High-intensity contrast agents in medical imaging

Thesis

UNRESTRICTED

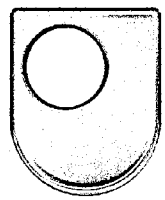

The Open University

High-Intensity Contrast Agents in Medical Imaging

Submitted for the degree of Doctor of Philosophy

David Peter Thomas Smith
M.Chem. (Hons) University of Wales, Bangor
M.Sc. University of Wales, Bangor

Chemistry and Analytical Sciences

Submission Date 31st of July 2008
Viva Date 10th of February 2009
Minor corrections submitted on 10th July 2009
Corrections accepted on 25th August 2009

DATE OF SUBMISSION : 11 AUGUST 2008
DATE OF AWARD : 25 AUGUST 2009

ProQuest LLC.
789 East Eisenhower Parkway
P.O. Box 1346
Ann Arbor, MI 48106 – 1346

Statement

The work embodied in this thesis was carried out by the author between October 2003 and March 2008 in the laboratories of the Department of Chemistry and Analytical Sciences, Open University, Walton Hall, Milton Keynes, under the supervision of Dr James Bruce and Prof. Peter Taylor.

I declare that the work presented here was the result of my own investigations, and that the material within this thesis has not been submitted, neither was it currently being submitted, for any other degree.

David Smith

March 2008

Abstract

This research project focused on the formation of novel, high-contrast MRI agents based on cyclen (1,4,7,10-tetraazacyclododecane) for the complexation of Gd^{3+}. The aim of the project was to attach a number of these gadolinium contrast agents to a silicon-based central scaffold. This would allow several cyclen units to be attached to the scaffold, producing a contrast agent in which the number of bound gadoliniums was limited only by the number of binding sites on the scaffold.

The Gd^{3+} was complexed in a ligand based on a tetrasubstituted cyclen (1,4,7,10-tetraazacyclododecane) in which three of the four amines were used for attachment of carboxylic acids for complexation to the gadolinium, while the fourth amine was used for the attachment of the linking arm used to bind to the silicon-based scaffold. Two types of cyclen ligand were investigated. Firstly, an eight-coordinate cyclen ligand based on acetic acid arms with but-3-enal for the binding arm, where the carbonyl on the but-3-enal was bound to the gadolinium to improve complex stability; and secondly, a seven-coordinate cyclen system consisting of succinic acid arms and a straight-chain alkene for the hydrosilylation reaction.

While the acetic acid based complexes failed due to stability issues, with the but-3-enal linking arm being hydrolysed during the deprotection of the acetic acid groups. As a result of this the research concentrated on the seven-coordinate ligand system. The advantage of the seven-coordinated system was that the extra non-coordinating three acid groups from the succinic acid on the cyclen would increase the solubility of the target molecules, and would also repel any anions in solution when used in biological systems.

The first scaffolds investigated were based on silsesquioxane cages. The experiments showed that this approach was problematic due to the decomposition of the cyclen system and the silsesquioxane cage to form an insoluble gel like product. This decomposition was found to be due to several unforeseen factors, which included the trapping of water with in the cyclen molecule, the decomposition of the cyclen ligand by the platinum catalyst producing a secondary amine. The decomposition of the silsesquioxane cage was inpart due to this secondary amine. Because of these problems an alternative scaffold was used. The new scaffold was based on silanes attached to a benzene ring, rather than to the siloxanes of the cages.

The MRI T2 relaxation rates showed that the complexes that contained one or two gadoliniums had a relaxivity in relation to molar concentration of complex of 4.8 $r_{1p}/mM^{-1}s^{-1}$ and 4.5 $r_{1p}/mM^{-1}s^{-1}$ (or 2.25 $r_{1p}/mM^{-1}s^{-1}$ per gadolinium) respectively, and so were similar to the commercial MRI contrast agent DOTA-Gd (4.3 $r_{1p}/mM^{-1}s^{-1}$). The trisubstituted scaffold compound 1,3,5-tris((pentane-sDO3A)dimethylsilyl)benzene-Gd3 (**247**) showed a marked increase in the relaxivity (13.1 $r_{1p}/mM^{-1}s^{-1}$) in relation to molar concentration, and 4.3 $r_{1p}/mM^{-1}s^{-1}$in relation to the gadolinium concentration.

The thesis is split into six chapters, with the first one covering the background of the MRI technique and current research into MRI contrast agents. The second chapter deals with the formation of the cyclen ligands. The third chapter is about the attachment of the cyclen ligands to the silicon scaffold. The fourth chapter concerns the formation of the lanthanide complexes and the measurements undertaken. The final two chapters involve the conclusion and the experimental section.

Acknowledgements

I would like to gratefully acknowledge my supervisors Dr James Bruce and Prof. Peter Taylor for all the support they have given me over the years of the project, and also the Open University for funding over the course of the project.

My thanks go to my wife, Dr Patricia Raggazon, for all her support during the research and writing stages of the project. I would also like to say thank you to my mum, Julie, and my brother, Adric, for all their support over the past years; and to Rory and Emma Stamp and Chris Hudson for all their continuing support.

In addition I would like to thank the following, for without them it would have been impossible to do the research in the lab: Allen Bowden, Pravin Patel, Colin Haynes, Graham Jeffs, Jill Clarke, Michael Batham and Susan Cooper; also Patrick O'Connell for his company in the lab. I thank too the teachers and lectures who have inspired me during my years of studies Mr Gill, Dr Robinson and Dr A. K. Croft

Dedication

To the people who believed in me and who lifted me up so I could reach for the stars.

Dedicated to the loving memory of my father

Contents

High-Intensity Contrast Agents in Medical Imaging _____ ***1***

Statement _____ **2**

Abstract _____ **3**

Acknowledgements _____ **5**

Dedication _____ **6**

Contents _____ **7**

Figures _____ **14**

Tables _____ **20**

Graphs _____ **21**

Equations _____ **21**

Abbreviations: _____ **22**

Chapter 1: Introduction _____ **23**

1.1: Principles of MRI and NMR _____ 24

1.2: MRI image enhancement by contrast agents _____ 32

1.3: Solomon–Bloembergen–Morgan equation _____ 35

1.4.1: Methods of improving the efficacy of contrast agents _____ 37

1.4.2: Effect of hydration number on a contrast agent _____ 38

1.4.3: Effect of the rotational correlation time on a contrast agent _____ 39

1.4.4: Effect of water exchange rate between lanthanides and the surrounding bulk water_45

1.5: Why is cyclen used in contrast agents? _____ 47

1.6.0: Classification of MRI contrast agent _____ 48

1.6.1: Extracellular fluid agents _____ 48

1.6.2: Blood-pool contrast agents _____ 50

1.6.3: Particulate / polymeric-based contrast agents _____ 51

1.6.4: Liposomal-based contrast agents _____ 52

1.6.5: Receptor-Induced Magnetic Enhancement (RIME) agents _____ 54

1.6.6: Non-clinical research contrast agents ____ 55

1.7.1: Aim of the thesis ____ 59

1.7.2: Silicon cages ____ 63

1.7.3: Properties of silicon cages ____ 64

1.7.4: Methods of forming bonds between silsesquioxanes and cyclens ____ 68

1.7.5: Hydrosilylation-based bond formation ____ 70

Chapter 2.0: Formation of the cyclen moiety – results and discussion ____ 73

2:1: Strategies for the substitution of cyclen ____ 74

2.2.1: Synthesis of 1-pent-4-enoyl-1,4,7,10-tetraazacyclododecane (**66**) ____ 76

2.2.2: Synthesis of 1-pent-4-enoyl-1,4,7,10-tetraazacyclododecane (**66**) via the 1+3 Route78

2.2.3: Protected cyclen route for the synthesis of 1-pent-4-enoyl-1,4,7,10tetraazacyclododecane(**87**) ____ 80

2.2.4:Conclusion ____ 86

2.3: Nomenclature for hex-acid cyclen systems ____ 87

2.4.1: Synthesis of a malonic acid-armed cyclen, mDO3A (**31**) ____ 89

2.5.1: Synthesis of a succinic acid substituted cyclen (**9**), butene-sDO3A ____ 96

2.5.2: Synthesis of butene-sDO3A-(ethyl) (**101**) ____ 98

2.5.3: Synthesis of butene-sDO3A-(ethyl) (**101**) by Route C (1+3) ____ 101

2.5.4: Synthesis of diethyl 2-bromosuccinate (**103**) ____ 107

2.5.5: Synthesis of butene-sDO3A-(ethyl) (**101**) from 1-but-3-en-1-yl-1,4,7,10-tetraazacyclododecane (**106**) ____ 108

2.6.1: Route D (3+1) for the synthesis of butene-sDO3A-(ethyl) (**101**) ____ 110

2.7.1: A study of the reaction between cyclen and diethyl 2-bromosuccinate ____ 117

2.8.1: Method for improving yields of the reaction between diethyl 2-bromosuccinate and cyclen ____ 118

2.8.2: Synthesis of (E)-3-(ethoxycarbonyl)acrylic acid (**125**) ____ 121

2.9.1: Conclusion ____ 123

2.10.1: Synthesis of sDO3A-(ethyl) (**107**) via Michael addition with diethyl maleate (**126**) and diethyl fumarate (**130**) ____ 126

2.11.1: Synthesis of butene-sDO3A-(ethyl) (**101**) from sDO3A-(ethyl) (**107**) ____ 129

2.11.2: Synthesis of pentene-sDO3A-(ethyl) (**133**) from sDO3A-(ethyl) (**107**) ____ 131

2.12: Conclusion 132

2.13.1: Hydrolysis of sDO3A-(ethyl) (**107**), butene-sDO3A-(ethyl) (**101**) to give the acids sDO3A and butene-sDO3A 133

2.13.2: Acid-catalysed hydrolysis of sDO3A-(ethyl) (**107**) 134

2.13.3: Base-catalysed hydrolysis of sDO3A-(ethyl) (**107**) to form sDO3A (**32**) 138

2.14.1: Purification of sDO3A (**32**) by ion-exchange chromatography 139

2.14.2: Cation-exchange chromatography of sDO3A (**32**) 140

2.14.3: Anion-exchange chromatography of sDO3A (**32**) 141

2.14.4: Conclusion 142

Chapter 3.0: Silicon–cyclen chemistry 143

3.1: Catalysts used in hydrosilylation reactions. 144

3.2: Reaction of pentene-sDO3A-(ethyl) with T_8H_8 147

3.2.1: Formation of T_8H_8 147

3.2.2: Model reaction of N,N-diethylbut-3-en-1-amine and T_8H_8 148

3.2.3: Reaction of butene-sDO3A-(ethyl) (**101**) with T_8H_8 (**33**) 150

3.2.4: Reaction of butene-sDO3A-(ethyl) (**101**) with $Q_8M_8^H$ (**38**) via Speier's catalyst 155

3.2.5: Reactions of pentene-sDO3A-(ethyl) (**194**) with $Q_8M_8^H$ (**38**) *via* Karstedt's catalyst 157

3.3: Investigation into the stability of pentene-sDO3A-(ethyl) (**133**) in the presence of a platinum catalyst 159

3.4: Alternative route to the formation of Q_8(pentene-sDO3A-(ethyl))$_8$ 161

3.5: Mechanism for the decomposition of silsesquioxane cages 164

3.6: Reaction of butene-sDO3A-(ethyl) (**133**) with simple siloxanes and silanes 171

3.7.1: Use of dimethylsilane$_n$-benzenes as the scaffold for the attachment of pentene-sDO3A-(ethyl) via hydrosilylation 174

3.7.2: Synthesis of ((pentane-sDO3A(ethyl))dimethylsilyl)$_n$- benzene via Route *H* 177

3.8: Modelling of side reactions between pentene-sDO3A-(ethyl) and dimethylsilylbenzene noticed in Route *H* 181

3.9.1: The synthesis of ((pentane-sDO3A(ethyl))dimethylsilyl)$_n$- benzene via Route *I* 184

3.10: Hydrolysis of the ethyl ester protecting groups on the ((pentane-sDO3A(ethyl))dimethylsilyl)n-benzene 190

Chapter 4.0: Complexation and luminescence and relaxivity studies of ((pentane-sDO3A (ethyl))dimethylsilyl)n benzene's 195

4.1: Complexation of the sDO3A-(ethyl)-ligands and the aDO3A-ligands with Gd^{3+} and Eu^{3+} 196

4.2.1: Luminescent studies of sDO3A–(ethyl)–Eu-based complexes, sDO3A–Eu-based complexes and the organosilicon Eu^{3+} complexes 198

4.2.2: Results and analysis of the Eu^{3+} emission spectra for the Eu^{3+} complexes 200

4.3.1: Determination of the water coordination number (*q*) for the Eu^{3+} complexes 206

4.3.2: Calculation of the Eu^{3+} water hydration number for the Eu^{3+}-complexed ligands 207

4.3.3: Results and analysis of the water coordination numbers of the Eu^{3+} complexes 208

4.4.1: Relaxivity measurements of the Gd^{3+} complexes 210

4.4.2: Relaxation results for the synthesised Gd^{3+} complexes 212

4.5: Conclusion 215

Chapter 5.0: Conclusion 217

5.1: The formation of sDO3A-(ethyl) (**107**) and sDO3A (**32**) 218

5.2: Silsesquioxane cage-based contrast agents 220

5.3: Silylbenzene based contrast agents 221

5.4: Further work on silsesquioxane-cyclen compounds 221

5.5: Further work on silylbenzene-based contrast agents 224

Chapter 6: Experimental Section 226

6.1: Synthesis of 1-pent-4-enoyl-1,4,7,10-tetraazacyclododecane (**66**) 227

6.2: Synthesis of 1,4,7,tetraaza-cyclodecane-1,4,7-tricarboxylic acid tri-*tert*-butyl ester (tri-Boc-cyclen) (**72**) 227

6.3: Synthesis of 1-pent-4-enoyl-4,7,10,tetraaza-cyclodecane-1,4,7-tricarboxylic acid tri-*tert*-butyl ester (**73**), Scheme C 228

6.4: Synthesis of 1-pent-4-enoyl-1,4,7,10-tetraazacyclododecane (**66**) from 1-pent-4-enoyl-4,7,10-tetraaza-cyclodecane-1,4,7-tricarboxylic acid tri-*tert*-butyl ester (**73**) 229

6.5: Synthesis of 1,4,7,10-tetraazacyclododecane-1,4,7-tricarbaldehyde 229

6.6: Synthesis of 10-pent-4-enoyl-1,4,7,10-tetraazacyclododecane-1,4,7-tricarbaldeyde (**75**) version 1 230

6.7: Synthesis of 10-pent-4-enoyl-1,4,7,10-tetraazacyclododecane-1,4,7-tricarbaldeyde (**75**), version 2 ____ 230

6.8: Synthesis of 1-pent-4-enoyl-1,4,7,10-tetraazacyclododecane (**66**) ____ 231

6.10: Synthesis of s-(bromomethyl)-2-methylmalonic acid (**89**) ____ 233

6.11: Synthesis of dimethyl 2-(bromomethyl)-2-methylmalonate (**96**) ____ 234

6.12: Synthesis of diethyl 2-(bromomethyl)-2-methylmalonate (**95**) ____ 235

6.13: Synthesis of 1-but-3-en-1-yl-1,4,7,10-tetraazacyclododecane (**106**) ____ 235

6.16: Synthesis of 7-but-3-en-1-yloctahydro-5*H*-2a,4a,7,9a-tetraazacycloocta[1,2,3-*cd*]pentalene (**115**) ____ 238

6.20: Synthesis of diethyl 2-bromosuccinate (**103**) ____ 242

6.21: Synthesis of butene-sDO3A-(ethyl) (**101**) from 1-but-3-en-1-yl-1,4,7,10-tetraazacyclododecane (**106**) ____ 244

6.22: Synthesis of sDO3A-(ether) (**107**) from cyclen (**9**) ____ 244

6.24: Purification method (1) – biphasic separation: silica chromatography eluted with DCM (70%), THF (30%) ____ 245

6.25: Purification method (2) – biphasic separation: silica chromatography eluted with DCM 95%, MeOH 5% ____ 246

6.26: Purification method (3) – biphasic separation: alumina chromatography eluted with DCM 95%, MeOH 5% ____ 247

6.27: Purification method (4) – biphasic separation: alumina chromatography eluted with DCM 70%, THF 30% ____ 248

6.28: Purification method (5) – biphasic separation: alumina chromatography eluted with DCM 99%, MeOH 1% ____ 248

6.29: Synthesis of sDO3A-(ethyl) (**103**) via cyclen (**9**) using Sep-Pak columns. ____ 250

6.30: Reaction of diethyl 2-succinate (**103**) with potassium carbonate to form diethyl maleate (**126**) ____ 251

6.31: Synthesis of sDO3A-(ethyl) (**107**) from cyclen (**9**) via caesium carbonate version 1_252

6.32: Synthesis of sDO3A-(ethyl) (**107**) from cyclen (**9**) via caesium carbonate version 2_253

6.32.1: Work-up method 1: Chromatography ____ 254

6.32.2: Work-up method 2: Vacuum distillation ____ 254

6.33: Reaction of diethyl 2-bromosuccinate (**103**) with potassium carbonate to form diethyl malate 256

6.34: Synthesis of sDO3A-(ethyl) (**107**) from diethyl maleate 256

6.36: Synthesis of sDO3A-(ethyl) (**107**) via diethyl maleate (126) – scaled-up version (final version) 258

6.37: Synthesis of butene-sDO3A-(ethyl) (**101**) via sDO3A-(ethyl) (**107**) 259

6.38: Synthesis of pentene-sDO3A-(ethyl) (**133**) from sDO3A-(ethyl) (**107**) 260

6.39: Hydrolysis of sDO3A-(ethyl) (**107**) to form sDO3A (**32**) – DCl method 262

6.40: Hydrolysis of sDO3A-(ethyl) to form sDO3A via formic acid 263

6.41: Hydrolysis of butene-sDO3A-(ethyl) (**101**) to form butene-sDO3A (**105**) via 1.4M formic acid 263

6.44: Preparation of ion-exchange resins 266

6.44.2: Cation-exchange resin preparation 267

6.44.3: Anion-exchange resin preparation 267

6.45: Cation-exchange chromatography of reaction solution from the hydrolysis of sDO3A-(ethyl) (107) via NaOD 267

6.49: Formation of T_8H_8 $[HSiO_{3/2}]_8$ (**33**) 270

6.50: Formation of *N,N*-diethylbut-3-en-1-amine (**156**) 270

6.51: Reaction of *N,N*-diethylbut-3-en-1-amine (**156**) with T_8H_8 to form compound (**167**) 272

6.51: Reaction of *N,N*-diethylbut-3-en-1-amine with Q_8H_8 to form compound (**168**) 272

6.52: Reaction of butene-sDO3A-(ethyl) (**101**) with T_8H_8 (**33**) via Speier's catalyst – version 1 273

6.53: Reaction of butene-sDO3A-(ethyl) (**101**) with T_8H_8 (**33**) via Speier's catalyst – version 2 274

6.54: Reaction of butene-sDO3A-(ethyl) (**101**) with T_8H_8 (33) via Speier's catalyst dried over molecular sieve 275

6.54.1: Chloroform extraction 275

6.54.2: Toluene extraction 276

6.56: Reaction of butene-sDO3A with Q_8H_8 via Speier's catalyst 278

6.57: Reaction of pentene-sDO3A (**133**) with Q_8H_8 via Karstedt's catalyst 279

6.58: Test reaction of T_8H_8 (**33**) with Speier's catalyst 280

6.59: Formation of Q_8-(1-bromobutane)$_8$ (**166**) 280

6.60: Reaction of Q_8(1-bromopentene)$_8$ (**166**) with sDO3A-(ethyl) (**107**) to form compound (**167**) 281

6.61: Reaction of triethoxysilane (**13**) and butene-sDO3A-(ethyl) (**101**) 282

6.62: Reaction of 1,1,3,3,5,5 hexamethyl-trisiloxane (**182**) with butene-sDO3A-(ethyl) (**101**)283

6.63: Reaction of triethylsilane (**181**) with butene-sDO3A-(ethyl) (**101**) to give compound (**186**) 285

6.64: Formation of tri-(dimethylsilyl) benzene (**193**) 286

6.65: Reaction of tri-(dimethylsilyl) benzene (**193**) with pentene-sDO3A-(ethyl) (**133**) to form 1,3,5-tris((pentane-sDO3A(ethyl))dimethylsilyl) benzene (**189**) 287

6.65.1: Distillation results: 288

6.66: Reaction of pentene-sDO3A-(ethyl) (**133**) with bis(dimethyl silyl)benzene (**192**) to form 1,4-bis((5-bromopentyl) dimethylsilyl) benzene (**198**) 289

6.67: Synthesis of bis(succinate)dimethyl phenylsilane (**196**) 292

6.68: Formation of diethyl 2-(diethylamino)succinate (**197**) 293

6.69: Reaction of diethyl 2-(diethylamino)succinate (**197**) with dimethylphenyl silane (**190**) 294

6.71: Stability of pentene-sDO3A-(ethyl) (**133**) with Karstedt's catalyst 295

6.72: Synthesis of (5-bromopentyl)dimethyl(phenyl)silane (**191**) 296

6.73: Formation of 1,4-bis((5-bromopentyl)dimethylsilyl)benzene (**198**) 297

6.74: Synthesis of 1,3,5-tris((5-bromopentyl)dimethylsilyl)benzene (**199**) 298

6.75: Synthesis of (pentane-sDO3A-(ethyl))dimethyl(phenyl)silane (**187**) 299

6.76: Synthesis of 1,4-bis((pentane-sDO3A(ethyl))dimethylsilyl) benzene (**188**) 301

6.77: Synthesis of 1,3,5-tris((pentane-sDO3A(ethyl))dimethylsilyl) benzene (**189**) 302

6.78: Hydrolysis of (sDO3A- (ethyl)-pentyl)dimethyl(phenyl) (**187**) to form (pentane-sDO3A-)dimethyl(phenyl)silane (**200**) 303

6.80: Hydrolysis of 1,3,5,-tris-(sDO3A-(ethyl)-pentyl)dimethyl(phenyl) (**232**) to form 1,3,5-tris((pentane-sDO3A)dimethylsilyl)benzene (**202**) 306

6.81: Luminescence emission defaults 307

6.82: Formation of pentene-sDO3A-(ethyl)-Gd (**203**) 308

6.83: Formation of butene-sDO3A-(ethyl)-Eu (**204**) 308

6.86: Formation of sDO3A-Gd (**207**) 310

6.87: Formation of sDO3A-Eu (**208**) 311

6.88: Formation of sDO2A-Gd (**209**) 311

6.89: Formation of sDO2A-Eu (**210**) 312

6.93: Formation of (pentane-sDO3A-)dimethyl(phenyl)silane-Eu (**213**) 315

6.94: Formation of 1,4-bis((pentane-sDO3A)dimethylsilyl)benzene-Gd_2 (**214**) 315

6.95: Formation of 1,4-bis((pentane-sDO3A)dimethylsilyl)benzene-Eu_2 (**215**) 316

6.96: Formation of 1,3,5-tris((pentane-sDO3A)dimethylsilyl) benzene-Gd_3 (**216**) 316

6.98: MOPS buffer – (10mmol) 318

6.99: Anionic background, simulated extracellular environment 318

Chapter 7: References 319

Figures

Figure 1.1.1: Radiogram of my left shoulder, showing possible detail obtainable using x-rays 24

Figure 1.1.2: Image of a typical MRI scan 25

Figure 1.1.3: Proton energy levels for different magnetic field strengths for ^1H NMR. 28

Figure 1.1.4: Diagram of the Spin–Spin interactions 30

Table 1.1.1: Table of relaxation times in milliseconds for tissues at 1 Tesla static magnetic field strength (42.6 MHz) and the percentage error. 31

Figure 1.2.1: Comparison of MRI images of the human knee. 33

Figure 1.3.1: Diagram showing the inner, second and outer water coordination spheres of DO3A-Gd 35

Figure 1.4.2.1: Structures of DO3A-Gd 38

Figure 1.4.3.2: Structure of P792 40

Figure 1.4.3.3: Different methods of increasing the rotational correlation times 41

Figure 1.4.3.4: Structure of NMS60-Gd 42

Figure 1.4.3.5: Example of a branched, fourth-generation dendrimer MRI contrast agent, where PAMAM G4 is functionalised with Gd-1BAM-DPTA 43

Figure 1.4.3.6: Structure of [Gd4dmpDO3A$_4$] 44

Figure 1.4.4.1: Structures of $[GdaDOTA]^{3-}$ and $[GdgDOTA]^{3-}$ 46

Figure 1.5.1: Structure of cyclen 47

Figure 1.5.2: The coordination of the lanthanide within the complexes 48

Figure 1.6.1.1: Structures of some extracellular contrast agents: 49

Figure 1.6.2.1: Structure of DOTA-$(BOM)_3$ 50

Figure 1.6.2.2: Structure of P760 51

Figure 1.6.4.1: Structure of a lipid membrane 52

Figure 1.6.4.2: Liposomal contrast agent with gadolinium at the centre 53

Figure 1.6.4.3: Liposomal contrast agent with gadolinium in the outer sphere 53

Figure 1.6.5.1: Structures of Structures of MS-325; and C_8-DOTP 55

Figure 1.6.6.1: Structures of DTPA-BMA 56

Figure 1.6.6.2: Structures of DO3A 57

Figure 1.6.6.3 Structures of gDO3A 58

Figure 1.6.6.4: Intramolecular binding of gDO3ALn 59

Figure 1.7.1.1: The target molecule 60

Figure1.7.1.2: The secondary target molecule 61

Figure 1.7.1.3: Change in the oscillations of the siloxane cage with linked cyclen–Ln pendant arms. 62

Figure 1.7.1.4: Structures of mDO3A and sDO3A 63

Figure 1.7.2.1: Types of silicon chains and rings 64

Figure 1.7.3.1: Some useful cages 65

Figure 1.7.3.2: Structures of lanthanide-silsesquioxane complexes 67

Figure 1.7.3.3: Mechanism for decomposition of a T8 cage via a primary amine 68

Figure 1.7.4.1: Retrosynthesis analysis of the target molecule for the formation of the Si–C bond 69

Figure 1.7.5.1: Addition of an alkene 70

Figure 1.7.5.2: Alcoholysis of $HSi(OEt)_3$ 71

Figure 1.7.5.3: Reaction of triethoxyhydrosilane (**47**) with propanoic acid (**49**) to form triethoxysilyl propionate (**50**) 72

Figure 2.1.1: The two strategies for asymmetric cyclens: top, 1+3 strategy; bottom, 3+1 strategy 74

Figure 2.1.2: pK_as of cyclen in water; conditions 25 °C, 0.1M $NaNO_3$ 75

Figure 2.1.3: Products of over-alkylation. Left: the over-alkylated product from the 1+3 strategy. Right the over-alkylated product from the 3+1 strategy 76

Figure 2.2.1.1: Retrosynthetic analysis of compound (**60**) 77

Figure 2.2.1.2: Two reaction pathways for the formation of the ethyl ester form of pent-4-enoyl-DO3A 78

Figure 2.2.2.1: The 1+3 route for the synthesis of 1-pent-4-enoyl-1,4,7,10-tetraazacyclododecane 79

Figure 2.2.2.2: Reaction products of cyclen and pent-4-enoyl chloride 80

Figure 2.2.3.1: Second method for the formation of 1-pent-4-enoyl-1,4,7,10-tetraazacyclododecane 81

Figure 2.2.3.2: Formyl-protected cyclen route for the synthesis of compound (**66**) 82

Figure 2.2.3.3 Synthesis of triformyl cyclen 83

Figure 2.2.3.4: Structure of monoformyl-protected product 84

Figure 2.2.3.5: Hydrolysis of compound (**75**) to form 1-pent-4-enoyl-1,4,7,10-tetraazacyclododecane 86

Figure 2.2.4.1: Structure of 4-bromobut-1-ene (**78**) 87

Figure 2.3.1: Examples of different compounds based on DO3A 88

Figure 2.4.1.1: Structures of oxalic acid 89

Figure 2.4.1.2: Decarboxylation of malonic acid compounds 89

Figure 2.4.1.3: Structure of proposed methylated malonic acid group to prevent decarboxylation 90

Figure 2.4.1.4: Retrosynthetic analysis of compound 91

Figure 2.4.1.5: Mechanism for the formation of 2-(bromomethyl)-2-methylpropane-1,3-diol 92

Figure 2.4.1.6: Formation of 2-(bromomethyl)-2-methylmalonic acid 93

Figure 2.4.1.7: Formation of ester-protected 2-(bromomethyl)-2-methylmalonic acid ____ 94

Figure 2.4.1.8: Structure of 2-(methoxycarbonyl)-3-bromo-2-methylpropanoic acid ____ 95

Figure 2.4.1.9: Proposed mechanism for the decarboxylation of 2-(bromomethyl)-2-methylmalonic acid ____ 95

Figure 2.5.1.1: Structure of succinic acid ____ 96

Figure 2.5.1.2: Retrosynthetic analysis of butene-sDO3A ____ 97

Figure 2.5.2.1: Routes C (1+3) and D (3+1) for the synthesises of butene-sDO3A ____ 99

Figure 2.5.2.2: The four possible products from the reaction of cyclen with diethyl 2-bromosuccinate ____ 100

Figure 2.5.3.1: Formation of the mono-alkene cyclen, 1-but-3-en-1-yl-1,4,7,10-tetraazacyclododecane ____ 101

Figure 2.5.3.2: Formation of 10-but-3-en-1-yl-1,4,7,10-tetraazacyclododecane-1,4,7-tricarbaldehyde (____ 102

Figure 2.5.3.3: Side product of the alkylation reaction ____ 102

Figure 2.5.3.4: Reaction of cyclen and DMF-DMA ____ 103

Figure 2.5.3.5: Reaction of tricyclic amine with 4-bromobut-1-ene ____ 104

Figure 2.5.3.6: Reaction mechanism for the deprotection of compound (**121**) ____ 105

Figure 2.5.3.7: Hydrolysis of (**121**) ____ 107

Figure 2.5.4.1: Synthesis of diethyl 2-bromosuccinate ____ 108

Figure 2.5.5.1: Synthesis of butene-sDO3A-(ethyl) ____ 109

Figure 2.5.5.2: By-products from the formation of butene-sDO3A-(ethyl) ____ 110

Figure 2.6.1.1: Route for the 3+1 route to butene-sBDO3A-(ethyl) ____ 111

Table 2.6.1.1: The $[M^{+1}]$ ions of the starting material and the products of formation of sDO3A-(ethyl) ____ 112

Table 2.6.1.2: Results from comparative purification techniques ____ 115

Table 2.6.1.3: Relative solvent strength based on polarity ____ 116

Figure 2.8.2.1: Reaction path for the synthesis of (E)-3-(ethoxycarbonyl)acrylic acid 121

Figure 2.8.2.2: Structures of the two isomers of the monoethyl acrylic acids and the free acids 122

Figure 2.9.1.1: Products of the reaction of diethyl 2-bromosuccinate 123

Figure 2.9.1.2: Mechanism of the E2 reaction of diethyl 2-bromosuccinate 124

Figure 2.10.1.1: Mechanism for the Michael addition of diethyl 2-bromosuccinate 127

Figure 2.11.1.1: Formation of butene-sDO3A-(ethyl) 130

Figure 2.11.2.1: Formation of pentene-sDO3A-(ethyl) 132

Figure 2.13.1: Structure of Karstedt's catalyst 133

Figure 2.13.2.1: The C2–D2 symmetry of 1,7-sDO2A 135

Figure 2.13.2.2: The decomposition of sDO3A 136

Figure 2.13.2.3: Probable structures of the products from the hydrolysis of butene-sDO3A-(ethyl) 137

Figure 2.14.1.1: The charged ion sites for ion exchange 140

Figure 3.1.1: Structure of Karstedt's catalyst 144

Figure 3.1.2: Catalytic reaction mechanism for Speier's catalyst 146

Figure 3.2.1.1: Formation of T_8H_8 147

Figure 3.2.2.1: Synthesis of N,N-diethylbut-3-en-1-amine 148

Figure 3.2.2.2: Hydrosilylation reaction of N,N-diethylbut-3-en-1-amine 149

Figure 3.2.2.3: The different NMR environments and their NMR signal ppm for $Q_8M_8^H$ 150

Figure 3.2.3.1: Reaction of butene-sDO3A-(ethyl) (**101**) with T_8H_8 (**33**) 152

Figure 3.2.3.2: The silicon environment corresponding to −21.4 ppm 153

Figure 3.2.3.3: Structure of butane-sDO3A-(ethyl) 155

Figure 3.2.4.1: Reaction of butene-sDO3A-(ethyl) 156

Figure 3.3.1: Decomposition of pentene-sDO3A-(ethyl) 160

Figure 3.3.2: Complex formed during the inhibition of Karstedt's catalyst by fumarate 161

Figure 3.4.1: Formation of Q_8M_8(1-bromobutane)$_8$ (**166**) 162

Figure 3.4.2: Formation of Q_8(pentane-sDO3A-(ethyl))$_8$ (**187**) 163

Figure 3.5.1: The different reactions of pentene-sDO3A-(ethyl) 165

Figure 3.5.2: Decomposition of $Q8M8^H$ 166

Figure 3.5.3: Reaction of $Q_8M_8^H$ (38) with compound (**170**) 167

Figure 3.5.4: Linking of an incompletely condensed silsesquioxane 168

Figure 3.5.5: Decomposition of T8H8 169

Figure 3.5.6: Formation of –(O-Si$(CH_3)_2$-O)n- 170

Figure 3.6.1: Structure of triethoxysilane 172

Figure 3.6.2: Decomposition of 1,1,3,3,5,5-hexamethyl-trisiloxane 173

Figure 3.6.3: Structure of triethylsilane-butane-sDO3A-(ethyl) 174

Figure 3.7.1.1: Structure of the new core sDO3A-(ethyl) systems 175

Figure 3.7.1.2: Two routes for the synthesis of (pentane-sDO3A-(ethyl)-(dimethylsilyl)benzene 176

Figure 3.7.1.3: Synthesis of 1,3,5,tri-(dimethylsilyl)benzene 177

Figure 3.7.2.1: Reaction of pentene-sDO3A-(ethyl) 179

Figure 3.7.2.2: Reaction of pentene-sDO3A-(ethyl) 180

Figure 3.8.1: Reaction of diethyl maleate 182

Figure 3.8.2: Synthesis of diethyl 2-(diethylamino)succinate 183

Figure 3.9.1: Synthesis of (5-bromopentyl)dimethyl(phenyl)silane 184

Figure 3.9.2: Structures of 1,4-bis((5-bromopentyl)dimethylsilyl)benzene 185

Table 3.9.1: Results of the reactions between 5-bromopent-1-ene (134) and dimethylsilyl benzene (190), 1,4,bis-(dimethylsilyl)benzene (192) or 1,3,5-tri-(dimethylsilyl)benzene (193) 186

Figure 3.9.3: Synthesis of (pentane-sDO3A-(ethyl))dimethyl(phenyl)silane 187

Figure 3.9.4: Structure of 1,4-bis((pentane-sDO3A(ethyl))dimethylsilyl)benzene 189

Figure 3.9.5: Structure of 1,3,5-tris((pentane-sDO3A(ethyl))dimethylsilyl)benzene 190

Figure 3.10.1: Hydrolysis of (pentane-sDO3A-(ethyl))dimethyl(phenyl)silane 190

Table 3.10.1: Reaction yields of the hydrolysis of compounds (187) and (188) 191

Figure 3.10.2: Structures of 1,4-bis((pentane-sDO3A)dimethylsilyl)benzene 192

Table 4.1.1: Ligands complexed, with the lanthanide used and the yield of products 197

Figure: 4.2.1.1: Energy levels of Eu^{3+} below 30 000 cm^{-1} 199

Figure 4.4.2.1: Possible configuration of the cross-binding seen within 1,3,5-tris((pentane-sDO3A)dimethylsilyl)benzene-Gd_3 215

Figure 5.4.1: Possible formation of sDO3A-(ethyl)-T8 223

Figure 5.5.1: Formation of the novel silylbenzene cores 2,3,4,5,6-pentadimethylsilaneanaline 225

Tables

Table 1.1.1: Table of relaxation times in milliseconds for tissues at 1 Tesla static magnetic field strength 31

Table 2.6.1.1: The $[M^{+1}]$ ions of the starting material and the products of formation of sDO3A-(ethyl) (= $[M–Br]^{+1}$ ion)* 112

Table 2.6.1.2: Results from comparative purification techniques 115

Table 2.6.1.3: Relative solvent strength based on polarity 116

Table 3.9.1: Results of the reactions between 5-bromopent-1-ene and dimethylsilylbenzene, 1,4,bis-(dimethylsilyl)benzene or 1,3,5,tri-(dimethylsilyl)benzene 186

Table 3.9.2: Results of the reaction between(5-bromopentyl) dimethyl (phenyl)silane, 1,4-bis((5-bromopentyl)dimethylsilyl)benzene and 1,3,5-tris((5-bromopentyl)dimethylsilyl)benzene and sDO3A-(ethyl) 188

Table 3.10.1: Reaction yields of the hydrolysis. 191

Table 4.1.1: Compounds complexed, with the lanthanide used and the yield of products 197

Table 4.3.3.1: Lifetime data for Eu^{3+} complexes to calculate Q values 208

Table 4.3.3.2: K_{H2O} and K_{D2O} values for sDO2A-Eu and sDO3A-Eu. 210

Table 4.4.2.1: Results of relaxation measurements. 213

Table 4.4.2.3: Table of comparative complexes. 213

Graphs

Graph 1.4.3.1: Plot of the relaxivity per gadolinium versus molecular weight of contrast agent 43

Graph 4.2.2.3: Emission spectrum of DOTA-Eu 203

Graph 4.2.2.5: Emission spectrum of sDO3A-(ethyl)-Eu 205

Graph 4.2.2.6: Emission spectrum of Ph-(Si-(Me)3-Pentene-sDO3A-Eu 205

Graph 4.2.2.7: Emission spectrum of Ph-(Si-(Me)3-Pentene-sDO3A-Eu)$_2$ 205

Graph 4.4.1: Example of the plot of $1/T_1$ against concentration for 1,4-bis((pentane-sDO3A)dimethylsilyl)benzene-Gd$_2$ (214) 232

Equations

Equation 1.1.1: 25

Equation 1.1.2: 26

Equation 1.1.3: 26

Equation 1.2.1: 33

Equation 1.2.2: 35

Equation 1.3.1: 35

Equation 1.3.2: 35

Equation 1.3.3: 35

Equation 1.4.1: 37

Equation 1.4.3.1: 38

Equation 2.6.1.1: 113

Equation 4.3.2.1: 203

Equation 4.3.2.2: 203

Equation 4.3.2.3: 204

Abbreviations:

BOC: *tert*-butyl carbamate protection group.

DCM: Dichloromethane.

DO3A: Tri-*tert*-butyl 1,4,7,10-tetraazacyclododecane-1,4,7-triacetate.

sDO3A: Succinic acid DO3A.

mDO3A: Malonic acid DO3A.

gDO3A: Glutamic acid DO3A.

aDO3A: Adipic acid DO3A.

EtOH: Ethanol.

FTIR: Fourier Transform Infra Red spectroscopy.

HRMS: High Resolution Mass Spectroscopy

IMS: Industrial Methylated Spirits.

LCMS: Liquid Chromatography Mass Spectroscopy.

Ln: Lanthanide.

MeOH: Methanol.

MRI: Magnetic Resonance Imaging.

MADLI: Matrix-Assisted Laser Desorption/Ionization

NMR: Nuclear Magnetic Resonance.

Rf: Retention factor.

T_1 : Spin-lattice relaxation.

T_2 : Spin-Spin relaxation.

TEA: Triethylamine.

THF: Tetrahydrofuran.

TLC: Thin Layer Chromatography.

Chapter 1: Introduction

1.1: Principles of MRI and NMR

Medical Imaging is a powerful diagnostic tool used in modern medicine, allowing the non-invasive examination of patients, such as diagnosis of problems or investigation of neural activity. The term 'Medical Imaging' relates to several different methods of imaging, which are characterised by the energy sources used and the method of detection. The main distinction is between ionising and non-ionising sources.

There are several different techniques of medical imaging that use ionising radiation, either as an external source – for example, in radiography or fluoroscopy – or as an internal source, as seen in Positron Emission Tomography (PET). While these techniques produce good images, there is a limited time they can be used owing to the effect of ionising radiation on the tissues (Figure 1.1.1).

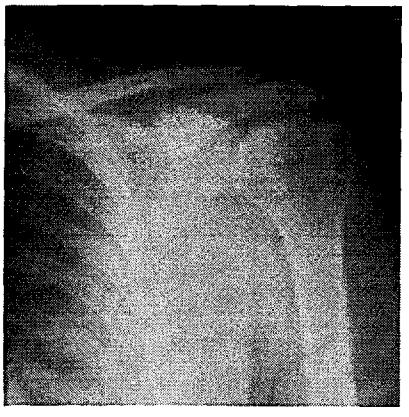

Figure 1.1.1: Radiogram of my left shoulder, showing possible detail obtainable using x-rays.

Non-ionising medical imaging techniques include Ultrasound and Magnetic Resonance Imaging (MRI). MRI is based upon Nuclear Magnetic Resonance (NMR). The application of NMR to a biological sample was first reported in 1971 by

Raymond Damadia, who discovered that certain mouse tumours gave elevated relaxation times when compared to those of non-cancerous tissue. In 1973 Paul Lauterbur[1] proposed using magnetic field gradients to distinguish between NMR signals originating from different locations, as the strength of the field is proportional to the radiofrequency. Between 1974 and 1980 further developments in detection and sensitising methods allowed for the first image of the human head to be published in 1978 by Clow and Young[2]. Since the introduction of the first MRI scanner at Hammersmith Hospital, London, with a field strength of 0.15T, the technique has greatly improved, to the point where a field strength of 3T is now commonplace in hospitals[3, 4] (Figure 1.1.2).

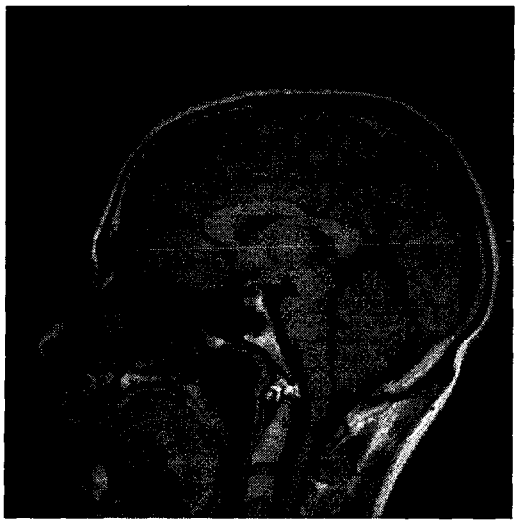

Figure 1.1.2: Image of a typical MRI scan.[5]

NMR and MRI rely on the interaction of atomic nuclei possessing a spin angular momentum with a magnetic field. The magnetic moment of the nucleus due to the nuclear spin arises from the spins of the individual protons and neutrons within the nucleus. This is seen as the angular momentum, where the rotation of the nucleus is around the central axis. This is shown in *Equation 1.1.1*, where *I* is the spin quantum number of the nucleus, and *h* is Planck's constant at 6.626 068 96 x 10^{-34} J s.

$$|I| = (h/2\pi)\sqrt{I(I+1)}$$ ***Equation 1.1.1***

Nuclei with an even mass number have spin quantum numbers as even multiples of ½ (I = 0, 1, 2...), while nuclei with odd mass numbers will have odd multiples of ½ (I = ½, 3/2...). A nucleus with I = 0 is insensitive to magnetic fields. The most commonly studied nuclei have a quantum number of 1/2, such as ^{1}H, ^{13}C, ^{31}P and ^{29}Si.[6, 7]

In practice, the subject is placed within the magnet of the MRI, whereupon the protons of the water molecules in the body are magnetised and align themselves with the magnetic field along the longitudinal axis. As the aligned protons cannot be measured, they need to be tipped out of alignment by the use of a pulsed radiofrequency (RF) into the *x*- or *y*-axis. As the proton realigns with the magnetic field the proton emits a pulse of energy in the form of radio waves, which are then detected by the MRI. It is also useful to probe the proton population with a second RF pulse to aid in the detection of the relaxation rate.

The strength of the signal received depends upon the relaxation of the protons within its environment such as proton concentration, viscosity of the tissue and changes in chemical shift because of pH and proton exchange.[3] It is important to note that MRI does not focus on a single molecule, but the protons in a local environment, thus the signal emitted by the protons will vary in its wavelength depending on the statistical populations of the area.

The energy needed to change the proton from one energy level, and thus spin state, to another is shown in *Equation 1.1.2*, where B_0 is the magnetic field strength. [8, 9]

$$\Delta E = \frac{h\gamma}{2\pi} B_0 \qquad \textbf{Equation 1.1.2}$$

It is possible to introduce energy in the form of radiofrequencies (v_1) to effect the transition between the energy levels in a fixed magnetic field of a known strength (B_0). The radiofrequency for a known magnetic field in an MRI can be calculated using *Equation 1.1.3*[8, 9] where γ is the magnetogyric ratio, which is the fundamental nuclear constant of the nuclei being monitored. In the case of ^1H, $\gamma = 2.675$ [$s^{-1}T^{-1}$] [10].

$$v_1 = \frac{\gamma}{2\pi} B_0 \qquad \textbf{Equation 1.1.3}$$

When the protons are in the magnetic field, the initial populations of the energy levels are determined by thermodynamics, as described by the Boltzmann distribution. This means that the lower energy level (N_α) will contain slightly more nuclei than the higher level (N_β). It is possible to excite these nuclei into a higher level with electromagnetic radiation. In the case of NMR with a magnetic field of 9.4 Tesla, a radiofrequency of 400 MHz is needed to effect the transition of the proton between the spin states. In MRI the magnetic field is lower than that of NMR; therefore the energy needed to affect the spin states is lower. For example, if an MRI has a magnetic field strength (B_0) of 1.5 Tesla, the energy gap between the two spin states is 64 MHz (Figure 1.1.3).

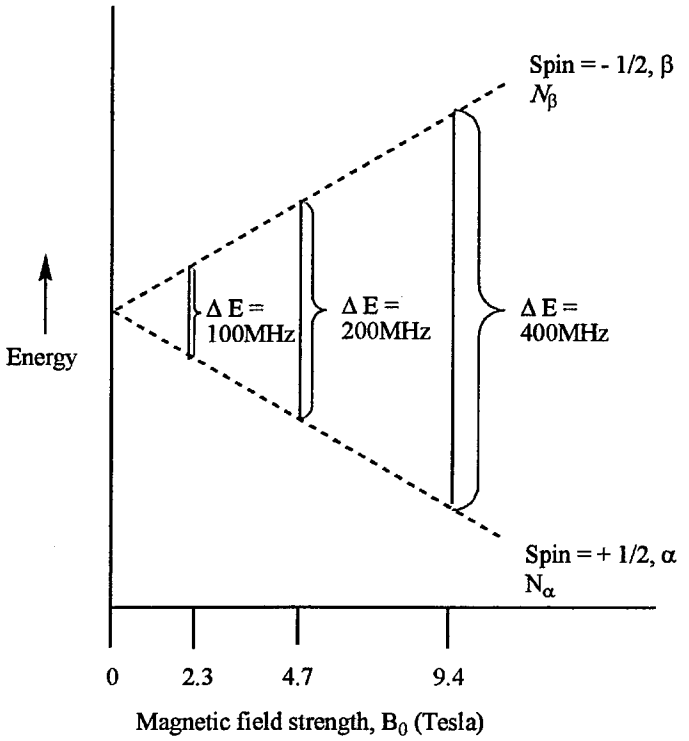

Figure 1.1.3: Proton energy levels for different magnetic field strengths for ^1H NMR.

The protons then return to alignment via a process called 'relaxation'. There are two different types of relaxation that occur in NMR and MRI. The first type of relaxation is known as T_1 relaxation and involves a return of the protons to the original alignment with the static magnetic field. This is expressed as longitudinal or spin-lattice relaxation. The term 'spin-lattice' refers to the interactions of the protons (spins) with their surroundings (lattice). This interaction causes a release of energy as the protons return to the original energy state of alignment.[11] Owing to the slow molecular motion of the fat molecules, T_1 relaxation occurs more rapidly – hence a shorter time T_1. Water molecules have higher mobility when compared to fat molecules; this movement induces inefficiency in the relaxation of the protons, as they do not have the possibility of interaction; therefore the loss of energy to other nuclei is slower. That results in greater values of T_1, as it takes longer for the proton

spins to realign with the main magnetic field. Also T_1 times are highly dependent on the field strength of the MRI scanner.[3]

The second type of relaxation, referred to as T_2, is transverse or spin–spin relaxation. The protons are aligned at right angles to the magnetic field. The energy is lost by the interaction of the proton spin with the spin of a neighbouring proton. This interaction reduces the phase coherence and cuts the signal strength down to 37% of its original strength. This loss in signal strength occurs because the magnetic moments of the random-orientated protons tend to cancel each other out (Figure 1.1.4). The T_2 times for different environments arise because water is less efficient in the exchange of energies than fat is, meaning that fat has shorter T_2 times compared with water, which has increased T_2 times.[12]

The rate at which the relaxation occurs differs, depending on the local environment in which the proton is found. T_1 times may be of the order of several hundred milliseconds, whereas T_2 times are of the order of tens of milliseconds. This is due to spin–spin interactions being more efficient than spin–lattice interactions.[11]

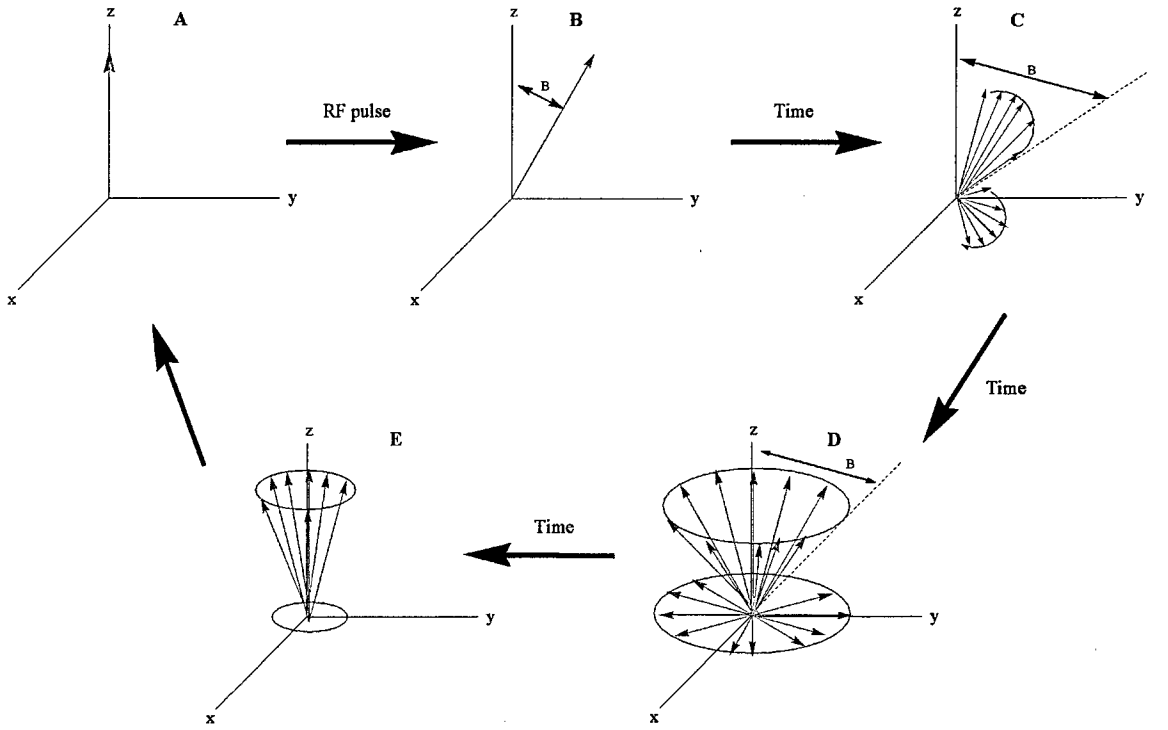

Figure 1.1.4: Diagram of the Spin–Spin interactions, showing the path of signal loss over time. A: The magnetic moment is aligned with the magnetic field. B: After the RF pulse (1) the magnetic moment can be represented as a single vector. C: The vector begins to break up as a result of localised non-uniformities in the applied field. The components of the vector move into the xy plane. D: The vectors spread out in an even pattern, cancelling each other out. E: With time, the cone representing the vectors narrows until the vector is again aligned with the magnetic field.[11]

Signal pulses are applied in specific sequences that depend on the technique used. There are several different techniques and each has several different subcategories, depending on whether T_1 or T_2 is being measured. Biological materials are distinguished by their T_1 and T_2 values, but the exact values are not unique for the different tissues (Table 1.1.1). The different values seen in T_1 or T_2 measurements arise from the correlation time of the water molecules in tissues. In liquids and semisolids the water molecules are free to rotate, while small molecules within the

liquid have higher rotational correlation times and have a greater chance of interacting with neighbouring molecules. This interaction between molecules allows relaxation to occur more rapidly and so the relaxation time is shorter.[11]

TISSUE	*T1*	*% +/-*	*T2*	*% +/-*
Skeletal muscle	732	18	47	27
Liver	423	22	43	32
Kidney	589	27	58	41
Adipose	241	28	84	42
Brain				
Grey matter	813	17	101	12
White matter	683	17	92	23

Table 1.1.1: Table of relaxation times in milliseconds for tissues at 1 Tesla static magnetic field strength (42.6 MHz) and the percentage error.[11]

This interaction of the spin and the microenvironment allows the distinction between water in bone, fats, muscles, body cavities, etc. in the MRI scan. However, the difference between tissue types can be hard to identify. Whilst with a large amount of time it is possible to find the optimum contrast between any tissues, it is not practical in a clinical setting. One way around this problem is by the use of contrast agents, which alter the relaxation rates.

While MRI is a more complex application of NMR spectroscopy, there are several differences which are apparent. The first is in the detail of information gained. An NMR instrument has a greater magnetic strength and thus has a greater resolution, due to the increase in the range of radiofrequencies available. There are two methods of obtaining an NMR spectrum. The first is continuous-wave, which uses a fixed radiofrequency pulse for the excitation of the protons. The different proton

environments are analysed by changing the current within the magnet, thus altering the magnetic field so that different protons are excited.[8] The second NMR method involves a Fourier transformation, where the radio pulse contains several different frequencies, scanning the whole range of the spectrum; this is used in the presence of a fixed magnetic field.[8] In MRI only a small set of radiofrequencies are used, as it is the relaxation time of the water in different environments that are being monitored, so structural information about the nuclear environment is not needed.

The second major difference between MRI and NMR is the way in which the sample is analysed. In NMR the sample is spun at around 17Hz; this creates a homogenous field within the sample tube and therefore in the probe. In MRI it is not possible to do this, and instead the MRI must focus on a small section or voxel of the subject at a time. This is done by the use of a secondary magnetic field in the form of a field gradient, which can change the strength of the magnetic field over the whole of the bore in all three axes. By changing the field strength in a certain location the resonance conditions for certain radiofrequencies are created, allowing for only the protons in that voxel to contribute to the image.

1.2: MRI image enhancement by contrast agents

The contrast within an MRI image is what allows for the identification of the tissues and fluids, owing to the signal strengths of the different environments. As the environments are similar, the detail that can be extracted from the image is limited. To improve the contrast between the tissues a contrast agent is employed. Contrast agents alter the rate of relaxation of the protons in nearby water molecules. T_1

agents shorten the longitudinal relaxation time, allowing a faster recovery of the spins to their thermodynamic equilibrium. That allows subsequent pulses to be formed without diminution in the signal intensity. In T_1 images, the shortened T_1 leads to an increase in the intensity, and thus the brightness of the image. T_2 agents shorten the transverse relaxation time, leading to a decrease in the MRI signal intensities. The effect of a contrast agent can be seen in the diagram below, which shows a comparison of images with no contrast agent and with a T_1 contrast agent (Figure 1.2.1).

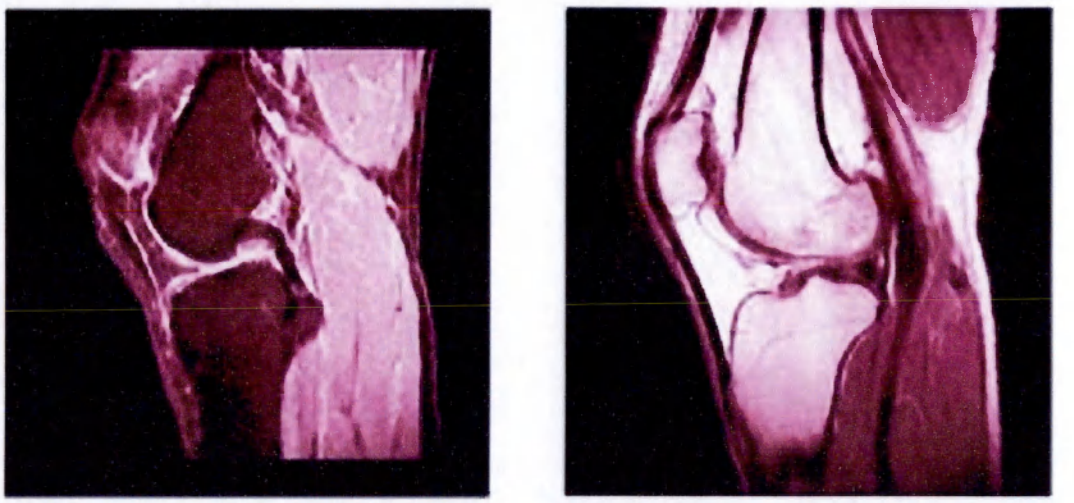

Figure 1.2.1: Comparison of MRI images of the human knee: normal contrast (left); with T_1 contrast agent (right).[13, 14]

The gadolinium(III) ion is the core of the great majority of T_1 contrast agents owing to its paramagnetic properties, which arise from the seven unpaired electrons of the gadolinium. Electrons, like atomic nuclei, have spin and magnetic moments. The magnetic moment of an electron is 100 times greater than that of a nucleus. However, owing to the alignment of electrons in the orbital shells with electrons of an

alternate spin, the magnetic moment has a net sum of zero in molecules and diamagnetic ions. The magnetic moment in a magnetic field is seen when an electron is unpaired in ions such as Gd^{3+} and Mn^{2+}, with 7 and 5 unpaired electrons, respectively; or in molecules such as organic free radicals with 1 unpaired electron, and diatomic oxygen.

In the case of paramagnetic contrast agents the tumbling of the Gd^{3+} ion in solution develops an alternating magnetic field, which interacts with the smaller magnetic moments of the protons of the surrounding water molecules. These dipolar magnetic interactions have natural random fluctuations that reduce both the longitudal (T_1) and the transverse (T_2) relaxation times for the protons by increasing the rate of dephasing.[7, 11]

The observed solvent relaxation rate $(1/T_i)_{obs}$ is the combination of the paramagnetic $(1/T_i)_p$ and diamagnetic $(1/T_i)_d$ relaxation rates (where i = 1 or 2), as shown in *Equation 1.2.1*

$$(1/T_i)_{obs} = (1/T_i)_d + (1/T_i)_p \qquad \textbf{\textit{Equation 1.2.1}}$$

The relaxivity (r_i) is defined as the gradient of the concentration-dependent term of *Equation 1.2.2*, and is commonly expressed in $mM^{-1}s^{-1}$.

$$(1/T_i)_{obs} = (1/T_i)_d + r_i[Gd] \qquad \textbf{\textit{Equation 1.2.2}}$$

1.3: Solomon–Bloembergen–Morgan equation

Paramagnetic relaxation can be divided into three types, based on the way in which the water coordinates to the Gd complex. These are the inner-sphere type, where the water complexes directly with the gadolinium; and the second sphere, where the water interacts with the surface of the gadolinium complex. It is as a result of the outer-sphere relaxation effect that compounds with a water coordination number of zero are able to have a relaxation effect on water.[15] (Figure 1.3.1).

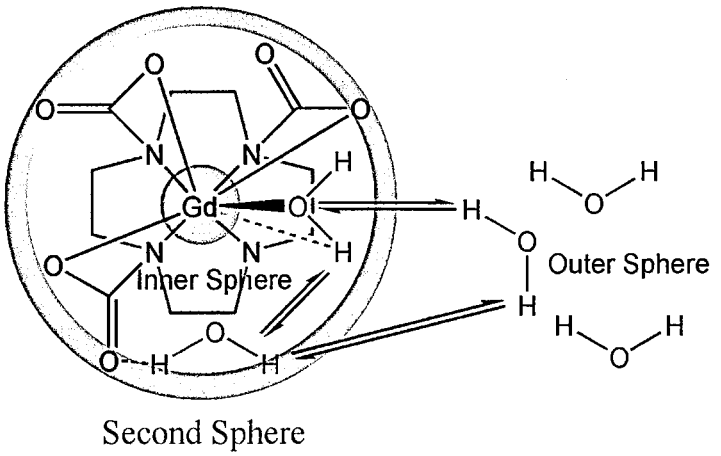

Figure 1.3.1: Diagram showing the inner, second and outer water coordination spheres of DO3A-Gd

The inner sphere is where the solvent is directly coordinated with the Gd(III) ion. The outer sphere includes the water molecules adjacent to the complex next to the bulk water. The Solomon–Bloembergen–Morgan equations are used to calculate the relaxation rates for the inner sphere. The lifetime and the relaxation rate of the solvent molecules in the inner sphere ($_{IS}$) can be expressed by Equations 1.3.1 to 1.3.3:

$$\frac{1}{T_1^{IS}} = \frac{qP_m}{T_{1m} + \tau_m}$$ ***Equation 1.3.1***

$$\frac{1}{T_1^{IS}} = qP_m \frac{1}{\tau_m}\left[\frac{T_{1m}^{-1}\left(\tau_m^{-1} + T_{2m}^{-1}\right) + \Delta\omega_m^2}{\left(\tau_m^{-1} + T_{2m}^{-1}\right)^2 + \Delta\omega_m^2}\right]$$ ***Equation 1.3.2***

$$\Delta\omega_{obs}^{IS} = qP_m\left[\frac{\Delta\omega_m}{\left(1 + \tau_m T_{2m}^{-1}\right)^2 + \tau_m^2\Delta\omega_m^2}\right]$$ ***Equation 1.3.3***

Where P_m is the mole fraction of the bound water nuclei; q is the water coordination number of the gadolinium ions; τ_m is the lifetime of the water molecule within the complex (this is the reciprocal of the water exchange rate, K_{ex}); and $\Delta\omega$ refers to the difference in the chemical shift between the paramagnetic and diamagnetic reference. The subscript (m) refers to the relaxation rate of the water molecule in the inner sphere.[16]

If the water exchange rate is fast the main factor influencing relaxation in the inner sphere is the q value. While if the water exchange rate is slow, i.e. $\tau_{1m} << \tau_m$ then the exchange rate itself becomes the main factor influencing the relaxation rate in the inner sphere.

For the majority of current monomeric Gd(III) complexes the inner and outer sphere mechanisms contribute approximately equal amounts to the observed relaxivity. However it is easier to affect the inner sphere relaxivity than the relaxivity induced by

the outer sphere. The contribution of the outer and second spheres can be increased by Increasing the number of hydrogen bonding sites on the complex by using non coordinating groups such as carboxylic acids, esters and amines. These can affect the relaxivity by ordering the second sphere of water molecules around the surface of the complex, allowing them to be relaxed and facilitate the interchange between the inner and the outer sphere. The eq 1.3.1 shows the how the inner sphere relaxivity may be influenced by the properties of the complex, these are the q value, and the rotational correlation times.

1.4.1: Methods of improving the efficacy of contrast agents

There are several ways in which the contrast-agent efficiency can be improved. Since the number of paramagnetic nuclei available is limited, one of the routes to increasing efficiency is to alter the ligands to improve the inner-sphere water relaxation.[17] This is seen in the inner-sphere relaxivity equation (*Equation 1.4.1*):

$$r_1^{IS} = \frac{q/[H_2O]}{(T_{1m} + \tau_m)} \qquad \textit{Equation 1.4.1.}$$

where T_{1m} is the T_1 of the water hydrogen in the inner-sphere, and $[H_2O]$ is the concentration of water in mMol. To increase relaxivity (r^{IS}_1), the T_{1m} or τ_m would have to be decreased, or q would have to be increased. [15]

1.4.2: Effect of hydration number on a contrast agent

The hydration number plays a major role in the effectiveness of the contrast agent. The vast majority of contrast agents are mono-aqua-based (i.e. q = 1), although there is an increasing number of di-aqua species being reported. The problem with di-aqua species is that they have reduced kinetic and thermodynamic stability with respect to acid- or cation-mediated dissociation.[18] This makes them potentially unsuitable for safe use *in vivo*, although there are some agents – such as DO3A-Gd (**1**) – that are sufficiently stable to be safe *in vivo*. The effect of increasing the q value can be seen between DOTA-Gd (**2**) and DO3A-Gd (**1**). The removal of one of the arms increases the relaxivity by 45%, from 4.2 to 6.0 $r_{1p}{}^{a}/mM^{-1}\ s^{-1}$.[19] (Figure 1.4.2.1).

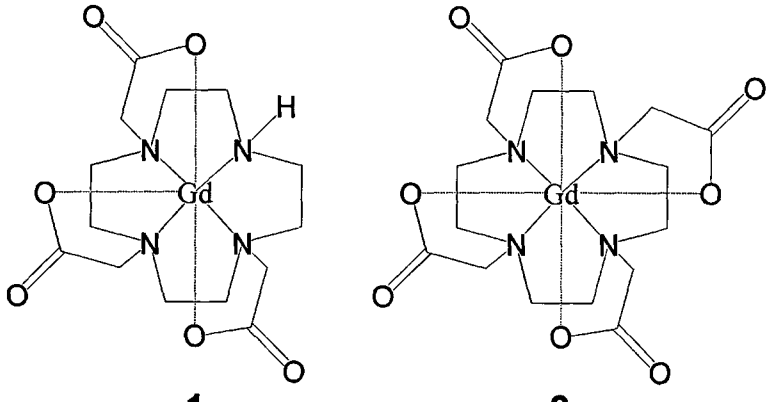

Figure 1.4.2.1: Structures of DO3A-Gd (1) and DOTA-Gd (2)

1.4.3: Effect of the rotational correlation time on a contrast agent

Rotational correlation time (τ_{ci}) is controlled by three factors, which are molecular rotation, electronic relaxation and chemical exchange rate of water molecules. Studies have shown that the dominant factor is the molecular rotation time (τ_R).[15]

$$\frac{1}{\tau_{ci}} = \frac{1}{\tau_m} + \frac{1}{\tau_R} + \frac{1}{\tau_{ie}}; i = 1,2$$

Equation 1.4.3.1

The molecular rotation time is influenced by the molecular weight. For a small-molecule contrast agent such as DOTA-Gd (**2**), the rotational correlation time is of the order of 0.1 ns, giving a relaxivity of 4.2 $mM^{-1}S^{-1}$ [19], while RIME-type agents (Receptor Induced Magnetic Enhancement – where a contrast agent attaches to a protein or large biomolecule) have a time of 10.0 ns. Intermediate high molecular weight compounds such as P792 (**3**) have a rotational time of $\tau_R \approx 2$ ns, with a relaxivity of 25.5 $mM^{-1}S^{-1}$ [20] (Figure 1.4.3.2). RIME agents are discussed in detail later in section 1.6.5, dealing with types of contrast agent.

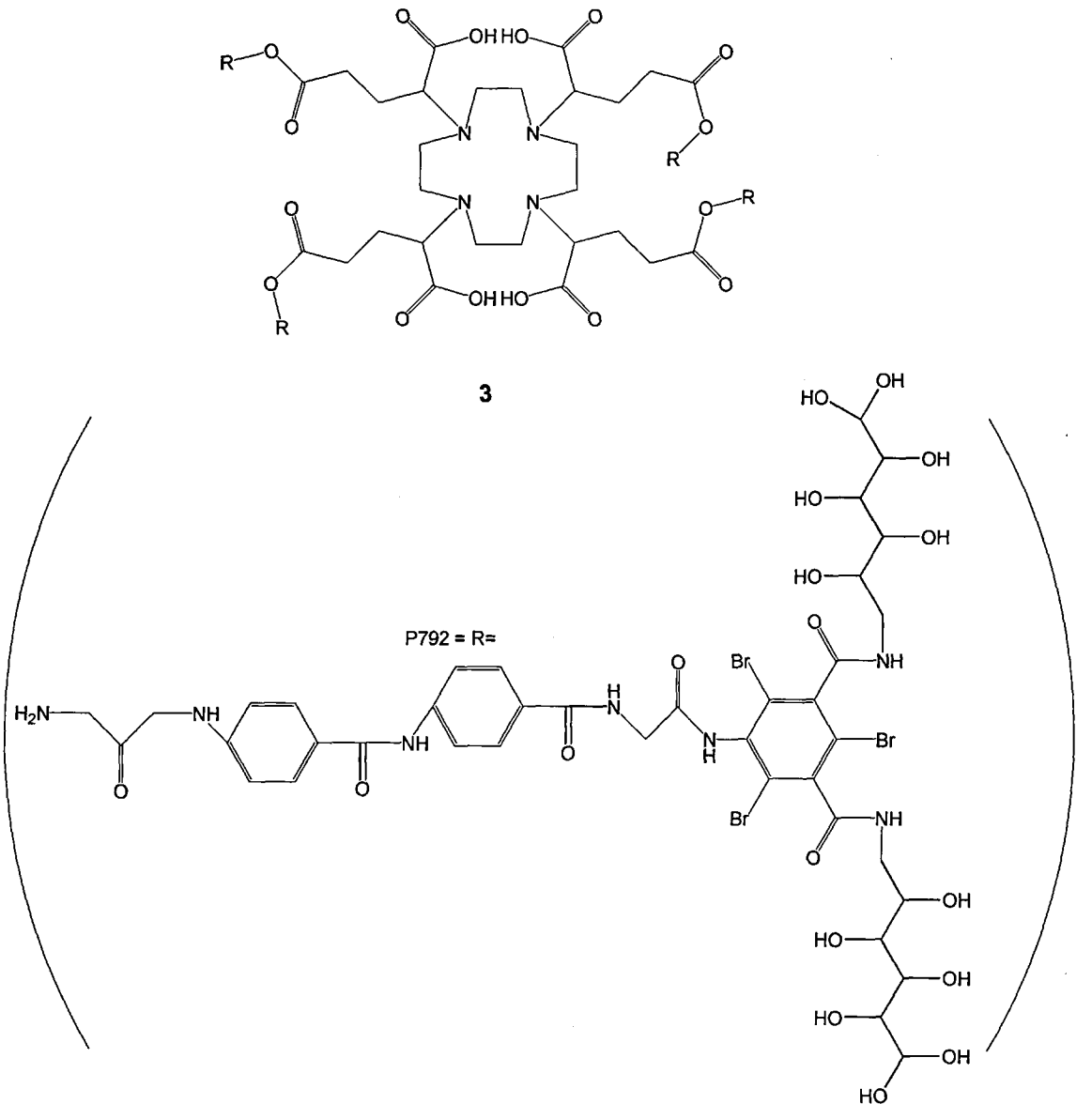

Figure 1.4.3.2: Structure of P792 (3)

There are several ways of increasing the rotational times of the molecule through increasing its size by making it a part of a linear oligomer; using a branched molecule, where the lanthanide groups are on the terminal ends of the chains radiating from the central core; or creating a barycentre, where the lanthanide group is placed centrally within the molecule (Figure 1.4.3.3).

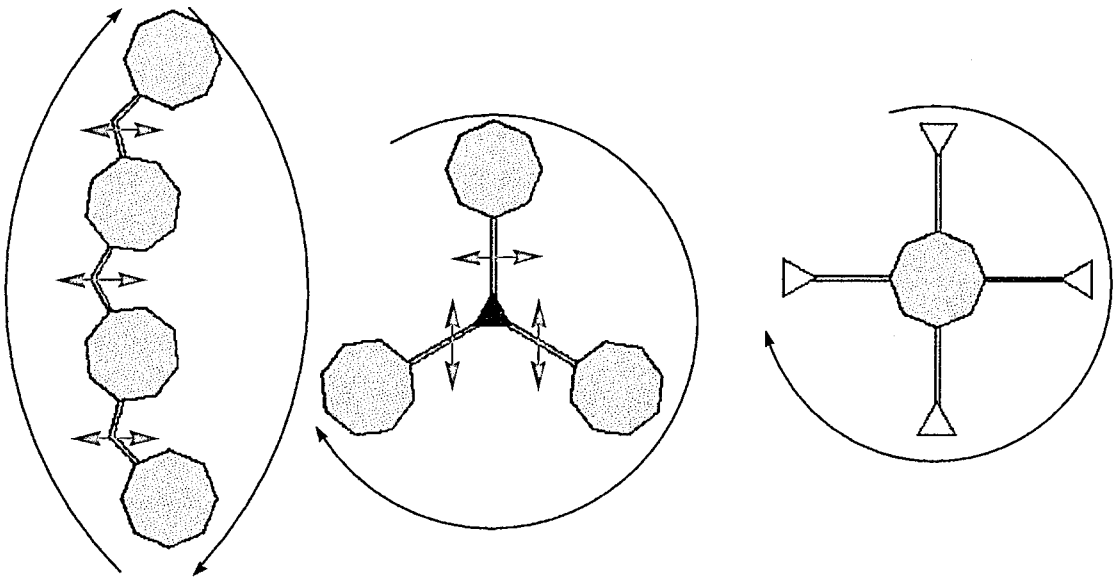

Figure 1.4.3.3: Different methods of increasing the rotational correlation times: (a) linear oligomer; (b) branched; (c) barycentre.[15] Key: Red corresponds to Gd^{3+} complex; yellow corresponds to stable groups to add mass; dark blue corresponds to a stable central core. The black arrows show the movement of the molecule, and the purple arrows show the movement of the Gd-ligand group within the molecule.

A linear oligomer may be formed by linking several contrast-agent groups together to form a linear chain. This is seen in contrast agents such as NMS60-Gd (**4**) [21] (Figure 1.4.3.4). The problem with linear oligomers is that they will undergo anisotropic rotation around the linking arms, where the linked Gd-complexes move directionally and are independent of each other as the molecule rotates. This in effect limits the advantages gained by the formation of the linear oligomer.

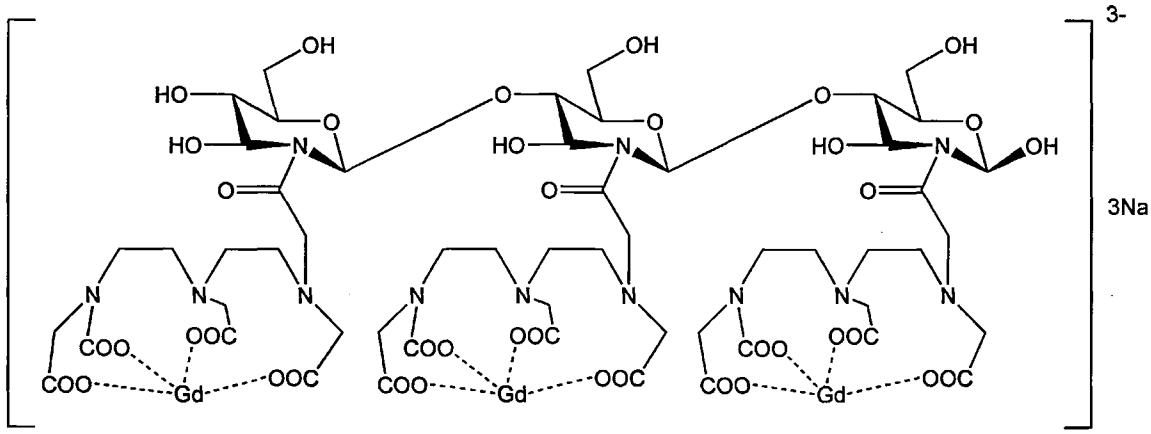

4

Figure 1.4.3.4: Structure of NMS60-Gd (4)

The second approach is the formation of a branched polymer- or dendrimer-based contrast agent. This is where the Gd-complexes are attached by organic chains to a central core. The size of the dendrimer will have an impact on the rotational dynamics, as larger molecules rotate at a slower speed and so have higher rotational correlation times than those of smaller molecules with lower rotational correlation times. The amount of branching in the dendrimer is denoted by the generation number. For example, PAMAM-Gd-1BAM-DPTA (**5**) [22] is a fourth-generation dendrimer which is denoted as G4 (Figure 1.4.3.5). The PAMAM (polyamidoamine) core has attached 50 Gd-1BAM-DPTA functional groups. The relaxivity of this dendrimer is 12.2 $r_{1p}/mM^{-1}\ s^{-1}$, which is three times greater than that of DOTA-Gd (**3**) at 4.2 $r_{1p}/mM^{-1}\ s^{-1}$ [19, 22], while the relaxivity per Gd^{3+} is 0.244 $r_{1p}/mM^{-1}\ s^{-1}$. The compound's half-life within the body before being excreted ($t_{1/2}$) is 87 minutes, compared to DOTA-Gd (**2**) at 36 minutes, which allows for more scans for the same dosage of contrast agent.[23]

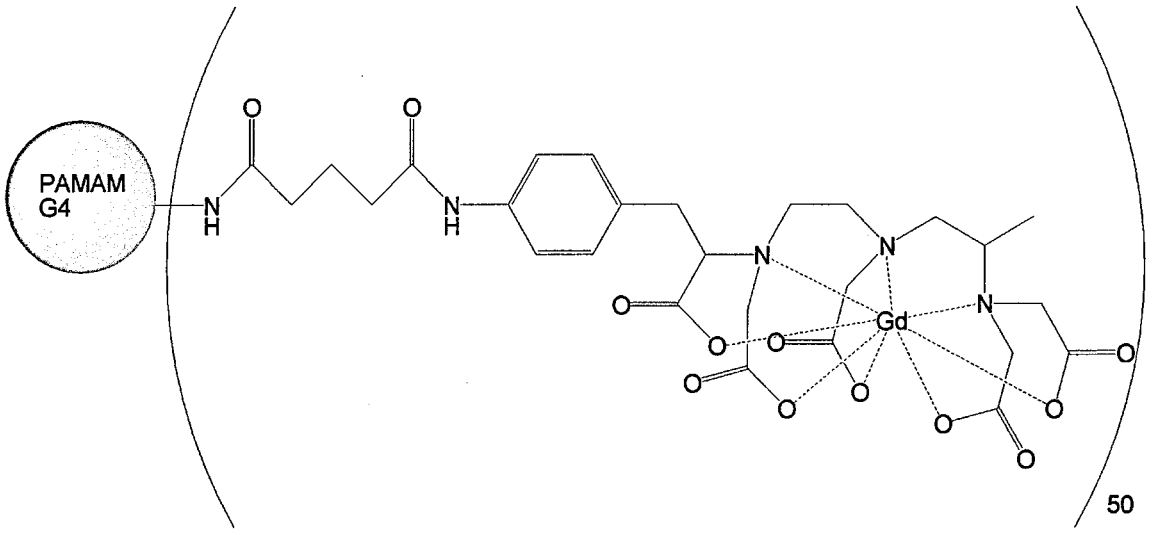

5

Figure 1.4.3.5: Example of a branched, fourth-generation dendrimer MRI contrast agent, where PAMAM G4 is functionalised with Gd-1BAM-DPTA.[22]

The effect of increasing the mass, and thus increasing the rotational correlation time, can be seen in the linear relationship between relaxivity per Gd(III) and molecular weight[16], as shown in Graph 1.4.3.1.

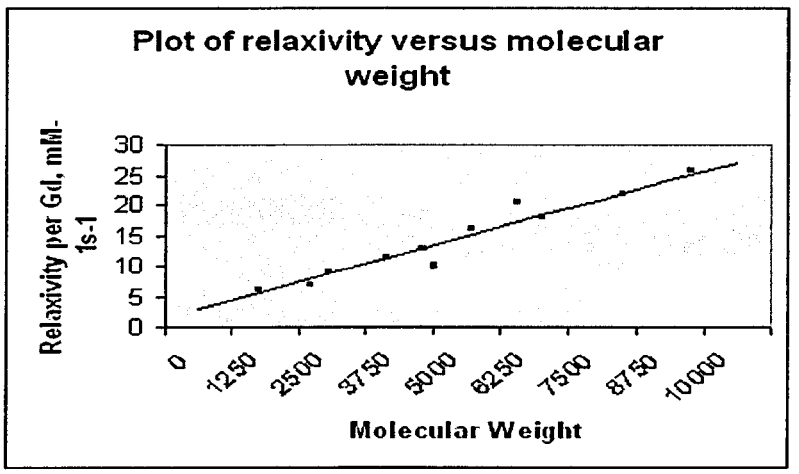

Graph 1.4.3.1: Plot of the relaxivity per gadolinium versus molecular weight of contrast agent (20 MHz).[18]

An example of a dendrimer-type contrast agent is the tetra-gadolinium(III) complex [Gd_4dmpDO3A_4] (**6**), which is based on 4 DO3A-Gd (**1**) groups attached to a dimethylpropane framework. The complex has a relaxivity of 28.13 $mM^{-1}s^{-1}$ (24 MHz, 35 °C, pH 5.6) [24], which is 4.7 times the value for GdDO3A of 6.0 $mM^{-1}s^{-1}$ (20 MHz, 20 °C).[25]. This is caused by a combination of the increasing rotational correlation time and the increase in the concentration of the gadolinium(III). It should be noted that the complex shows a relaxivity of 28.13 $mM^{-1}s^{-1}$, giving a relaxation per Gd(III) of 7.03 $mM^{-1}s^{-1}$, which is an increase of 16% [24] (Figure 1.4.3.6).

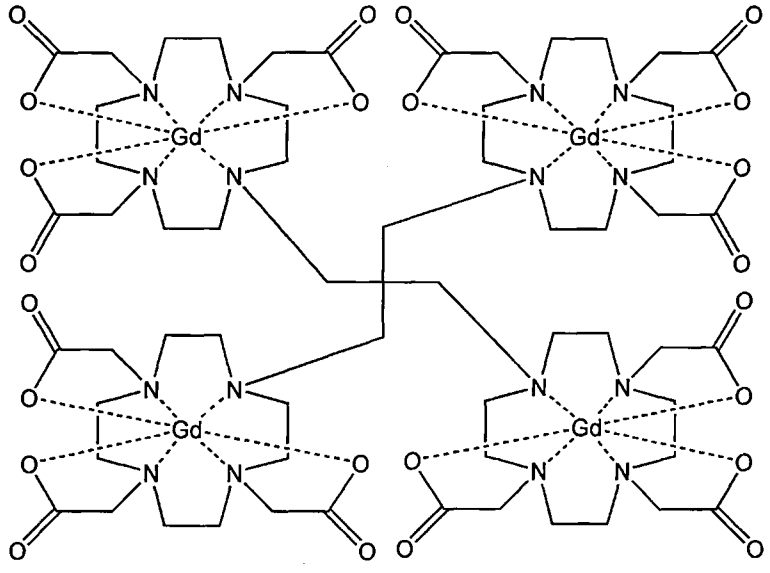

6

Figure 1.4.3.6: Structure of [Gd4dmpDO3A$_4$] (6)

The third method is to simply increase the mass of a single complex molecule, which may be achieved in two ways. The first possibility is the attachment of polymeric arms, such as PEG (poly(ethylene glycol)); this increases the mass of the molecule up to 5 KDa [26] by forming a barycentre-type contrast agent. An alternative method of increasing the mass is through the binding of the contrast agent to a biological protein *in vitro*, as in the case of RIME agents.

The drawback to barycentre-type molecules is that if the rotational time of the molecule becomes too low, then the relaxivity of the molecule will drop owing to water exchange inefficiencies in the water diffusion rate. This is due to the relaxed water molecule being released from the contrast agent and then becoming re-coordinated to the agent, reducing the number of molecules which can be relaxed in a given time frame.[15]

1.4.4: Effect of water exchange rate between lanthanides and the surrounding bulk water

The water exchange rate is an important factor in the ability of a contrast agent to induce relaxivity. On the one hand, if the water exchange rate is too slow the relaxation effect is not transmitted effectively to the bulk water; on the other hand, if the water exchange rate is too fast the water coordinates to the Gd^{3+} ion, but does not dwell long enough to be relaxed.

The rotational diffusion rate also has an effect on the size of the window of the optimum time for water exchange, producing a relaxivity with 20% of the maximum. For a compound with τ_R = 0.1 ns, then the optimum window is between 1 and 1000 ns, while if τ_R = 1 ns then the window is reduced to between 3 and 200 ns. If the τ_R is increased to 10 ns, then the window is even smaller, at 2–30ns.[15] This increase in the coordination lifetime effectively reduces the relaxation of the agent to a few per cent of the theoretical limit, because of long water-coordination lifetimes.[27]

The rate of water exchange is also affected by the structure of the contrast agent. A small change in the structure can make a marked difference to the lifetime of the

coordinated water molecule.[28] An example can be seen in $[GdaDOTA]^{3-}$ (**7**) and $[GdgDOTA]^{3-}$ (**8**), where an increase of one carbon in a chain can change the water exchange lifetime (T_m/ns) from 68 ns to 200 ns. This limits the relaxivity of the complex, as the longer the lifetime of the water exchange rate, the lower will be the relaxivity[29] (Figure 1.4.4.1). The water exchange rate is also influenced by the isomeric structure of the Gd^{3+} complex. For example, the three isomeric forms for $[GdgDOTA]^{3-}$ are (RRRR), (RRRS) and (RSRS), which have corresponding water exchange rates of 68, 140 and 270 ns at 298K.[30] This shows that the twisted square–antiprismatic isomer increases the time in which the water is bound, thus reducing the water exchange rate. The effect of this changing of the water exchange rate can be seen in the relaxivity values, which are approximately 7.7, 7.6 and 6.8 $mM^{-1}s^{-1}$ respectively at 20 MHz, 25 °C.[30]

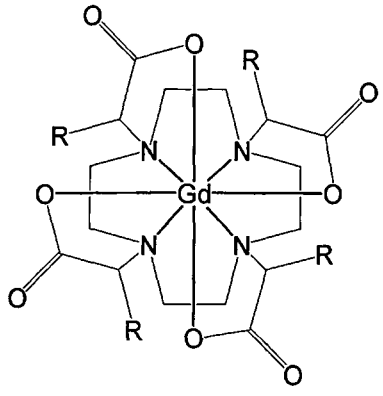

R = $(CH_2)_2CO_2^-$ = $[GdaDOTA]^{3-}$ (**7**)
R = $(CH_2)_3CO_2^-$ = $[GdgDOTA]^{3-}$ (**8**)

Figure 1.4.4.1: Structures of $[GdaDOTA]^{3-}$ and $[GdgDOTA]^{3-}$

1.5: Why is cyclen used in contrast agents?

Cyclen (**9**) (Figure 1.5.1), when substituted with suitable pendant arms, such as acetic acid in the case of DOTA (**13**), will readily form stable complexes with lanthanides such as gadolinium to give DOTA-Gd (**2**). Cyclen-based compounds will also complex with a wide range of different metals, such as Eu(III), Cu(II), Ni(II), Co(II),[31] Cd(II), Pb(II) and Rh(II).[32, 33] The stability of the cyclen/cation complex is due to the stabilisation afforded to the complex by the macrocycle effect, which forms complexes with high thermodynamic stability and kinetic inertness. Also, they are able to satisfy 7 of the 9 coordination sites required by the lanthanide metal ions.[34, 35]

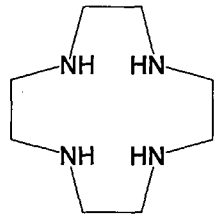

9

Figure 1.5.1: Structure of cyclen (9)

In the cyclen-based molecules, four of the coordination sites on the lanthanide are filled with the lone pairs of the nitrogens of the cyclen ring (**10**), with three more sites occupied by the lone pairs of the carbonyl oxygen of the esters (**11**), or directly via the oxygen anion of the acid groups (**12**) (Figure 1.5.2). This chemical flexibility makes the cyclen an ideal substructure for contrast agents.

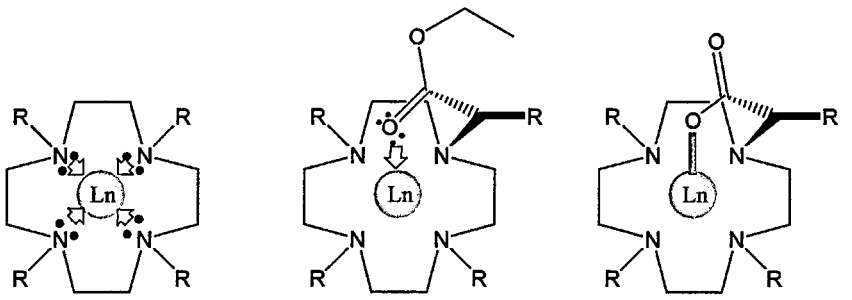

Figure 1.5.2: The coordination of the lanthanide within the complexes

A key requirement of any pharmaceutical metal complex is the formation of stable chelates. This prevents the toxic effect that the free metal ions may have upon the body. The gadolinium may replace metals within the body, especially the metals present in metallo-proteins and enzymes, and that could alter the biochemical systems. Also, the toxicity can be affected by the pharmacokinetic properties of the agent, since the longer the duration in the body, the greater will be the risk of a toxic effect occurring.

1.6.0: Classification of MRI contrast agent

Contrast agents can be grouped into loosely bound classes according to their properties, structural make-up and mode of use, and a particular agent can belong to more than one group.

1.6.1: Extracellular fluid agents

DOTAREM^{TM} (DOTA-Gd) (**2**) is the most commonly used extracellular agent[36], owing to its strong contrast effect and relatively low cost. GdDOTA-4AmP^{-5} (**14**) is a DOTA (**13**) -based extracellular agent that allows the non-invasive measurement of

pH within the body of the subject.[37] The change in pH is seen in the increase of relaxation, which is governed by the phosphonate group that catalyses the proton exchange in the bulk water. For example, at pH 2–4 the enhancement is 25%, whereas at pH 6–9 the enhancement effect is increased to 84%.[38]

The ability to detect differences in the pH gradient of tissues helps in the detection of certain cancers, as the cancer cells are slightly more acidic compared to normal tissue, with a difference of 0.1–0.2 in pH. The variation is caused by differences in metabolic pathways in the tissue types. The pH difference induces a gradient change in the extracellar environment, which can be signalled by the contrast agent[39] (Figure 1.6.1.1).

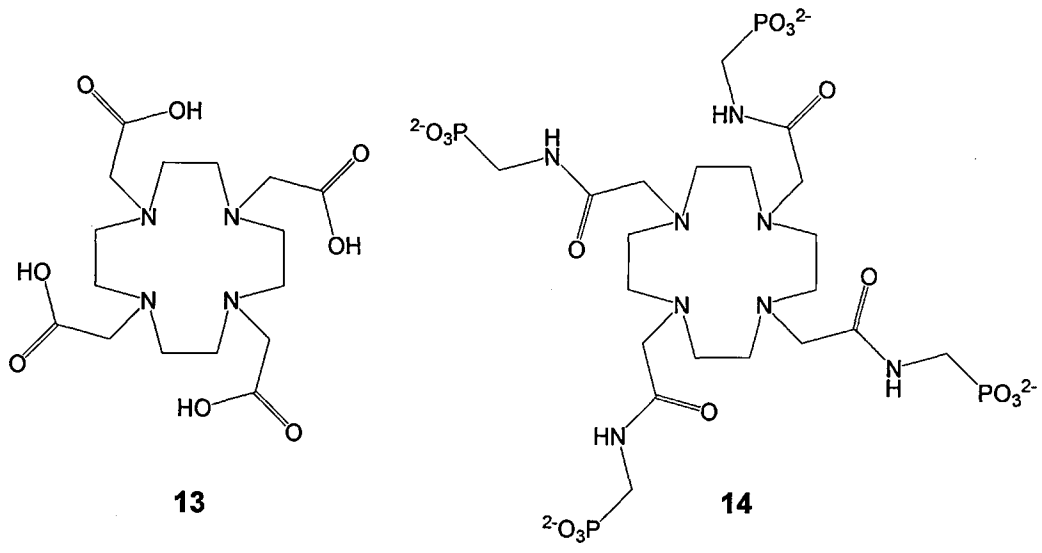

Figure 1.6.1.1: Structures of some extracellular contrast agents: (13) DOTA; (14) GdDOTA-4AmP-5

1.6.2: Blood-pool contrast agents

Blood-pool agents enhance the vascular structures of the subject, so are therefore used as an alternative to X-ray angiography. For example, abnormal angiogenesis can be seen in developing tumours.[16] The efficiency of the blood-pool agents depends upon the time the agents spend in circulation, their tendency not to redistribute in the interstitial space, and the resistance to glomerular filtration in the kidney. Best results are achieved by the use of high-molecular-weight MRI contrast agents. DOTA-$(BOM)_3$ (**15**) is a DOTA (**13**) derivative with benzyloxymethyl (BOM) groups. The BOM groups are hydrophobic, which helps them to bind to HSA (Human Serum Albumin). This substance is used as an angiographic MRI contrast agent, with a relaxivity of 53.2 $mM^{-1}s^{-1}$ [36] (Figure 1.6.2.1).

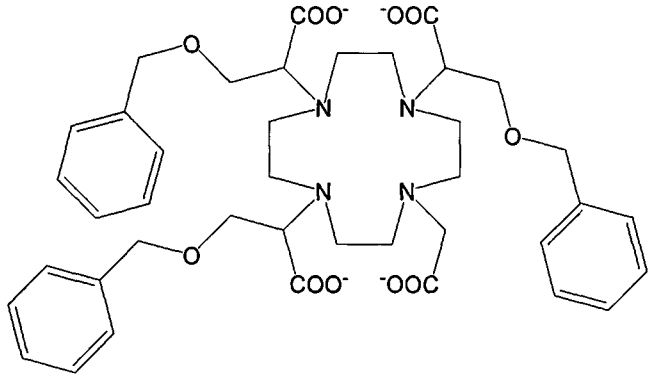

15

Figure 1.6.2.1: Structure of DOTA-$(BOM)_3$ (15)

Not all blood-pool agents need to bind to proteins; an example is blood-pool agent P760 (**16**), with relaxivity of 24.7 $mM^{-1}s^{-1}$ (60 MHz, 310K).[40] This large relaxivity is due to the size of the complex conferring a slow rotational time[20] (Figure 1.6.2.2).

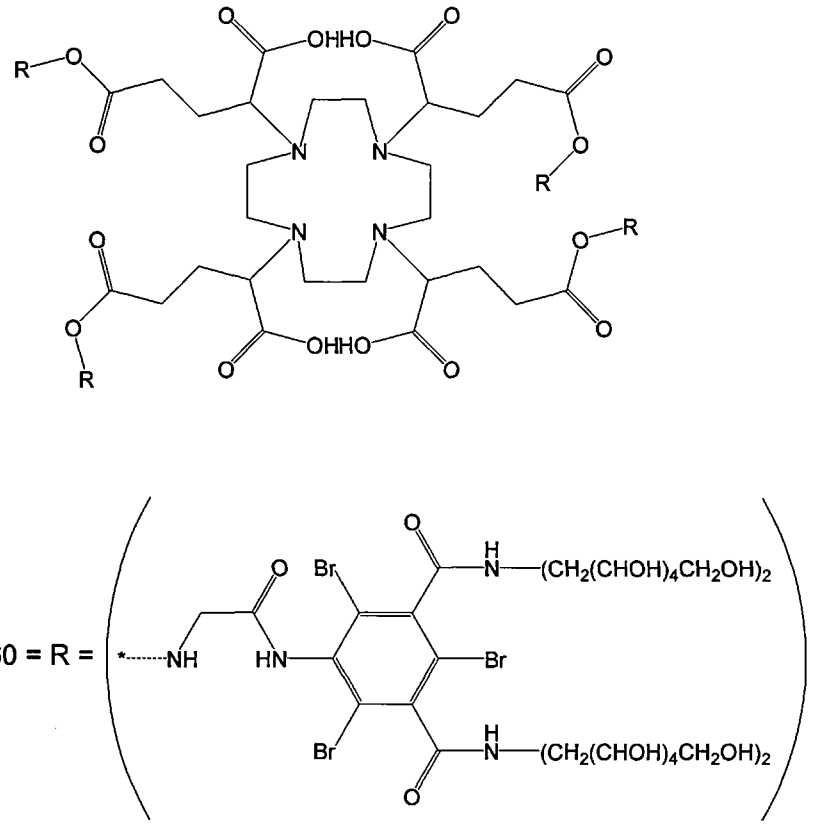

16

Figure 1.6.2.2: Structure of P760 (16) [20, 40]

1.6.3: Particulate / polymeric-based contrast agents

Particulate and polymeric contrast agents are macromolecular contrast agents, and are a subset of blood-pool agents. Owing to their large size these contrast agents increase the blood retention times by avoiding glomerular filtration, while also affecting the rotational correlation times of the molecule.[41] However, particulate agents such as ultra-small superparamagnetic iron oxides (USPIOS) decrease rapidly in the bloodstream owing to reticulo-endothelial affinity, and they may also be phagocytosed by macrophages in the liver, spleen and bone marrow – although dextran coatings help to reduce this effect.[41] Several particulate contrast agents have been found to be effective in human trials: examples are particulate contrast

agents such as gadolinium(III)-loaded zeolite clays, like Gadolite™, and more recently nanoparticles consisting of gadolinium(III) bound with methacrylic acid–ethyl acrylate copolymer encapsulated within a polymeric shell,[42, 43] which allows the sequestration of the gadolinium ion while still enabling water exchange. Other polymeric contrast agents have been developed using gadolinium chelating agents coupled with high-molecular-weight biological proteins such as HAS,[44] or polymers such as polyaminoacids (polylysine) or oligosaccharides (dextrans or dendrimers).[45] There have been several polymeric contrast agents that have a high gadolinium content; for example, polylysine-GdDTPA[46] has up to 70 gadolinium(III) ions per molecule. The addition of biocompatible polymers such as PEG or MPEG to the contrast agent provides protection from interaction with blood cells and plasma proteins, as well as increasing the molecular mass of the agent.

1.6.4: Liposomal-based contrast agents

Liposomal agents are based on a spherical vessel made from lipid compounds, which possess both hydrophilic and hydrophobic properties. The lipids then combine to form a membrane with the hydrophilic groups on one side and the hydrophobic ones on the other side. These vessels have high biocompatibility[47] (Figure 1.6.4.1).

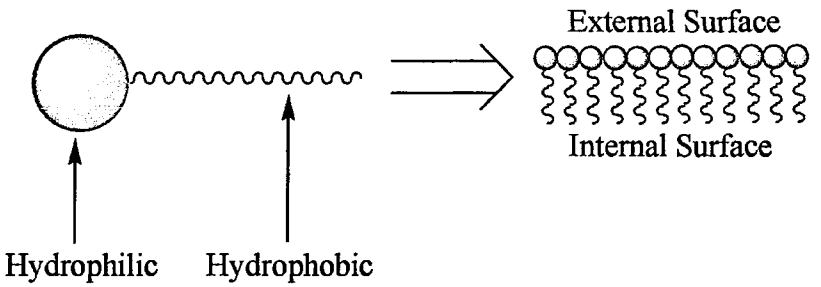

Figure 1.6.4.1: Structure of a lipid membrane

There are two main types of liposomal contrast agent. In the first, the liposome incorporates the metal ion – for example iron, manganese or gadolinium – within the centre of the lipid membrane structure[48] (Figure 1.6.4.2).

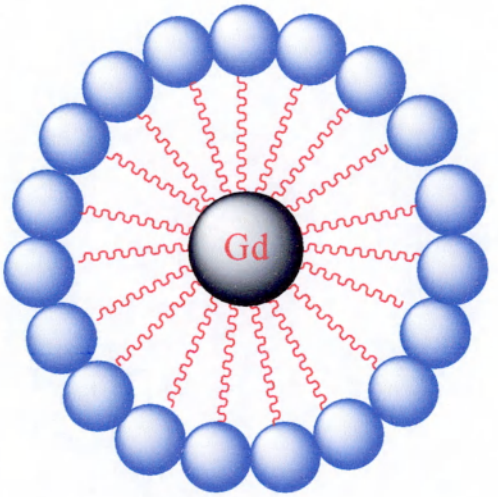

Figure 1.6.4.2: Liposomal contrast agent with gadolinium at the centre

In the second type the gadolinium is complexed with a ligand, to which is attached a long hydrophobic chain. These types of liposomal agent can mimic the behaviour of the circulating cells in situations where direct labelling of the cells would cause problems, such as in the case of red blood cells, which need high amounts of contrast agent to achieve a good contrast. The main problem with liposomal contrast agents is that the membranes are easily disrupted or taken up by the reticular-endothelial system[49] (Figure 1.6.4.3).

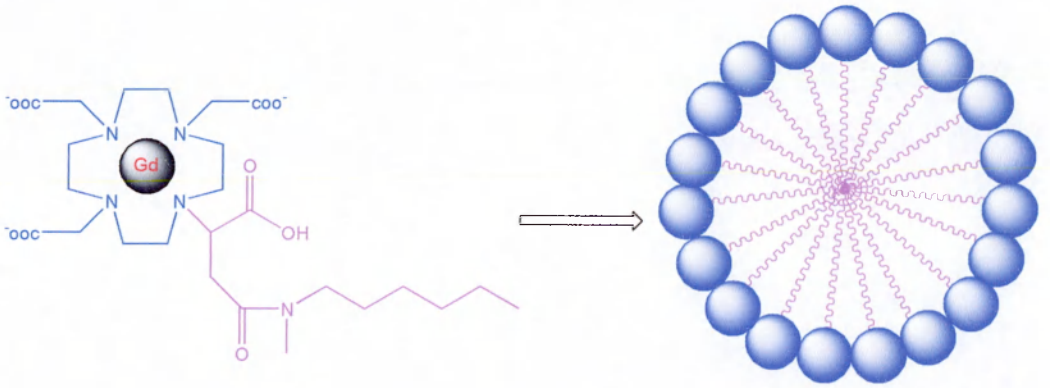

Figure 1.6.4.3: Liposomal contrast agent with gadolinium in the outer sphere

One way around this is the surface modification of the liposomes, for example by PEG grafting, which increases the lifetime of the contrast agent. Polymerisation of the lipid layer can also achieve the same effect. Liposomal agents have a high relaxivity, owing to their high molecular weight and the restricted free rotation of the low-molecular-weight species within the cavity of the vesicle.[16, 50]

1.6.5: Receptor-Induced Magnetic Enhancement (RIME) agents

Receptor-Induced Magnetic Enhancement, or RIME, agents are contrast agents that bind to the targeted biomolecule. For example, EP-2104R is currently in phase 2a clinical trials as a RIME agent for binding to fibrin, for use in the imaging of coronary thrombosis.[51] Another example of a RIME agent is MS-325 (**16**), produced by EPIX pharmaceuticals. MS-325 (**16**) reversibly binds via a non-covalent bond to the blood protein albumin, allowing the imaging of the blood vessels for up to one hour.[52] MS-325 (**17**) binds to the albumin via an aromatic ring set. The increased MRI contrast relaxivity is due to the decrease in rotation speed arising from the presence of aromatic rings that bind to albumin.[46] C_8-DOTP (**18**) was also found to bind to HAS and has been approved for clinical use. C_8-DOTP binds to the albumin in several places via the fatty-acid chain[53] (Figure 1.6.5.1).

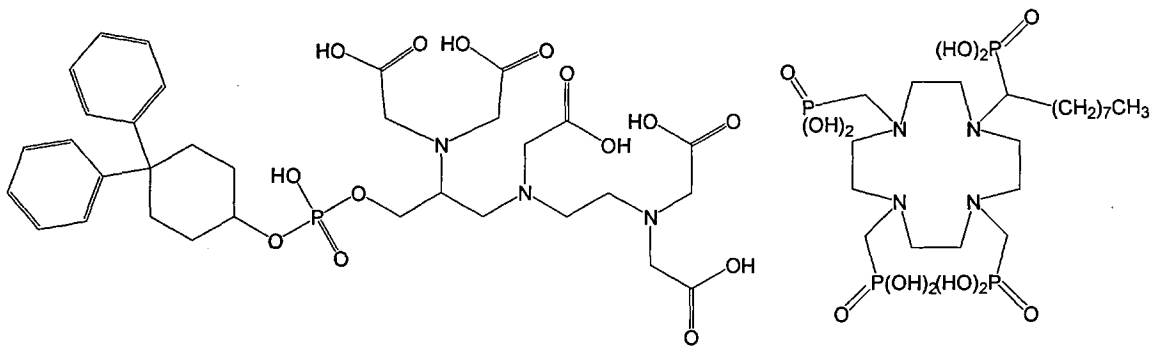

17 18

Figure 1.6.5.1: Structures of (17) MS-325; and (18) C_8-DOTP

1.6.6: Non-clinical research contrast agents

One area of current research into MRI contrast agents is in complexes which have a *q* value of 2. These have two main problems: stability of the complex, and complexation with anions within the environment. While the stability of GdDO3A (**21**) may be slightly lower than that of DOTA-Gd (**3**) – with logK_{eq} M^{-1} values of 21.2 and 25.8 respectively at 25 °C with tetramethylammonium chloride (0.1M)[54] – that is still greater than some compounds used in animal studies, such as DTPA-BMA (**19**) [55], with a logK_{eq} M^{-1} value of 16.84 at 25 °C with tetramethylammonium chloride (0.1M).[18] The stability can be increased by small changes that increase the steric hindrance in the structure and limit arm movement, thus limiting the rate of dissociation; for example, DO3A-BMA (**20**) has a logK_{eq} M^{-1} of 25.3 [18] (Figure 1.6.6.1).

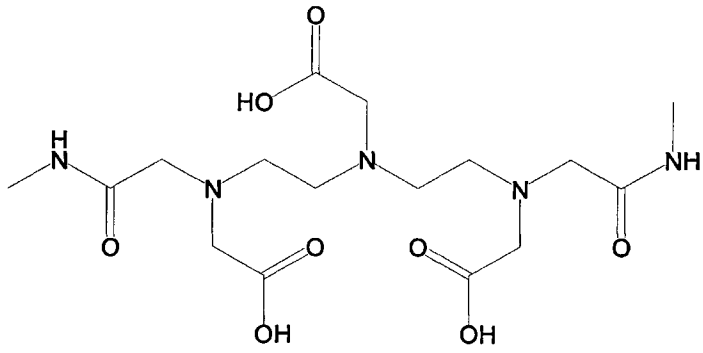

19

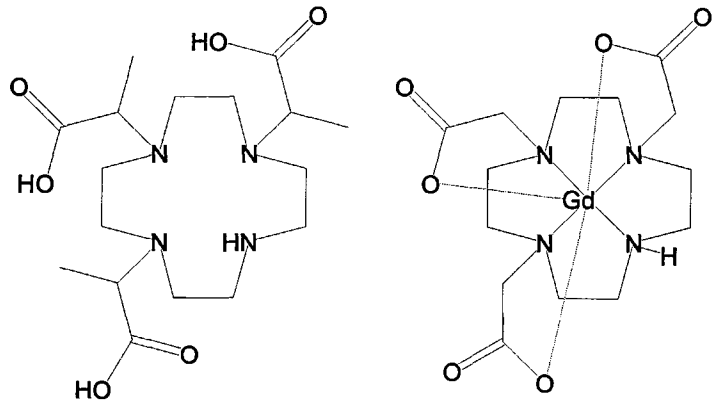

20 21

Figure 1.6.6.1: Structures of DTPA-BMA (19) DO3A-BMA (20) [18] **and Gd-DO3A (21)**[56]

The main problem with compounds with two water binding sites is that the inner-sphere water molecules can be replaced by anions such as phosphate, carbonate, lactate or HAS, which are found within biological environments.[15, 29, 57] This poses a problem, as the anions coordinate to the Gd^{3+}, effectively reducing the *q* value to 1 or 0. This lowering in the *q* value has a direct effect on the relaxation value for the complex; the unwanted complexation of these anions can be limited by the Gd^{3+} complex having a net negative charge. This has been achieved by the use of di-acid pendant arms such as adipic acid (**24**) and glutaric acid (**23**) (Figure 1.6.6.2). These have been used in several different complexes based on DOTA (**13**) and DO3A (**22**).[30, 58, 59]

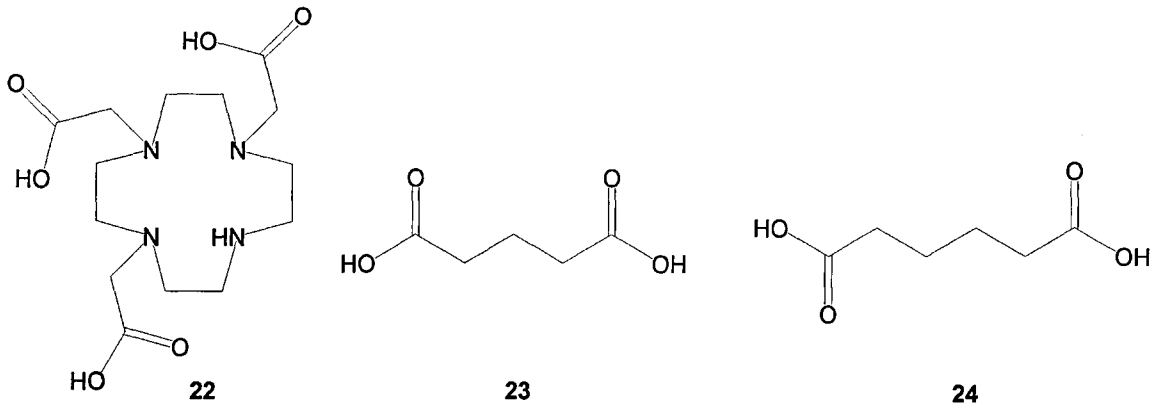

Figure 1.6.6.2: Structures of DO3A (22), glutaric acid (23) and adipic acid (24)

The two compounds of interest based on DO3A (**22**) are gDO3A (**25**) and aDO3A (**26**), with relaxivity values of 12.3 $mM^{-1}s^{-1}$ and 5.4 $mM^{-1}s^{-1}$ respectively. These are higher than that for Gd(DOTA) (**3**) at 4.2 $mM^{-1}S^{-1}$ under the same conditions (20 MHz, 298K, pH 7.2).[19] The change in the relaxivity is due to the increase in the number of coordinated water molecules, and also to the negative charge of the contrast agent, which has the effect of increasing the hydrophilic nature of the molecule. This causes a decrease in the water exchange times, thus improving contrast.[60] This can be seen in the difference between Gd(aDO3A) and Gd(DO3A), which had a relaxation value of 6.0 $mM^{-1}S^{-1}$ [19] (Figure 1.6.6.3).

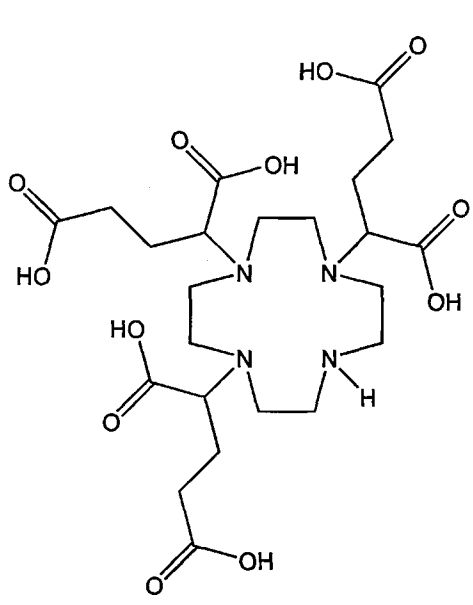

25

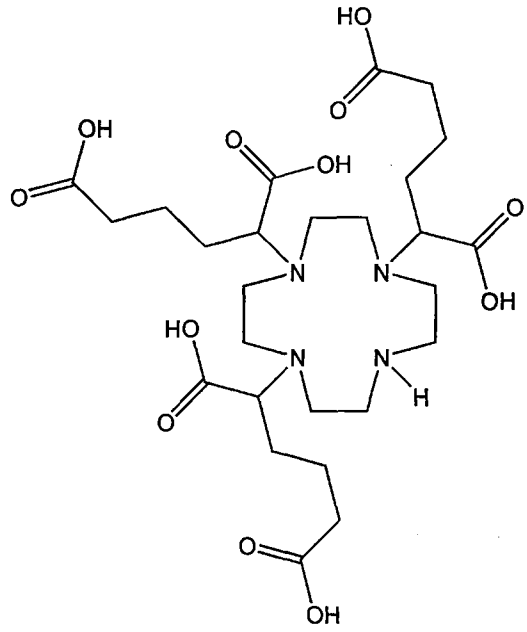

26

Figure 1.6.6.3 Structures of gDO3A (25) and aDO3A (26)

The difference in the relaxivity between the gadolinium complexes of gDO3A (**25**) and aDO3A (**26**) is due to intramolecular binding; the second carboxylic acid on the redundant glutaric acid arm binds with the Ln, reducing the *q* values of the complex. This intramolecular binding occurs at pH > 8 for the case of Eu-gDO3A, which has been shown to displace one of the water binding sites on the Ln. The effect is less apparent with Eu-aDO3A, owing to the increased ring strain of the eight-membered ring as compared to the seven-membered ring (**28**) formed by the cross binding of gDO3A (**25**) [19] (Figure 1.6.6.4).

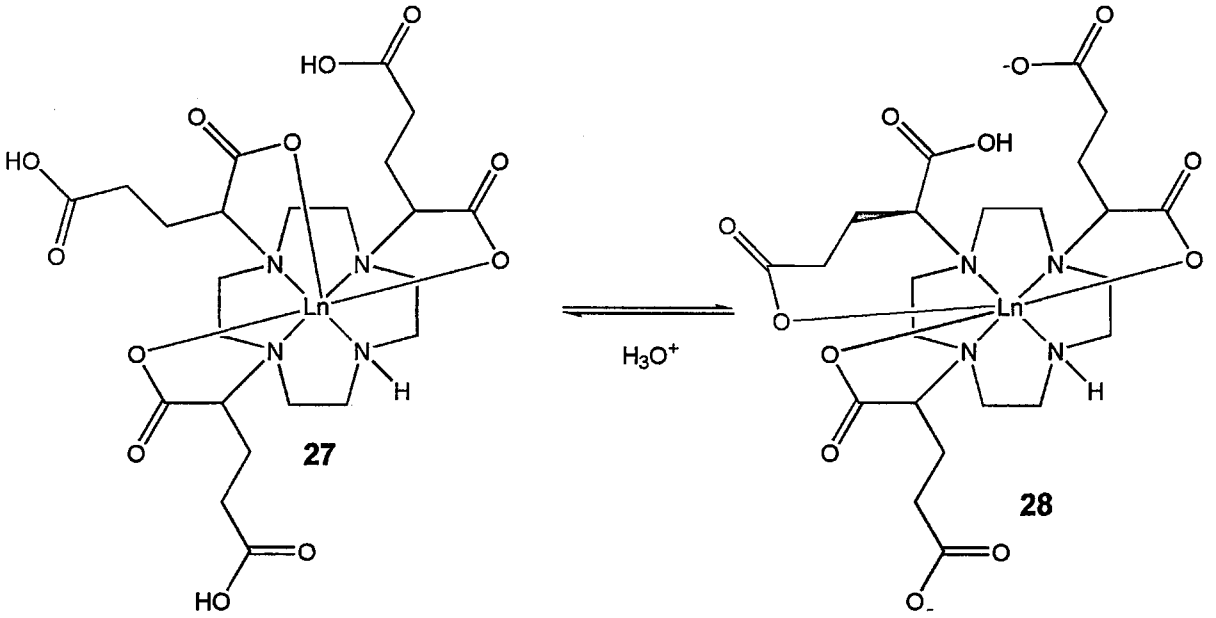

Figure 1.6.6.4: Intramolecular binding of gDO3ALn

1.7.1: Aim of the thesis

A key objective in MRI contrast-agent research is to devise covalently linked or non-covalently bound conjugates that efficiently promote the rate of relaxation of the bulk water proton signal. The target molecule (**29**) consists of a central core consisting of a silsesquioxane cage, (see Section 1.7.2) to which several Gd^{3+} satellite complexes are attached via linker arms. This silsesquioxane cage would impart to the molecule the rigidity needed to reduce the internal movement of the molecule, which would have an effect upon the overall relaxivity (Figure 1.7.1.1). This asymmetrically tetra substituted cyclen would provide eight coordination sites for the Gd(III) to bind, along with an alkene for attachment to the silsesquioxane core.

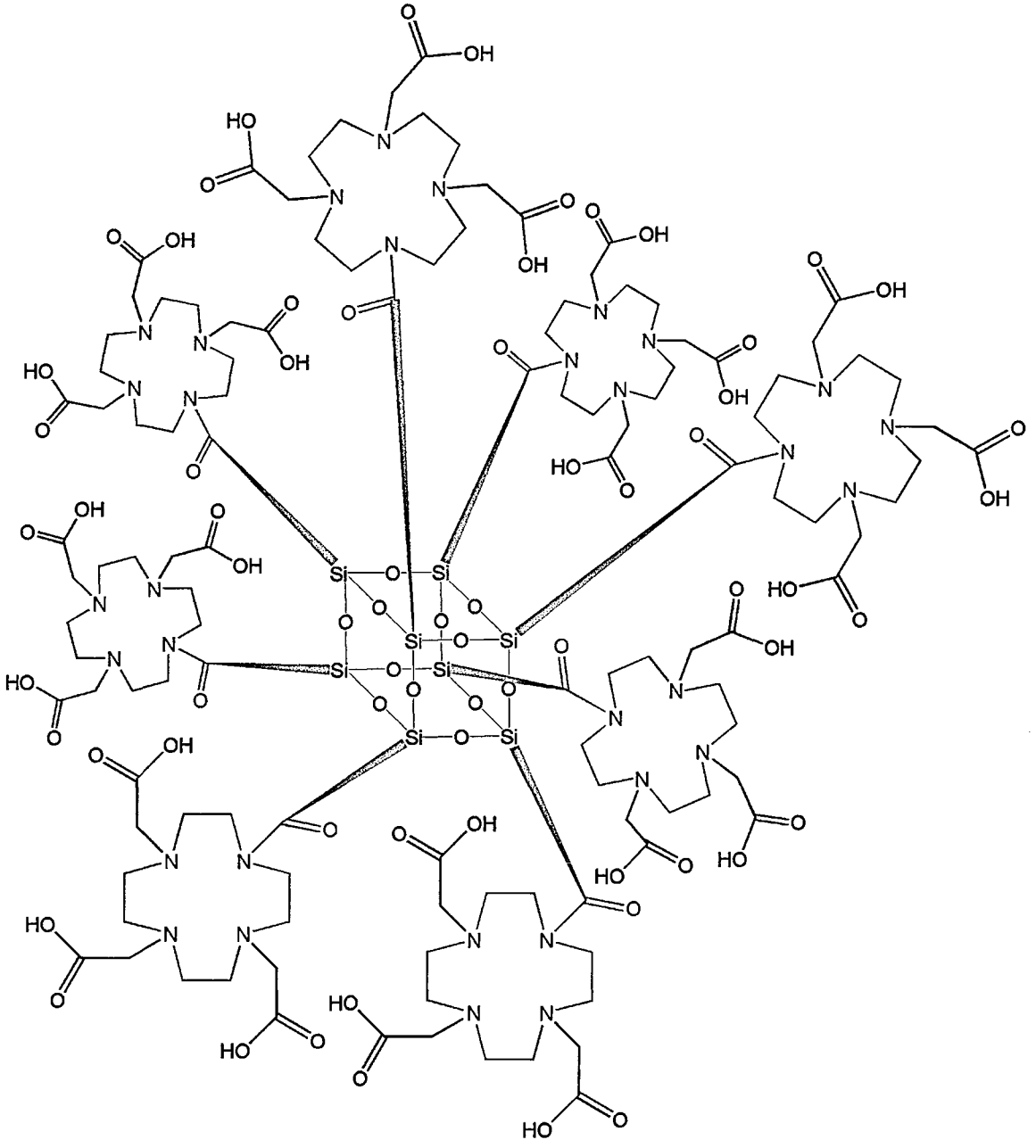

29

Figure 1.7.1.1: The target molecule (29), a dendrimer-based contrast agent with a silsesquioxane core and up to eight Gd-Cyclen tendrils.

The second target molecule (**30**) is based on a di-acid-armed cyclen (Figure 1.7.1.2). Compared to lanthanides, such molecules would have greater stability when complexed than the DO3A (**22**) -based molecules discussed earlier. This added stability would allow for the molecule to have a coordination number of 7, and hence

an hydration number of 2 by replacing the complexing linking arm seen in the first target molecule with a non-complexing linking arm, such as a straight-chain alkene.

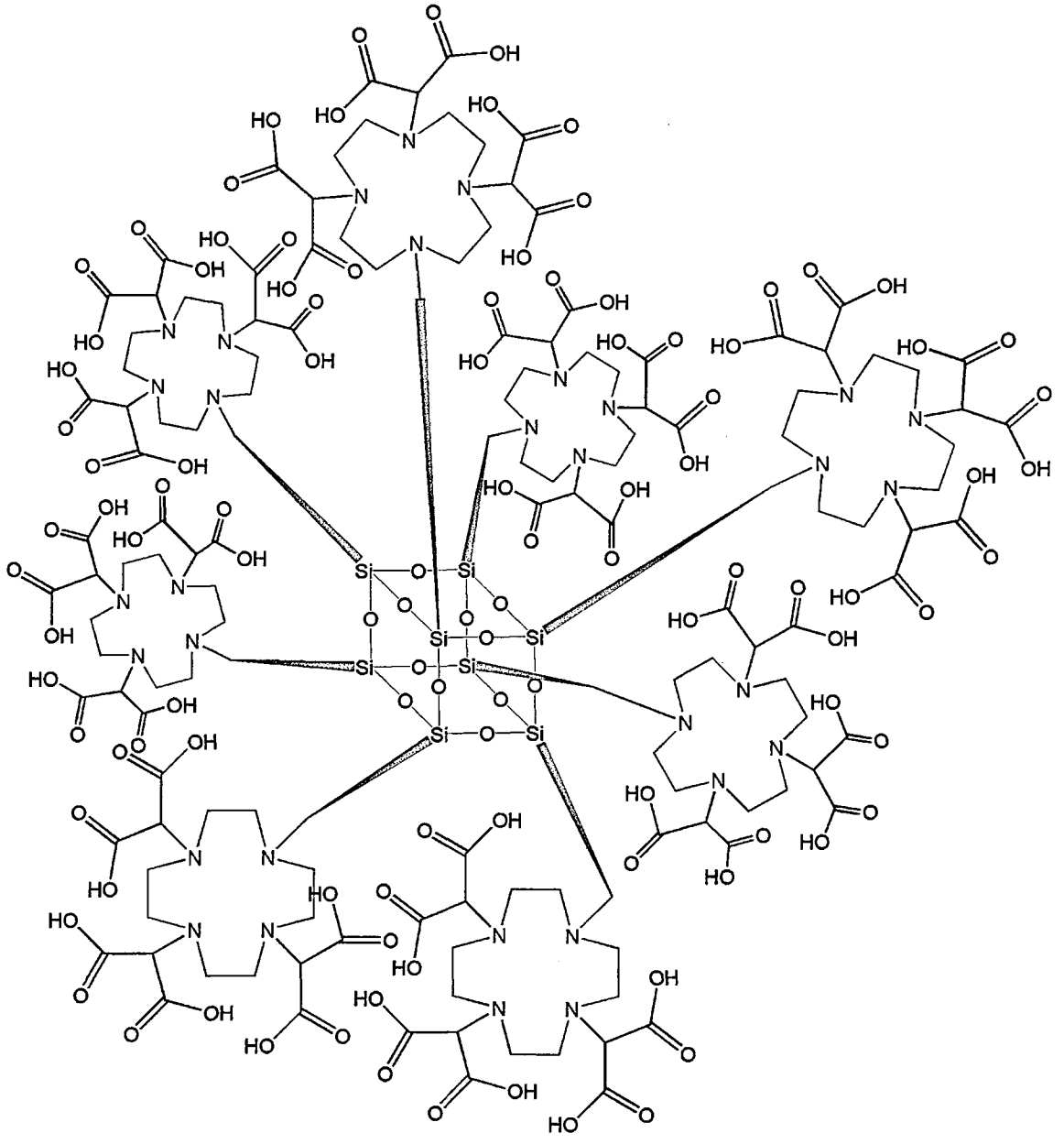

30

Figure1.7.1.2: The secondary target molecule (30)

As discussed earlier, di-acid compounds such as gDO3A present a problem with cross-binding within the molecule. The length of the carbon chain between the two carboxylic acid groups is important, owing to the possibility of intermolecular

complexation between two cyclen–Ln pendant arms once attached to the siloxane cage. This would be more likely with a longer-chain acid such as adipic acid (**24**), as used in aDO3A (**26**). This pendant–pendant binding would reduce the anisotropic rotation of the cyclen–Ln pendant arms in relation to the central siloxane cage by increasing the rigidity of the molecule. Whilst this reduction of the anisotropic rotation would lead to greater relaxation, it would cause a reduction in the *q* value, thus effectively reducing the relaxation value of the complex (Figure 1.7.1.3).

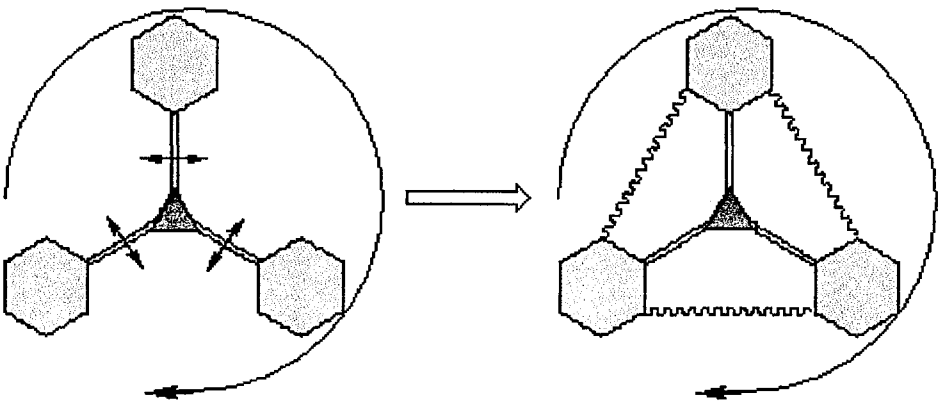

Figure 1.7.1.3: Change in the oscillations of the siloxane cage with linked cyclen–Ln pendant arms.

A cyclen based on glutaric acid (**23**), such as gDO3A (**25**), would reduce the possibility of pendant–pendant binding occurring, owing to the shorter chain length. However, the intramolecular binding discussed earlier would mean that the gain from the increasing *q* value would be lost. One way around this intramolecular binding would be the use of a shorter chain length, such as with malonic and succinic acids, to give mDO3A (**31**) and sDO3A (**32**) (Figure 1.7.1.4). These shorter chains would

increase the ring strain between the second acid group and the lanthanide, thereby making intramolecular binding more difficult.

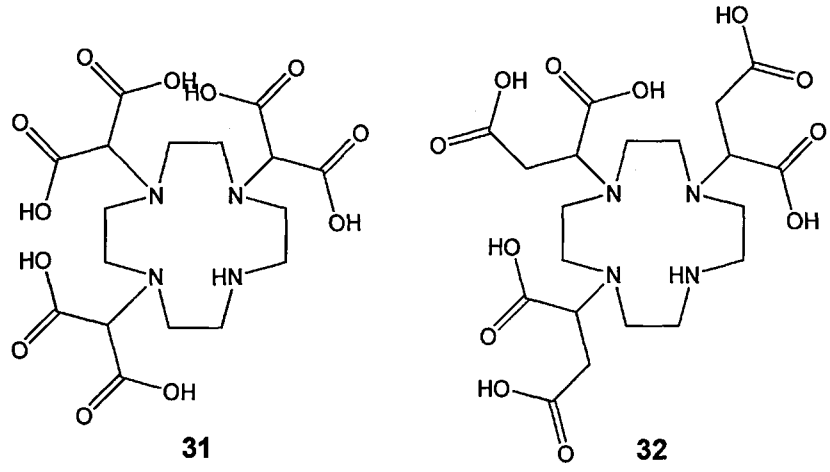

Figure 1.7.1.4: Structures of mDO3A (31) and sDO3A (32)

1.7.2: Silicon cages

At the core of the dendrimer molecule is a silsesquioxane, a six-faced Si–O–Si cube with a formula of Si_8O_{12} (**33**). Silicon can form stable chains interlinked with oxygen (**34**). These chains can form rings (**35**), which when cross-linked form cages of various sizes. The cubic cages have the benefit of having eight corner sites for addition of ligands or the attachment of, for example, biological coordinating systems to form RIME-type agents. The advantage gained by the use of the silsesquioxane cage would be the rigidity to the molecule that it would impose on the dendrimer structure (Figure 1.7.2.1).

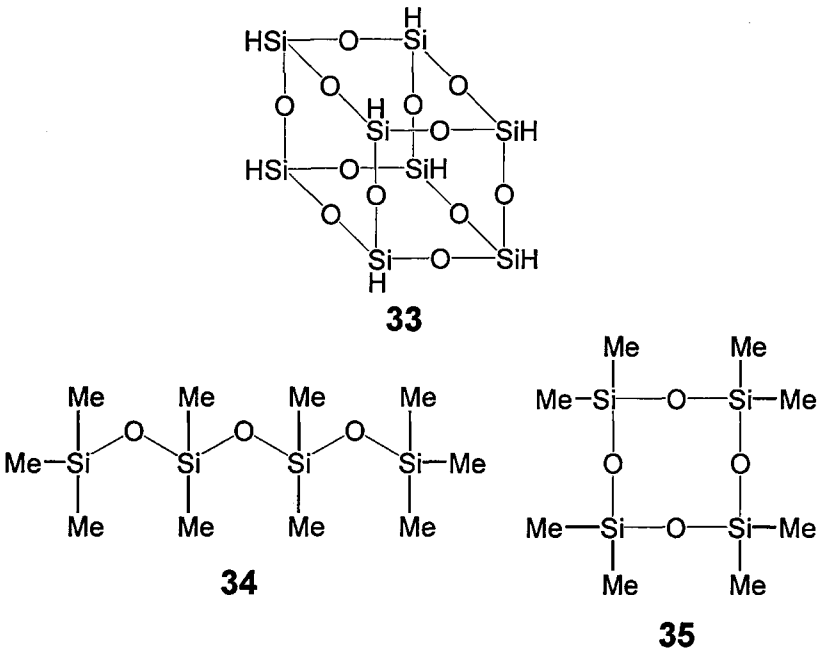

Figure 1.7.2.1: Types of silicon chains and rings

1.7.3: Properties of silicon cages

Silsesquioxanes or polysilsesquioxanes[61] have a general formula of $(RSiO_{1.5})_n$, forming a cube in the case where $n = 8$. They are often referred to as T_n compounds, where n is the number of silicon atoms in the compound. Silicon compounds are often referred to in general by a letter corresponding to the number of oxygen atoms bound to the silicon; D means di-oxygen functional, T is tri-oxygen functional and Q stands for tetra-oxygen functional. Under the right conditions, silicon can also form 5 oxygen bonds. The most studied type of double-ring silicate system is the cubic (Si_8O_{12}) silicate, or T8. Octahydridosilsesquioxane, ($H_8Si_8O_{12}$) or (T_8H_8) (**33**), was first prepared in 1959 with yields of 0.1% by Muller et al.[62] It was improved upon by Agaskar et al.[63] to give a mixture of $H_8Si_8O_{12}$ (**33**) and $H_{10}Si_{10}O_{15}$, with yields of 27%. Silsesquioxanes may be prepared by the condensation of tri-functional silanes. The cage system contains a functional group at each of the corners; in the case of T_8H_8 (**33**) the functional groups are hydrogens, and in the case of $Q_8M_8^H$ (**38**) the

functional groups are oxysilanes. Generally they are stable and, depending on the functional groups, they are also inert to most reagents.[64] Their inertness is a result of the stability and strength of the silicon–oxygen bond and the silicon–carbon bonds.[65]

Silsesquioxanes are divided into two main classes, functional and non-functional, depending on whether the group can undergo other reactions. The non-functional silsesquioxanes contain groups such as alkyl or aryl, whereas the functional silsesquioxanes can contain a range of organic functional groups such as vinyl, alcohol and carboxylic acid esters. There are several synthetically useful cages, such as Si–H (**33**), Si–OH (**36**), Si–vinyl (**37**), and O–Si–Me_2H (**38**); (**36**) and (**38**) are examples of Q_8 cages (Figure 1.7.3.1).

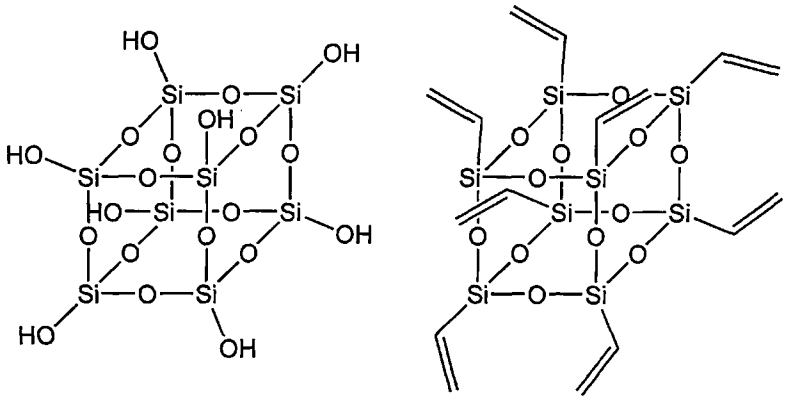

36 **37**

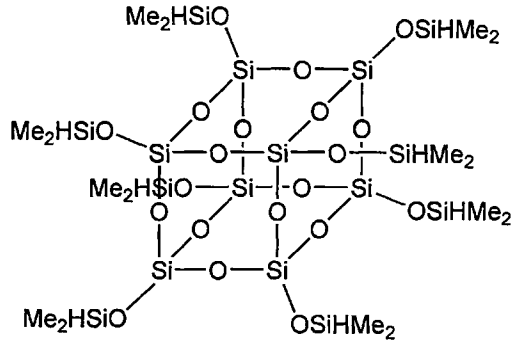

38

Figure 1.7.3.1: Some useful cages

Silsesquioxanes are often used in the coating industry, as a precursor for silicon oxycarbide ceramics, as a nanofiller for load-bearing plastics[66], or as a scaffold for molecular nanotechnology.[67] They are also used as copolymers, when the chain is extended with suitable functional groups to form a dendrimer species in the shape of a star. The group of compounds formed in this way are often referred to as octopus-silsesquioxanes. The functional groups of the cubes may also be able to cross-link with other monomers, dendrimers or Polyhedral Oligomeric Silsesquioxanes (POSS).

Another important group of silsesquioxanes are the incompletely condensed polyhedral oligosilsesquioxanes (**39**), which contain essentially a silsesquioxane cage missing one of its corners. These silsesquioxanes may be formed by hydrolytic condensation reactions of alkyl or aryltrichlorosilanes,[68] in a similar manner to the formation of the T_8H_8 (**33**) cages. An alternative preparation is the incomplete hydrolysis of octa-polyhedral silsesquioxanes ($R_8Si_8O_{12}$) with strong acids, such as $HBF_4.OMe_2$ or triflic acid (CF_3SO_3H), over a period of several hours at room temperature or in a brief reflux[64, 69]

It is important to note that the silsesquioxane cages are completely condensed before they are used for imaging agents, owing to the possible formation of a complex between the lanthanide and the incompletely condensed polyoligosilsesquioxane cage. These complexes form dimeric lanthanides, where two lanthanide–silsesquioxanes come together to form a stable complex (**40**) at low temperature, which may be capped with a strong donor ion such as pentamethyldiethylenetriamime to form a stable complex (**39**).[70] These complexes

are stable in non-aprotic solvents, have limited solubility, and their stability in aqueous solution is limited owing to their ease of hydrolysis[71] (Figure 1.7.3.2).

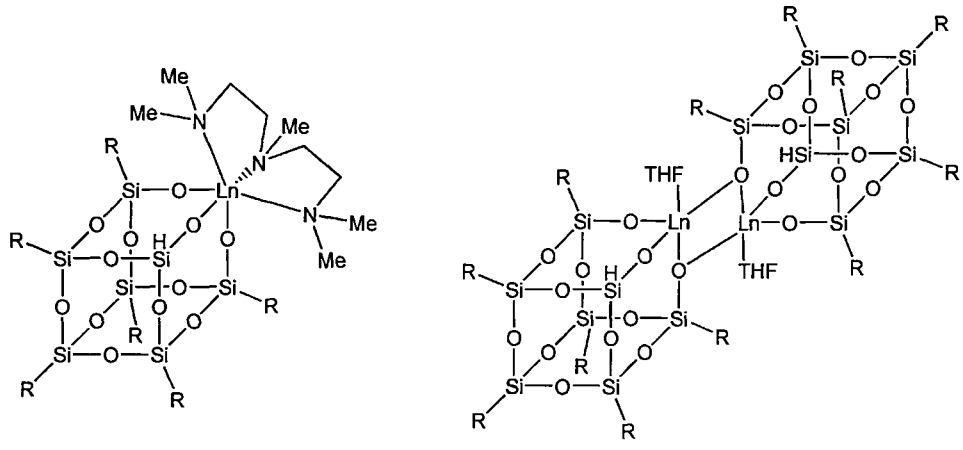

39 40

Figure 1.7.3.2: Structures of lanthanide-silsesquioxane complexes[70]

While the silsesquioxanes cage may be stable in acid and neutral conditions, the cage can undergo decomposition in a basic environment. This occurs slowly when the compound is exposed to an amine such as Et_3N in wet solvents, but much more slowly when in anhydrous solvents.[72] The reaction with the base Et_4NOH (aqueous) in THF has been investigated as a method for producing incompletely condensed silsesquioxanes.[73] Amine-induced hydrolysis is more common when the amine in question is a primary amine, such as compound (**41**). The amine breaks the Si–O bond to form an intermediate structure (**42**), which would then undergo condensation with another Si–OH group or, if water is present, would form Si–OH directly (**43**) [74] (Figure 1.7.3.3).

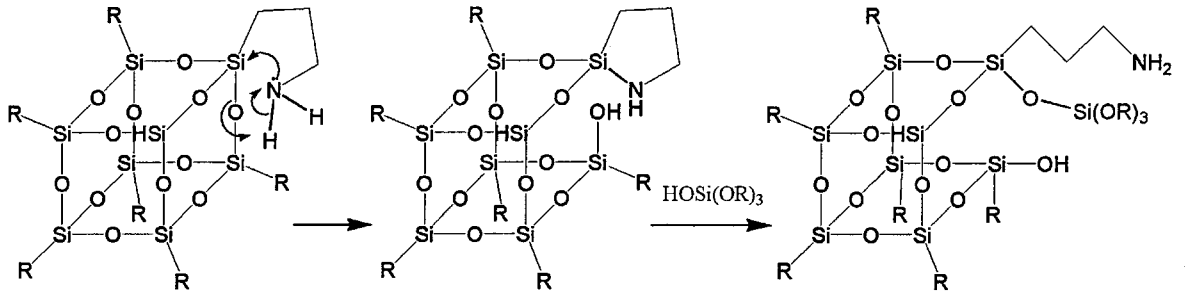

41 42 43

Figure 1.7.3.3: Mechanism for decomposition of a T8 cage via a primary amine[74]

1.7.4: Methods of forming bonds between silsesquioxanes and cyclens

The linking reaction between a substituted cyclen and a silsesquioxane is the key step in the formation of the target ligands. There are several ways to form Si–C bonds, such as the direct reaction – used in industry – of silicon with an alkyl halide using a metal catalyst such as silver, nickel or copper under high temperatures, which yields a mixture of reaction products. Other laboratory Si–C-based bond formations are based on the formation of a carbanion; such methods include Grignard-type reactions using a silyl halide such as Me_3SiCl, with RMgX in ether The alkali metals lithium and sodium can also be used in the formation of the Si–C bond[75]

The problem with these methods is that they rely on the generation of a carbanion, which may react with the cyclen system. An alternative, which does not rely on the formation of a carbanion, is hydrosilylation[75]. This is the reaction of an alkene with Si–H to form an Si–C bond, using platinum catalysis. The alkene butene-mDO3A (**44**) would be attached to the cyclen via a short arm (Figure 1.7.4.1). The length of

the arm linking the cyclen ligand to the silsesquioxane cage is critical to limiting the amount of anisotropic rotation which could occur, in the same manner as in the oligomers seen in section 1.4.3.

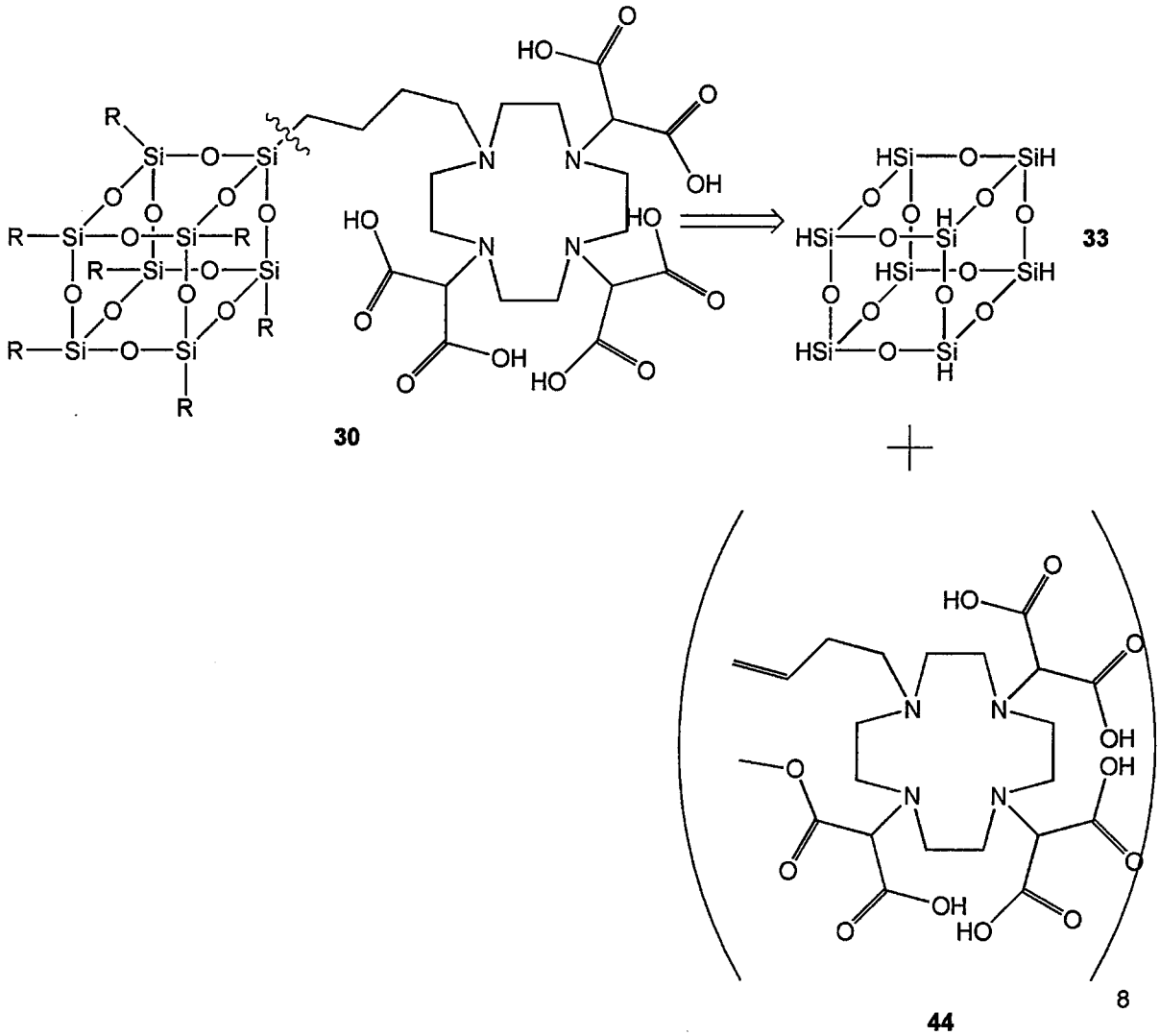

Figure 1.7.4.1: Retrosynthesis analysis of the target molecule for the formation of the Si–C bond

1.7.5: Hydrosilylation-based bond formation

Hydrosilylation is the addition reaction of Si–H across a π bond, such as in alkenes and alkynes, forming an Si–C bond by taking advantage of the low strength of the Si–H bonds. This is performed using two main methods, radical and transition-metal catalysis, with the latter being the more synthetically useful. The main transition metal used as a catalyst in hydrosilylation is platinum, normally as chloroplatinic acid (H_2PtCl_6) in propan-2-ol.

The formation of the bond is favoured because of the increase in bond strength. This provides a good synthetic route for the attachment of arms with different functional groups to the octahydridosilsesquioxane (T_8H_8) (**33**). Another advantage of platinum catalysts is that they are tolerant of a wide range of function groups and would not be expected to react with the esters and amines of the compound[76-78] (Figure 1.7.5.1).

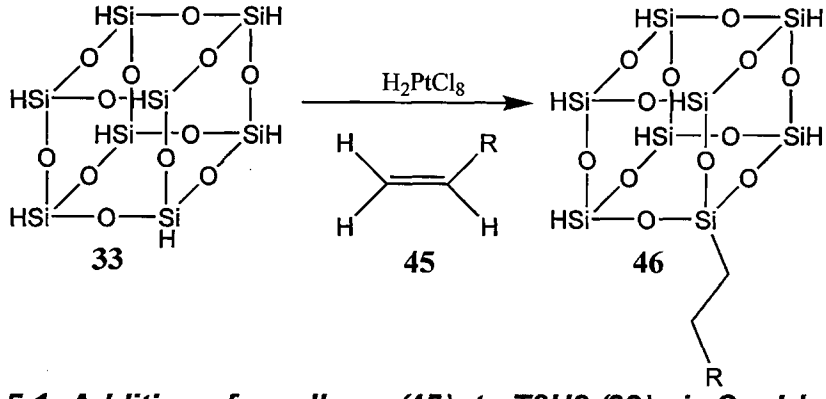

Figure 1.7.5.1: Addition of an alkene (45) to T8H8 (33) via Speir's catalyst to give the substituted silsesquioxane cage (46) [61]

There are possible side reactions which could occur with the hydrosilylation reaction between the alkene–cyclen and the hydrosilane. These side reactions are caused by

the difference between the bond energies of Si–H and Si–O, suggesting that hydrosilanes would react rapidly with alcohols. Alcoholysis reactions with hydrosilanes are kinetically quite slow under neutral conditions. For example, the ethanolysis of $HSi(OEt)_3$ (**47**) needs to be performed in a sealed tube at a temperature of 100 °C, producing $Si(OEt)_4$ (**48**) with yields of 50% (Figure 1.7.5.2).

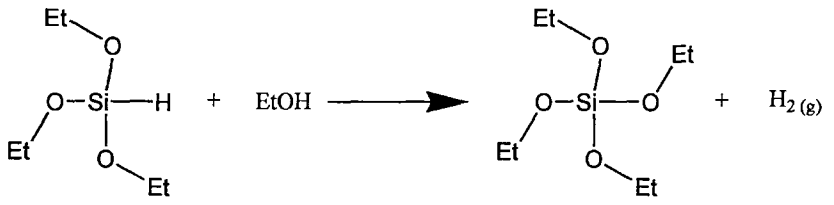

47 **48**

Figure 1.7.5.2: Alcoholysis of $HSi(OEt)_3$ (47) with ethanol to form $Si(OEt)_4$ (48) and hydrogen gas

To be able to react with an alcohol in a synthetically useful way, hydrosilanes need the presence of a strong acid, a base, radical conditions or the presence of metals such as colloidal copper or a transition metal, for example palladium and nickel complexes.[79-81] Bases are typically more efficient as catalysts than are acids, but both have the drawback of being able to hydrolyse the ester-protecting group of the carboxylic acid on the ligand. This is crucial, as the carboxylic acid, propanoic acid, (**49**) can react with the triethoxyhydrosilane (**47**) to form the corresponding silyl carbonate, triethoxysilyl propionate (**50**) (Figure 1.7.5.2).

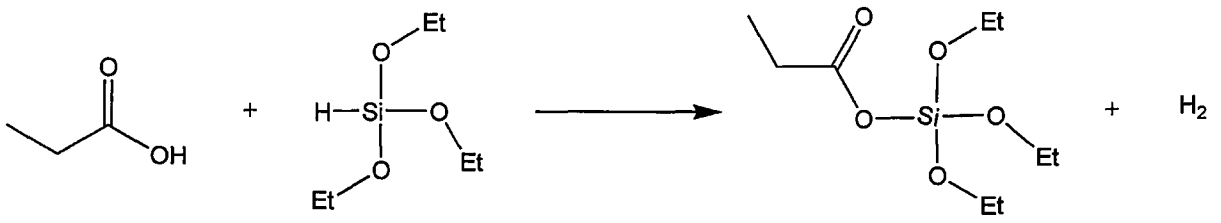

49 **47** **50**

Figure 1.7.5.3: Reaction of triethoxyhydrosilane (47) with propanoic acid (***49***) to form triethoxysilyl propionate (***50***)

Thus the cyclen ligand must be attached to the silsesquioxane cage before the hydrolysis of the esters and the formation of the lanthanide complexes; otherwise the three unbound carboxylic acid groups would react with other cages to form an insoluble polymer. To avoid the unwanted hydrosilylation between the carboxylic acids and the silsesquioxane cage, the other Si–H sites on the silsesquioxane would have to be protected, or have their functionality changed to avoid unwanted side reactions.

Chapter 2.0: Formation of the cyclen moiety – results and discussion

2.1: Strategies for the substitution of cyclen

There are two main synthetic strategies possible for the asymmetric derivatisation of cyclen (**9**), depending on the way in which the different arms are attached (Figure 2.1.1). Each strategy has its own problems, which will be discussed later. The first method is referred to as the 1+3 strategy, where the first step is the attachment onto one of the nitrogens of the alkene linking group for the attachment to the siloxane cage (**51**); that is followed by the attachment of the complexing arms onto the three remaining nitrogens (**53**). The second method is referred to as the 3+1 strategy, where the first step is the attachment of the complexing arms to the three nitrogens (**52**), followed by the attachment of the linking group on the fourth nitrogen (**53**).

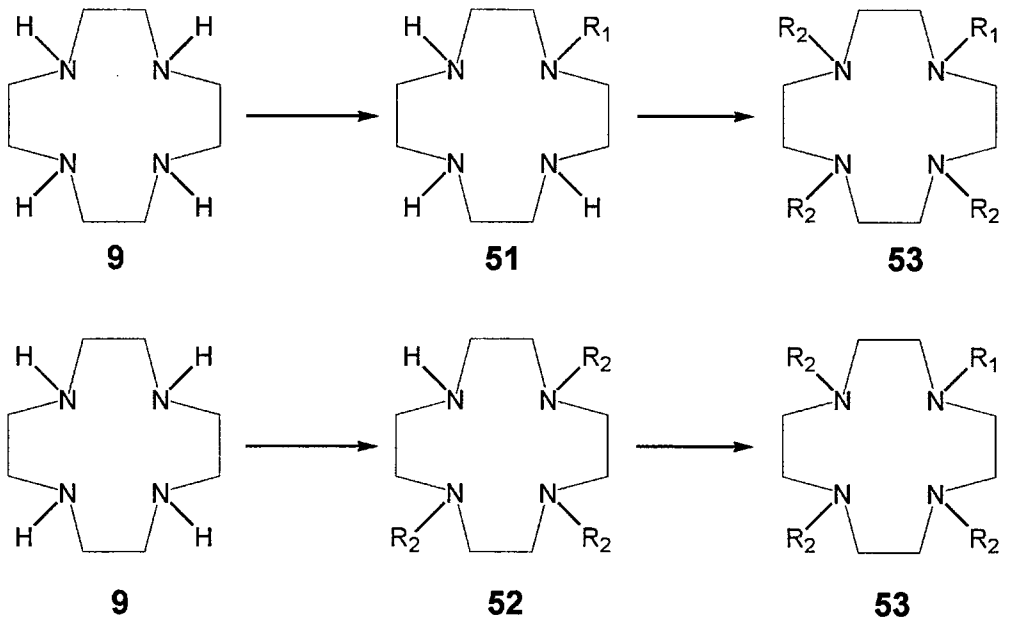

Figure 2.1.1: The two strategies for asymmetric cyclens: top, 1+3 strategy; bottom, 3+1 strategy

Both the 1+3 and 3+1 routes have similar problems with over-substitution during the asymmetric substitution of cyclen (**9**). This is possibly due to two factors: the pK_a of the amines and the steric effect of the groups. The pK_a of the amines varies depending upon the extent of quarterisation and can be split into two phases. The first two protonations have higher pK_a values – between 10.6 ($^{+}/_{-}$ 0.1) (**54**) and 9.6 ($^{+}/_{-}$ 0.1) (**55**) – while the second set of protonations have lower pK_a values – between 1.7 ($^{+}/_{-}$ 0.11) (**56**) and 0.8 ($^{+}/_{-}$ 0.1) (**57**) [82, 83] (Figure 2.1.2).

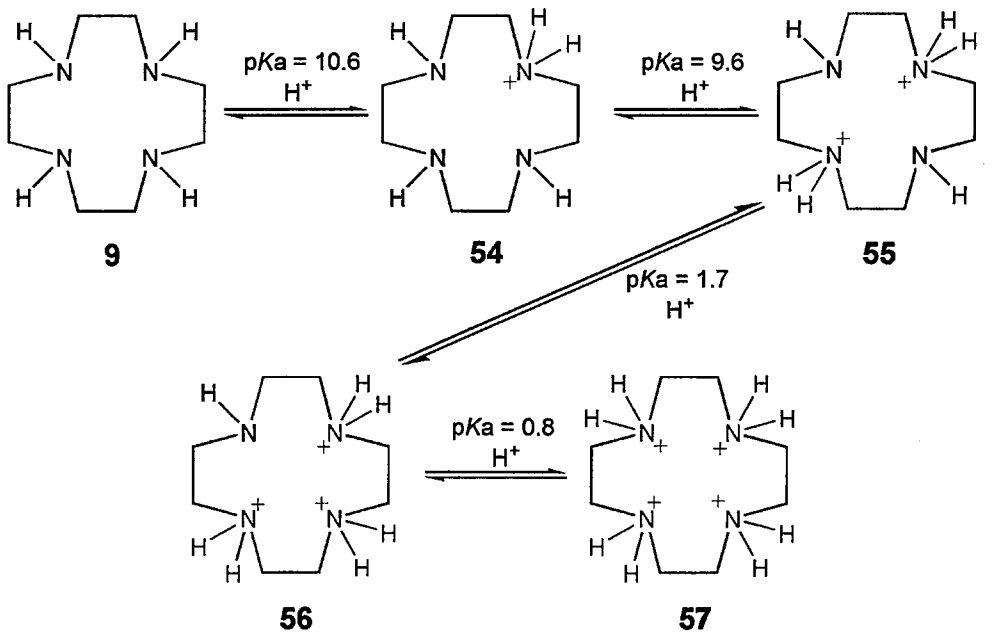

Figure 2.1.2: pK_as of cyclen in water; conditions 25 °C, 0.1M $NaNO_3$ [82, 83]

This grouping of the pK_as proves to be a problem with the asymmetric substitution, as the conditions needed to alkylate one of the nitrogens are ideal for the alkylation of the other nitrogen within the pK_a pair. This over-alkylation was a key problem in both routes. In the 1+3 route over-alkylation occurs on the nitrogen, *trans* to the first site of alkylation (**58**). In the 3+1 route the over-alkylation produces a tetrasubstituted cyclen (**59**) (Figure 2.1.3).

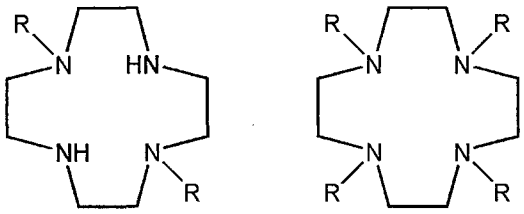

58 **59**

Figure 2.1.3: Products of over-alkylation. Left: the over-alkylated product from the 1+3 strategy. Right the over-alkylated product from the 3+1 strategy

There are several ways to prevent over-alkylation in both routes. The first was to use a higher dilution and/or arrange for the number of equivalents of the alkylation arms to be slightly less than that of the cyclen. Alternatively, it might be prevented by the use of a suitable protection group such as BOC (*N*-tert-butoxycarbonyl).

2.2.1: Synthesis of 1-pent-4-enoyl-1,4,7,10-tetraazacyclododecane (66)

The first cyclen system investigated was based upon DO3A (**22**), with the linking arm between the cyclen and the siloxane being pent-4-enoyl chloride (**63**), which has the functionalities of the acid chloride for the substitution reaction on the cyclen as well as the alkene needed for the hydrosilylation reaction onto the silicon cage. The pent-4-enoyl chloride (**63**) arm would need to be attached to the cyclen (**9**) before the hydrosilylation reaction with T_8H_8 (**33**) could be performed, to prevent possible side reactions between the siloxane and the acid chloride (Figure 2.2.1.1).

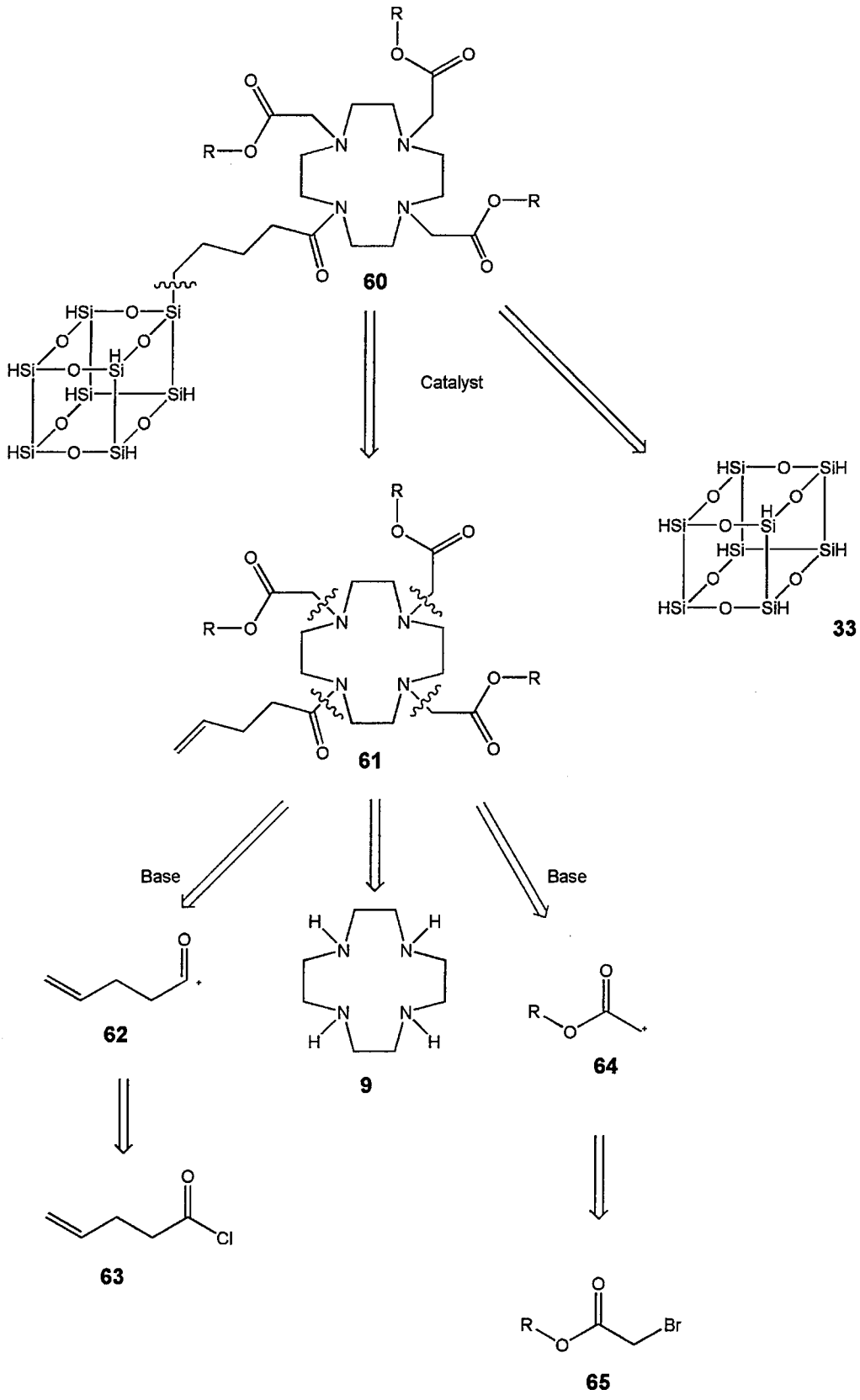

Figure 2.2.1.1: Retrosynthetic analysis of compound (60)

There are two possible routes to the formation of pent-4-enoyl-DO3A (**61**). The first, labelled Route A (Figure 2.2.1.2), is the 1+3 route, where the cyclen (**9**) is first acylated with pent-4-enoyl chloride (**63**) to give the monosubstituted cyclen (**66**), which was then reacted with ethyl 2-bromoacetate (**65**) to give the target molecule (**61**). The second route, labelled Route B, is the 3+1 route, where the cyclen (**9**) was first alkylated by ethyl 2-bromoacetate (**65**) to give the trisubstituted cyclen (**67**), which was then acylated by pent-4-enoyl chloride (**63**) to give the target molecule (**61**).

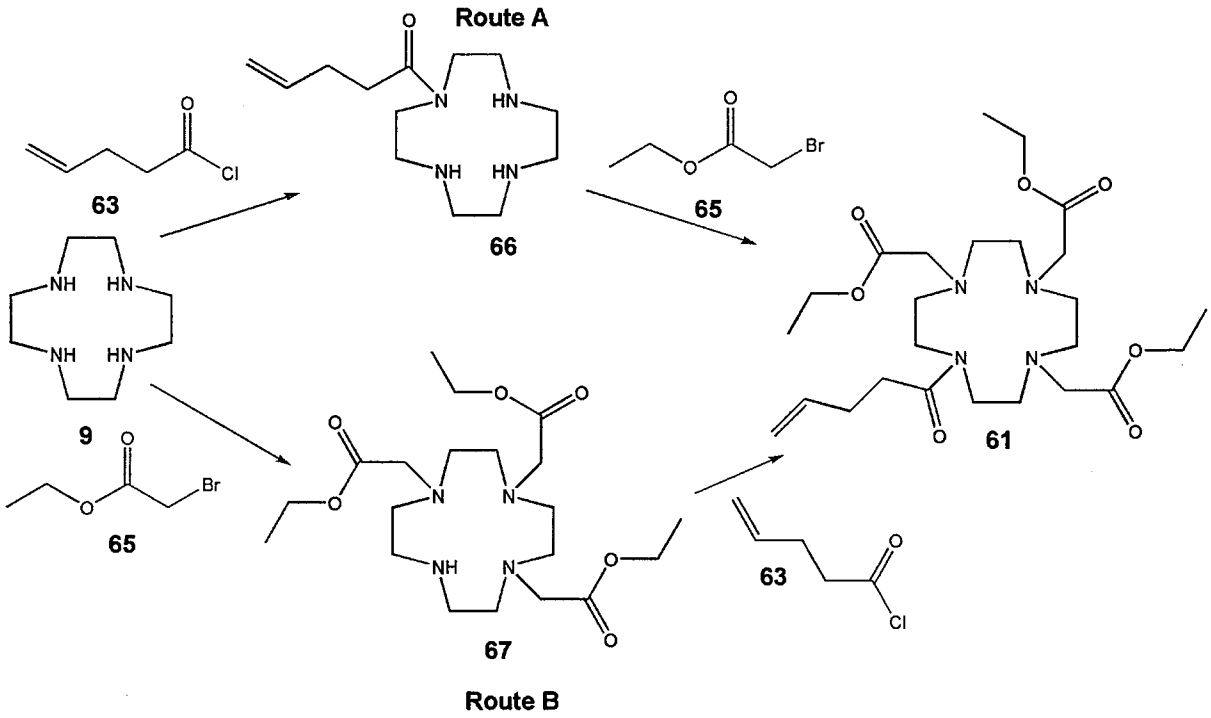

Figure 2.2.1.2: Two reaction pathways for the formation of the ethyl ester form of pent-4-enoyl-DO3A (61)

There are two methods for the formation of 1-pent-4-enoyl-1,4,7,10-tetraazacyclododecane (**66**). The first was the direct alkylation of the cyclen (**9**) by pent-4-enoyl chloride (**63**) (Figure 2.2.2.1). In the second method the cyclen (**9**) was first protected on three of the nitrogens, and then reacted with pent-4-enoyl chloride (**63**) before being deprotected to give the 1-pent-4-enoyl-1,4,7,10-tetraazacyclododecane (**66**).

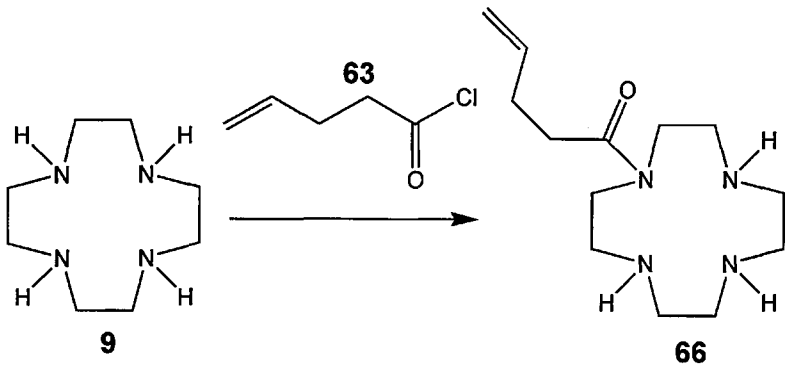

Figure 2.2.2.1: The 1+3 route for the synthesis of 1-pent-4-enoyl-1,4,7,10-tetraazacyclododecane (66)

In the first method the pent-4-enoyl chloride (**63**) was reacted with cyclen (**9**), using powdered activated molecular sieve and anhydrous chloroform. The molecular sieve has two functions in this reaction: the first is to act as an acid scavenger, removing the HCl produced, and the second is to remove any residual water present, thus preventing the hydrolysis of the acid chloride.[84]

The LCMS of the crude reaction product showed that the reaction had produced a mixture of substituted cyclens ranging from 1 to 4 substituted cyclens with the following m/z results 255.21 [M(**66**)$^{+H}$], 337.21 [M(**68**)$^{+H}$], 419.31 [M(**69**)$^{+H}$] and 501.33 [M(**70**)$^{+H}$] (Figure 2.2.2.2). The separation of the reaction products proved to

be unsuccessful, by TLC (chloroform 90%, methanol 10% on silica) RF 0.01. So the second method, using the tri-protected cyclen, was investigated.

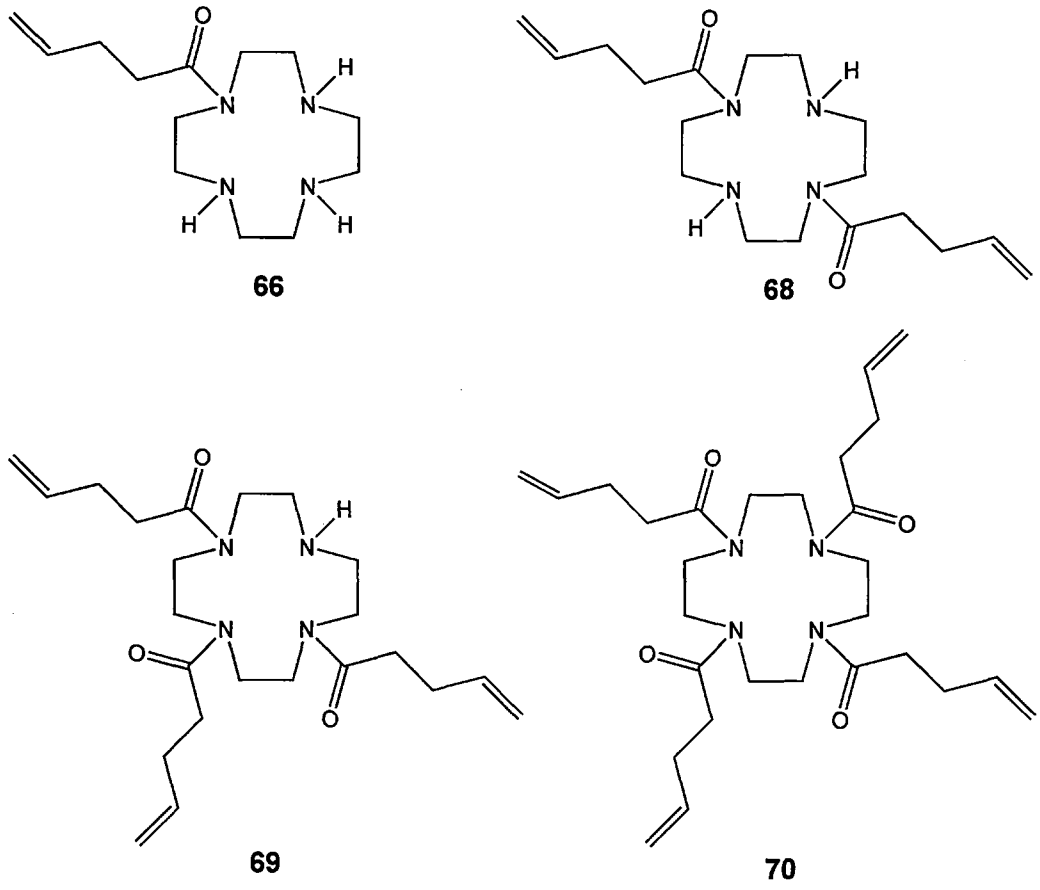

Figure 2.2.2.2: Reaction products of cyclen (9) and pent-4-enoyl chloride (63)

2.2.3: Protected cyclen route for the synthesis of 1-pent-4-enoyl-1,4,7,10-tetraazacyclododecane (87)

In the second method the cyclen is first protected with di-*tert*-butyldicarbonate (**71**) to give the tri-BOC-cyclen (**72**) giving yields of 40%, proven by ^{1}H NMR, ^{13}C NMR and FTIR which showed the presence of the carbonyl at 1691 cm^{-1}. The tri-BOC-cyclen is then alkylated with pent-4-enoyl chloride (**63**) to give the fully substituted cyclen

(**73**). That would then be deprotected to give 1-pent-4-enoyl-1,4,7,10-tetraazacyclododecane (**66**) (Figure 2.2.3.1).

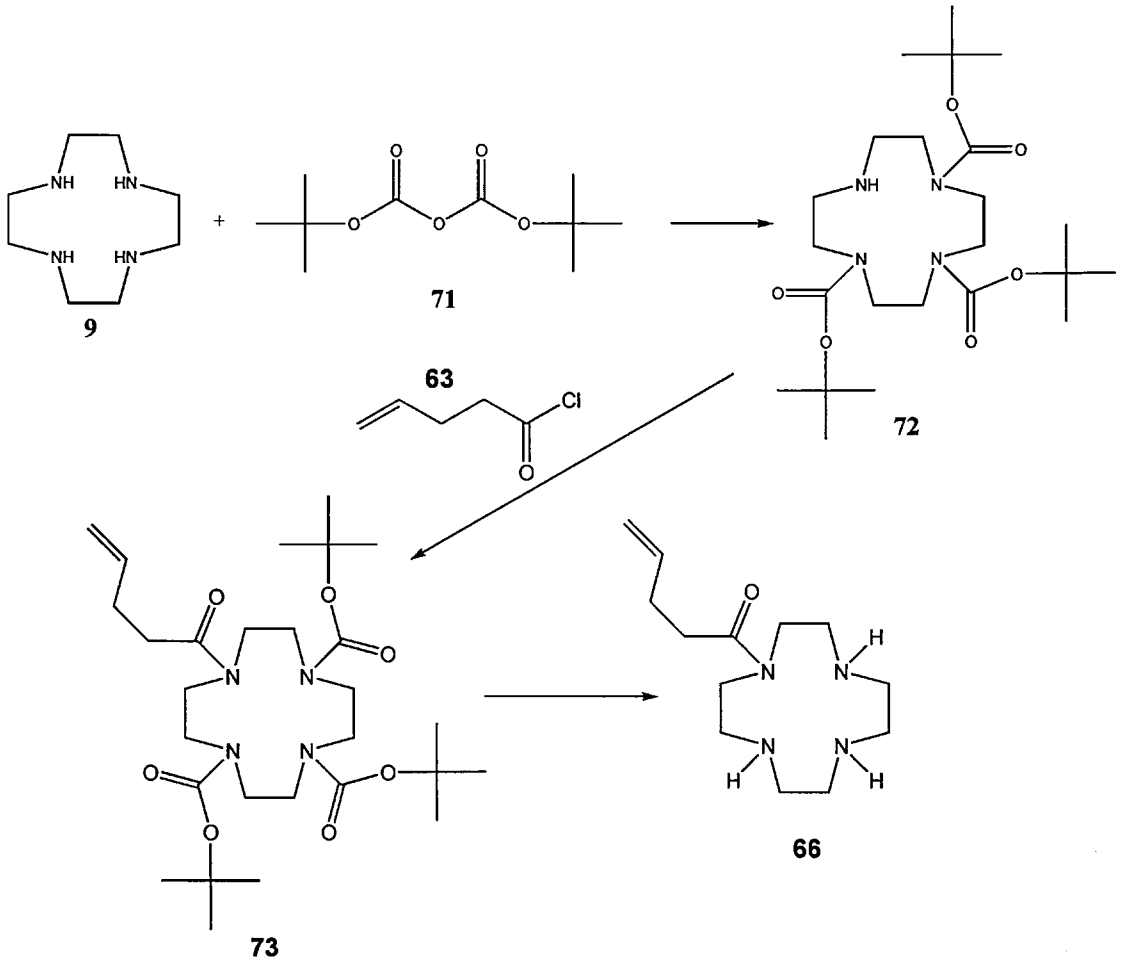

Figure 2.2.3.1: Second method for the formation of 1-pent-4-enoyl-1,4,7,10-tetraazacyclododecane (66).

Tri-BOC-cyclen (**72**) was dissolved in chloroform and powdered molecular sieve added as before, to which a solution of pent-4-enoyl chloride (**63**) in chloroform was added dropwise. The reaction mixture was chromatographed on alumina using chloroform (95%) and methanol (5%) as the eluant. A clear oil was produced in a yield greater than 60%. The ^{1}H NMR showed the presence of the alkene at 4.92 (H2) and 5.76 (H) ppm, The compound was also confirmed by ^{13}C NMR, FTIR and LCMS (555.72 [M(**73**)$^{+H}$]

The next step in the synthesis was the removal of the BOC protecting groups using trifluoroacetic acid, monitored by LCMS, to give 1-pent-4-enoyl-1,4,7,10-tetraazacyclododecane (**66**). While this step did remove the BOC groups, the TFA removed the pent-4-enoyl group from the cyclen as well. LCMS 173.19 [M(**9**)$^{+H}$], 255.24 [M(**66**)$^{+H}$] (trace only).

The removal of the linking arm rendered the method of protection using BOC-groups void. Therefore alternative protection was investigated, using milder conditions for the removal of the protection groups. Formyl protection of cyclen, 1,4,7,10-tetraazacyclododecane-1,4,7-tricarbaldehyde (triformylcyclen) (**74**), is a synthetically useful procedure used for the regio-selective substitution of cyclen and the formyl groups can easily be removed using weak acids or bases.[85, 86] (Figure 2.2.3.2).

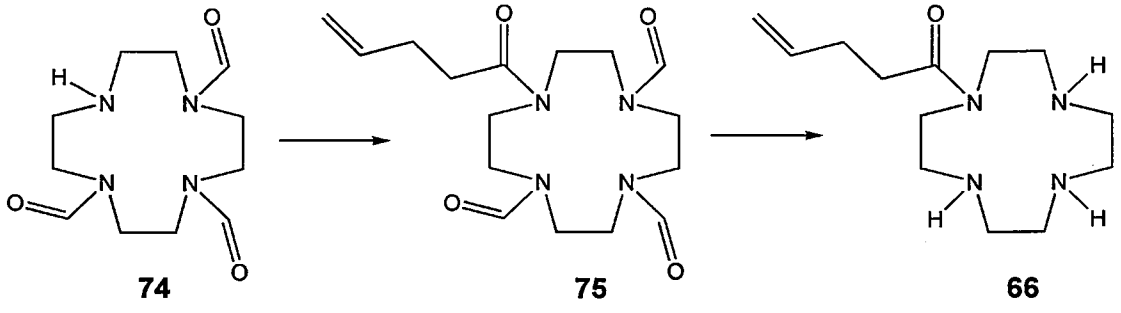

Figure 2.2.3.2: Formyl-protected cyclen route for the synthesis of compound (66)

1,4,7,10-tetraazacyclododecane-1,4,7-tricarbaldehyde (triformylcyclen) (**74**) was synthesised by the reaction of 2,2,2-trichloroethane-1,1-diol (**76**) (chloral hydrate) with cyclen (**9**) dissolved in ethanol and heated to 60 °C for 3 hours. The crude product, consisting of mainly di- and trisubstituted cyclen, was purified using silica

chromatography with a short silica column, eluting with a solution of 89.9% DCM, 10% MeOH and 0.1% ammonia solution (35%). This process eluted the target molecule in a yield of 80%, with a retention factor (R_f) of 0.25. The solution was then dried over magnesium sulfate and the organic solvents removed using reduced pressure to give a transparent viscous oil in 84% yield[87] The product was confirmed by LCMS [257.39 [M(74)$^{+H}$], FTIR which showed the presence of the carbonyl at 1669 cm^{-1} and the carbonyl was also confirmed by ^{1}H and ^{13}C NMR at 8.06ppm and 162.71 ppm respectively. (Figure 2.2.3.3).

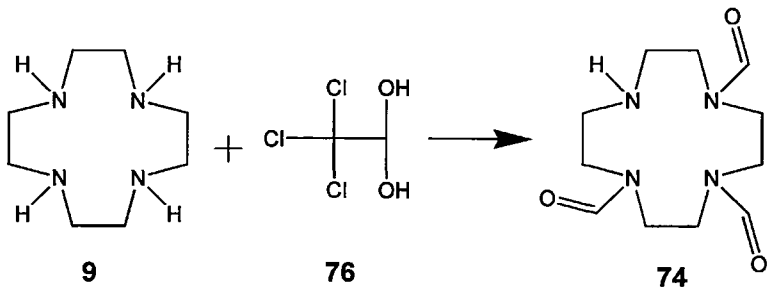

Figure 2.2.3.3 Synthesis of triformyl cyclen (74)

The triformyl cyclen (**74**) was reacted with pent-4-enoyl chloride (**63**) in chloroform with powdered activated molecular sieve. The reaction produced a mixture of compounds, as seen in the LCMS which showed that the target molecule 10-pent-4-enoyl-1,4,7,10-tetraazacyclododecane-1,4,7-tricarbaldeyde (**75**) was present as a minor trace, along with a mixture of pent-4-enoyl substituted cyclens. This was due to the acidic nature of the molecular sieve[88] removing the formyl protecting groups from the cyclen, allowing the pent-4-enoyl chloride (**63**) to produce polysubstituted cyclens. The attempted separation of the target compound on silica failed, resulting in a mixture of different compounds that eluted all at the same time.

To prevent the loss of the formyl protecting groups by the side reaction with the molecular sieve, potassium carbonate was used as the base. The removal of the residual acid chloride was achieved by the reaction of TEA with the excess pent-4-enoyl chloride to form the corresponding salts. This method prevents the formation of HCl, as would happen in, for example, biphasic extraction using water and chloroform.

The potassium carbonate was removed from the chloroform by filtration, and TEA was added to the reaction and stirred for 30 minutes to neutralise the acid chloride. The solvents were removed using reduced pressure, followed by high vacuum to remove any remaining TEA. The crude oil was then dissolved in acetone, causing the TEA-Cl present in the crude product to form a precipitate that was filtered from the reaction mixture. The solvent was then removed and the crude oil passed though a silica chromatography column eluted with 90%DCM, 10%MeOH and 0.1% ammonia solution. The 10-pent-4-enoyl-1,4,7,10-tetraazacyclododecane-1,4,7-tricarbaldeyde (**75**) was then added to a solution of sodium hydroxide solution (0.2M) to yield the deprotected cyclen 1-pent-4-enoyl-1,4,7,10-tetraazacyclododecane (**66**). The LCMS of the product showed the target molecule at 254.31 [M(**66**)$^{+H}$] along with a trace of the monoformyl-protected product (**77**) at 282.48 [M(**77**)$^{H+}$ (Figure 2.2.3.4).

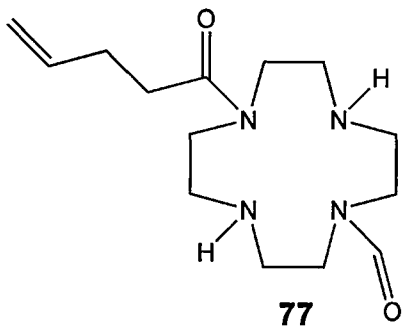

77

Figure 2.2.3.4: Structure of monoformyl-protected product (77)

The LCMS is sensitive to sodium ions, this leads to ion saturation of the detector, thus reducing the signal output of the LCMS. In an attempt to remove the sodium ions, a 2 ml fraction of the reaction was removed and freeze-dried. The product was extracted from the solid by using $CDCl_3$. The ^{13}C NMR indicated that the hydrolysis reaction had worked, by the loss of carbonyl peaks at 162 ppm corresponding to the formyl groups. The LCMS of the $CDCl_3$ solution still showed, however, a large amount of ion saturation caused by the sodium ions. Because of the limited solubility an alternative method of removing the sodium ions was attempted, by retaining the product on a C18 reverse-phase column and eluting off the sodium hydroxide. The C18 stationary-phase-chromatography approach failed owing to the polar nature of the cyclen compound in basic solution, meaning that it was eluted along with the sodium hydroxide

An alternative way to neutralise the sodium hydroxide is with hydrochloric acid (0.2M), then removal of the salt formed using a C18 reverse-phase column. The LCMS spectrum showed that compound (**75**) had been hydrolysed to form a range of products at 254.37 [M(**66**) $^{H+}$]. 282.51 [M(**77**)$^{H+}$] and 171.41 [M(**9**)$^{+}$ ^{H}] which correspond to compounds (**66**), (**77**) and cyclen (**9**) respectively. This indicated that the linking group could be hydrolysed from the cyclen compound rendering this route unfeasible. (Figure 2.2.3.5).

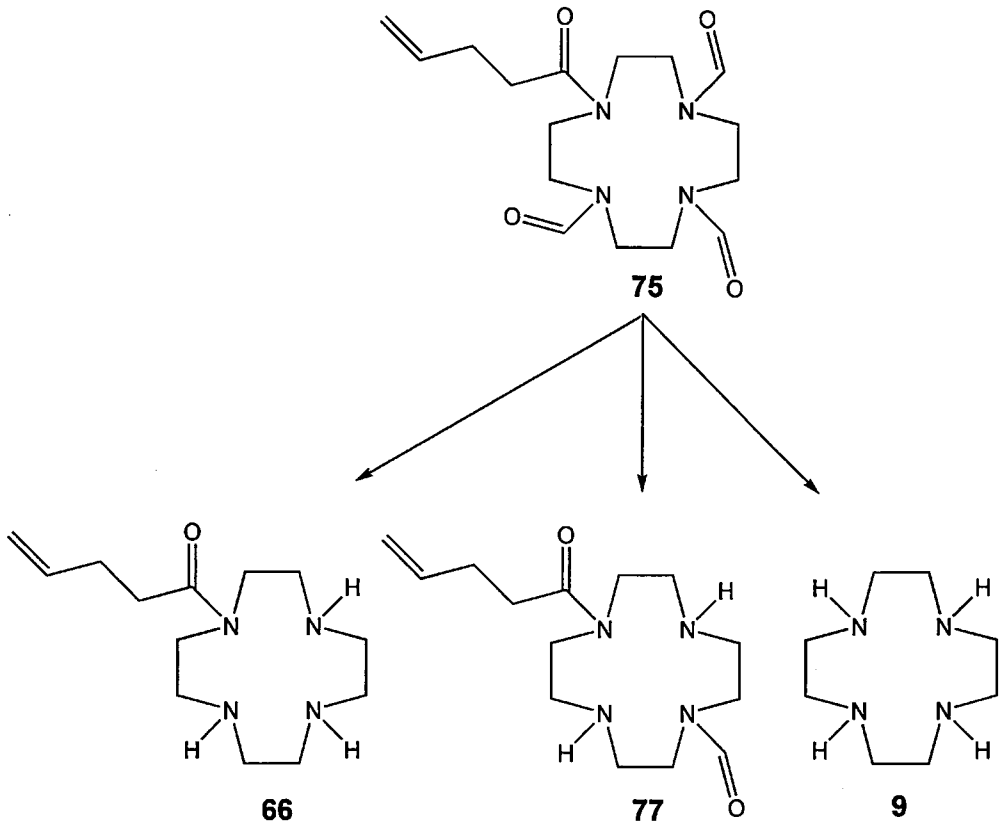

Figure 2.2.3.5: Hydrolysis of compound (75) to form 1-pent-4-enoyl-1,4,7,10-tetraazacyclododecane (66)

2.2.4: Conclusion

The failure to attach the carbonyl-based lining arm was due to the sensitivity of the arm to acids. This ease of elimination of the carboxyl linker arm presented a problem, as it would be easily removed at later stages of the synthesis. The main inconvenience would be the hydrolysis of the cyclen–siloxane cage to remove the ester protection groups. The nature of the silicon cage means that a strong base is not viable for carrying out this hydrolysis, as it would destroy the cage. The use of an acid for the hydrolysis would hydrolyse the linking arm of the cyclen, which would result in the decomposition of the target molecule. An alternative to the acid chloride arms is a haloalkene arm such as 4-bromobut-1-ene (**78**) (Figure 2.2.4.1). The use

of such an arm would change the water coordination number of the Gd–cyclen complex from q = 1 to q = 2, caused by the loss of the carbonyl group on the linking arm reducing the 8 coordinating ligands to 7.

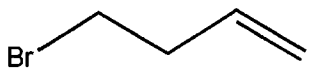

78

Figure 2.2.4.1: Structure of 4-bromobut-1-ene (78)

The loss of the coordinating arm would have an effect on the stability of the Gd–cyclen complex. The stability of 7 coordinate ligands can be improved by the use of di-acid pendant arms, for example aDO3A (**26**). This would allow the system to be more stable, while taking the advantage of the increases in q values. The solubility would also be improved owing to the extra acid groups.

2.3: Nomenclature for hex-acid cyclen systems

The IUPAC nomenclature produces extremely long names for the ligands studied in this project; therefore abbreviations will be used from this point onwards, based upon the system seen in Parker et al. in 2001. This uses the generic name of the acid groups as the first letter, followed by the generic core name. Thus, if the ligand has three adipic acid pendant arms it would be aDO3A (**20**); if the acid pendant arms were malonic acid it would be represented as mDO3A (**31**); and sDO3A (**32**) for succinic acid pendant arms. The fourth pendant arm is expressed before the DO3A

nomenclature, e.g. a butene-based arm attached to gDO3A (**79**) would be expressed as butene-gDO3A (**106**) (Figure 2.3.1).

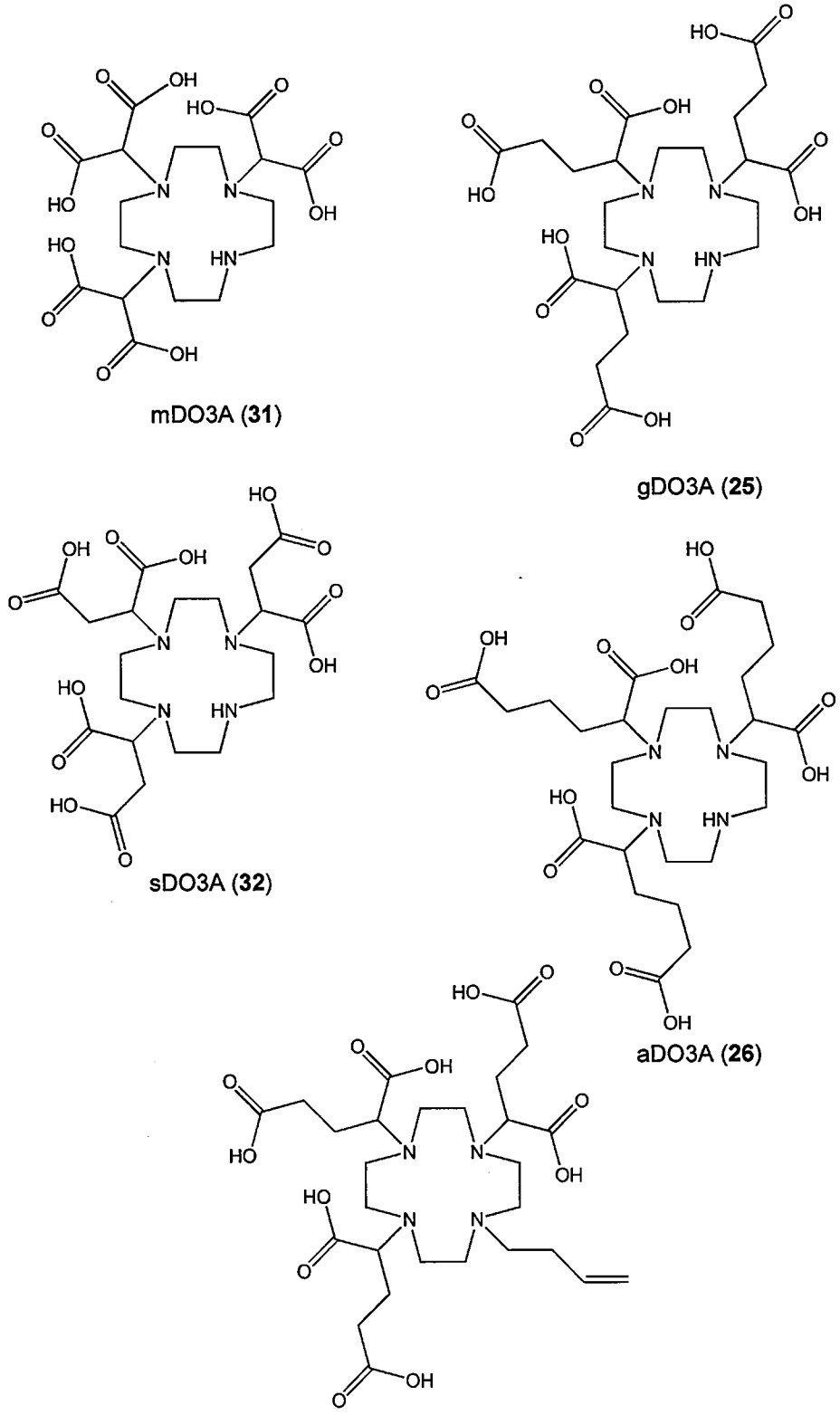

Figure 2.3.1: Examples of different compounds based on DO3A

2.4.1: Synthesis of a malonic acid-armed cyclen, mDO3A (31)

The first di-acid chosen was malonic acid (**80**); with a carbon chain length of 3 it is the shortest possible chain length that allows for modification for attachment to the cyclen. This is in contrast to oxalic acid (**81**), which has only the carbonyl carbons, and thus no position for possible attachment to the cyclen (Figure 2.4.1.1).

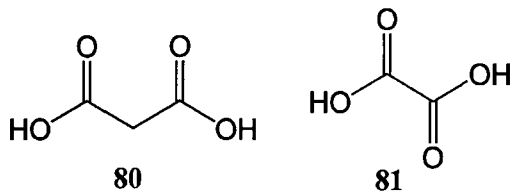

Figure 2.4.1.1: Structures of oxalic acid (81) and malonic acid (80)

Malonic acid (**80**) is not directly suitable as a ligand, owing to its ease of decarboxylation to form an acetic acid group (**84**)[88] via the decomposition of (**82**) to give the enolate (**83**), which converts to the mono-acid (**84**) by addition of a proton (Figure 2.3.1.2).

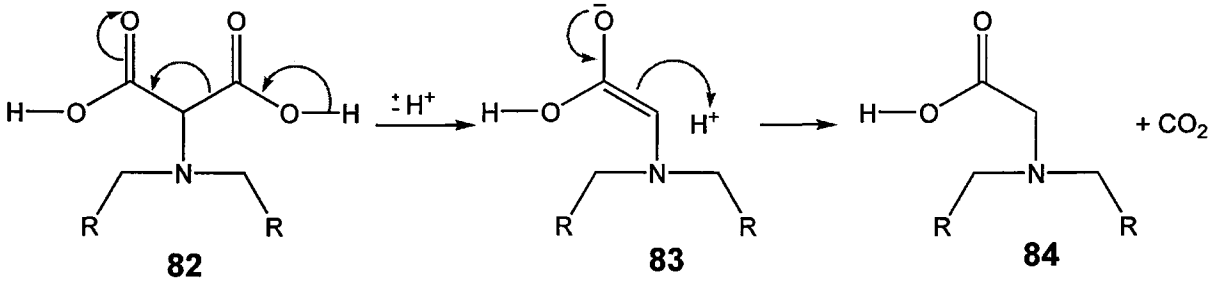

Figure 2.4.1.2: Decarboxylation of malonic acid compounds

The decarboxylation may be reduced by the addition of a methyl group to the central carbon; this improves the stability of the compound (**85**) (Figure 2.4.1.3).

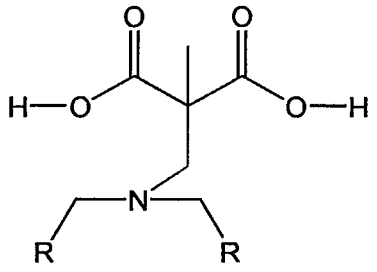

85

Figure 2.4.1.3: Structure of proposed methylated malonic acid group to prevent decarboxylation

The redesigned target molecule (**86**) can be prepared from three main reagents: the cyclen (**9**), the haloalkene 4-bromobut-1-ene (**78**), and the di-acid 2-(bromomethyl)-2-methylmalonic acid (**89**). The formation of the ligand arm occurs in several steps. The 2-(bromomethyl)-2-methylmalonic acid (**89**) is formed from the di-alcohol 2-(bromomethyl)-2-methylpropane-1,3-diol (**90**) by the oxidation of the primary alcohol group to a carboxylic acid, which is in turn synthesised from the oxetane 3-methyl-3-oxetanemethanol (**91**) by a ring-opening reaction. The 2-(bromomethyl)-2-methylmalonic acid (**89**) would need to be protected using a suitable ester protection group before the reaction with the cyclen ring (Figure 2.3.1.4).

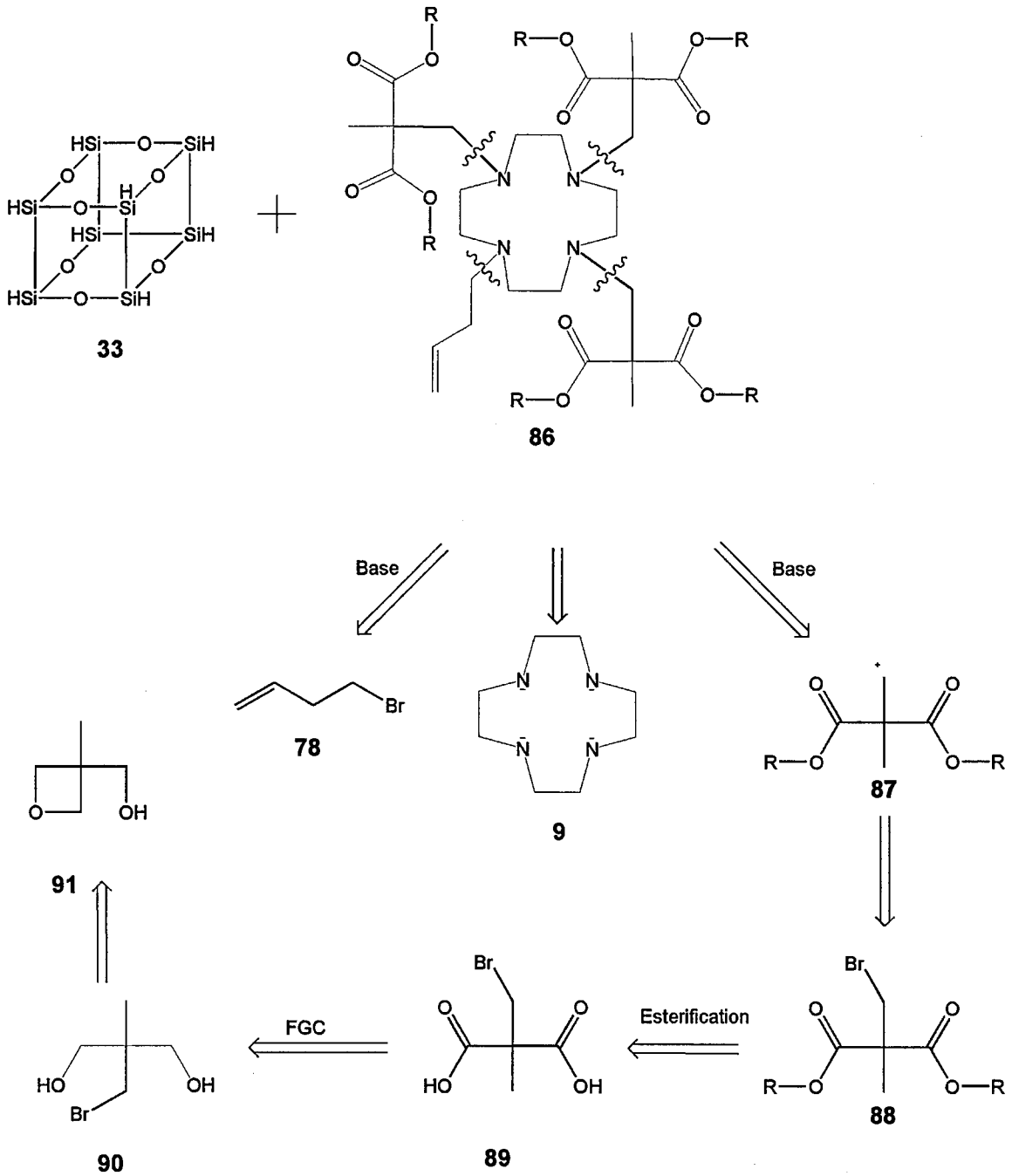

Figure 2.4.1.4: Retrosynthetic analysis of compound (86)

The first synthetic step in the synthesis of (**88**) is the ring-opening reaction of 3-methyl-3-oxetanemethanol (**91**) to form 2-(bromomethyl)-2-methylpropane-1,3-diol (**90**), catalysed by 40% hydrobromic acid added dropwise over one hour before

being heated to 90 °C for 16 hours (Figure 2.4.1.5). The reaction was cooled to 4 °C, at which temperature the product crystallises out of solution. The crystals were taken up into DCM and dried over magnesium sulfate, giving rise to a white solid product with a yield of 59%. The ^{1}H and ^{13}C NMR spectra correspond to the literature values.[89]

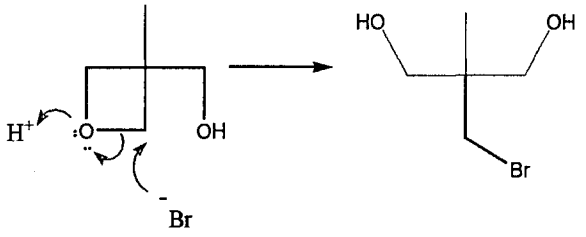

91 90

Figure 2.4.1.5: Mechanism for the formation of 2-(bromomethyi)-2-methylpropane-1,3-diol (90)

Primary alcohols can be oxidised to form carboxylic acids by several strong oxidising agents. The oxidation of 2-(bromomethyl)-2-methylpropane-1,3-diol (**90**) occurs in two steps, of which the first is the oxidation of the alcohol groups to the corresponding aldehyde groups. The aldehyde is then oxidised to form the carboxylic acid. The oxidation is carried out using Jones' reagent; a solution of chromic acid and sulfuric acid, which is added to a solution of the di-alcohol dissolved in acetone.[88] Since the reaction is highly exothermic, the Jones' reagent is added dropwise over a period of one hour. After this addition, the reaction is stirred for 16 hours at room temperature (Figure 2.4.1.6).

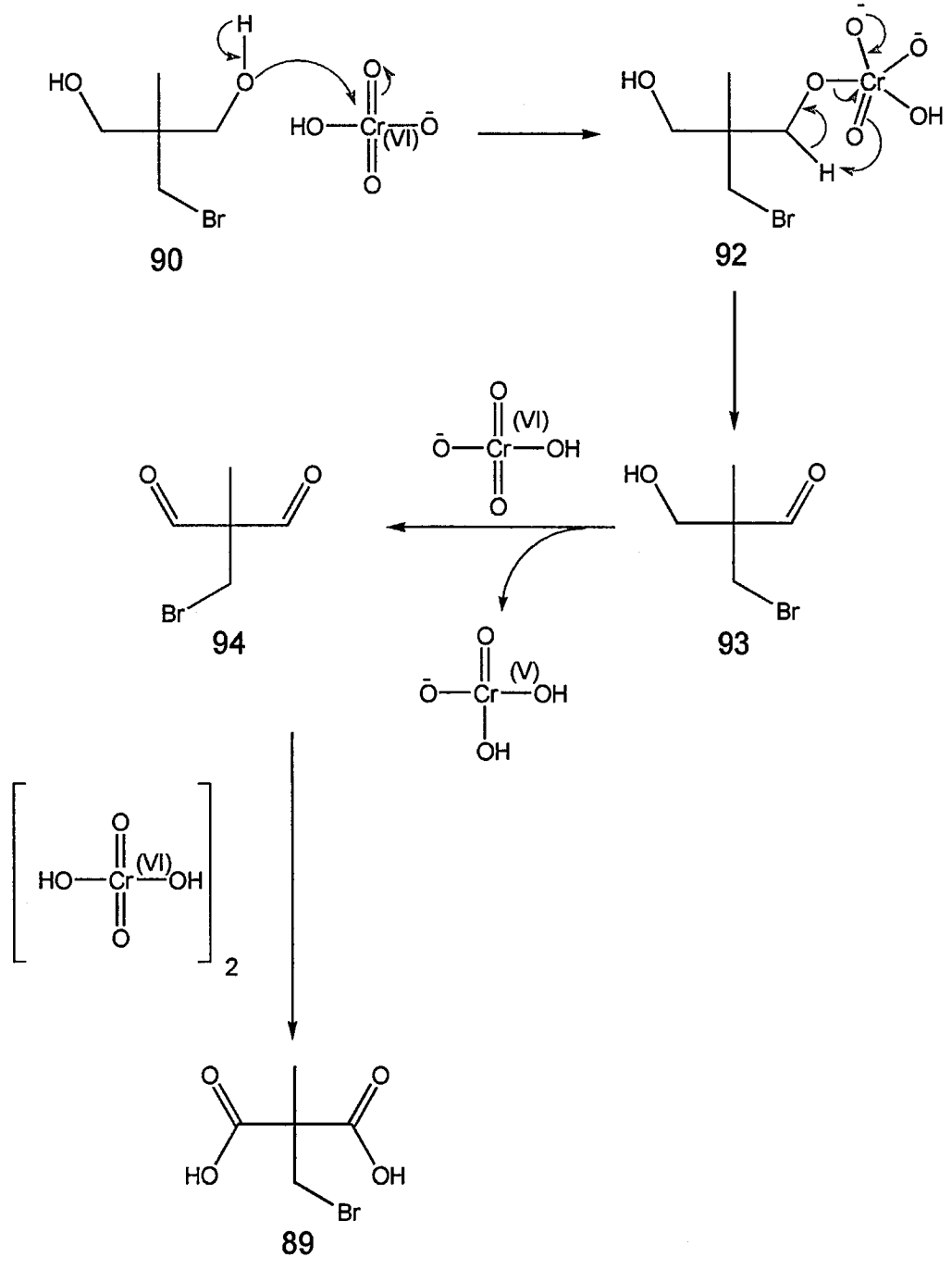

Figure 2.4.1.6: Formation of 2-(bromomethyl)-2-methylmalonic acid (89) from 2-(bromomethyl)-2-methylpropan-1,3-diol (90) via Jones' reagent in acetone

The reaction mixture was then poured into methanol (100 ml) and stirred for 30 minutes in order to quench the remaining $Cr^{(VI)}$ to $Cr^{(V)}$. The reaction changes colour from red to green during the quenching, owing to the reduction of the Cr^{6+} to Cr^{3+}. Methanol and acetone are removed using reduced pressure and the acid is

extracted from the aqueous layer using chloroform (2 x 50 ml) and diethyl ether (4 x 200 ml). The combined organic phase is dried and the solvent removed using reduced pressure. The reaction gives yields greater than 46%. The ^{1}H and ^{13}C NMR spectra matched the published data, and gave a MP of 128.1 °C compared to the literature value of 126.5 °C. [90]

The next step is the protection of the carboxylic acids by the formation of esters with a suitable protection group. Methanol was used in the first attempt, to form dimethyl 2-(bromomethyl)-2-methylmalonate (**96**) (Figure 2.4.1.7).

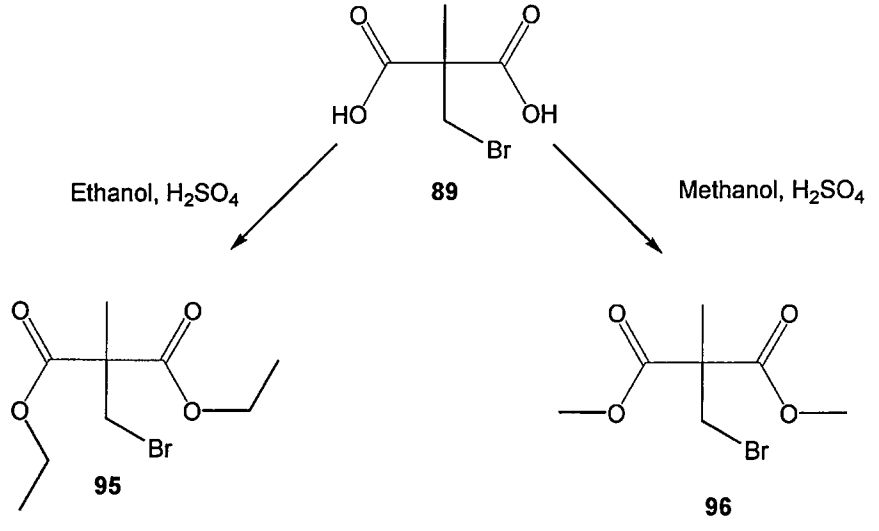

Figure 2.4.1.7: Formation of ester-protected 2-(bromomethyl)-2-methylmalonic acid

The reaction produced a monomethyl ester, 2-(methoxycarbonyl)-3-bromo-2-methylpropanoic acid (**114**), after 24 hours and showed no sign of the diester product by LCMS analyses. The reaction of the dicarboxylic acid with ethanol under the same conditions produced a trace amount of diethyl 2-(bromomethyl)-2-methylmalonate (**112**), in a yield of less than 2% (Figure 2.4.1.8)

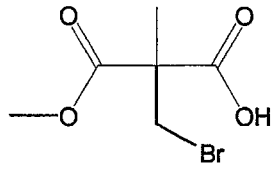

97

Figure 2.4.1.8: Structure of 2-(methoxycarbonyl)-3-bromo-2-methylpropanoic acid (97)

With no trace of the intermediate monomethyl ester compound (**97**) and the starting material, it was proposed that the starting material was being lost though decarboxylation of 2-(bromomethyl)-2-methylmalonic acid (**89**) to form 2-methylpropanoic acid (**99**). The decarboxylation also presented a major problem for the stability of the mDO3A–La complex, as any loss of a ligand arm would destabilise the complex[88, 91] (Figure 2.3.1.9).

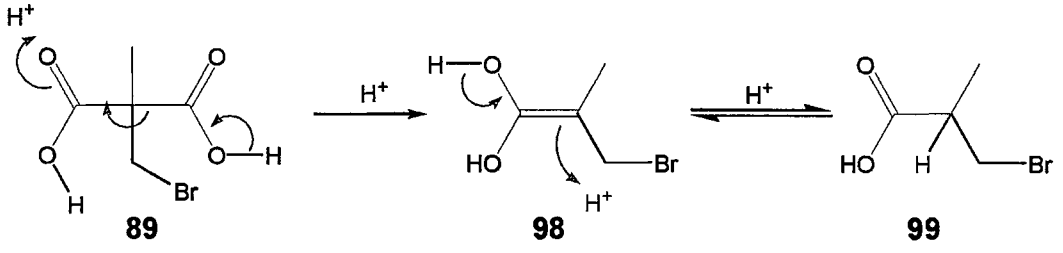

89 **98** **99**

Figure 2.4.1.9: Proposed mechanism for the decarboxylation of 2-(bromomethyl)-2-methylmalonic acid (89)

2.5.1: Synthesis of a succinic acid substituted cyclen (9), butene-sDO3A

Since the synthesis of mDO3A (**86**) was not feasible, an alternative molecule was proposed utilising succinic acid as the di-acid arm instead of malonic acid. Succinic acid (**100**), with its additional CH_2, would prevent the decarboxylation step from occurring (Figure 2.5.1).

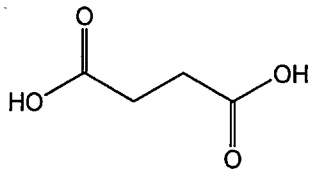

100

Figure 2.5.1.1: Structure of succinic acid (100)

The amount of cross-binding occurring should be lower than with the glutaric-based gDO3A (**25**), owing to the increased ring strain induced by the smaller ring system formed. The target molecule sDO3A (**32**) could be split into three reagent molecules; the core of the molecule was as before, cyclen (**9**); the ligand arms would be succinic acid (**100**); and the linking arm would be a haloalkene such as 4-bromobut-1-ene (**78**) (Figure 2.5.1.2).

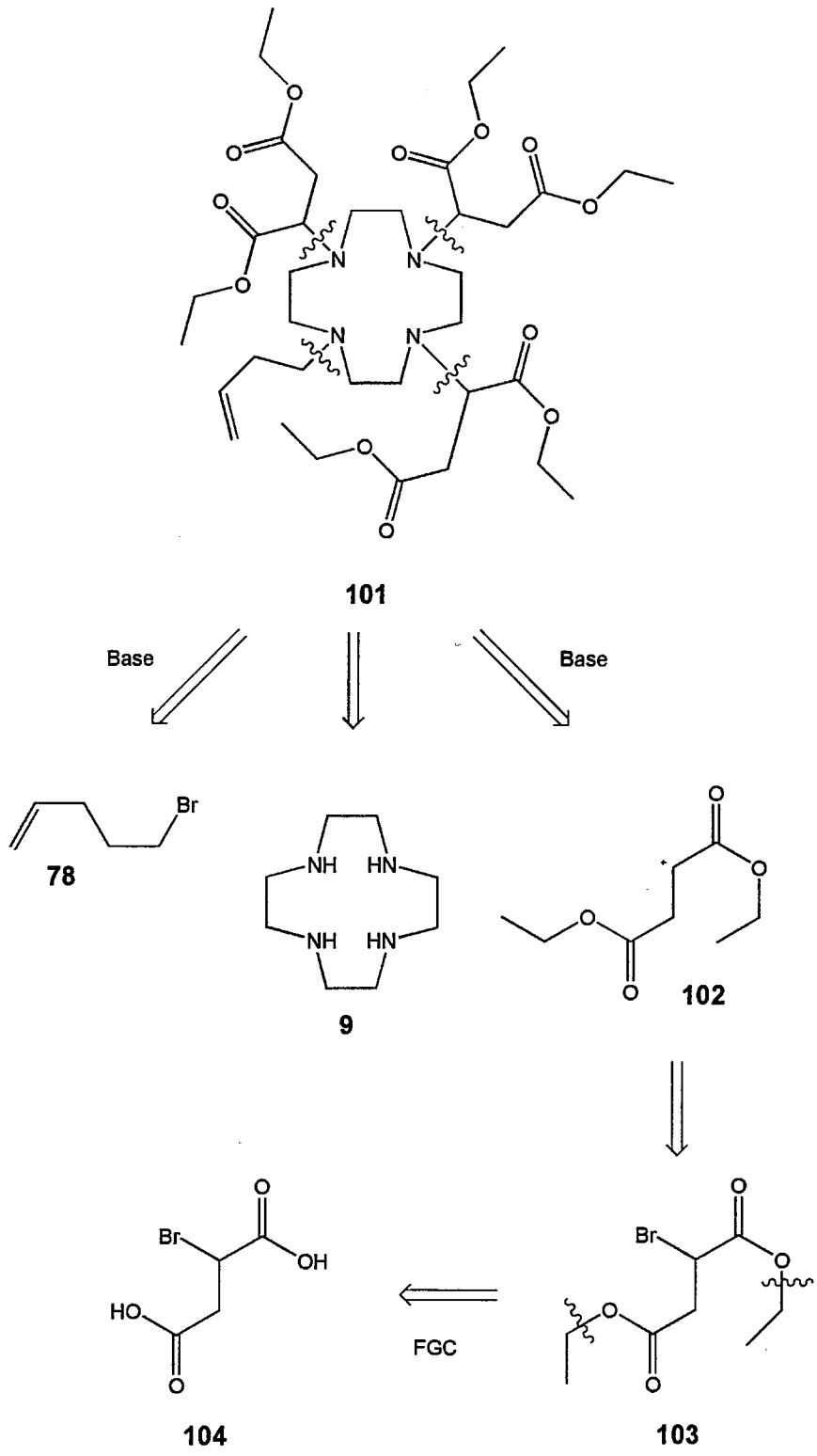

Figure 2.5.1.2: Retrosynthetic analysis of butene-sDO3A (101)

2.5.2: Synthesis of butene-sDO3A-(ethyl) (101)

As described in earlier routes, there are two possible pathways for the synthesis of butene-sDO3A-(ethyl) (**101**). Route C (figure 2.5.2.1) was the 1+3 route, while Route D (figure 2.5.2.1) was the 3+1 route. The first step in Route C (1+3) was the selective alkylation of the cyclen molecule with 4-bromobut-1-ene (**78**), to form compound (**106**). The direct alkylation of cyclen with 4-bromobut-1-ene (**78**) would result in multiple alkylation of the cyclen (**9**), and so protection groups are needed to prevent that from occurring. The second step, after deprotection of the remaining nitrogens, was the alkylation of the three remaining nitrogen atoms with the diethyl 2-bromosuccinate (**103**) to give the ethyl-protected butene-sDO3A-(ethyl) (**101**) (Figure 2.4.2.1).

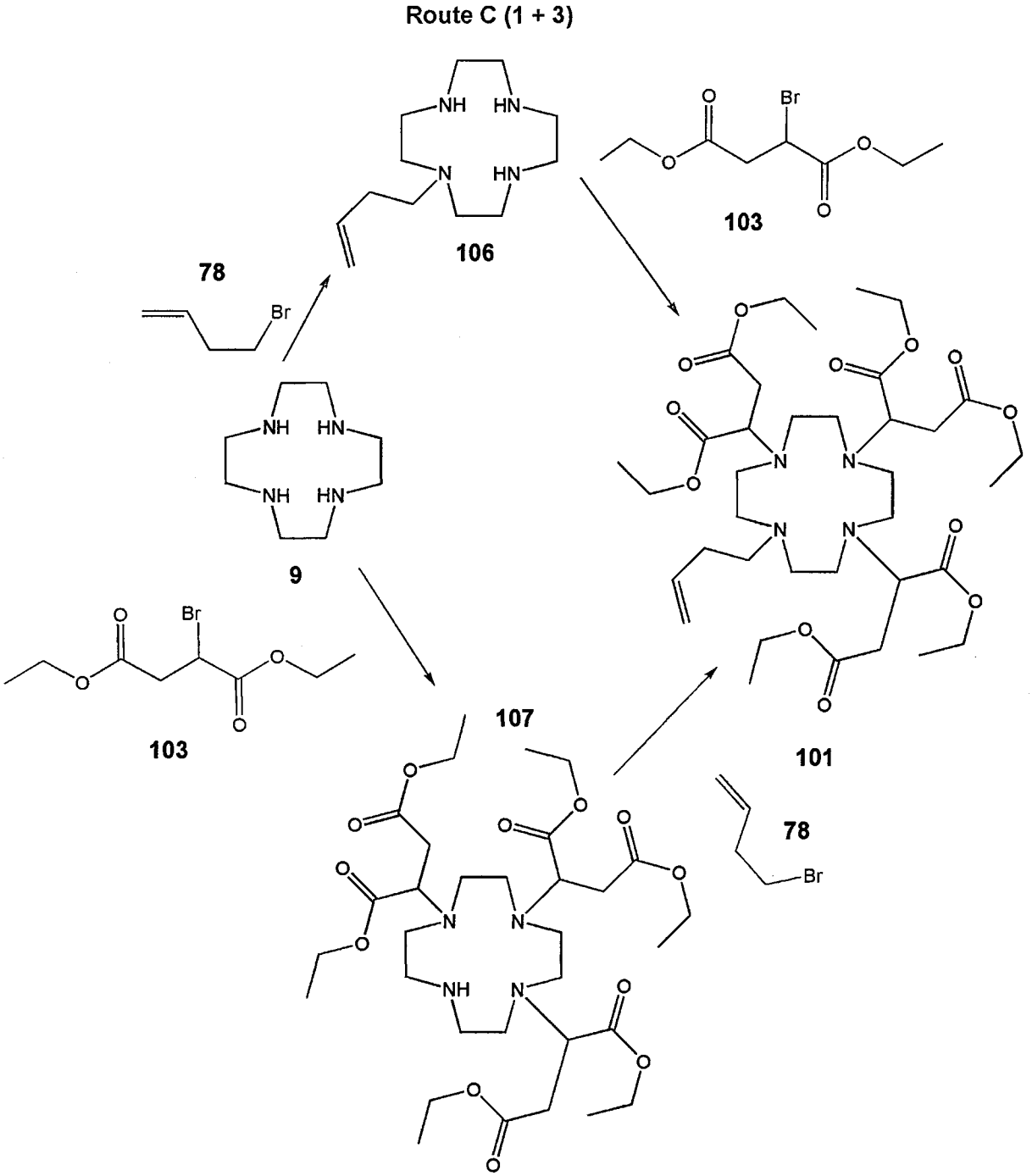

Figure 2.5.2.1: Routes C (1+3) and D (3+1) for the synthesises of butene-sDO3A (101)

The first step in Route D (3+1) was the alkylation of the cyclen with diethyl 2-bromosuccinate (**103**) to give sDO3A-(ethyl) (**107**). The second was the alkylation of sDO3A-(ethyl) (**107**) using 4-bromobut-1-ene (**78**) to give butene-sDO3A-(ethyl)

(**101**). The key for this route was the prevention of over-alkylation to yield sDO4A-(ethyl) (**110**), or under-alkylation to yield sDO1A-(ethyl) (**108**) and sDO2A-(ethyl) (**109**) (Figure 2.5.2.2). As the possible compounds have similar chemical properties, owing to the presence of amines and ethyl esters, they would need to be carefully separated using chromatographic methods.

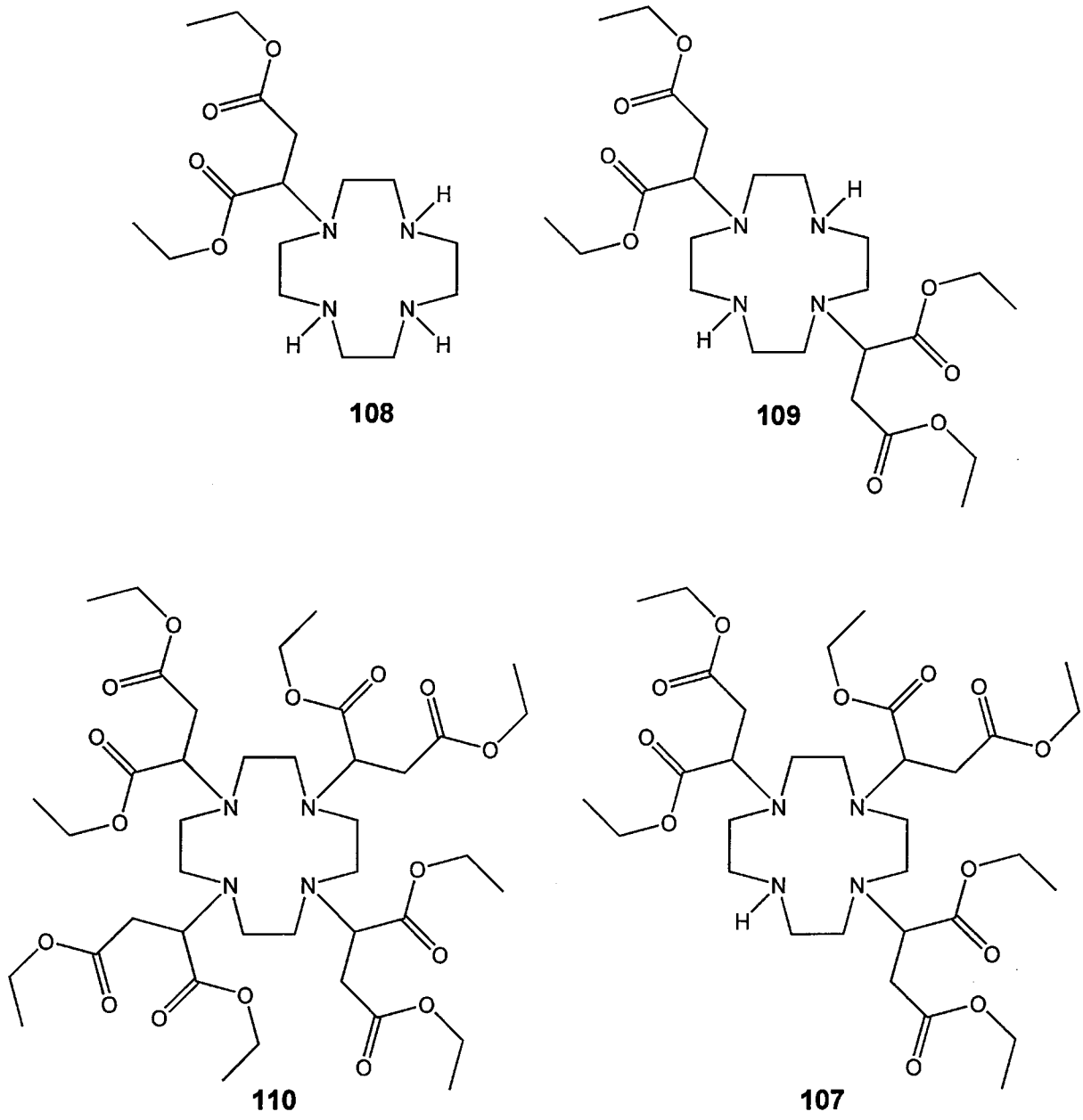

Figure 2.5.2.2: The four possible products from the reaction of cyclen (52) with diethyl 2-bromosuccinate (103)

2.5.3: Synthesis of butene-sDO3A-(ethyl) (101) by Route C (1+3)

The first step in the synthesis of the target molecule was the alkylation reaction between 4-bromobut-1-ene (**78**) and cyclen (**9**) to give the monosubstituted cyclen 1-but-3-en-1-yl-1,4,7,10-tetraazacyclododecane (**106**) (Figure 2.5.3.1).

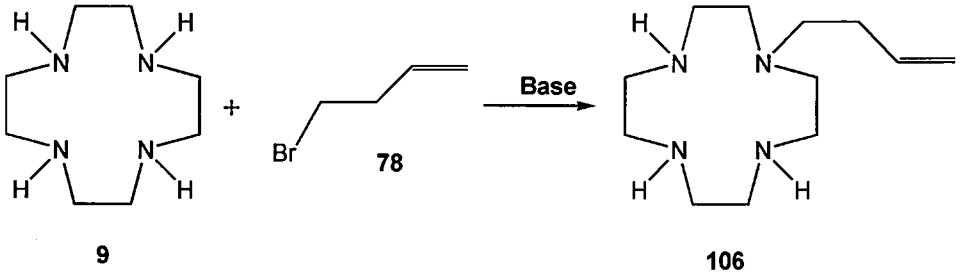

Figure 2.5.3.1: Formation of the mono-alkene cyclen, 1-but-3-en-1-yl-1,4,7,10-tetraazacyclododecane (106)

4-bromobut-1-ene (**78**), dissolved in acetonitrile, was added to the cyclen (**9**) as a cooled solution (−10 °C), dropwise over 4 hours. The reaction was monitored by LCMS, which showed the formation of the monoalkene cyclen (**106**), but with significant amounts of the di-alkene and tri-alkene substituted cyclens as seen by LCMS. Unfortunately it was not possible to separate these compounds, owing to their close R_f values (MeOH (5%) $CHCl_3$ (95%) Silica).

To overcome the over-alkylation, a protected cyclen methodology was sought. The first protected cyclen was triformylcyclen (**74**) from section 2.2.3, which was then reacted in anhydrous acetonitrile with a large excess of 4-bromobut-1-ene (**78**) using potassium carbonate as the base. The reaction was monitored using LCMS and was shown to reach completion after 72 hours. The solid residues were removed by

filtration and the solvent and the remaining 4-bromobut-1-ene (**78**) were removed using reduced pressure, yielding an oil (Figure 2.5.3.2).

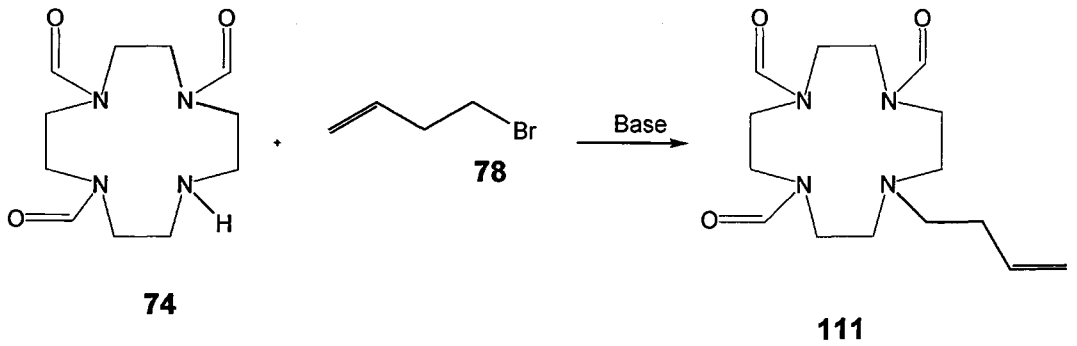

74 **78** **111**

Figure 2.5.3.2: Formation of 10-but-3-en-1-yl-1,4,7,10-tetraazacyclododecane-1,4,7-tricarbaldehyde (111).

During the alkylation step one of the formyl groups was lost, leading to the formation of a di-alkene cyclen (**112**) (Figure 2.5.3.3).as characterised by LCMS which showed both products (**111**) and (**112**) at 311.31 [M(**111**)$^{+H}$] and respectively 337.51 [M(**112**)$^{+H}$]. This loss of the formyl group was from hydrolysis caused by the base in the reaction. The separation of these two alkenes on alumina, eluting with DCM (90%) and MeOH (10%), was unsuccessful, producing a product in a yield of 19% which, by LCMS, was shown to be a mixture of compounds (**111**) and (**112**) 311.21 [M(**111**)$^{+H}$], 337.61 [M(**112**)$^{+H}$].

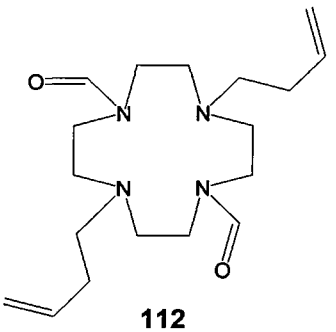

112

2.5.3.3: Side product of the alkylation reaction

Owing to the problems with the triformylcyclen, an alternative protection method was attempted. The tri-protected cyclen, octahydro-5H-2a,4a,7,9a-tetraazacycloocta[1,2,3-cd]pentalene (**113**) has been reported as having been used in a number of syntheses for the formation of monosubstituted cyclens.[92, 93] The advantage of this substrate was that the protecting group can be removed using aqueous acid or alkaline solutions, but it was stable in anhydrous conditions.

Octahydro-5H-2a,4a,7,9a-tetraazacycloocta[1,2,3-cd]pentalene (**113**) was synthesised from cyclen (**9**) and N,N-dimethylformamidedimethlyacetal (DMF-DMA) (**114**) in refluxing toluene. The solvent, along with by-products and excess reagents, was removed using reduced pressure to give a white, crystalline solid in a yield of 86% (Figure 2.5.3.4).

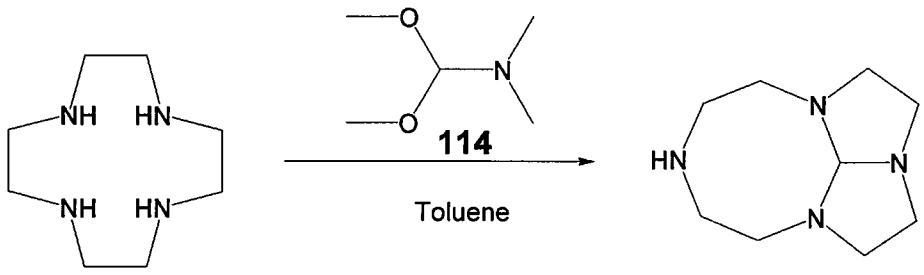

9 **113**

Figure 2.5.3.4: Reaction of cyclen (9) and DMF-DMA (113)

The product was confirmed by using both ^{1}H and ^{13}C NMR spectroscopy and comparison with the published data.[92, 93] The protecting group fixes the structure in one plane, forming a rigid system of 5- and 8-membered rings. This structure presents the lone pair of the unprotected amine to the outside of the ring system. The 4-bromo-but-1-ene (**78**) will undergo reaction with the lone pair of the protected

cyclen (**113**) to give the monosubstituted cyclen 7-but-3-en-1-yloctahydro-5H-2a,4a,7,9a-tetraazacycloocta[1,2,3-cd]pentalene (**115**). To prevent the 4-bromobut-1-ene (**78**) from undergoing decomposition, the reaction must be kept at a low temperature for the first 3 hours, after which the temperature was slowly raised to 25 °C. The product was purified by flash-column chromatography, using neutral alumina as the stationary phase to avoid deprotection of the cyclen and subsequent binding of the deprotected cyclen to the stationary phase. The chromatography column was eluted using a mixture of 97% chloroform with 3% methanol yielding 30% product, which was shown to be pure by a single LCMS ion peak at 237.18 [M(**115**)$^{+H}$] and the integration of the ^{1}H NMR spectra which showed the correct number of protons for the alkene and the cyclen. (Figure 2.5.3.5).

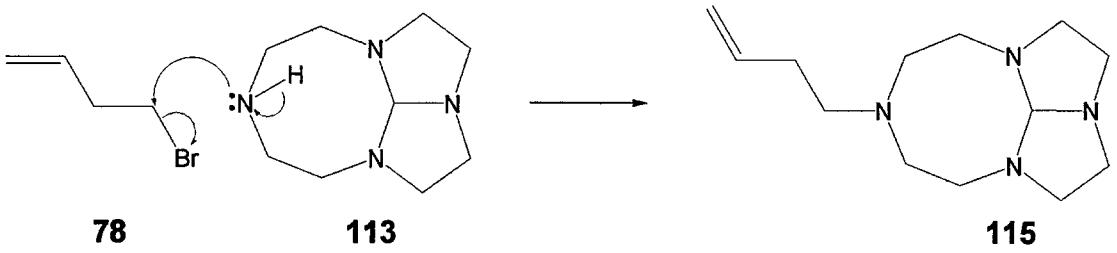

78 **113** **115**

Figure 2.5.3.5: Reaction of tricyclic amine (113) with 4-bromobut-1-ene (78)

The deprotection of the tricyclic alkene system (**115**) occurs in two steps. The first step was the hydrolysis of the protecting group to give the monoformamide 7-but-3-en-1-yl-1,4,7,10-tetraazacyclododecane-1-carbaldehyde (**121**). The second hydrolysis step was the removal of the formyl group to give the monoalkene-armed cyclen 1-but-3-en-1-yl-1,4,7,10-tetraazacyclododecane (**106**). The first hydrolysis was performed by refluxing the protected product in a solution of water and methanol (Figure 2.5.3.6).

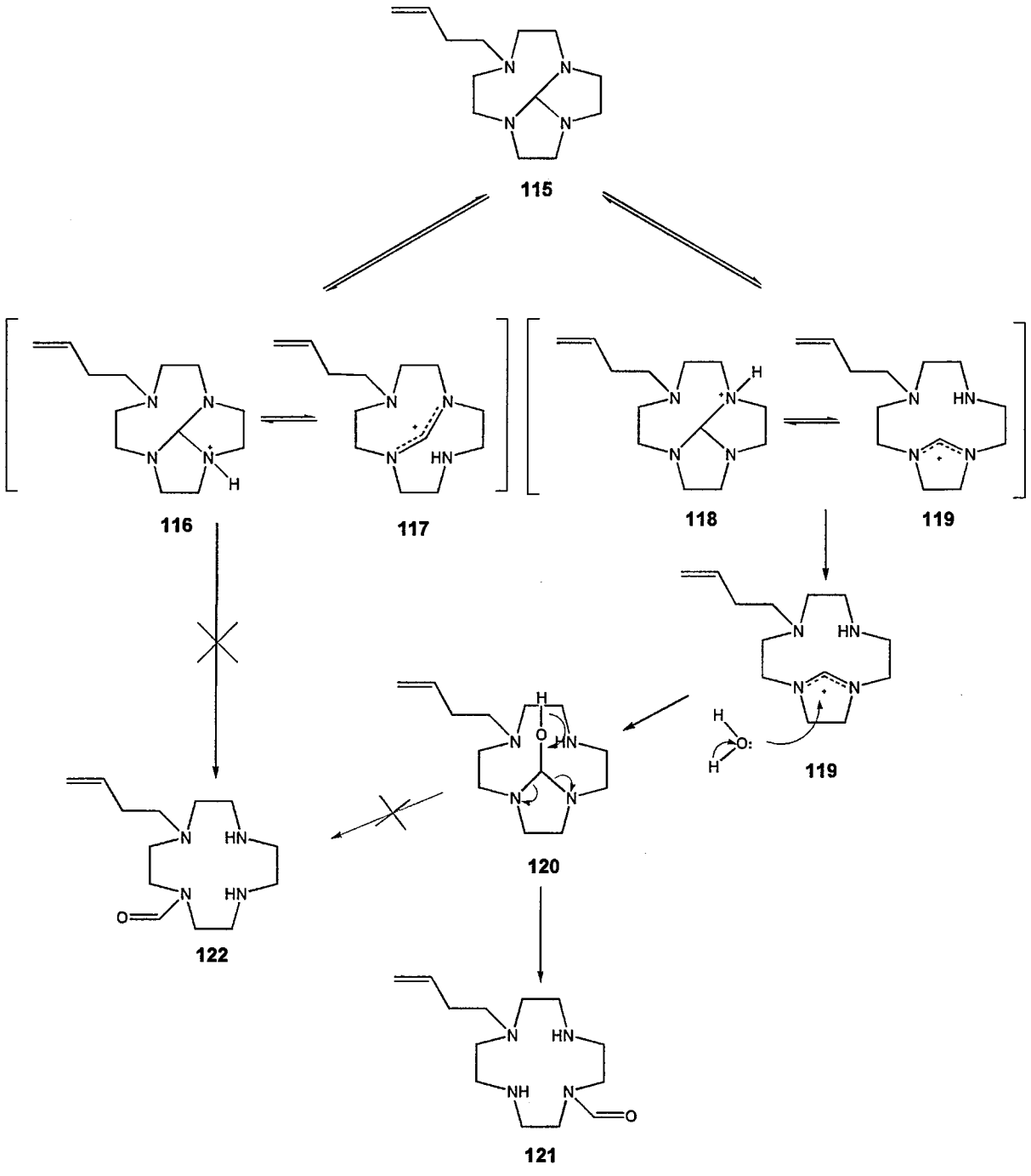

Figure 2.5.3.6: Reaction mechanism for the deprotection of compound (121).

This ring-opening step was highly regioselective for the formation of the 1,7-isomer (**121**), with only a trace of the 1,4 (**122**) isomer. The isomers were identified in the reaction product by ^{1}H-^{1}H-COSY and ^{1}H-^{13}C-COSY NMR spectroscopy, where the differences in the symmetries of the CH_2 groups of the cyclen were observed.[94] In

particular, in the ^{13}C-NMR the 1,4 (**122**) compound would have 9 carbon environments, whereas the 1,7 (**121**) compound would have 13 carbon environments. The formation of the bicyclic intermediate (**117**) was possibly prevented by the strain induced by the CH group adjacent to the N-4 and N-10 nitrogens. The hydrolysis of the five-membered ring in (**118**) would be expected to give both of the isomers (**121**) and (**122**), after carbonyl formation in the last step. The possible mechanism by which the 1,7(**121**) isomer was obtained as the main product could involve the addition of a water molecule to the cation (**119**), since the protonation of the N-10 nitrogen was more favourable than that of the N-7 nitrogen, owing to the interaction with N-1; the interactions with N-7 and N-4 are less favourable owing to N-4 being protonated.[95]

The removal of the formyl group may be carried out with either weakly acidic or basic conditions. As the use of an acid was inconvenient, owing to the loss of the alkene group in the presence of strong acids, the reaction was performed under basic conditions. The first alkali used was potassium hydroxide. The crude material was dissolved in methanol and added to potassium hydroxide (0.2M solution) and refluxed for 24 hours, after which the pH of the reaction was then carefully lowered to pH 7.00 using hydrochloric acid. The solvent was removed using reduced pressure to yield a white solid. The product was extracted using a biphasic method with dichloromethane and water; the organic layer was separated to yield a clear, yellow oil. The NMR analysis showed that the reaction was incomplete and consisted as a mixture of the N-4 and N-7 formyl isomers together with the monosubstituted cyclen (**106**) and cyclen (**9**). Presumably the addition of hydrochloric acid caused the decomposition of the alkene–cyclen (**106**), giving back the cyclen (**9**) starting material.

The second base attempted was ammonium hydroxide, which had the advantage of being volatile, allowing its removal by reduced pressure and thus limiting the need for acid neutralisation of any excess base. 7-but-3-en-1-yl-1,4,7,10-tetraazacyclododecane-1-carbaldehyde (**121**) was dissolved in 2% ammonia solution and heated to 105 °C in a sealed tube. The solvent was removed using reduced pressure to give a yellow transparent oil in a yield of 64% (Figure 2.5.3.7). The compound (**106**) was characterised by ^{1}H NMR spectra which showed the correct integration and peak pattern, ^{13}C NMR spectra showed that the carbonyl had been removed and that there was only 4 carbon environments on the cyclen. The LCMS showed single ion peak at (227.24 [M(**106**)$^{+1}$]), while the FTIR showed the absence of the carbonyl peak at 1980 cm^{-1}.

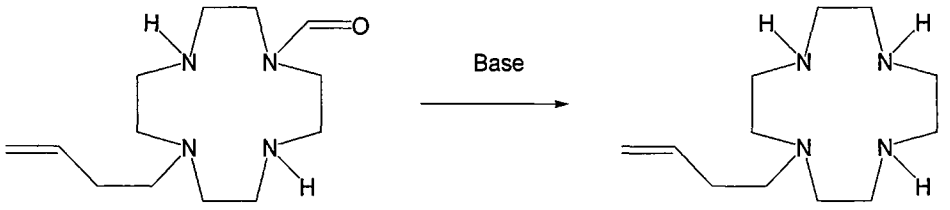

121 **106**

Figure 2.5.3.7: Hydrolysis of (121) to form 1-but-3-en-1-yl-1,4,7,10-tetraazacyclododecane (106)

2.5.4: Synthesis of diethyl 2-bromosuccinate (103)

The next step in the reaction with 1-but-3-en-1-yl-1,4,7,10-tetraazacyclododecane (**106**) was the addition of the succinate groups, to form butene-sDO3A-(ethyl) (**101**). This was achieved using 2-bromo-succinic acid. As the acid groups would cause problems with the hydrosilylation reaction later, they would have to be protected as

ethyl esters to give diethyl 2-bromosuccinate. Diethyl 2-bromosuccinate (**103**) was formed by the esterification of 2-bromo-succinic acid (**104**) in ethanol, with sulfuric acid as the catalyst. This reaction produced the diethyl ester, diethyl 2-bromosuccinate (**103**), in yields of greater than 89%. The diethyl 2-bromosuccinate (**103**) was then stored under argon and molecular sieves (type 3A) to remove any residual water. The diethyl 2-bromosuccinate (**103**) was confirmed by ^{1}H and ^{13}C NMR spectra, both of which showed the presence of the ethyl groups, while the ^{13}C NMR spectra also showed the down field shift of the carbonyl from 177ppm to 169ppm corresponding to the formation of the ethyl ester group. The FTIR showed a stretch at 1739 cm^{-1} which corresponds to the carbonyl of the ethyl ester group and LCMS which showed two ion peaks the first at 253 [M(103)$^{+H}$] which corresponds to the target molecule with a second at 174 [M(103) – Br^{+H}] which shows the target molecule with the loss of the bromide due to ionization conditions of the LCMS. (Figure 2.5.4.1).

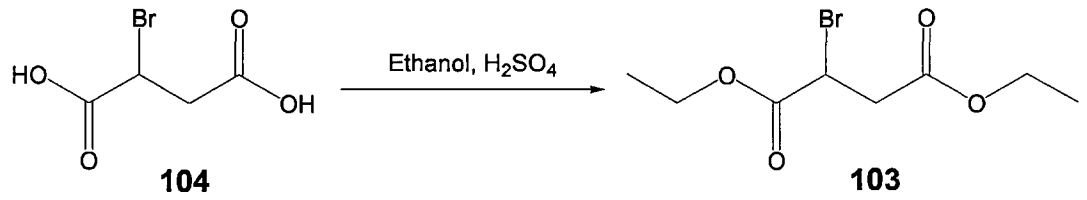

Figure 2.5.4.1: Synthesis of diethyl 2-bromosuccinate (103).

2.5.5: Synthesis of butene-sDO3A-(ethyl) (101) from 1-but-3-en-1-yl-1,4,7,10-tetraazacyclododecane (106)

The final step in this (1+3) strategy was the formation of butene-sDO3A-(ethyl) (**101**). The 1-but-3-en-1-yl-1,4,7,10-tetraazacyclododecane (**106**) was dissolved in

anhydrous acetonitrile, along with potassium carbonate. To this solution, excess diethyl 2-bromosuccinate (**103**) in anhydrous acetonitrile was added dropwise over several hours. The reaction was then heated to reflux for 48 hours (Figure 2.5.5.1).

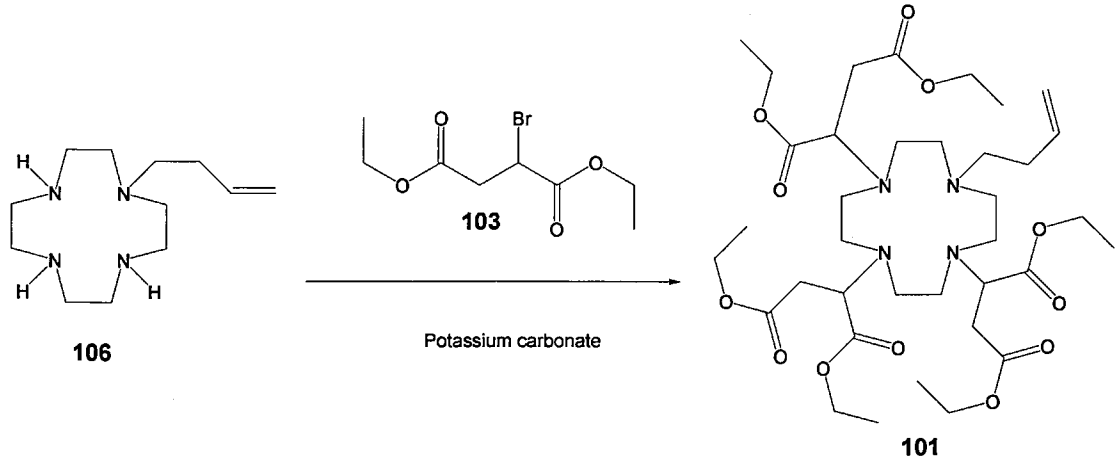

Figure 2.5.5.1: Synthesis of butene-sDO3A-(ethyl) (101)

LCMS analysis showed that the compound had formed small amounts of the trisubstituted cyclen (**123**), along with large amounts of the disubstituted species (**124**), this was seen as two ion peaks at 571.32 [M(**123**)$^{+H}$], 398.12 [M(**124**)$^{+H}$]. The ^{1}H NMR could not distinguish between compounds (**123**) and (**124**). There was no evidence of the target molecule, and modification by increasing the amount of diethyl 2-bromosuccinate (**103**) and/or reaction time did not improve the reaction.

The failure of the reaction could have been due to two factors. The first factor could have been due to the increasing amount of steric hindrance with every diester arm attached, because of the size of the diethyl succinate group (Figure 2.5.5.2). The second was that there was the possibility of the diethyl 2-bromosuccinate (**103**) undergoing an elimination reaction forming an alkene with the elimination of HBr. This elimination of HBr to form the corresponding alkene was not reported in similar

work by Parker[19] were the dimethyl 2-bromoglutamate and dimethyl 2-bromoadipate were reacted with cyclen to form gDO3A (**25**) and aDO3A (**26**)

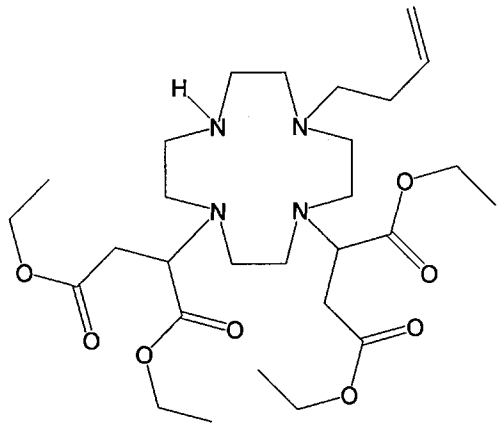

123

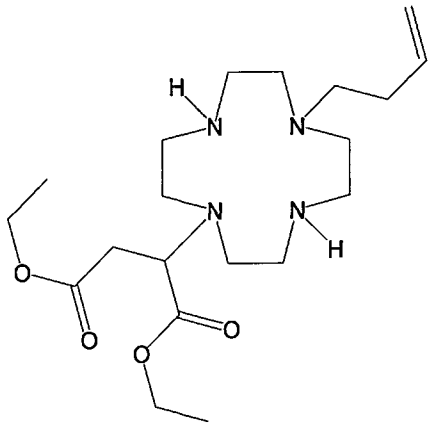

124

Figure 2.5.5.2: By-products from the formation of butene-sDO3A-(ethyl) (101)

2.6.1: Route D (3+1) for the synthesis of butene-sDO3A-(ethyl) (101)

Since the incomplete alkylation of (**106**) produced compounds (**123**) and (**124**), the alternative Route D (3+1) was investigated. The first step investigated was based on the synthesis of gDO3A (**25**), where dimethyl 2-bromoglutamate was reacted with cyclen (**9**).[96] In this case dimethyl 2-bromoglutamate was replaced with diethyl 2-bromosuccinate (**103**) (Figure 2.6.1.1).

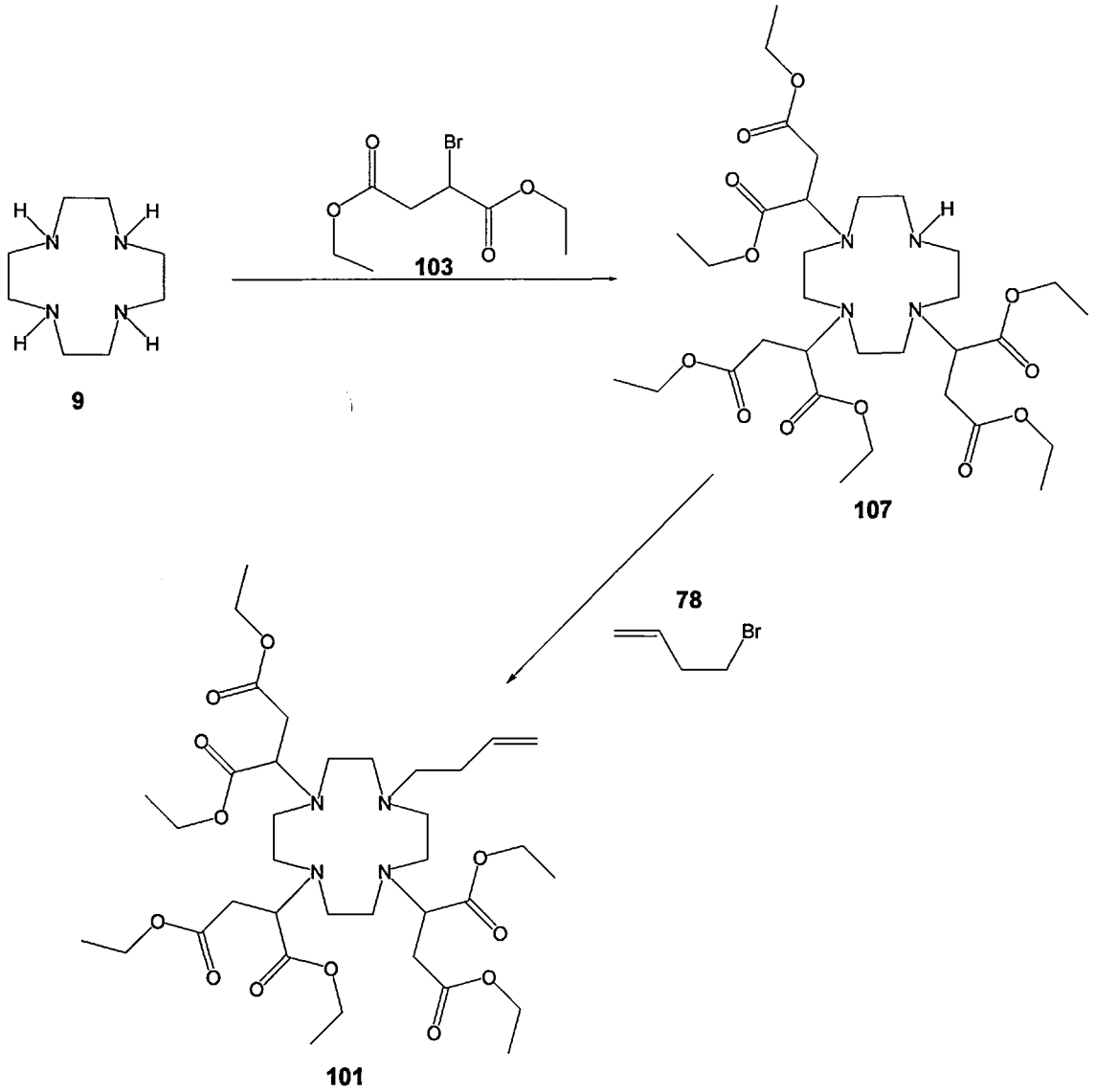

Figure 2.6.1.1: The 3+1 route for the formation of butene-sBDO3A-(ethyl) (101)

Cyclen (**9**) dissolved in anhydrous acetonitrile was reacted with diethyl 2-bromosuccinate (**103**) (3.1 eq) in the presence of potassium carbonate (3.4 eq). As this reaction was exothermic, the diethyl 2-bromosuccinate (**103**) was added in small aliquots of 0.5 ml and kept at −15 °C using a refrigerant bath consisting of crushed ice, industrial methylated spirits (IMS) and sodium chloride. The reaction was then left to stir under argon for 24 hours, while the refrigerant bath was allowed to warm up to room temperature over time. After this step samples were tested by LCMS,

which showed that the reaction did not go to completion, as only sDO1A-(ethyl) (**108**) and a trace of sDO2A-(ethyl) (**109**) could be identified.

To force the reaction in the direction of the desired product, another volume of diethyl 2-bromosuccinate (**103**) (1.3 eq) was used in the reaction, which was stirred for a further 24 hours. The reaction mixture was then filtered and the solvent was removed using reduced pressure. The crude product was shown by LCMS to consist of mainly sDO2A-(ethyl) (**109**), with a trace of sDO3A-(ethyl) (**107**). The products, sDO2A-(ethyl) (**109**) and sDO3A-(ethyl) (**107**), run at similar R_f values of 0.15 and 0.20 (MeOH (5%), $CHCl_3$ (95%)), which makes TLC monitoring of the reaction of limited use. The properties of the possible products are shown in Table 2.6.1.1.

.Compound	*Mass*	M^{+1}
Cyclen	172.17	173.17
sDO1A-(ethyl) (**108**)	344.24	345.24
sDO2A-(ethyl) (**109**)	516.32	517.32
sDO3A-(ethyl) (**107**)	688.39	689.39
sDO4A-(ethyl) (**110**)	860.46	861.46
Diethyl 2-bromosuccinate (**103**)	252	174.08*

Table 2.6.1.1: The [M^{+1}] ions of the starting material and the products of formation of sDO3A-(ethyl) (* = [M–Br]$^{+1}$ ion)

While the conditions of the LCMS were kept as gentle as possible (i.e. low voltage), to stop any fragmentation of the molecules, the diethyl 2-bromosuccinate (**103**)

appeared as the [M(**103**)–Br]$^{+1}$ ion, owing to electron impact-induced halogen elimination of the bromide ion.[97, 98] It should be noted that the percentage values measured by LCMS are qualitative, owing to the ease of ionisation of the compound. Both sDO2A-(ethyl) (**109**) and especially sDO3A-(ethyl) (**107**) can stick to the ionisation cone of the mass spectrometer for a substantial amount of time, and can distort the results of following measurements. This was compensated for by allowing a suitable time between runs and the use of base-line subtraction from the ion peak in the recording of the spectra. The crude reaction was chromatographed on silica eluted with chloroform (95%) and methanol (5%), producing sDO3A-(ethyl) (**107**) in 2.25% yield, as shown by ^{1}H spectra where the integration of the ethyl groups was in proportion to the protons in the cyclen / succinic groups at 1.21 ppm (H18, t, 4.7 Hz) and 2.52–2.91 (H22, m) respectively. The ^{13}C NMR spectra showed the presence of the carbonyl carbons at 170.94 ppm and 171.29 ppm and the secondary carbon attached to the amine at 60.70 ppm. The FTIR which showed stretches associated with both with the ethyl ester (1737 cm^{-1}) and amine (1464 cm^{-1}). The LCMS showed the product at 689.37 [M(**107**)$^{+H}$] and 728.37 [M(**107**)+ K^{+H}]

.

To increase the yield, the number of equivalents of diethyl 2-bromosuccinate (**103**) was increased from 4.2 to 6.2 equivalents relative to cyclen (**9**). The reaction conditions were the same as before. The reaction was monitored over a period of 72 hours by LCMS and was refluxed until there was no presence of sDO1A-(ethyl) (**108**) signal and the signal for sDO2A-(ethyl) (**109**) on the LCMS has been reduced as much as possible when compared to the sDO3A-(ethyl) (**107**) signal. While this was not an accurate method of determining reaction product percentages, it was a good indication of the progress of the reaction. The reaction mixture was centrifuged

to compact the solids into a pellet, allowing the solvent layer to be decanted. The solvent was then removed using reduced pressure, yielding an oil that contained sDO2A-(ethyl) (**109**), sDO3A-(ethyl) (**107**), and diethyl 2-bromosuccinate (**103**) (LCMS analysis). This reaction method was used as a "universal method" for the syntheses of sDO3A-(ethyl) (**107**), which was used to produce the crude product for the following purification methods.

The first method of purification, taken from the literature, was based on biphasic solvent separation, by which the isolation of gDO3A-(methyl) was performed.[96] The crude product was taken up into DCM and then washed with water to remove the excess diethyl 2-bromosuccinate (**103**), sDO1A-(ethyl) (**108**) and any remaining potassium carbonate and cyclen (**9**). While the water removed the sDO1A-(ethyl) (**108**), it did not completely remove the sDO2A-(ethyl) (**109**), as shown by LCMS. The resulting product was then chromatographed on silica gel using a mixture of DCM 70% and THF 30%, changing to DCM 66.5%, THF 30%, MeOH 3% and ammonium solution (33% strength) 0.5% as the eluent. This process separated the two compounds, but only by a small amount, as they eluted at virtually the same time from the column. The reaction gave yields of less than 1.1% of sDO3A-(ethyl) (**107**). As this compound would be needed for several further steps, this was not a feasible method of purification of the compound. The second purification method attempted involved column chromatography. Several solvent systems were investigated for the separation of the crude reaction product, along with different stationary phases (Table 2.6.1.2). The solvent strength was calculated using *Equation 2.6.1.1* and Table 2.6.1.3.

Purification method	*Solvent 1*	*Solvent 2*	*Solvent 3*	*Solvent 4*	*Yield of sDO3A-Ethyl)*	*Solid Phase*	*Solvent strength*
1	DCM 66.5%	THF 30 %	MeOH 3%	Ammonia 0.5%	1.10%	Silica	0.48
2	DCM 95%	MeOH 5%	---	---	3.70%	silica	0.44
3	DCM 95%	MeOH 5%	---	---	Mixture	Alumina	0.44
4	DCM 70%	THF 30%	---	---	Mixture	Alumina	0.46
5	DCM 99%	MeOH 1%	---	---	5.60%	Alumina	0.42

Table 2.6.1.2: Results from comparative purification techniques

$$\frac{(solventA\%(strength)) + (solventB\%(strength))}{100} = eluant\_strength$$

Equation 2.6.1.1

Solvent	*Strength*
Methanol	0.95
Ethanol	0.88
Propan-2ol	0.82
Acetonitrile	0.65
Ethyl Acetate	0.58
THF	0.57
Acetone	0.56
DCM	0.42
Chloroform	0.40
Diethyl Ether	0.38
Toluene	0.29
Hexane	0.01

Table 2.6.1.3: Relative solvent strength based on polarity

The most effective solvent system for elution was a mixture composed of DCM 99% and MeOH 1%, using alumina as the stationary phase. This gave yields of around 5.5%, with minimum contamination of sDO2A-(ethyl) (**109**). The main obstacle was the excess diethyl 2-bromosuccinate (**103**) acting as a co-solvent in the chromatography column. The co-solvent effect was seen as an increase in the polarity of the solvent, which decreased the retention times. This was shown by co-spotting samples of the purified sample with and without the diethyl 2-bromosuccinate (**103**), which showed a marked difference in the Rf values. The

samples with diethyl 2-bromosuccinate (**103**) gave an Rf of 0.55, while the sample without diethyl 2-bromosuccinate (**103**) gave an Rf of 0.32 ($CDCl_3$ 99%, MeOH 1%).

2.7.1: A study of the reaction between cyclen and diethyl 2-bromosuccinate

The crude reaction product was produced using the "universal method" mentioned in Section 2.6.1 to see if an elimination reaction was occurring in the reaction for the formation of sDO3A-(ethyl). The TLCs of the reaction crude were rerun using glass-backed plates to which was bound Si-60 (Si-60 refers to the average size of the silica particles as 60 μm, this was comparable to the silica used in the column chromatography, where as the TLC media used in the previous TLC was a polymer backed with a silica gel partial size of 25 μm. With the closer partial of the TLC plates to that of the silica gel of the column chromatography, better models of the purification system could be produced and thus refine the chromatography technique. As the plates contain no fluorescent indicator, so were developed using a potassium permanganate spray. The plates were previously washed with the solvents used in the elution of the plates. This gives a plate which has a closer match of Rf values to that of the actual chromatography column under the same conditions.

A range of solvent combinations was explored. The aim was to adjust the polarity of the solvent so that the R_f of the target compound was 0.20, while the non-desired compounds were less than R_f 0.10 or greater than R_f 0.30. This led to an ideal eluent of DCM 95% and EtOH 5%. The chromatography columns used in the subsequent study were Sep-Pak columns containing 25 grams of Si-60 in a 60 ml syringe body. Sep-Pak was a pre-packaged, disposable chromatography cartridges supplied by

Waters (Milford, Massachusetts, USA) which have consistency between each cartridge. The column was primed using vacuum and eluting solvent, then 200 ml of eluting solvent was passed though the Sep-Pak to fully saturate the eluent. The Sep-Pak was then loaded with 500 mg of the crude oil and the solvent passed through, collecting the eluent in 20 ml fractions. The fractions were examined using a combination of TLC and LCMS. This method successfully separated the crude extract, giving a pure sample at R_f 0.19 for sDO3A-(ethyl) (**107**). The diethyl 2-bromosuccinate (**103**) was seen at R_f 0.91, while at R_f 0.55 a new compound was found. The new compound was diethyl maleate (**126**), which was confirmed by NMR, LCMS and FTIR analysis. The formation of the diethyl maleate (**126**) from diethyl 2-bromosuccinate (**103**) was confirmed by an experiment in which diethyl 2-bromosuccinate (**103**) was heated in the presence of potassium carbonate at 60 ^{o}C for 72 hours. This conversion was achieved with a yield of 87%.

2.8.1: Method for improving yields of the reaction between diethyl 2-bromosuccinate (103) and cyclen (9)

One possible method of improving yields would be to change the base (potassium carbonate) to a more reactive, such as caesium carbonate. The increase in reactivity by the use of caesium carbonate stems from two main factors. The first was the lower ion pairing of caesium carbonate compared to potassium carbonate, due to caesium having a lower charge density because of its increased cationic radius while retaining the same charge. This allows greater accessibility of the ion to the reaction. The second effect was that caesium carbonate was more soluble in acetonitrile than was potassium carbonate, allowing for a greater number of ions to be available. [99]

Caesium carbonate has been used in several cyclen (**9**) -based reactions once the cyclen (**9**) had already undergone substitution.[96, 100, 101] The caesium carbonate reactions were first performed in the same manner as those of the potassium carbonate reactions. The diethyl 2-bromosuccinate (**103**) was dissolved in acetonitrile and added dropwise over a period of two hours. LCMS showed that the main products of the reaction were as expected: sDO2A-(ethyl) (**109**) and sDO3A-(ethyl) (**107**). The crude extract was chromatographed on alumina using DCM (99%) and MeOH (1%) as the eluent. The product was isolated in a yield of 5.6% and characterised by ^{1}H, ^{13}C NMR and FTIR spectroscopy which were identical to the spectra for sDO3A-(ethyl) (**107**) produced by using potassium carbonate as the base with in the reaction. The LCMS showed the product at 689.38 [M(**107**)$^{+H}$].

Careful monitoring of the reaction by LCMS gave an indication that the reaction had not gone to completion. Since the cyclen (**9**) was soluble in the diethyl 2-bromosuccinate (**103**) the reaction was attempted using solvent free conditions, as a way of increasing the concentration. As the addition of the caesium carbonate was highly exothermic, the reactions were kept at low temperature in an ice/salt/IMS bath. The cyclen (**9**) was dissolved in 6.9 eq of diethyl 2-bromosuccinate (**103**), along with 4.8 equivalents of caesium carbonate. The reaction was heated at 60 °C for 24 hours. The LCMS suggested that the reaction had gone to completion, with no sign of sDO1A-(ethyl) (**108**) and sDO2A-(ethyl) (**109**) present. The reaction mixture was taken up into DCM and the solids removed. Since the LCMS showed that the only compounds in the crude product were sDO3A-(ethyl) (**107**) and excess diethyl 2-bromosuccinate (**103**), the crude product was washed with water, which removed the majority of the diethyl 2-bromosuccinate (**103**) from the organic layer. The organic

layer was washed with water to yield 6.6% of sDO3A-(ethyl) (**107**), with only a trace of diethyl 2-bromosuccinate (**103**). While a small amount of sDO3A-(ethyl) (**107**) would be expected to be lost in the water layer during the purification, its yield was still too low. The reaction was repeated with 9.6 eq of diethyl 2-bromosuccinate (**103**) with 5 eq of caesium carbonate. After 10 minutes the LCMS showed that the reaction contained a mixture of cyclen (**9**), diethyl 2-bromosuccinate (**103**) and both sDO1A-(ethyl) (**108**) and sDO2A-(ethyl) (**109**), but no sDO3A-(ethyl) (**107**). The reaction was then stirred for 48 hours at room temperature, after which the LCMS showed that the reaction contained sDO2A-(ethyl) (**109**) along with traces of sDO1A-(ethyl) (**108**) and sDO3A-(ethyl) (**107**). As the LCMS results suggested that the sDO3A-(ethyl) (**107**) had been produced only in trace amounts, the reaction was heated for another 48 hours at 60 °C. The LCMS showed that this reaction had produced mainly sDO3A-(ethyl) (**107**), with only a trace of sDO2A-(ethyl) (**109**). Critically, there was no sign of diethyl 2-bromosuccinate (**103**) being present. The reaction mixture was dissolved in DCM and the solids removed by centrifuge. The sample was split into two aliquots. The first sample underwent column chromatography on silica with elution with DCM (95%) and MeOH (5%), to yield a pure sample of sDO3A-(ethyl) (**107**) (1.1%), characterised by ^{1}H and ^{13}C NMR, FTIR spectroscopy and LCMS data which matched the known spectras for sDO3A-(ethyl) (**107**). The solvent from the second sample was removed and the sample purified using high-vacuum distillation. At 60 ^{0}C a white solid formed on the side of the condenser. No other products were extracted from the oil, as it had decomposed giving a viscous black oil.

2.8.2: Synthesis of (E)-3-(ethoxycarbonyl)acrylic acid (125)

The white solid obtained via the high-vacuum distillation was shown to be (E)-3-(ethoxycarbonyl)acrylic acid (**125**) by ^{1}H and ^{13}C NMR and FTIR spectroscopy, and had a melting point (MP) of 68 °C based on the literature values of 66–70 °C.[102, 103] The MP of the *cis* (Z) isomer was 180 °C[104]). The formation of the acrylic acid (**125**) could occur in two possible steps (Figure 2.8.2.1). The first step involves the formation of diethyl maleate (**126**) by the elimination of HBr, as with the side reaction seen with potassium carbonate in section 2.7.1. The second step involves the hydrolysis of diethyl maleate (**126**), with the alkene undergoing rearrangement to the (E) isomer, the acrylic acid (**125**). [103, 105]

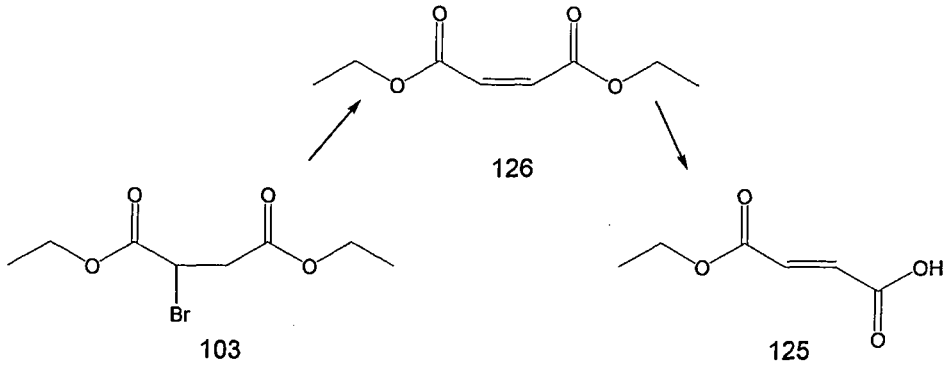

Figure 2.8.2.1: Reaction path for the synthesis of (E)-3-(ethoxycarbonyl)acrylic acid (125)

This pathway was confirmed by the reaction of diethyl 2-bromosuccinate (**103**) with caesium carbonate. Upon addition of the diethyl 2-bromosuccinate (**103**) to the carbonate, the reaction released a large amount of heat and HBr gas. The gas was identified by the use of wet pH indicators. LCMS and NMR spectroscopy showed that (E)-3-(ethoxycarbonyl)acrylic acid (**125**) had been formed, and the sample had

the strong smell associated with acrylic acids. The reaction was then heated to 60 °C for 1 hour, giving a mixture of diethyl 2-bromosuccinate (**103**) and (E)-3-(ethoxycarbonyl)acrylic acid (**125**), as shown by the ^{1}H spectra which showed protons at 7.66ppm with C-C coupling as associated with the trans isomer at 15.70 Hz. The ^{13}C NMR spectra showed that there were six different carbon environments present at 14.05, 61.60, 132.54, 135.84, 164.65, 170.21ppm. The (E)-3-(ethoxycarbonyl)acrylic acid (**125**) was removed using vacuum distillation. The corresponding (Z) isomer, (Z)-3-(ethoxycarbonyl)acrylic acid (**127**), was not found in the sample. This was supported by the literature, which shows that the hydrolysis of diethyl 2-bromosuccinamate (**103**) produces fumaric acid (**129**), owing to the (E) isomer being more stable[106] (Figure 2.8.2.2).

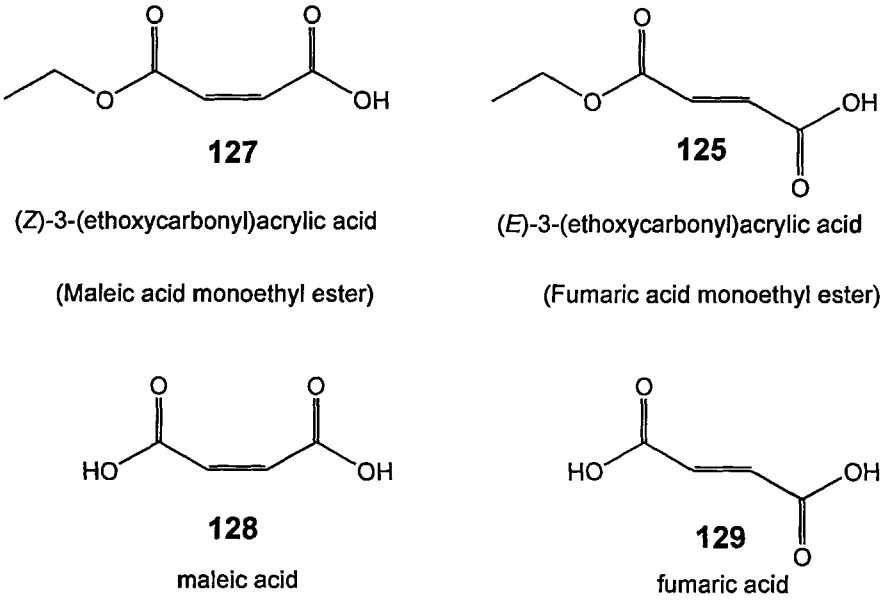

Figure 2.8.2.2: Structures of the two isomers of the monoethyl acrylic acids and the free acids

2.9.1: Conclusion

There are two main problems presented with the use of diethyl 2-bromosuccinate (**103**) as a starting material in the formation of sDO3A-(ethyl) (**107**). The first was the elimination of the bromide to form the alkene, with diethyl maleate (**126**) as a significant product from the reaction of diethyl 2-bromosuccinate (**103**) when in the presence of potassium carbonate, and with the formation of (E)-3-(ethoxycarbonyl)acrylic acid (**125**), when diethyl 2-bromosuccinate (**103**) was in the presence of caesium carbonate (Figure 2.9.1.1). The second problem with diethyl 2-bromosuccinate (**103**) was that it changes the Rf values of the reaction products. This causes both sDO2A-(ethyl) (**108**) and sDO3A-(ethyl) (**107**) to be eluted from the chromatography column at the same time reducing the usable yield of sDO3A-(ethyl) (107).

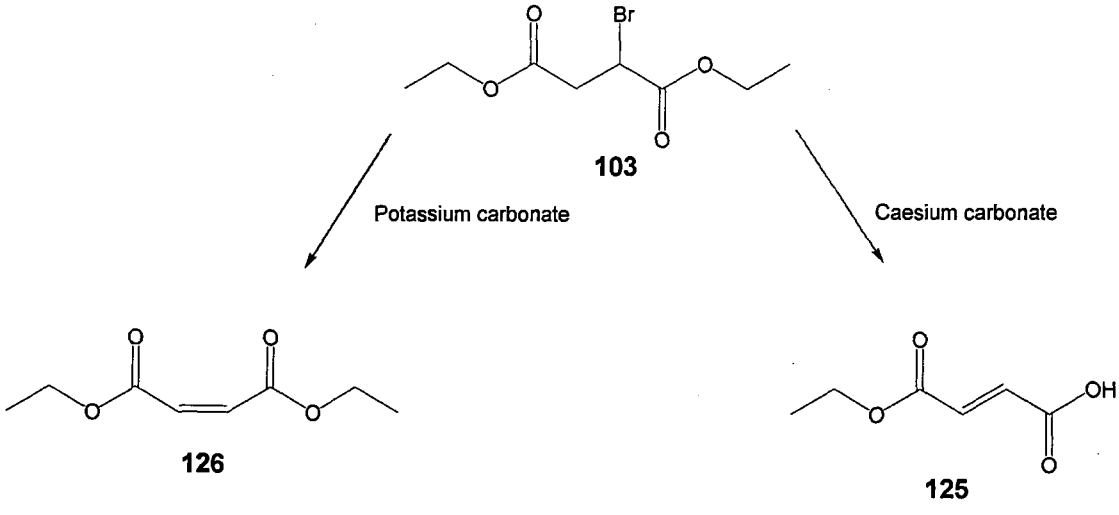

Figure 2.9.1.1: Products of the reaction of diethyl 2-bromosuccinate (103) with potassium carbonate and caesium carbonate, producing diethyl maleate (126) and (E)-3-(ethoxycarbonyl) acrylic acid (125)

The alkene formed from diethyl 2-bromosuccinate (**103**) was by an E2 elimination pathway, which was favoured by secondary halides in the presence of a strong base.[107] The base attacks the neighbouring hydrogen to the bromide on the diethyl 2-bromosuccinate (**103**) (Figure 2.9.1.2). This E2 elimination occurs in competition with S_N2 addition reaction between the diethyl 2-bromosuccinate (**103**) and the cyclen (**9**). In this case the elimination was faster than the substitution reaction. This indicates that the reaction was going down an alternative pathway to that of the substitution reaction between the diethyl 2-bromosuccinate (**103**) and cyclen (**9**).

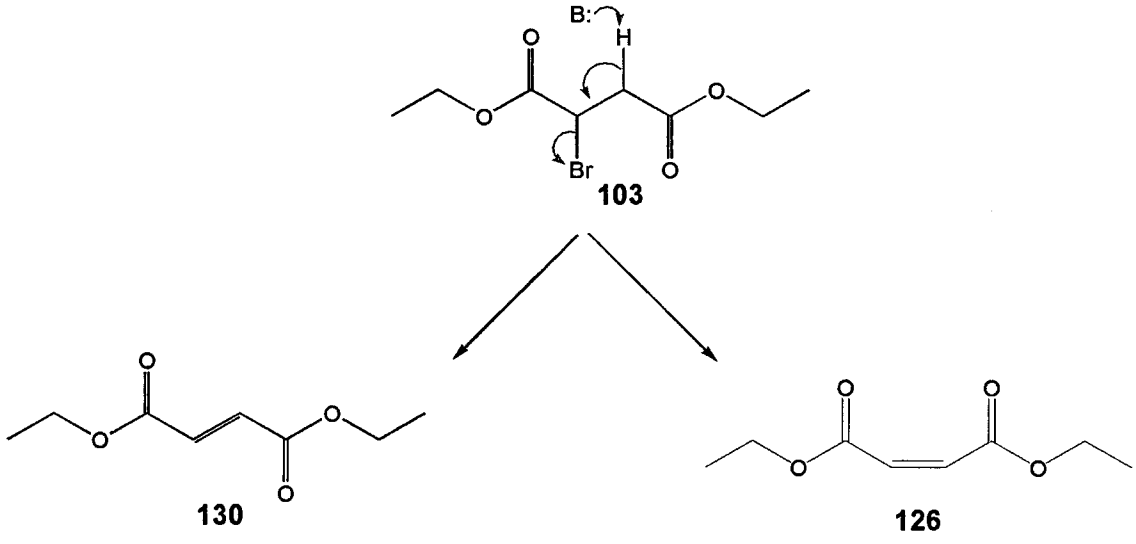

Figure 2.9.1.2: Mechanism of the E2 reaction of diethyl 2-bromosuccinate (103) with a strong base to form diethyl fumarate (130) and diethyl maleate (126)

With the alkene produced by the elimination reaction between diethyl 2-bromosuccinate and the base being adjacent to two electron withdrawing groups makes it acceptable to react with the amine of the cyclen (**9**). This was due to the carbonyl groups stabilising the formation of the carbanion making the alkene formed (diethyl maleate (**126**) or diethyl fumarate (**130**)) an excellent nucleophile. This leads to an alternative synthetic pathway for the formation of sDO3A-(ethyl) (**107**) though

the use of the Michael addition of diethyl maleate (**126**) or diethyl fumarate (**130**) with cyclen (**9**)

2.10.1: Synthesis of sDO3A-(ethyl) (107) via Michael addition with diethyl maleate (126) and diethyl fumarate (130)

The Michael addition reaction has been traditionally performed in protic solvents, with a catalytic amount of alkali[88]. The Michael addition requires a nucleophile acceptor and a nucleophilic donor. A nucleophile acceptor could be α,β-unsaturated carbonyl compound, or a ester, nitrile, amide or nitro compound.

In this case the Michael acceptor was the alkene in the diethyl maleate (**126**) or diethyl fumarate (**130**). These are excellent Michael acceptors, owing to the electron-withdrawing effect of both carbonyl groups. The Michael donor was the lone pair on the nitrogen of the cyclen (**9**) (Figure 2.10.1.1). Several methods have been reported for the reaction of a 1-2 alkene with a cyclen, giving a range of products from monosubstituted to tetra-substituted cyclens.[108-110] There have also been several reports of the reaction of diethyl maleate with secondary amines such as diethylamine.[111]

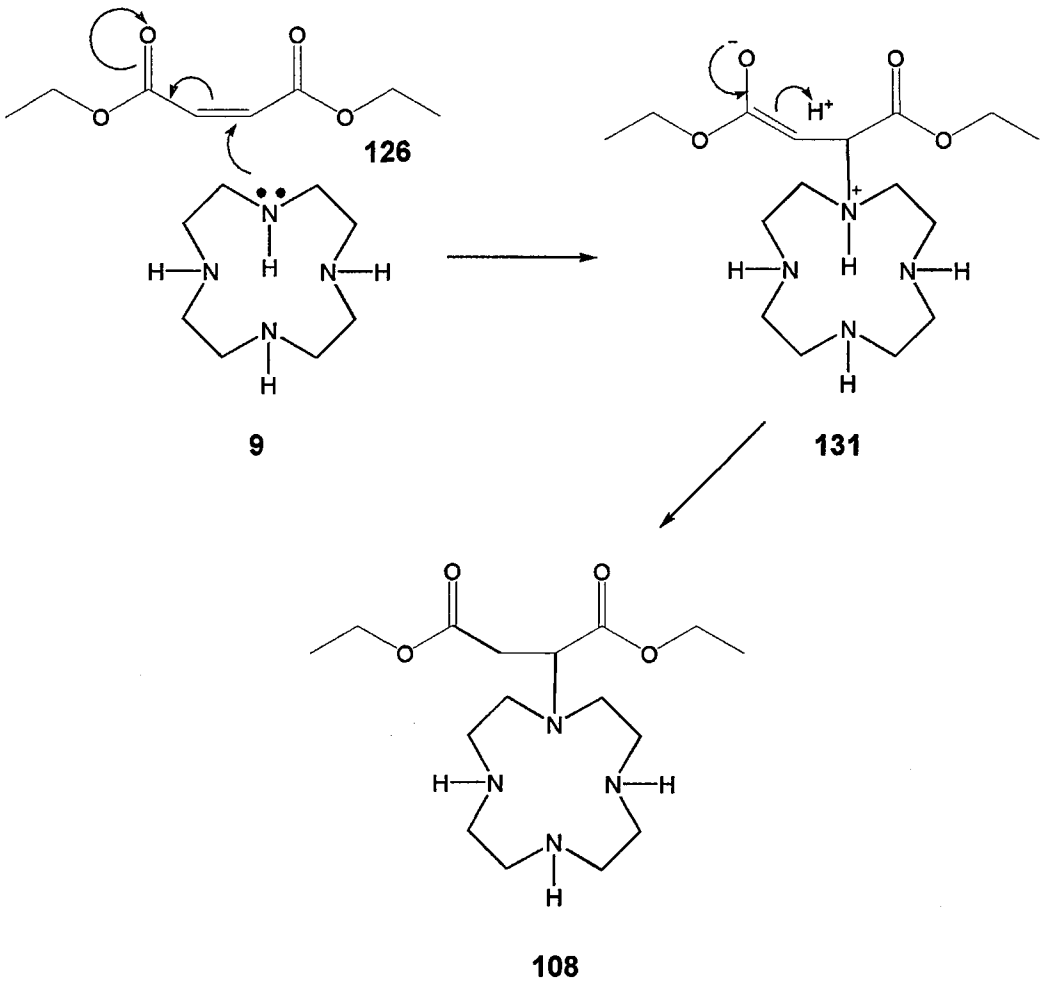

Figure 2.10.1.1: Mechanism for the Michael addition of diethyl 2-bromosuccinate (126) with cyclen (9) for the formation of sDO1A-(ethyl) (108)

The reactions were run under identical conditions using acetonitrile as the solvent and potassium carbonate as the base. The alkene was added in a ratio of 5.4 eq to that of cyclen. Both reactions yielded sDO3A-(ethyl) (**107**), as has been reported in the literature.[112] There was no difference between the two alkenes in terms of reaction yields.

The use of the alkenes diethyl maleate (**126**) and diethyl fumarate (**130**) has a marked effect on the Rf values in the chromatography of the crude reaction product. In the reaction using diethyl maleate (**126**) and diethyl fumarate (**130**) the Rf

difference between sDO2A-(ethyl) (**109**) and sDO3A-(ethyl) (**107**) was greater than when diethyl 2-bromosuccinate (**103**) was used. This was due to the co-solvent effect noted earlier.

The main synthesis of sDO3A-(ethyl) (**107**) was scaled up to 3g of cyclen (**9**) allowing for the synthesis of greater amount of product. This was performed in acetonitrile with 3.3 eq of potassium carbonate and 14 eq of diethyl maleate (**126**) in acetonitrile. The reaction was heated to 80 °C for 72 hours. The chromatography protocol had to be modified to make purification of the crude oil possible. Since the amount of the crude material to be loaded onto the column was too large, direct addition of the oil to the column was not feasible, owing to uneven band separation occurring during the loading of the product. This was prevented by adsorbing the crude product onto the silica before addition to the column, by dissolving the crude oil in DCM and then adding silica (10 g of silica per 1 g of crude). The solvent was then removed, using reduced pressure, to yield a sticky powder. The powder was added to the top of the column and compacted in the same manner as before. After the compaction a layer of sand (3 cm) was placed on the top to prevent movement of the silica during the addition of the eluent. This methodology replicates the benefits of the Sep-Pak columns, by reducing air/solvent pockets within the chromatography bed to allow for a greater resolution within the column and thus better separation. The column was then eluted with a mixture of DCM 95%, EtOH 5%. The sDO3A-(ethyl) (**107**) was found at R_f 0.20, giving a yield of over 35%. The product was confirmed by HRMS predicted 711.3787 [M(**107**)+Na^{+H}], found 711.3792 [M(**107**)+Na^{+H}], The FTIR and the ^{1}H and ^{13}C NMR spectra matched the spectra of the known sDO3A-(ethyl) (**107**) samples.

2.11.1: Synthesis of butene-sDO3A-(ethyl) (101) from sDO3A-(ethyl) (107)

The final step in the synthesis of butene-sDO3A-(ethyl) (**101**) was the reaction of sDO3A-(ethyl) (**107**) with 4-bromobut-1-ene (**78**) via the remaining amine group of the cyclen, in a nucleophilic reaction. The reaction was performed in anhydrous acetonitrile, with potassium carbonate as the base. The main problem was stopping the 4-bromobut-1-ene (**78**) from reacting with itself, and this was achieved by lowering the temperature of the reaction to around −15 °C using an ice/salt/IMS bath, before the addition of the 4-bromobut-1-ene (**78**). The reaction was then allowed to warm up slowly to room temperature over a period of several hours. The solid was removed from the reaction by filtration, and the solvent and excess of 4-bromobut-1-ene (**78**) were removed using reduced pressure. The crude product was identified using LCMS and then passed through a silica chromatographic column using DCM 95 % and EtOH 5% as eluent, giving an oil in a yield of greater than 75%. It was noticed in the LCMS of the crude reaction that the butene-sDO3A-(ethyl) (**101**) underwent a Menshutkin reaction, where the tertiary amine was converted to the quaternary ammonium salt (**132**).[88] This effect was seen mainly in reactions that contained a large excess of 4-bromobut-1-ene (**78**). This by-product was removed on work-up using chromatography (Figure 2.11.1.1).

The ^{1}H NMR spectra showed the presence of the protons of the alkene at 4.93 and 5.71 ppm and the integration fitted the proposed structure. The ^{13}C NMR spectra confirmed the presence of the alkene at 115.31 ppm and 137.09 ppm and the spectra also showed the N-CH carbon of the succinate groups. The HRMS calculated 743.4437 [M(**101**)$^{+H}$], found 743.4445 [M(**101**)$^{+H}$], the FTIR showed the presence of a stretch associated with the alkene at 2982 cm^{-1}, the ethyl ester at 1723 cm^{-1} and the amine at 1461 cm^{-1}.

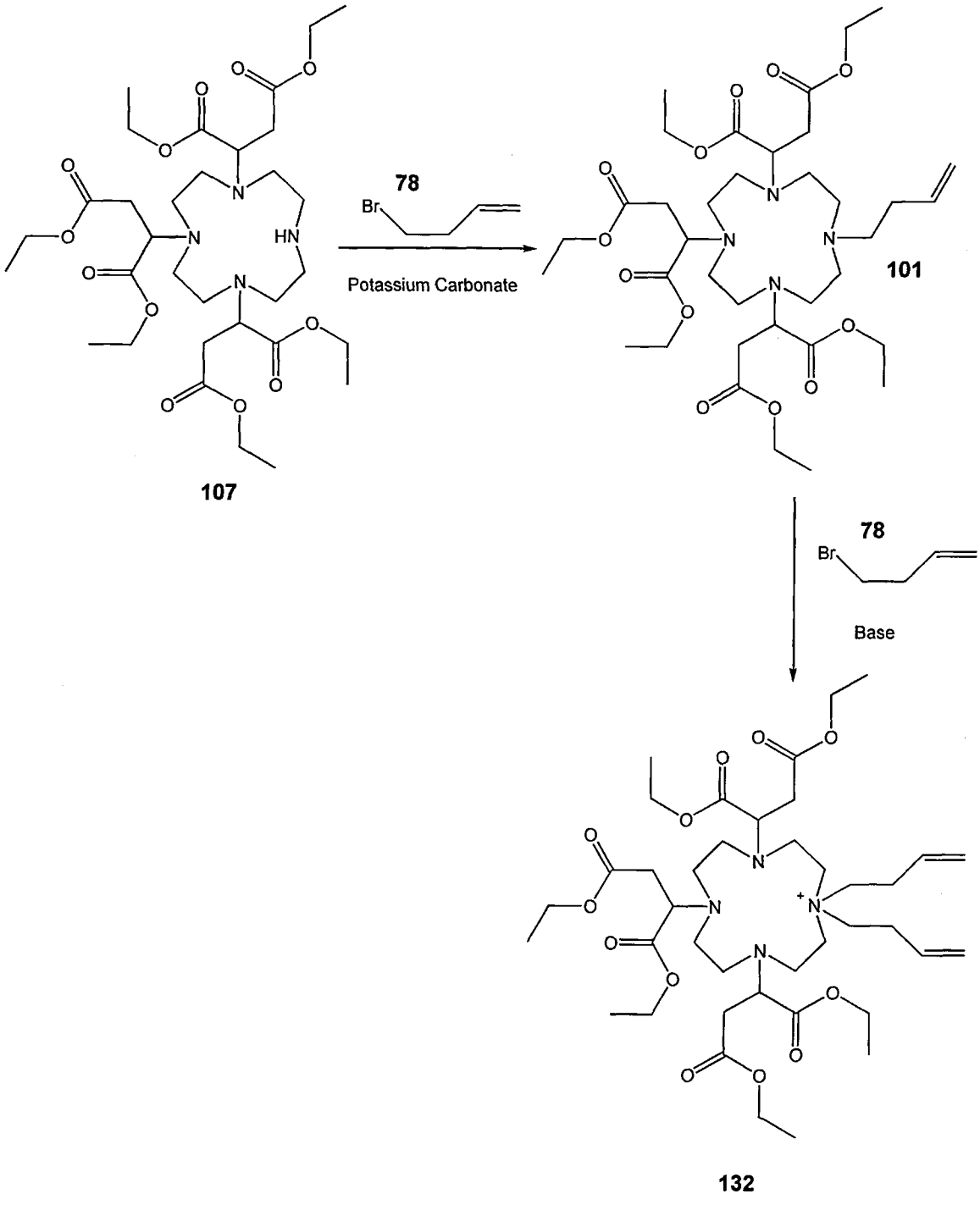

Figure 2.11.1.1: Formation of butene-sDO3A-(ethyl) (101) and a quaternary ammonium compound (132)

2.11.2: Synthesis of pentene-sDO3A-(ethyl) (133) from sDO3A-(ethyl) (107)

An alternative linker arm, was based on 5-bromopent-1-ene (**134**) and was also synthesised to form pentene-sDO3A-(ethyl) (**133**). The reaction was performed in anhydrous acetonitrile, to which potassium carbonate and sDO3A-(ethyl) (**107**) were added. The temperature of the reaction was adjusted to −15 °C using an ice/salt/IMS bath, before the addition of the 5-bromopent-1-ene (**134**). The reaction was then warmed up slowly to room temperature over a period of several hours. The solid was then removed from the solvent along with any excess 5-bromopent-1-ene (**134**). The crude product was passed through a silica chromatographic column using DCM 95% and EtOH 5% as eluent, giving a yield of 62%. (Figure 2.11.2.1). The target compound was identified by using ^{1}H NMR which showed the alkene at 4.92 ppm and 5.72 ppm, and the integration fitted the predicted structure. The ^{13}C NMR showed the alkene at 115.30 ppm and 137.11 ppm and showed the presence of the extra carbon environment when compared to butene-sDO3A-(ethyl) (101). The FTIR showed the alkene at 2981 cm^{-1} the ethyl ester at 1728 cm^{-1} and the amine at 1448 cm^{-1}. The HRMS showed an ion at 757.4590 [M(**133**)$^{+H}$] which matched the predicted ion of 757.4593 [M(**133**)$^{+H}$].

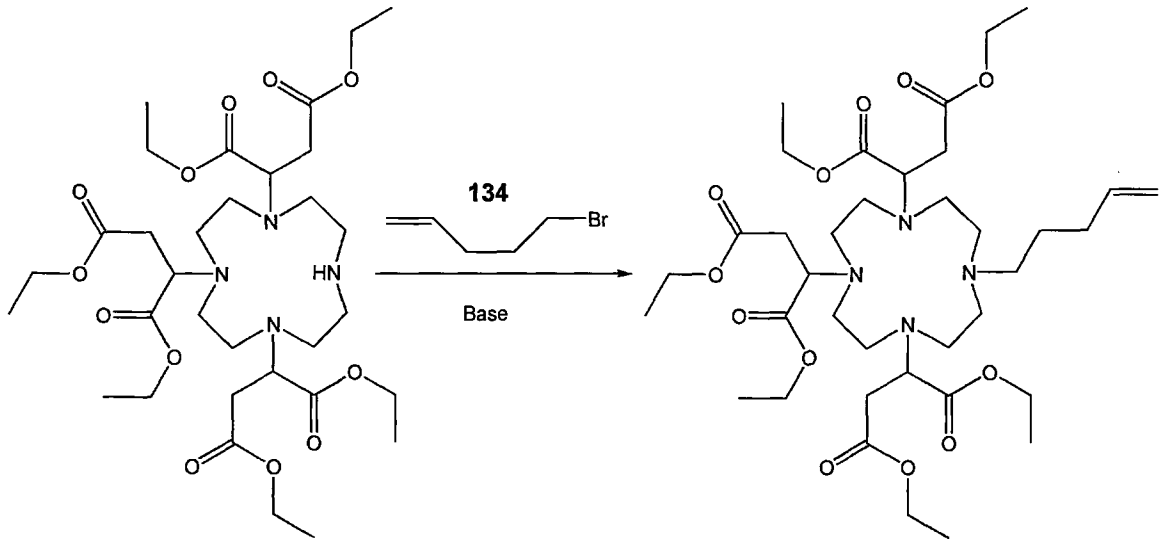

Figure 2.11.2.1: Formation of pentene-sDO3A-(ethyl) (133)

2.12: Conclusion

Following the successful synthesis of sDO3A-(ethyl) (**107**), butene-sDO3A-(ethyl) (**101**) and pentene-sDO3A-(ethyl) (**133**), they can be employed in the preparation of lanthanide complexes in one of two ways. The first was hydrolysis to form the associated carboxylic acids of the ethyl esters; these are sDO3A (**32**), butene-sDO3A (**105**) and pentene-sDO3A (**135**). These compounds would then be complexed with Gd^{3+} and Eu^{3+}. The second approach was to react the alkene-sDO3A-(ethyl)'s with the silicon cages as in Chapter 3. These compounds would then be hydrolysed and complexed with Gd^{3+} and Eu^{3+}.

2.13.1: Hydrolysis of sDO3A-(ethyl) (107), butene-sDO3A-(ethyl) (101) to give the acids sDO3A and butene-sDO3A

The final step in the synthesis of butene-sDO3A (**105**) and sDO3A (**32**) was the hydrolysis of butene-sDO3A-(ethyl) (**101**) and sDO3A-(ethyl) (**107**). The reaction was monitored using a combination of LCMS and ^{1}H and ^{13}C NMR techniques. The NMR integration and position of the ^{1}H NMR signals for the protons attached to carbon [1], relative to the protons attached to carbons [5] and [8], can be used to measure the progress of the hydrolysis reaction (Figure 2.13.1.1).

The integration of the proton attached to carbon [1] was used as a standard, as it was present in both the ester and acid compounds, whereas the integration of the protons attached to carbons [8] and [5] will vary with the number of ester groups in the molecule and these are seen at 1.18 ppm on the ^{1}H NMR spectra. The chemical shift of the proton attached to carbon [1] depends on the shielding produced by the different carbonyl groups on carbons [6] and [3]. When both of the carbonyls are ethyl esters, the chemical shift of the protons attached to carbon [1] was at 4.1 ppm; while when the carbonyls [6] and [3] are carboxylic acids the shift goes upfield to 3.8 ppm.

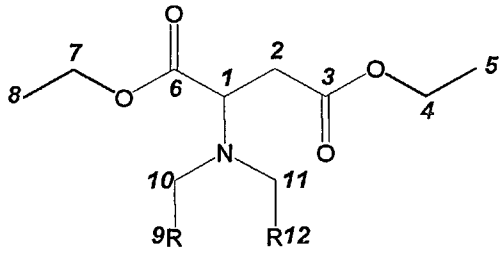

136

Figure 2.13.1: Structure (136), showing the numbering of the carbon atoms in the ligand-arm section of sDO3A-(ethyl) (107)

Alternatively, when the carbonyl [6] was an ethyl ester and the carbonyl [3] was a carboxylic acid, the chemical shift moves downfield to 4.13 ppm. When the carbonyl [6] was an acid and the carbonyl [3] was an ethyl ester, the peak shifts upfield to 3.78 ppm. This variability of chemical shift makes it possible to monitor which of the ester groups are being removed during the reaction, by measuring the integration between the peaks as well as their ppm.

2.13.2: Acid-catalysed hydrolysis of sDO3A-(ethyl) (107)

The reaction was performed in D_2O, as then it was possible to monitor the reaction by NMR spectroscopy without the need for purification. The hydrolysis was performed using DCl in D_2O to reduce the HOD signal in the NMR. The reaction was heated at 90 °C in a sealed tube to prevent the loss of DCl over the 18-hour reaction time, after which the NMR spectra showed the presence of the ester groups. The heating was continued for another 18 hours until the ester peaks were no longer present. The DCl was removed using reduced pressure and the D_2O removed by freeze-drying. The solid was then dissolved in water and freeze-dried. This step removed all traces of DCl and replaced the deuterium on the carboxylic acid groups with protons. The ^1H NMR spectra showed that the protons at 1.18 ppm had been removed indicating that the ester groups had been removed. The proton associated with position [1] had been shifted from 4,1ppm to 3.5ppm. LCMS spectra showed that during the hydrolysis one of the succinic acid arms had been removed 231.35 [1/2M(**138**)-NaCl^{+H}], 403.69 [M(**138**) $^{+H}$], 439.97 [M(**109**)Cl^{+H}]. The product was the only one from the reaction and was identified as the chloride salt, with yields of 92%. The structure of sDO2A has two possible regioisomers: the 1,4-sDO2A (**137**), with

C_2 and D_2 symmetry, and the 1,7-sDO2A (**138**), with D_2 symmetry. The synthesised product was shown to have 1,7 substitution. This conclusion was based on the ^{13}C NMR of the carbon environments of the cyclen ring. The 1,7-sDO2A (**138**) has two carbon environments, whereas the 1,4-sDO2A (**137**) has 4 carbon environments (Figure 2.13.2.1).

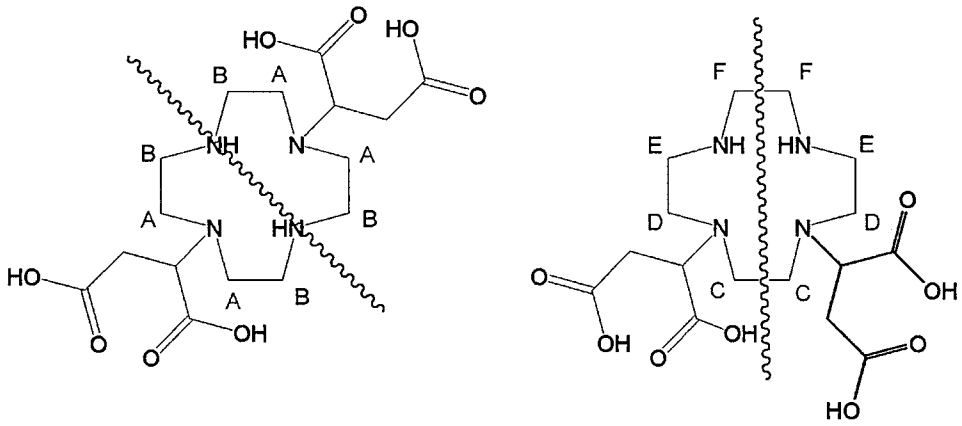

1-7-sDO2A (**138**) 1-4-sDO2A (**137**)

Figure 2.13.2.1: The C2–D2 symmetry of 1,7-sDO2A (138) and D2 symmetry of 1,4-sDO2A (137)

This suggests that the sDO3A (**32**) was decomposing via an elimination mechanism, whereby the leaving group of the protonated nitrogen leads to the formation of the formate. The fumaric acid was seen in the ^1H NMR spectrum of the crude reaction product at 7 ppm (Figure 2.13.2.2).

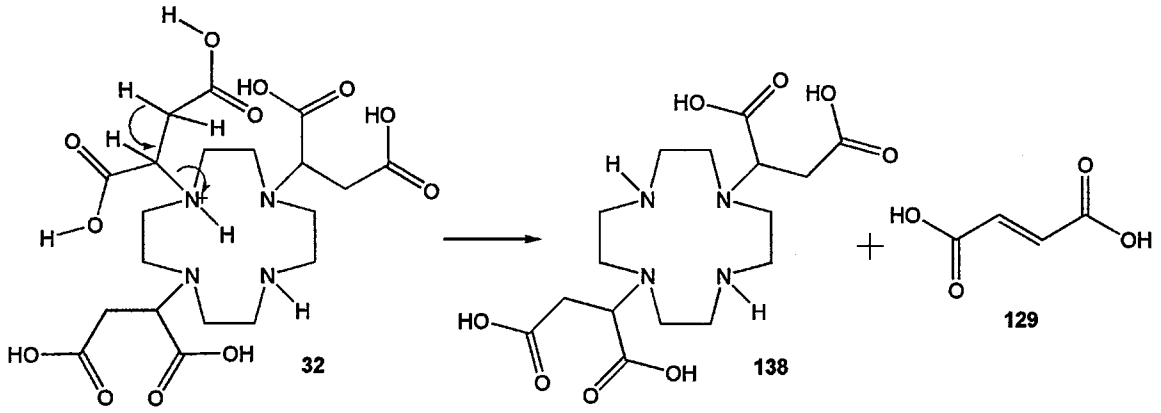

Figure 2.13.2.2: The decomposition of sDO3A (32) to form sDO2A (138) and fumaric acid (129).

As the hydrochloric acid-catalysed hydrolysis formed sDO2A (**138**) from sDO3A-(ethyl) (**107**), an alternative, weaker acid was investigated. Formic acid was chosen for its high volatility. It was first dissolved in a small amount of ethanol, to assist the solubility of the ester in the acid solution. Because of the low boiling point of the formic acid, the reaction was performed in a sealed tube, heated to 90 °C for 24 hours. The water and the formic acid were removed by lyophilisation, freezing the sample in liquid nitrogen and placing under vacuum. To remove all traces of formic acid from the sample the lyophilisation was repeated by dissolving the sample in ultra-pure water and repeating the lyophilisation step three times. The resulting solid was then dissolved in D_2O. The NMR spectra showed that the deprotection of the ester was incomplete, and increasing the time for the hydrolysis did not lead to further hydrolysis.

The hydrolysis of butene-sDO3A-(ethyl) (**101**) was attempted using formic acid in parallel with the hydrolysis of sDO3A-(ethyl) (**107**). The butene-sDO3A-(ethyl) (**101**) was dissolved in 1.4M formic acid solution, and heated for a period of 48 hours at 60 °C. However, the NMR spectra showed that no hydrolysis had occurred, so the

reaction was heated to 70 °C for a further 24 hours. The ^{1}H NMR spectra showed that two of the ester groups had been hydrolysed to form the corresponding carboxylic acids (**139**) and (**140**). This was confirmed by the reduction in the integration of the CH_3 signal in the ^{1}H NMR corresponding to the ester group. The loss of the ester group was also seen in the ^{13}C NMR, by the appearance of a third peak corresponding to a carboxylic acid group (Figure 2.13.2.3).

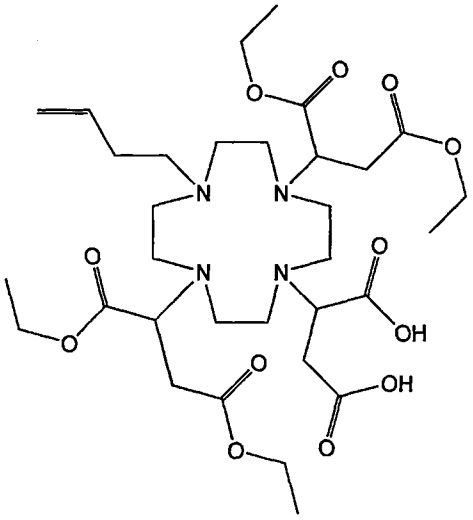

139

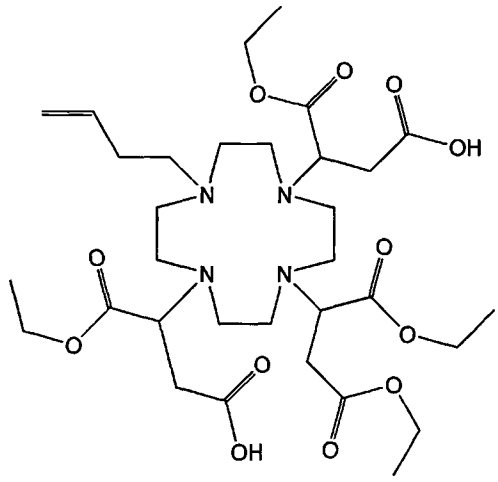

140

Figure 2.13.2.3: Probable structures of the products from the hydrolysis of butene-sDO3A-(ethyl) (101)

Stronger conditions were tested, in which butene-sDO3A-(ethyl) (**101**) was dissolved in 2.2M formic acid and heated to 80 °C for 48 hours. The mass spectrum of the resulting product showed a mixture of products. These were identified as sDO2A-(ethyl) (**109**), butene-sDO2A-(ethyl) (**123**) and butene-sDO3A (**105**), with the butene-sDO2A-(ethyl) (**123**) being the major compound. The reaction showed two types of decomposition; the first was the loss of a succinate arm to give butene-sDO2A-(ethyl) (**123**), in the same manner as the HCl hydrolysis of sDO3A-(ethyl) (**107**). The

second form of decomposition was the loss of the butene arm to produce sDO3A-(ethyl) (**107**), which then decomposed to give sDO2A-(ethyl) (**109**).

Since this decomposition occurred in the hydrolysis of both sDO3A-(ethyl) (**107**) and butene-sDO3A-(ethyl) (**101**) to produce the corresponding sDO2A compounds, and also because decomposition via the loss of the alkene was seen in the formic acid hydrolysis reaction of desBDO3A, an alternative route for the hydrolysis of sDO3A-(ethyl) (**107**) and butene-sDO3A-(ethyl) (**101**) was sought.

2.13.3: Base-catalysed hydrolysis of sDO3A-(ethyl) (107) to form sDO3A (32)

The next method of hydrolysis was a base-catalysed reaction. The main problems with the use of a base such as potassium hydroxide, sodium hydroxide or lithium hydroxide involve the removal of the excess base and the removal of the inorganic salts formed in the reaction, owing to the high polarity of the target molecule and its high solubility in water. There are several methods for removing the salts and the excess hydroxide, which will be discussed later.

The first attempt at the alkaline hydrolysis employed 1M sodium hydroxide. One problem that arose in the monitoring of the reaction via LCMS was that ion suppression occurred in the LCMS due to the presence of the metal ions, since they are charged and present in high numbers. These metal ions swamp the detector, reducing its ability to detect high molecular masses. When this ion-suppression effect was combined with the multiply charged states of the compounds, it makes analysis of the reaction mixture virtually impossible using this technique. One solution was to perform the trial reactions in D_2O in the same manner as the DCl

reaction. This allowed a small sample of the reaction mixture to be removed and analysed using ^{1}H NMR. The reaction was performed in a sealed, screw-topped tube, to limit deuterium exchange with water in the atmosphere. The analysis showed that no reaction took place over a period of 1.5 hours at room temperature. This was shown as before, based on the integration of the protons attached to carbon [1] relative to those attached to carbon atoms [8] and [5]. The temperature of the reaction was increased to 80 °C and maintained for 24 hours. After this the reaction was cooled and a sample was removed and analysed via H^{1} NMR spectroscopy, which showed the loss of the protons due to the cleavage of the ethyl ester groups.

2.14.1: Purification of sDO3A (32) by ion-exchange chromatography

Cyclen-based compounds will form stable complexes with sodium and will temporarily complex both lithium and potassium. These metal ions need to be removed owing to the competitive binding with the gadolinium at the complexation stage. The sDO3A (**32**) has the ability to be separated on both cation and anion resins, depending on the pH, because the compound has a secondary amine, which when protonated (**141**) will interact with the cation-exchange resin, while the carboxylic acid groups (**142**) can interact with the anion-exchange resin (Figure 2.14.1.1).

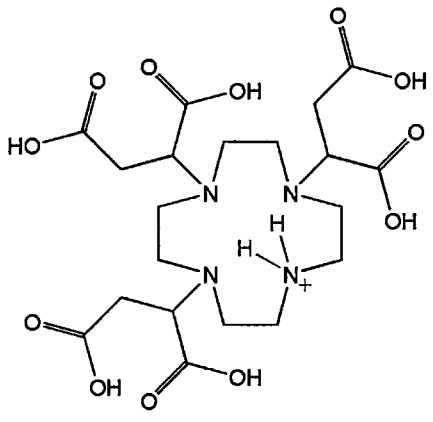

141

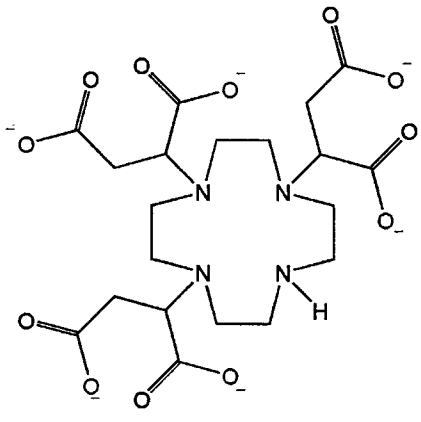

142

Figure 2.14.1.1: The charged ion sites for ion exchange

2.14.2: Cation-exchange chromatography of sDO3A (32)

Cationic ion-exchange chromatography was performed using Dowex 50W x 8, a strong sulfonic acid-based exchange resin. The resin was used in the H^+ form. The sDO3A (**32**) and sodium hydroxide solution were passed slowly though the ion-exchange column. The pH was monitored after every 5 ml of eluent, showing a decrease in the pH of the eluent from pH 6 to pH 3. This confirmed the absorption of the sodium cation and the sDO3A (**32**). The pH decrease was due to the release of H^+ ions from the ion-exchange resin.

After the pH of the eluent stabilised, showing complete absorption of the ions, the column was eluted with a solution of ammonia (2%) at a rate of 4 ml per minute. Ammonia solution was used since the resin has a higher affinity for Na^+ than for NH_4^+, thus allowing the elution of the hex-acid as the ammonium salts while the Na^+ ions remain on the resin.[113] The pH then rose over time, showing a step increase, and then stabilising at pH 11. At this point the sDO3A (**32**) was eluted off the ion-

exchange chromatography column. The negative ion LCMS showed the presence of the sDO3A (**32**) as the diammonium salt. The positive spectra showed no trace of sodium ions. The water and ammonia were removed using lyophilisation. ^{1}H and ^{13}C NMR data showed that the sample contained both sDO3A (**32**) and sDO2A (**138**).

2.14.3: Anion-exchange chromatography of sDO3A (32)

Since sDO2A (**138**) was formed from sDO3A (**32**) while undergoing ion-exchange chromatography, owing to the highly acidic conditions on the surface of the resins, an alternative to the cation-exchange resin was employed: an anion-exchange resin. With anion-exchange resins the lower the selectivity of the counter ion, the more readily it exchanges with an ion of similar charge.

As anion-exchange chromatography relies on the flushing of the metal ion from the resin bed, it was possible to use Li^{+} ions. The advantage of LiOH was that it was a "milder" base than NaOH and KOH and leads to less decarboxylation. The sDO3A-(ethyl) (**107**) was dissolved in a small volume of 1M LiOH, and heated in a sealed tube at 90 °C for 38 hours. The LCMS showed complete removal of the ester arms, with no production of sDO2A (**138**). The resin used was analytical grade Bio-Rad AG1 A4I, which was a quaternary ammonium-based resin. The resin was prepared in the OH^{-} form, as the sDO3A (**32**) would bind to the resin and the Li^{+} ion would be carried through with the eluent. The reaction solution of sDO3A (**32**) and LiOH was added to the resin column and eluted with water until the pH was stabilised, showing the complete elution of the LiOH. The column was then eluted with a gradient of formic acid (1M) in water (3.3% increase in 1M formic acid per minute verse water),

and the pH was monitored every 5 ml. The product was eluted at pH 2.75 and monitored by LCMS. The fractions containing the product were then lyophilised, retaken up into water and lyophilised again. This process was repeated three times to remove any trace of the formic acid. The LCMS confirmed the presence of the sDO3A (**32**) ion, and the ^{1}H and ^{13}C NMR spectra showed that the ester had been hydrolysed to the acid, by the loss of the protons of the ethyl ester at 1.18 ppm, and the change in ppm of the proton at [1] from 4.1ppm to 3.83 ppm on the ^{1}H NMR spectrum. The ^{13}C NMR showed the change in ppm of the carbonyls from 170.93 and 171.46 to 174.9 and 177.3 ppm. The HRMS showed the target ion at 521.2088 [M(**32**)$^{+H}$], with the predicted ion at 521.2089 [M(**32**)$^{+H}$].

2.14.4: Conclusion

The acid-catalysed hydrolysis was unsuccessful owing to the decomposition of the alkene and of the succinate groups. The base-catalysed hydrolysis of sDO3A-(ethyl) (**107**) was successful and did not induce the decomposition that occurred with the acid-catalysed process. The cationic ion exchange proved problematic, with decomposition occurring during the eluting phase of the chromatography. This was circumvented by changing the solid-phase ion-exchange resin type to an anionic form; thus allowing the elution of the desired product with decomposition. The formic acid used in the elution meant that the butene-sDO3A (**105**) could not be purified without decomposition of the alkene occurring.

3.1: Catalysts used in hydrosilylation reactions.

The next stage in the synthesis was the attachment of the substituted cyclen to the silicon cage via the alkene arm. This reaction between the alkene and the Si–H was performed using a platinum catalyst. There are two main types of catalyst for the formation of Si–C bonds via hydrosilylation, both based on Pt species. The first investigated was Speier's catalyst, a solution of chloroplatinic acid (H_2PtCl_6) (**143**) in propan-2-ol (**144**), which was used with reactions involving T_8H_8 (**33**) cages; while the second catalyst, known as Karstedt's catalyst (**145**), was commonly used in reactions involving $Q_8M_8^H$ (**38**), although Speier's may also be used with the $Q_8M_8^H$.[58, 111, 112]

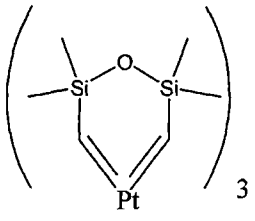

145

Figure 3.1.1: Active site in Karstedt's catalyst

There are two possible products from the reaction between the alkene and the silsesquioxane, depending on whether the hydrosilylation proceeds via α- or β-addition. In general most reactions go via α-addition with a trace of β-addition; the degree of β-addition depends upon the functionality of the alkene. In the case of butene-sBDO3A-(ethyl) the effect should be minimised, as the bulk steric effect of the cyclen system should hinder the formation of β-addition products [1].

The active Speier's catalyst (**143**) was formed by the reduction of $Pt^{(IV)}$ by the propan-2-ol (**144**) to give $Pt^{(II)}$ as $PtCl_4^{2-}$ (**146**) and propan-2-one (**147**). The $PtCl_4^{2-}$ (**146**) then binds with the alkene (**148**), displacing one of the chlorides and forming the complex (**149**). This complex then undergoes an oxidative addition with a silane (**150**) to form a $Pt^{(iv)}$ complex (**151**). This forms an intermediate complex (**152**), where the alkene was reduced. The complex then reacts with another alkene (**148**) molecule to give the $Pt^{(ii)}$ complex (**149**), whilst producing the target molecule (**153**) (Figure 3.1.2).

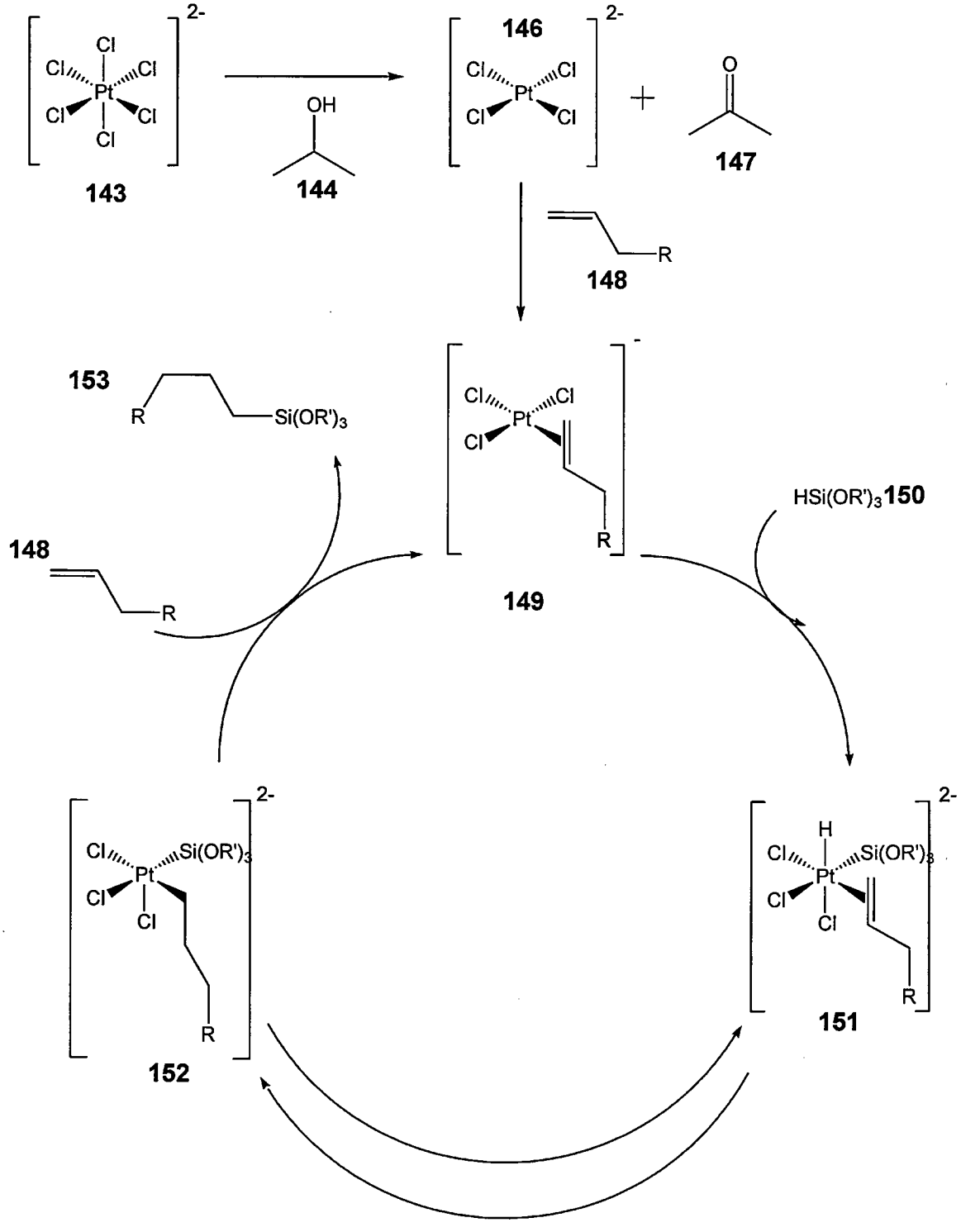

Figure 3.1.2: Catalytic reaction mechanism for Speier's catalyst

3.2: Reaction of pentene-sDO3A-(ethyl) with T_8H_8

3.2.1: Formation of T_8H_8

The first cage investigated was the silsesquioxane $[HSiO_{3/2}]_8$ (**33**), referred to as T_8H_8. T_8H_8 (**33**) was synthesised by the bi-phasic hydrolysis of trichlorosilane (**154**), yielding a white crystalline solid with a yield of up to 12%. The compound was confirmed by the ^{28}Si NMR peak at −84.44 ppm. The Si–H stretch in the FTIR was at 2169 cm^{-1}. These characteristic peaks are useful as a method of monitoring the reaction, as alternative methods, such as LCMS, are not suitable for these compounds owing to their poor ionisation ability. The size of the molecule will be close to the detection limits of the available equipment (Figure 3.2.1.1).

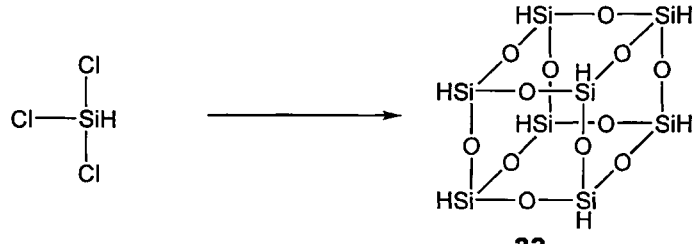

154 **33**

Figure 3.2.1.1: Formation of T_8H_8 (33) from trichlorosilane

3.2.2: Model reaction of N,N-diethylbut-3-en-1-amine and T_8H_8

The first reactions to be performed on the T_8H_8 (**33**) were reactions with the model ligand N,N-diethylbut-3-en-1-amine (**156**). This allowed the testing of the catalyst and the methodology. The model ligand N,N-diethylbut-3-en-1-amine (**156**) was synthesised from 4-bromobut-1-ene (**78**) and diethylamine (**155**) in anhydrous acetonitrile at 60 °C for 48 hours. The product was confirmed by ^{1}H and ^{13}C NMR, which showed the loss of the proton signal for the CH_2–Br group at 3.34 ppm. The FTIR and LCMS also confirmed the target product (Figure 3.2.2.1).

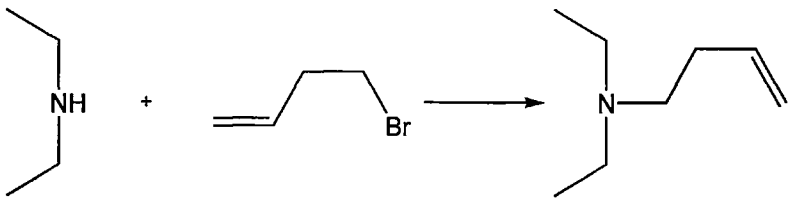

155 **78** **156**

Figure 3.2.2.1: Synthesis of N,N-diethylbut-3-en-1-amine (156)

N,N-diethylbut-3-en-1-amine (**156**) was then reacted with both T_8H_8 (**33**) and $Q_8M_8^H$ (**38**) in anhydrous toluene, using Speier's catalyst. Owing to the sensitivity of the reaction to water, the reactions were performed in a sealed, screw-top tube flushed with argon. The reactions were worked up by centrifugation to remove any solids formed in the reaction. The solvent was then removed and the crude product taken up in $CDCl_3$, leaving an insoluble residue (Figure 3.2.2.2).

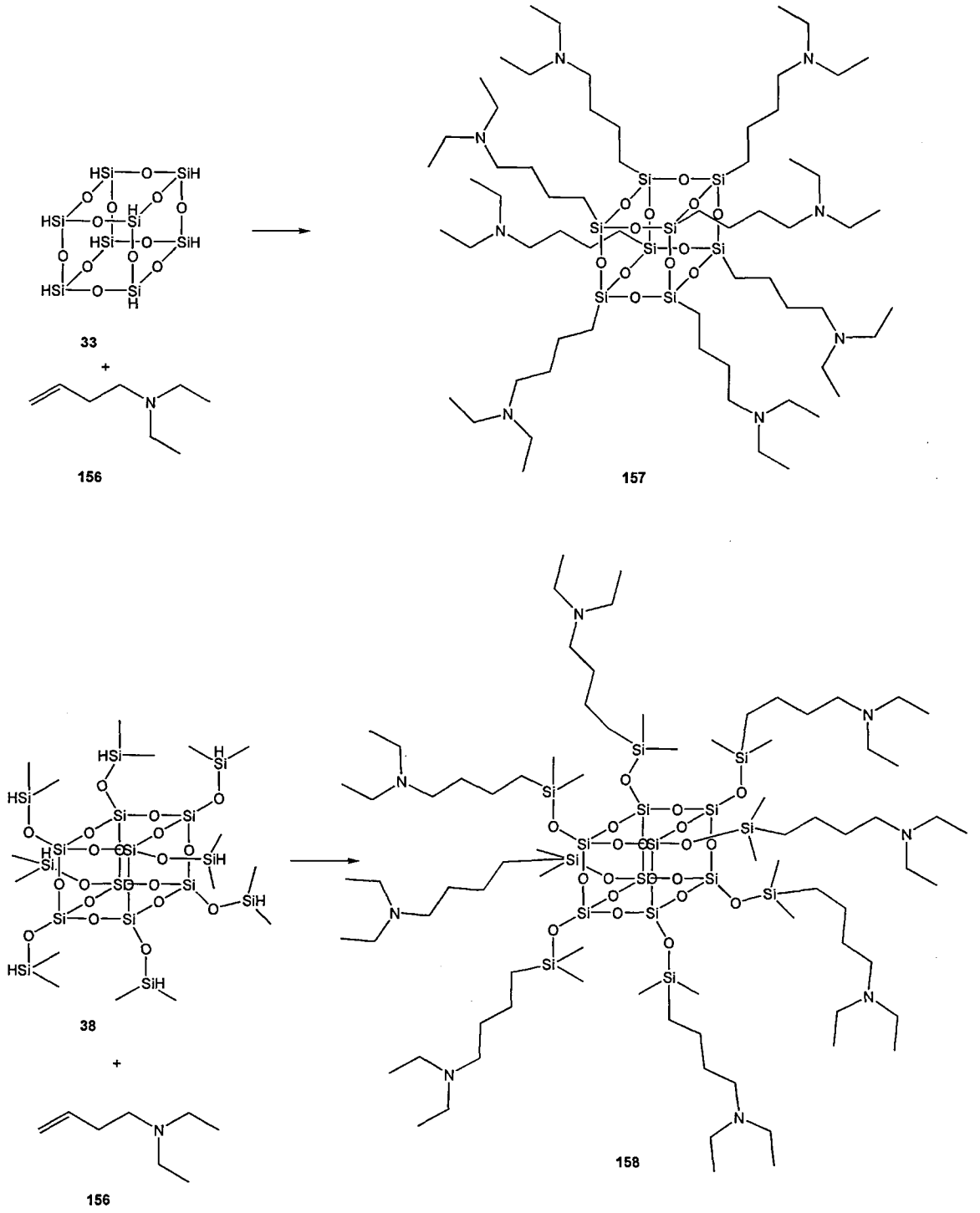

Figure 3.2.2.2: Hydrosilylation reaction of N,N-diethylbut-3-en-1-amine (156) with T_8H_8 (33) and $Q_8M_8^H$ (38) via Speier's catalyst.

The ^{29}Si NMR of the reaction mixture from T_8H_8 (**33**) showed that the signal had shifted downfield from −84.44 ppm to −66.0 ppm, in accordance with other alkyl T_8s with a extracted yield of 8mg, 85%. The ^{1}H and ^{13}C NMR showed that the alkene

had been removed by loss of the ^{1}H NMR signal at 4.98 and 5.73 ppm and signals in the ^{13}C NMR at 115.95ppm and 135.42ppm.

The NMR spectra of the reaction mixture from the $Q_8M_8^H$ complex (**158**) are more complex than those from the T_8H_8 complex (**157**), owing to the presence of two environments for the silicon (highlighted in red and purple). The ^{29}Si NMR shows a shift upfield from −0.78ppm to −11.31ppm upon hydrosilylation of the $HSi(CH_3)_2$ with the alkene. The chemical shift of the second silicon environment, the quaternary silicon (marked in purple), was shifted upfield from −107.79 ppm to −109.58 ppm. This shift was thought to be due to the N,N-diethylbut-3-an-1-amine group causing more shielding of the silicon (Figure 3.2.2.3). The reaction yielded 50mg of recoverable product.

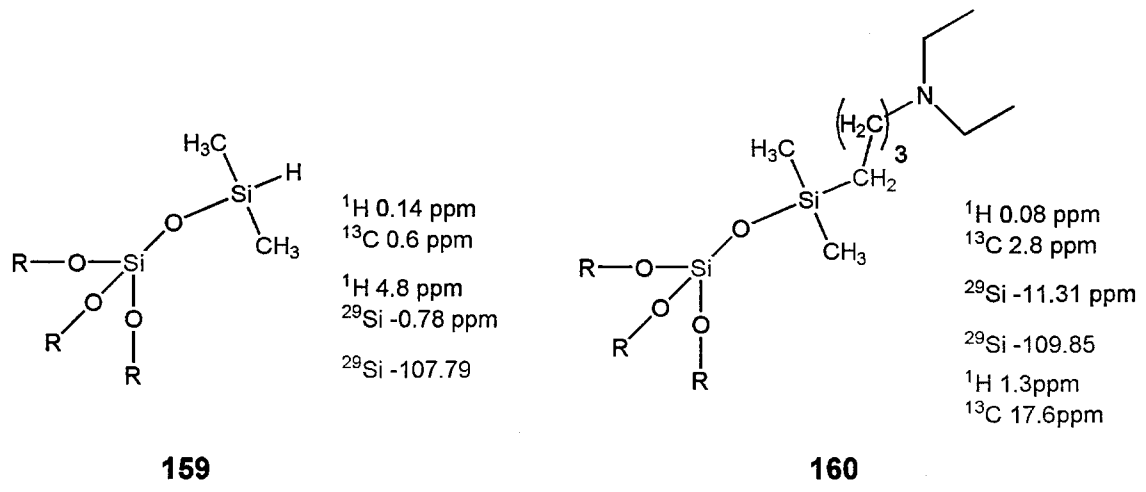

Figure 3.2.2.3: The different NMR environments and their NMR signal ppm for $Q_8M_8^H$ (159) and Q_8M_8-diethylbut-3-an-1-amine (160).

3.2.3: Reaction of butene-sDO3A-(ethyl) (101) with T_8H_8 (33)

As had been demonstrated in the model reaction, the prevention of water from entering the system was paramount. The reactions were performed in two types of reaction vessel. The first was a screw-topped reaction tube that was flushed with

argon and sealed with polytetrafluoroethylene (PTFE) tape. The second involved the use of a Schlenk line. All the glassware used in the hydrosilylation reactions was dried in an oven at 90 °C for a minimum of 3 hours, and cooled to room temperature in vacuum desiccators.

Butene-sDO3A-(ethyl) (**101**) and T_8H_8 (**33**) were combined with the Speier's catalyst and the reaction was heated to 80 °C for 24 hours; following that the product was dissolved in chloroform, which was then passed though an activated charcoal plug to remove the platinum from the reaction. The pooled eluent formed a mixture of solution and gel. The gel was extracted from the liquid by centrifugation. The liquid layer was decanted and the solvent was removed using reduced pressure, yielding a mixture of oil and solid. The mixture was dissolved in $CDCl_3$ and centrifuged to remove the insoluble gel. The sample was then analysed (Figure 3.2.3.1).

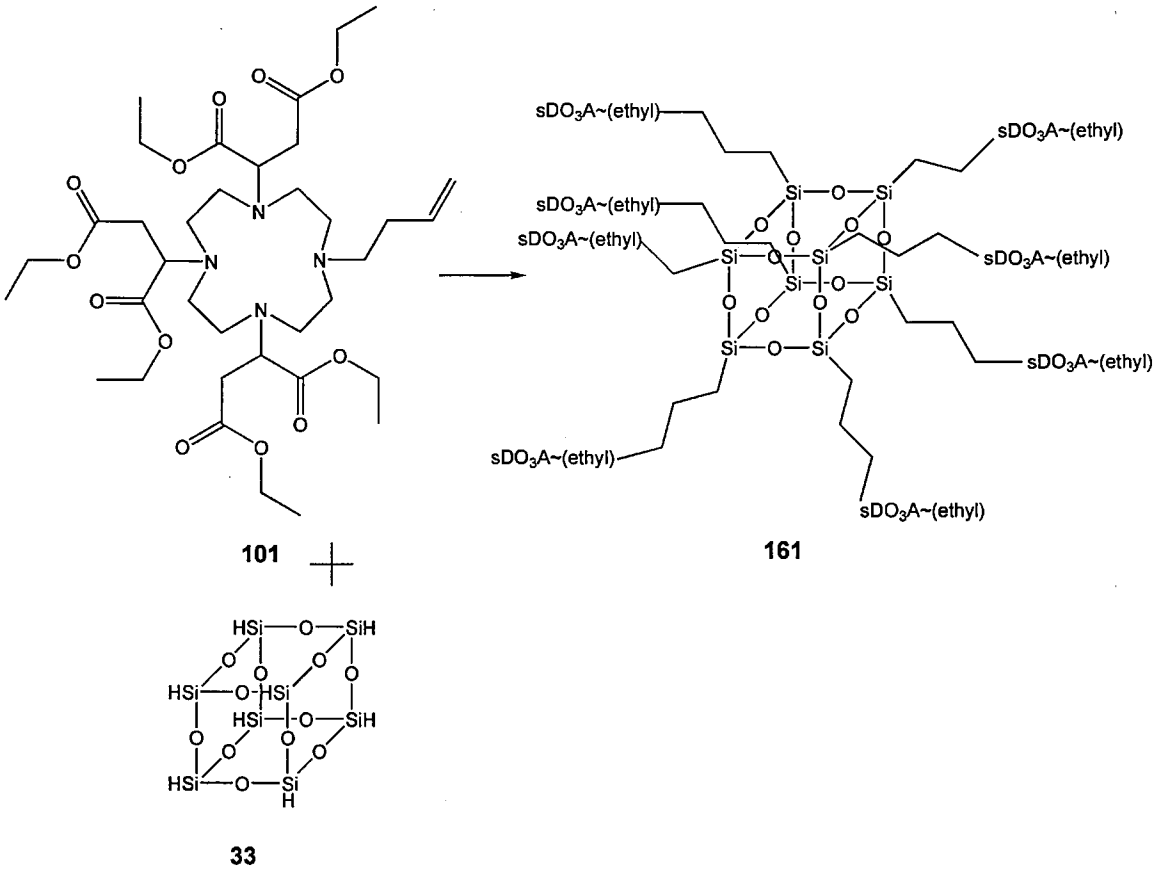

Figure 3.2.3.1: Reaction of butene-sDO3A-(ethyl) (101) with T_8H_8 (33)

The ^1H NMR of the original liquid layer showed that the alkene of the butene-sDO3A-(ethyl) (**101**) was still present and had not undergone the hydrosilylation reaction. The ^{13}C NMR also confirmed the presence of the alkene. The ^{29}Si NMR showed only the glass of the NMR tube. The gels from the first separation and the $CDCl_3$ extraction were dried under high vacuum, yielding small, spherical particles. Under the microscope (x 100) the particles were seen to be translucent and green in colour, with a glassy appearance.

Owing to the formation of the gel during filtration through activated charcoal, the reaction was repeated without the platinum-removal step. The reaction was set up as before. After being stirred at 80 °C for 24 hours, the reaction formed a gel within the reaction tube. The reaction was extracted using chloroform, which formed a precipitate. The precipitate was separated from the solution by centrifuge, yielding a gel, while the solution was decanted and the solvent removed using reduced pressure to yield a viscous oil, which was then taken up into $CDCl_3$. We attempted to dissolve the gel in hexane. The gel did not dissolve in hexane, but it formed a white solid, which when subjected to high vacuum to remove any residual solvent produced a glassy-looking product. ^1H NMR of the $CDCl_3$-soluble product showed that the sample was butene-sDO3A-(ethyl) (**101**), while ^{29}Si NMR gave a signal at −21.49 ppm, which was characteristic of a PDMS (Figure 3.2.3.2). This signal was characteristic of silicone grease. However, all the glassware had been washed with hexane at all stages of the reactions involving the cages and the formation of pentene-sDO3A-(ethyl) (**133**), in order to remove any residual grease, and the joints

within the glassware were sealed with PTFE tape. The ^{29}Si NMR needed a large number of scans to be able to detect the signal with no T or Q silicon's being visible in the ^{29}Si NMR spectra. This indicates that the silsesquioxane was undergoing hydrolysis of the silsesquioxane cage instead of the hydrosilylation reaction. This resulted in an insoluble polymer formed from the cage, while the unreacted alkene-sDO3A-(ethyl) went into solution.

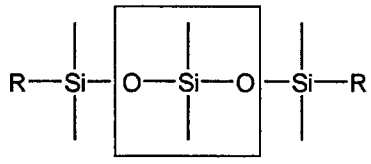

Figure 3.2.3.2: The silicon environment corresponding to −21.4 ppm

The formation of the gel in the second reaction suggested the presence of water in the starting materials. The butene-sDO3A-(ethyl) (**101**) with the six ester groups and the four amines was very hydrophilic and absorbs water readily. Owing to the range of chemical functional groups in the butene-sDO3A-(ethyl) (**101**), the most effective method for drying was the use of molecular sieves. Because of the viscous nature of butene-sDO3A-(ethyl) (**101**), a solvent would have to be used. Toluene was chosen for its high boiling point, its lack of reactivity to hydrosilylation reactions[75] and its non-polar properties, reducing water absorption from exposure to the air. The two pore sizes ideal for removal of water are 3 Å and 4 Å, with 4 Å being preferred for non-polar solvents. The molecular sieve was activated at 300 °C for 12 hours, cooled under vacuum and kept under argon. The butene-sDO3A-(ethyl) (**101**) was dissolved in toluene, to which the sieve was added and kept under argon for 24 hours, after which the solution was decanted onto a fresh sieve and kept for another 24 hours

under argon and sealed with a suba seal. The solution was then taken directly from the flask via syringe and used immediately in the reaction with T_8H_8 (**33**) to avoid moisture absorption. The reaction was heated to 80 °C for 48 hours, after which the solvents were removed using reduced pressure to yield the crude product. The crude product was shown by TLC (DCM 95%, EtOH 5%) to be a mixture of two products. The spot at Rf 0.56 co-spotted with butene-sDO3A-(ethyl) (**101**), while the second spot remained on the base line, and was the polymerised gel. The crude product was extracted first with $CDCl_3$, which left a residual gel that was dissolved in $C_6D_5CD_3$ to leave only a small amount of insoluble material. The ^1H and ^{29}Si NMR spectra of the chloroform-soluble component, by comparison with the NMR of the starting alkene, showed the product to be a mixture of mainly butene-sDO3A-(ethyl) (**101**) and butane-sDO3A-(ethyl) (**162**) (Figure 3.2.3.3). The $C_6D_5CD_3$ fraction showed butene-sDO3A-(ethyl) (101) in the ^1H NMR spectra. The ^{29}Si NMR showed the silicone grease at -21.40ppm. The spectra also showed two other peaks at -111.06 and -116.14 ppm. These two peaks correspond to quaternary silicon atoms. With the presence of the alkene on the amine indicate that the presence of this silicon compound was minimal.

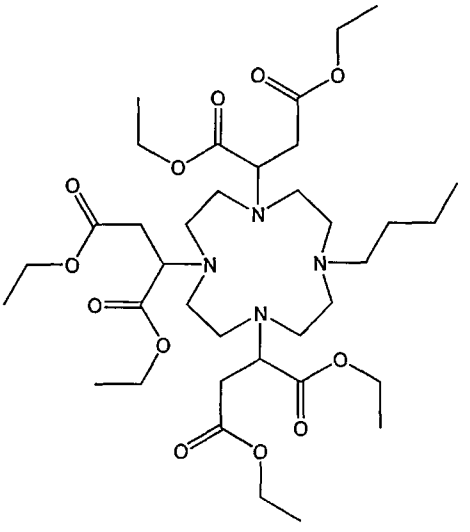

162

*Figure 3.2.3.3: Structure of butane-sDO3A-(ethyl) (**162**)*

The formation of butane-sDO3A-(ethyl) (**162**) was a result of the alkene reacting with the T_8H_8 via hydrosilylation, then decomposing to the alkane. There was a trace NMR signal in both the ^1H and ^{13}C NMRs at 0.04 ppm, and 0.94 ppm respectively. These peaks correspond to Si–CH_n bond formation, and are likely to be due to the grease.

3.2.4: Reaction of butene-sDO3A-(ethyl) (101) with $Q_8M_8^H$ (38) via Speier's catalyst

Owing to the T_8H_8 (**33**) readily undergoing hydrolysis, an alternative cage was investigated. Octakis(dimethylsilyloxy)silsesquioxane ($Q_8M_8^H$) (**38**) was less likely to undergo hydrolysis because of the lower reactivity of the $SiH(Me_2)(OR)$ when compared to $SiH(OR)_3$[75].

The first $Q_8M_8^H$ (**38**) reaction to form the Q_8M_8-butane-sDO3A-(ethyl) (**163**) was performed in toluene in which butene-sDO3A-(ethyl) (**101**) was dissolved, along with $Q_8M_8^H$ (**38**) to which Speier's catalyst had been added. The reaction was heated to 80 °C for 65 hours, while being monitored by FTIR looking at the Si–H stretch at 1694 cm^{-1}. The reaction was passed though an activated charcoal plug and the solvent was removed using reduced pressure to give a clear gum. The product was taken up into $C_6D_5CD_3$, leaving a residual gum-like product that formed a glassy product upon vacuum drying (Figure 3.2.4.1).

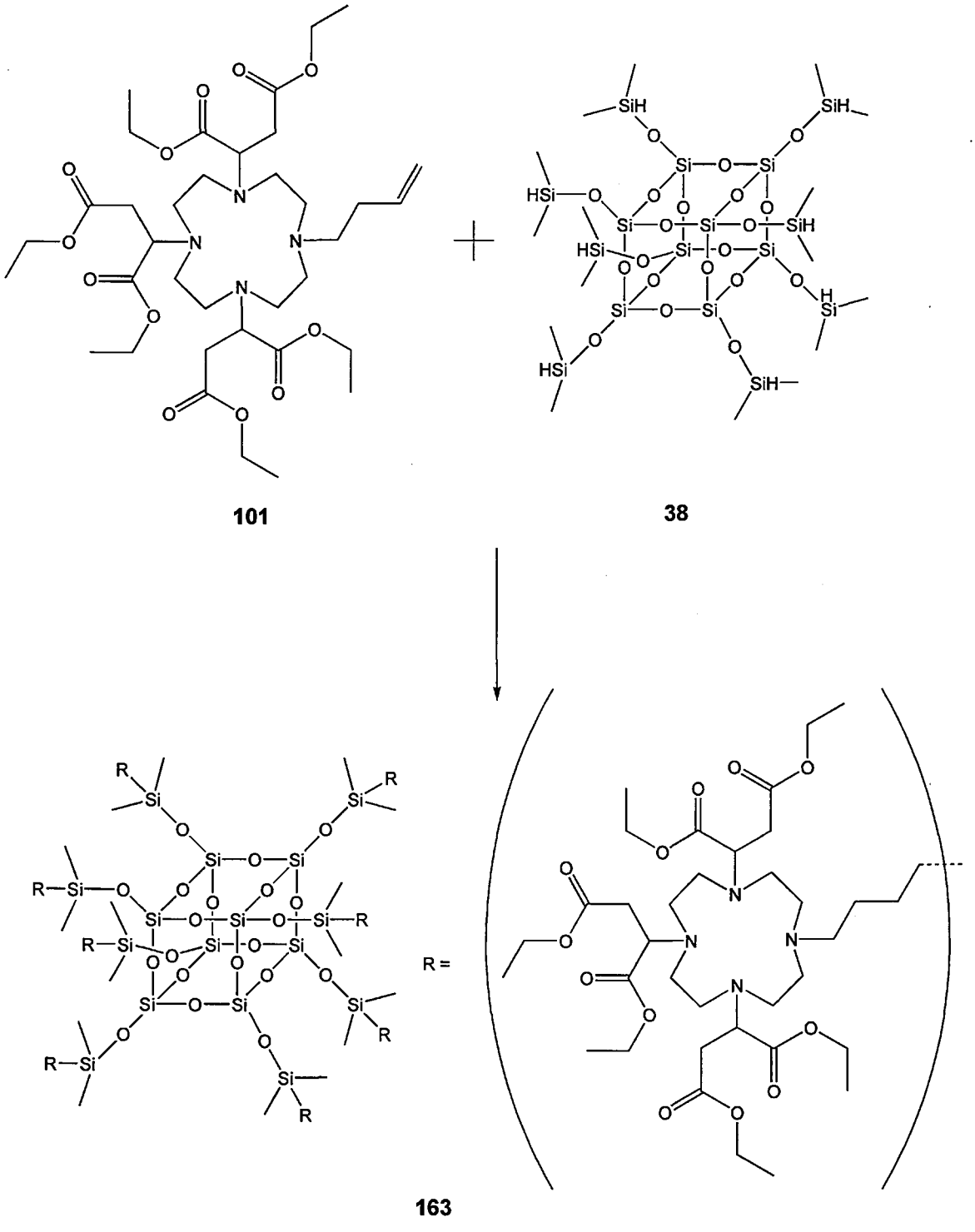

Figure 3.2.4.1: Reaction of butene-sDO3A-(ethyl) (101) with $Q_8M_8^H$ (38)

The ^{29}Si NMR showed that the cage had decomposed, with the major peak appearing at −21.47 ppm, and no sign of the peak for the $SiH(CH_3)_2$ group at −0.78 ppm. The ^{29}Si NMR did show very small trace peaks, which were just above the

background noise, at −1.10 and −11.23 ppm, corresponding to the formation of an Si–C bond. Since it appeared that the hydrolysis of $Q_8M_8^H$ (**38**) occurred during the reaction, an alternative method to the drying of butene-sDO3A-(ethyl) (**101**) over molecular sieve was investigated: namely, a Dean–Stark-based azeotropic distillation. The butene-sDO3A-(ethyl) (**101**) (400 mg) was dissolved into 38 ml of toluene, and the drying process was run for 4 hours, with 12 ml of solvent being removed. From this stock solution a 5 ml aliquot was taken and used in the experiment as before, with the Speier's catalyst and $Q_8M_8^H$ (**38**). The reaction produced a yellow gel, which on analysis by ^1H, ^{13}C and ^{29}Si NMR showed the same decomposition products as before in the T_8H_8 with the ^1H and ^{13}C NMR spectra showed the reaction product to be a mixture of butane-sDO3A-(ethyl) (**162**) and butene-sDO3A-(ethyl) (**101**), and the FTIR showed the loss of the Si–H stretch at 2144 cm^{-1} .

3.2.5: Reactions of pentene-sDO3A-(ethyl) (194) with $Q_8M_8^H$ (38) *via* Karstedt's catalyst

Since it seemed the decomposition of the $Q_8M_8^H$ (**38**) cages occurred with the Speier's catalyst, the alternative Pt-based Karstedt's catalyst (**145**) was investigated. The benefit of Karstedt's catalyst was that it was dissolved in toluene, which, unlike the 2-propanol used as a solvent in the Speier's catalyst, should not rapidly absorb water and thus catalyse the decomposition of the cages.

An alternative to butene-sDO3A-(ethyl) (**101**), pentene-sDO3A-(ethyl) (**133**), was employed. The pentene-sDO3A-(ethyl) (**133**) was dissolved in toluene and dried over 4 Å molecular sieve for 48 hours, as before. The reaction was catalysed using Karstedt's catalyst and heated to 80 °C for 18 hours. After the solvent had been

removed the residual platinum was removed by take-up of the crude product in dichloromethane. This was followed by refluxing the solution with activated charcoal, which was then removed using gravity filtration. The ^{1}H and ^{13}C NMR suggested a mixture of products, including pentane-sDO3A-(ethyl) (**133**), was confirmed by the absence of the alkene signals. The ^{29}Si NMR had a major peak at −21.49 ppm, but no peak corresponding to $HSi(CH_3)_2$. The signal arising from the Q Si–O–Si group had also disappeared, suggesting that $Q_8M_8^H$ (**38**) had undergone the same form of hydrolysis as the T_8H_8 (**33**).

The only other possible source of water was the catalysts. To see if that was causing the hydrolysis of the cage, the following test reaction was performed. The T_8H_8 (**33**) and Speier's catalyst were combined in anhydrous toluene, and heated to 80 °C for 48 hours. The solvents were removed to yield a white solid, which was shown by ^{1}H and ^{29}Si NMR and FTIR to be the unreacted T_8H_8 (**33**) cage.

This showed that the hydrolysis must arise from water in the butene/pentene-sDO3A-(ethyl) (**101**)/(**133**). There must be bound water within the sDO3A-(ethyl) structure or the amines of the cyclen, which was responsible for the hydrolysis seen in the cage reactions. This form of decomposition has been observed with primary, secondary and simple tertiary amines, where the decomposition was relatively rapid in wet solvents but much slower in anhydrous systems.[72-74] As the decomposition of both cages still occurred even after the appropriate alkene-sDO3A-(ethyl) had been dried, this suggests that the decomposition was catalysed by the amine groups of the cyclen. The earlier reaction with N,N-diethylbut-3-en-1-amine showed no decomposition of the T_8H_8 (**33**) and $Q_8M_8^H$ (**38**) cages. This suggests that the tertiary amines of the alkene–sDO3A-(ethyl) have no role in the decomposition. The only

possibility left was that the alkene–sDO3A-(ethyl) undergoes an elimination reaction with the platinum catalyst, forming a secondary amine by the loss of one of the succinate groups, and it was this amine group that catalyses the hydrolysis reaction.

3.3: Investigation into the stability of pentene-sDO3A-(ethyl) (133) in the presence of a platinum catalyst

The platinum catalyst itself could have been causing the decomposition of the alkene–sDO3A-(ethyl), producing a fumarate or maleate and, importantly, a secondary amine, which would catalyse the hydrolysis of the cage in the presence of water. The stability of the pentene-sDO3A-(ethyl) (**133**) in the presence of the platinum catalyst was investigated by dissolving pentene-sDO3A-(ethyl) (**133**) in $CDCl_3$ to which the catalyst had been added, and warming to 80 °C for 48 hours. Both Speier's and Karstedt's catalysts were used.

The analysis of the reaction of pentene-sDO3A-(ethyl) (**133**) with the Speier's catalyst by ^{1}H and ^{13}C NMR showed that a mixture of pentene-sDO3A-(ethyl) (**133**), propan-2-ol (**144**) and a trace amount of (Z)-3-(ethoxycarbonyl)acrylic acid (**127**) had been formed. The strongest evidence was obtained from the ^{13}C NMR. The carbonyl of the ethyl ester of the (E/Z)-3-(ethoxycarbonyl)acrylic acid (**125/127**) occurs at a characteristic position of around 164 ppm. In the reaction mixture the signal was between 175 and 178 ppm, suggesting the loss of an ethyl group from the pentene-sDO3A-(ethyl) (**133**).

The reaction of pentene-sDO3A-(ethyl) (**133**) with Karstedt's catalyst showed the formation of (Z)-3-(ethoxycarbonyl)acrylic acid (**127**), using both ^{1}H and ^{13}C NMR spectroscopy. The formation of the acrylic acid arises from the decomposition of the pentene-sDO3A-(ethyl) (**133**), forming pentene-sDO2A-(ethyl) (**164**) (Figure 3.3.1).

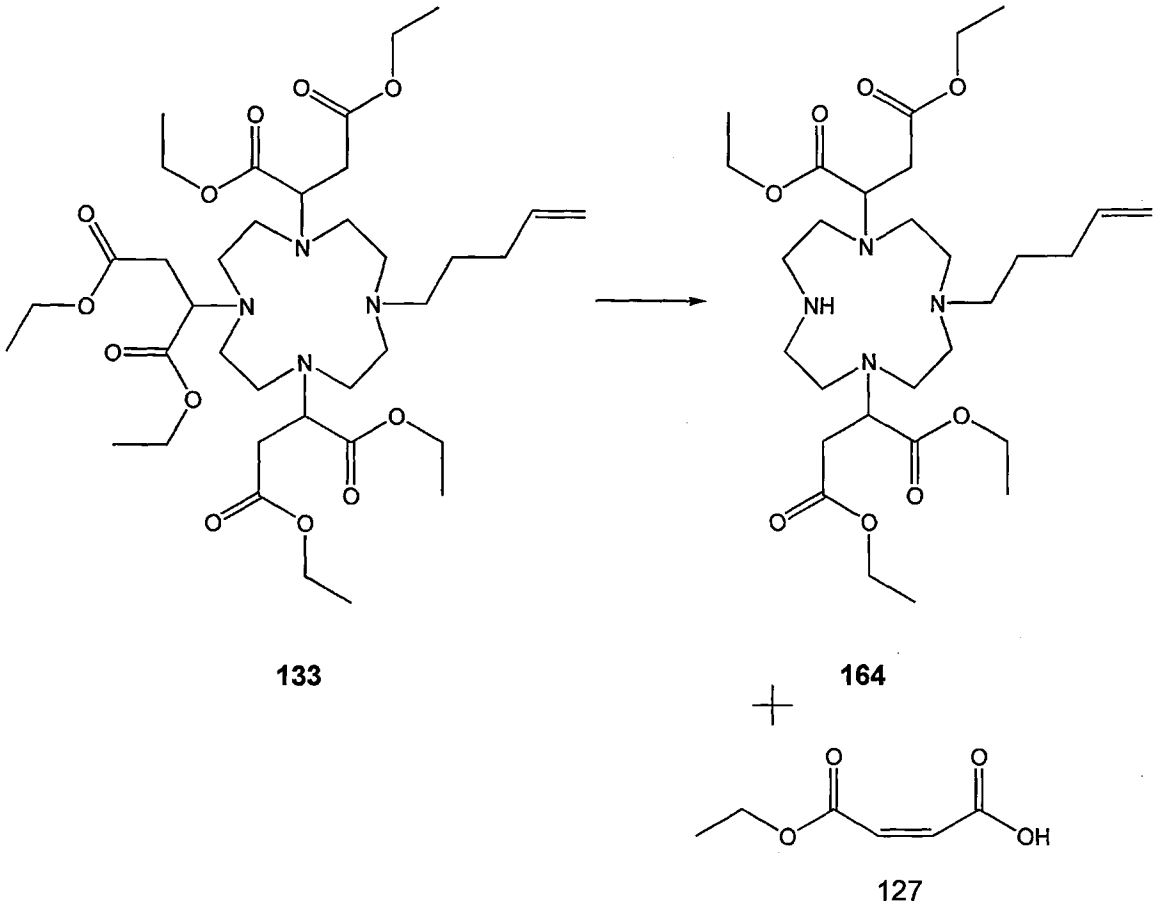

Figure 3.3.1: Decomposition of pentene-sDO3A-(ethyl) (133) to pentene-sDO2A-(ethyl) (164).

This suggests that in the hydrosilylation reaction a secondary amine was formed, which catalyses the hydrolysis of the siloxane cage with extraneous water. It has been reported that both maleate and fumarate inhibit Karstedt's catalyst by binding to the platinum, thus preventing hydrosilylation.[114, 115] Thus the corresponding acids

are formed in the decomposition reaction, leading to the inhibition of the catalyst by the alkene bonds next to carboxyl functional groups (Figure 3.3.2).

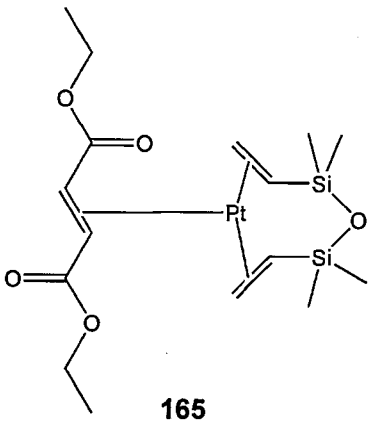

165

Figure 3.3.2: Complex (165) formed during the inhibition of Karstedt's catalyst by fumarate[115]

3.4: Alternative route to the formation of Q_8(pentene-sDO3A-(ethyl))$_8$

Clearly the direct hydrosilylation between the silsesquioxane cages and pentene-sDO3A-(ethyl) (**133**) failed because of the decomposition of pentene-sDO3A-(ethyl) (**133**) by the platinum catalyst. The most logical approach to preventing the decomposition was to remove the step where both the cyclen and platinum are present together. This was achieved by the hydrosilylation reaction being performed before the introduction of the sDO3A-(ethyl) (**107**) group.

The hydrosilylation reaction of $Q_8M_8^H$ (**38**) with 5-bromopent-1-ene (**134**) was performed to give Q_8-(1-bromopentane)$_8$ (**166**), which could then be reacted with sDO3A-(ethyl) (**107**) to give the target ligand. The first step was performed in toluene to which $Q_8M_8^H$ (**38**) and 20 eq of 5-bromopent-1-ene (**134**) were added. Speier's

catalyst was used for this reaction (Figure 3.4.1). The reaction yielded the product with a yield of 84%, as shown by ^{1}H, ^{13}C and ^{29}Si NMR spectroscopy. The ^{29}Si NMR gave two peaks at −11.32 ppm and −109.5 ppm, which was a result similar to the reaction product from N,N-diethylbut-3-en-1-amine (**156**) and $Q_8M_8^H$ (**38**).

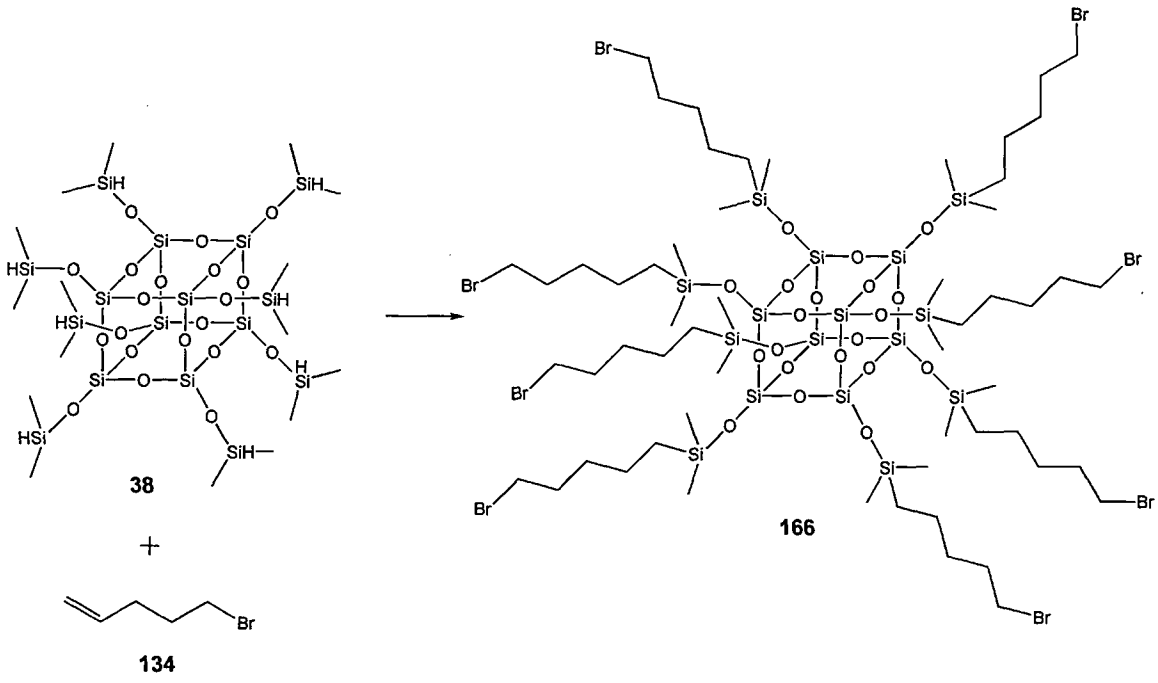

Figure 3.4.1: Formation of Q_8M_8(1-bromobutane)$_8$ (166)

The second step was performed in acetonitrile along with potassium carbonate, in the same manner as the synthesis of butene-sDO3A-(ethyl) (**101**) (Figure 3.4.2). The solids were removed from the reaction and the solvent by filtration to give a yellow solid after evaporation of the solvent. The product was extracted from the solid by DCM to give an oily product. The ^{1}H NMR showed the loss of the CH_2–Br group, indicating that the intended reaction had taken place. The ^{29}Si NMR, however, showed that a side reaction had occurred and the product had been decomposed, as before, giving a signal at −21.40 ppm. There was also a trace peak of an

unknown compound at −97.21 ppm. This decomposition was most likely due to the secondary amine catalysing the hydrolysis of the silicon cage, as before.

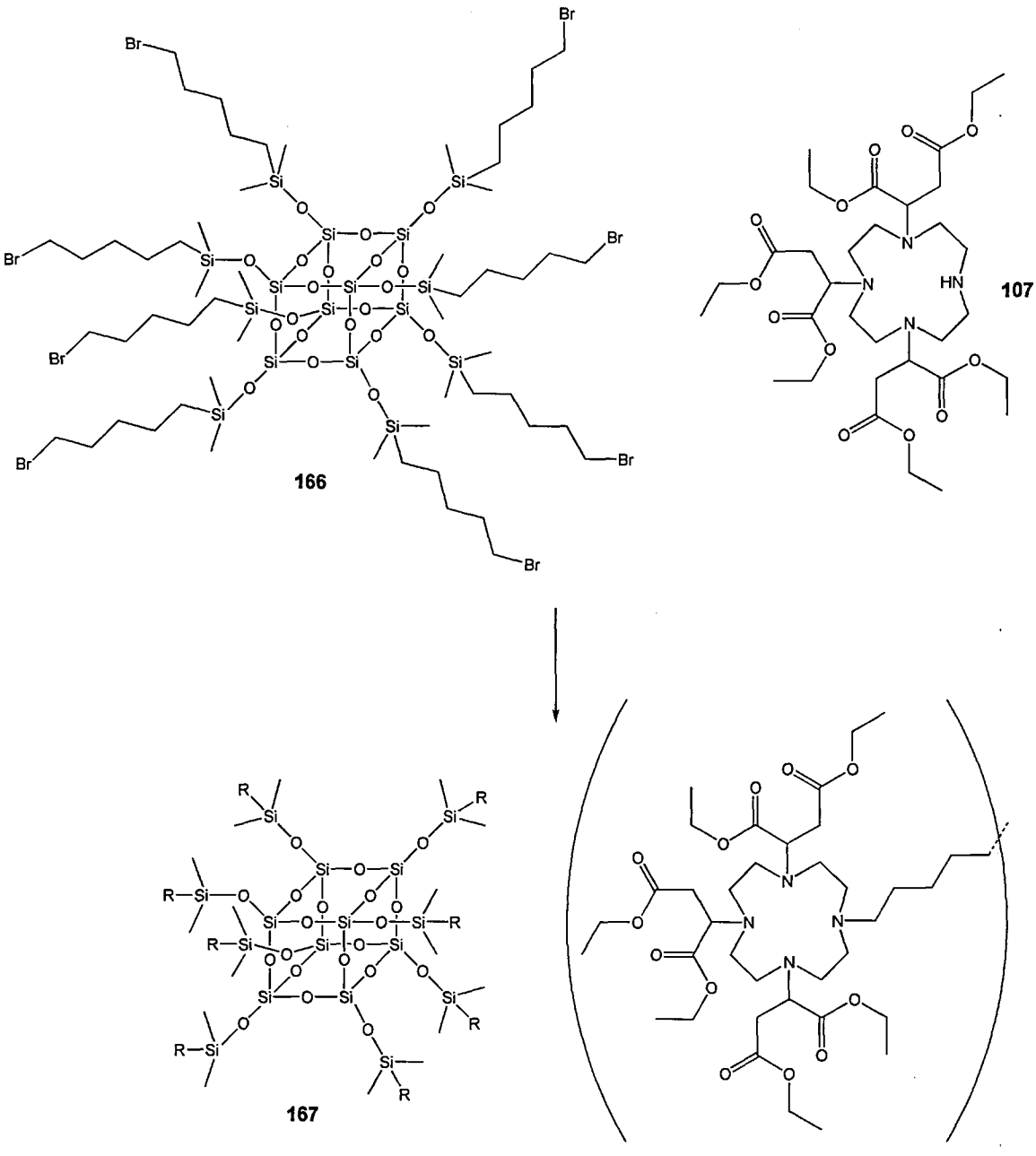

Figure 3.4.2: Formation of Q_8(pentane-sDO3A-(ethyl))$_8$ (187)

3.5: Mechanism for the decomposition of silsesquioxane cages

The main cause of the decomposition and polymerisation of the silsesquioxane cages was side reactions that occur when pentene-sDO3A-(ethyl) (**133**) reacts with the cages. It was noted earlier that NMR suggested the alkene had been removed by the hydrosilylation reaction (red arrow) with the silsesquioxane cage, showing that the intended reaction had worked. The problems occurred when the pentene-sDO3A-(ethyl) (**133**) reacted with the platinum catalyst and formed pentene-sDO2A-(ethyl) (**164**) and an acrylic acid (Figure 3.5.1.).

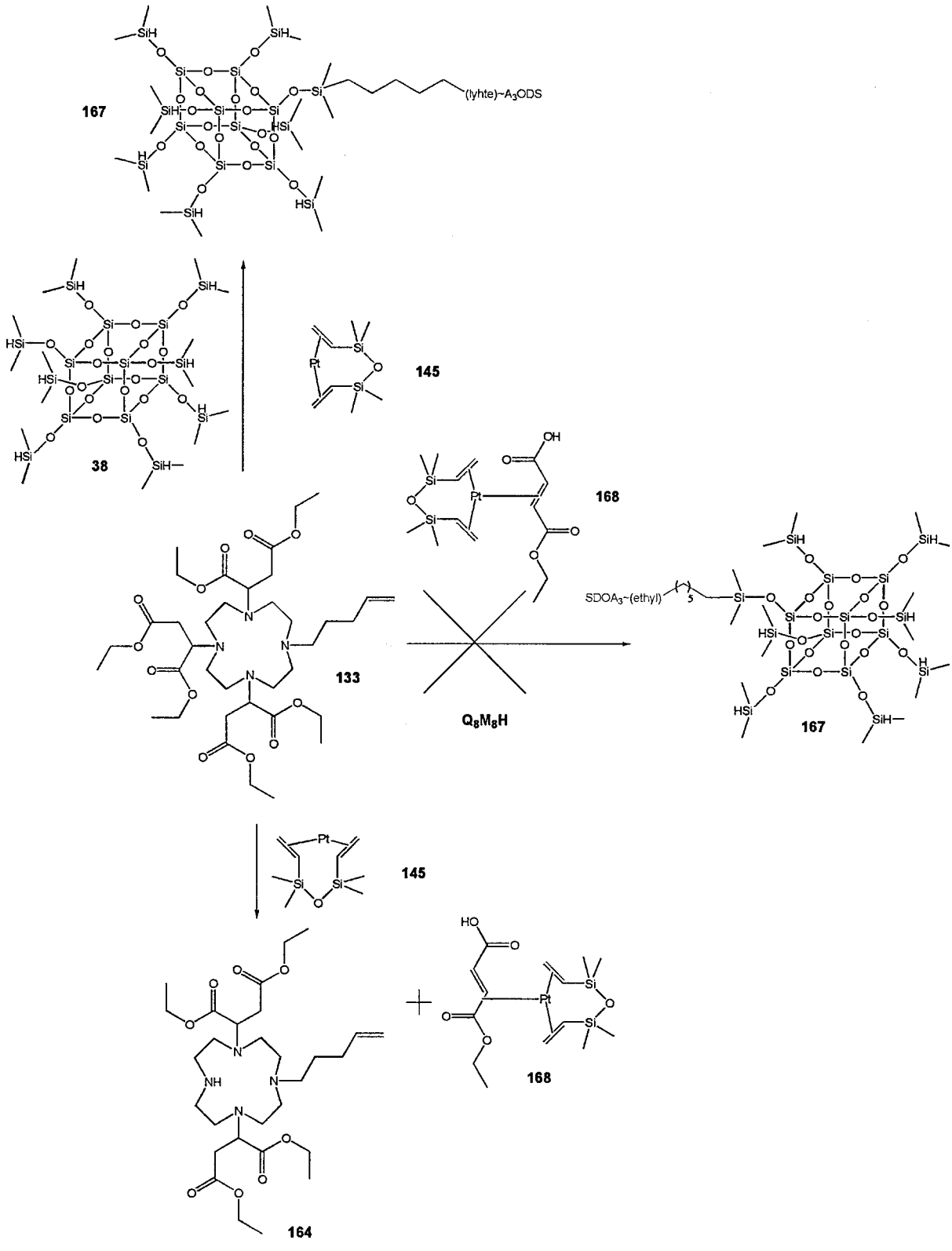

Figure 3.5.1: The different reactions of pentene-sDO3A-(ethyl)

The pentene-sDO2A-(ethyl) (**164**) can decompose both T_8H_8 (**33**) and $Q_8M_8^H$ (**38**) in the same fashion. There are three ways in which the $Q_8M_8^H$(**38**) can decompose. The first was the removal of the $SiH(CH_3)_2$ group by the pentene-sDO2A-(ethyl), producing an Si–OH group on the cage, which then undergoes a siloxane bond-forming reaction with another $Q_8M_8^H$ to form an Si–O–$Si(CH_3)_2$– bond. The pentene-sDO3A-(ethyl) (**164**) was re-formed by the reaction of the intermediate (**169**) with water, generating the silanol (**171**). The silanol produced would then react with the $Q_8M_8^H$ forming (**173**) (Figures 3.5.2 and 3.5.3).

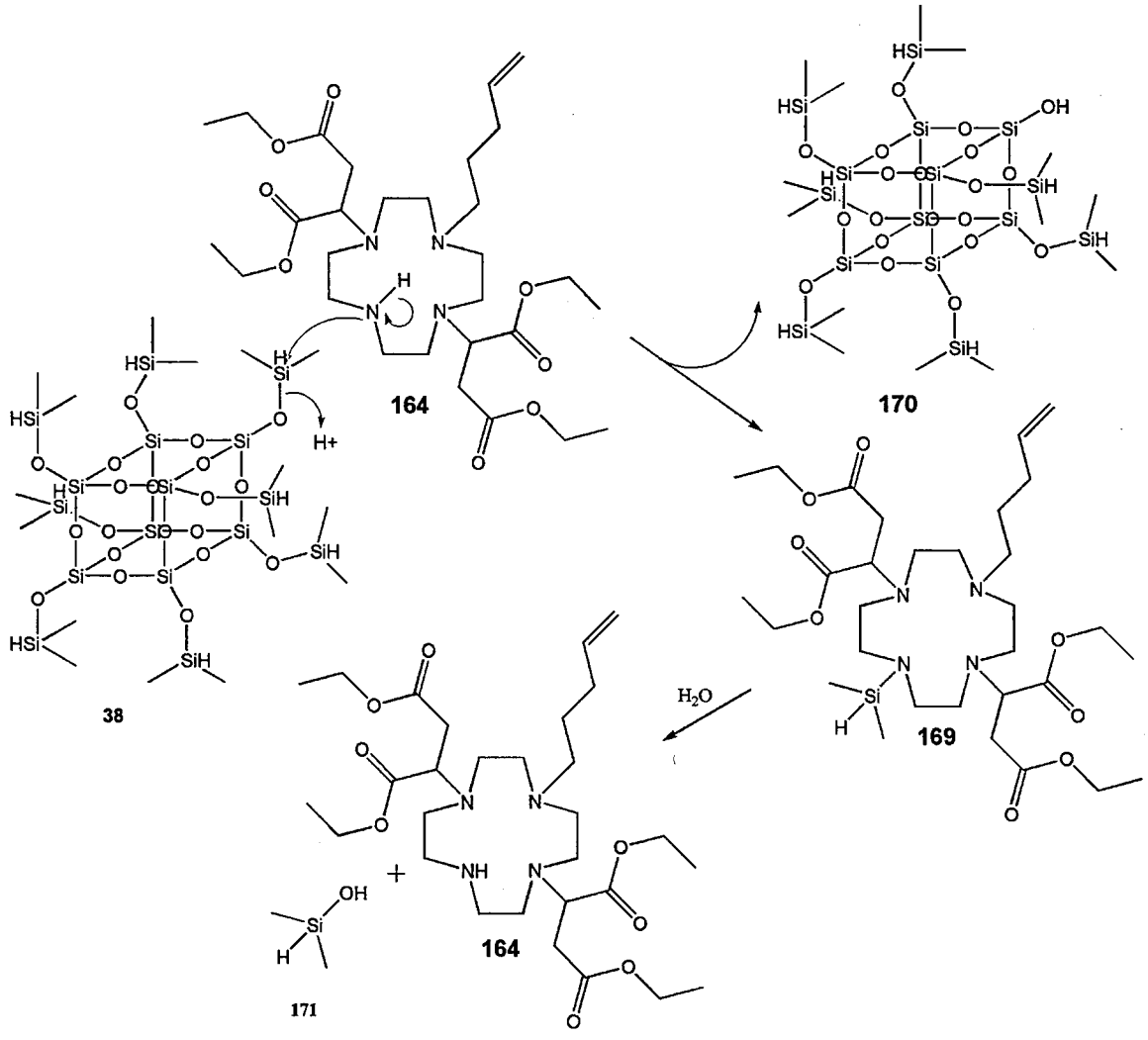

Figure 3.5.2: Decomposition of Q8M8^H (38) by pentene-sDO2A-(ethyl) (164).

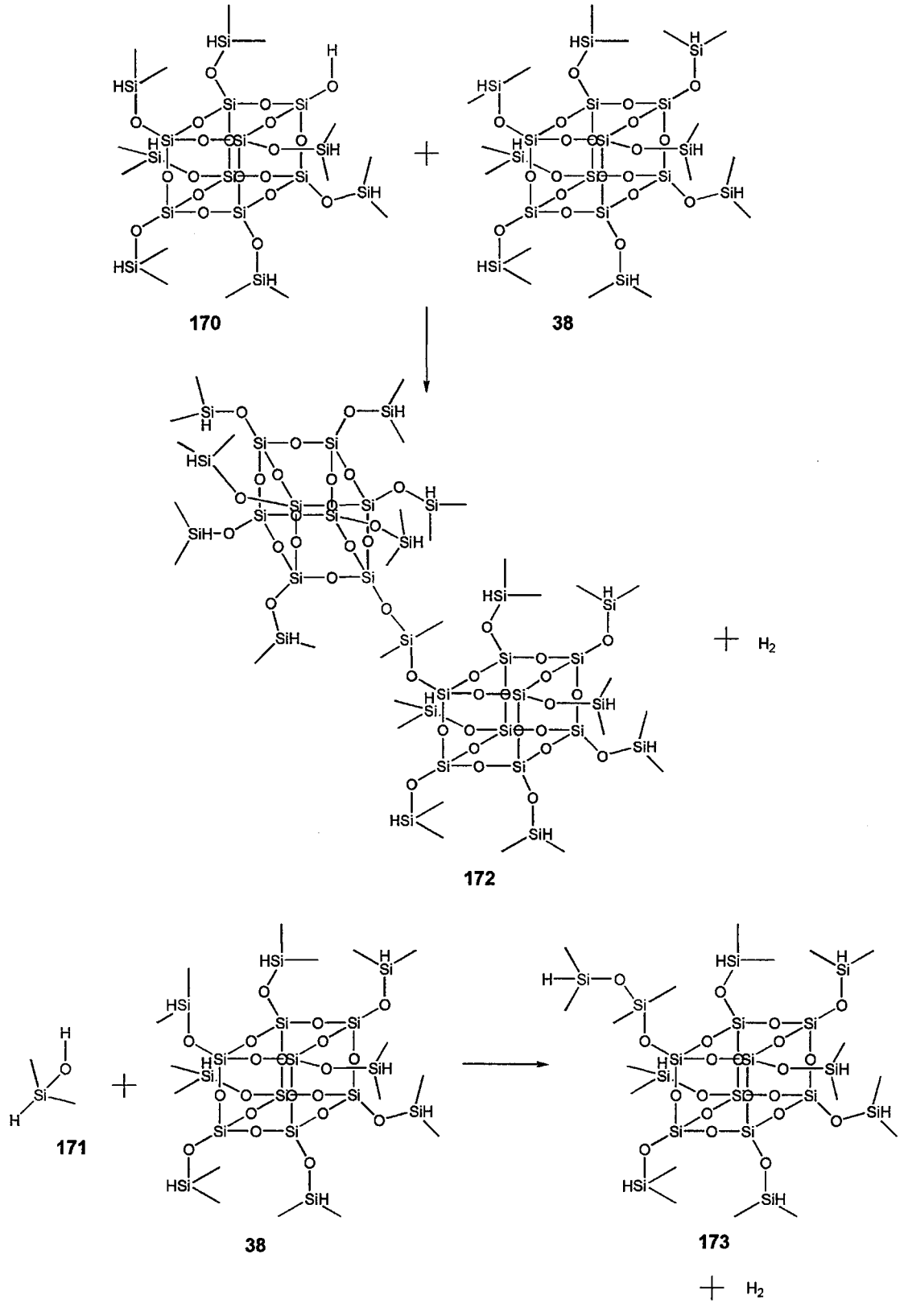

Figure 3.5.3: Reaction of $Q_8M_8^H$ (38) with compound (170)

The alternative reaction for the Si–OH group, for example compound (**170**), was to react with another unit of pentene-sDO2A-(ethyl) (**164**), producing a larger

compound which in turn reacts with $Q_8M_8^H$ (**38**), (**174**) leading to the incompletely condensed silsesquioxane (**175**)[72, 73] (Figure 3.5.4). This would then decompose into penetene-sDO2A-(ethyl) (**164**) and the linked cages (**176**). This would lead to an increases in the presence of -21 ppm in the ^{29}Si NMR and importantly it would continue to polymerise to form the insoluble gels seen in the reactions.

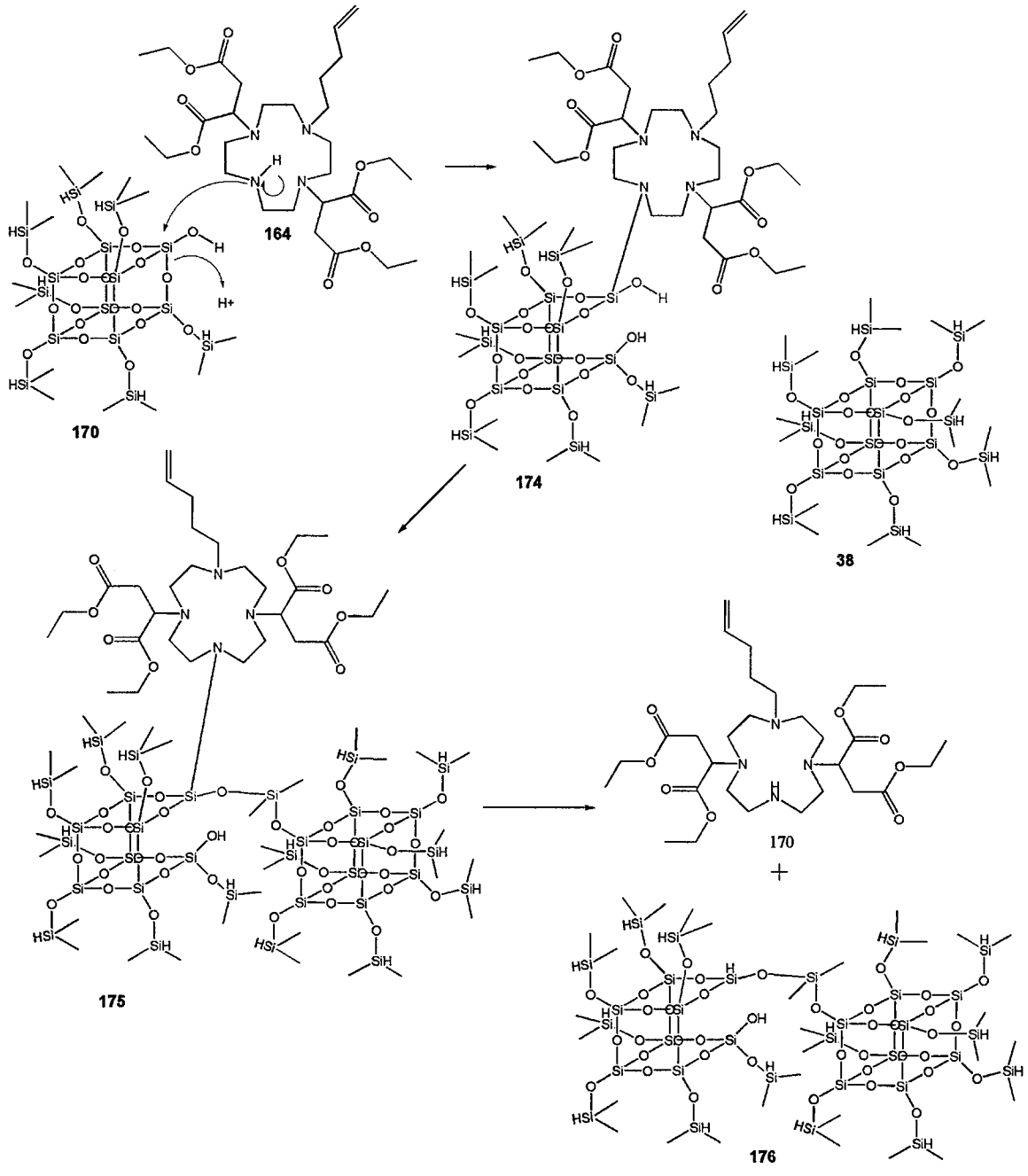

Figure 3.5.4: Linking of an incompletely condensed silsesquioxane (175) with $Q8M8^H$ (38)

The T_8H_8 (**33**) cage may undergo similar decomposition reactions to $Q_8M_8^H$ (**38**). The first reaction was the opening of the cage by reaction with pentene-sDO2A-(ethyl) (**164**), forming an intermediate compound (**176**), which then reacts with another T_8H_8 (**33**) or an incompletely condensed silsesquioxane (**177**) to give the polymerised product (**178**) (Figure 3.5.5).

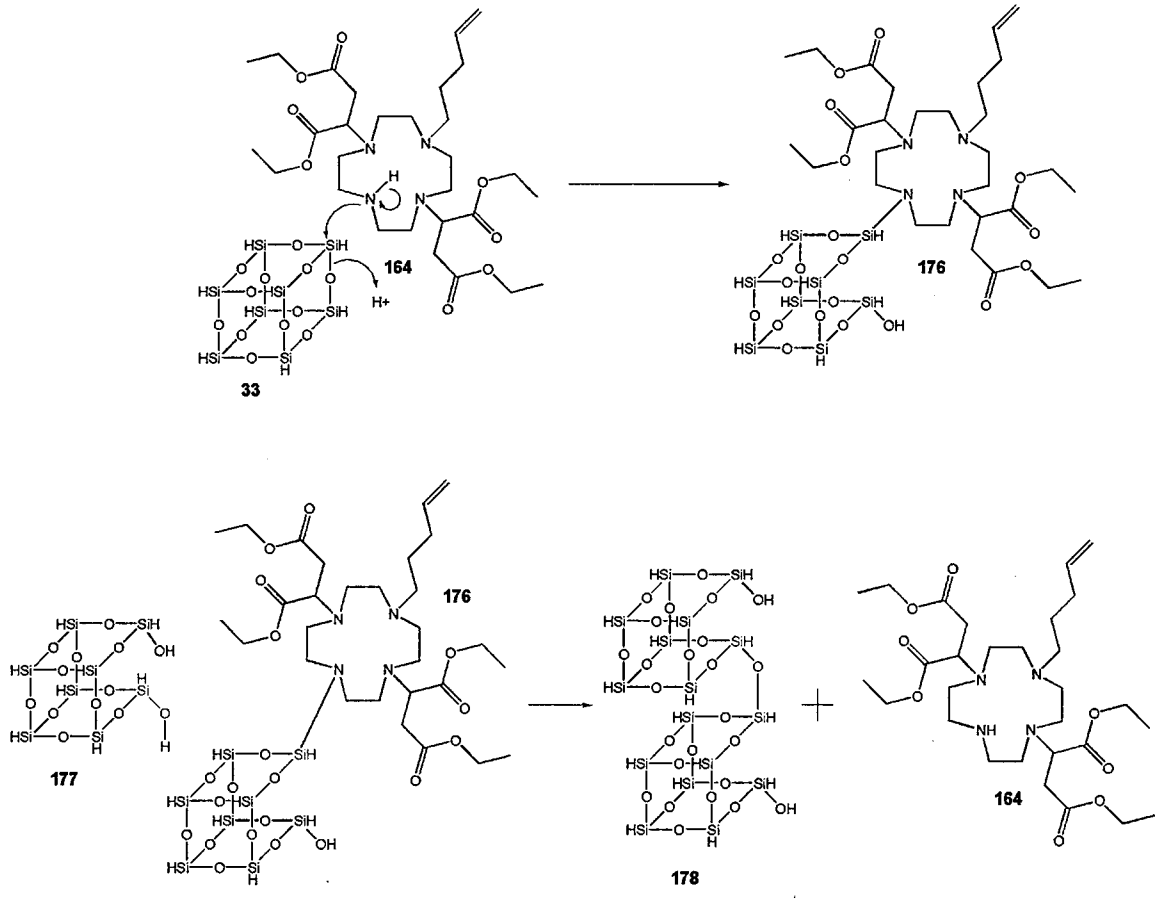

Figure 3.5.5: Decomposition of T8H8 (33) via pentene-sDO2A-(ethyl) (164)

These reactions can continue occurring with catalytic amounts of pentene-sDO2A-(ethyl) (**164**) in the presence of water, until the relative silsesquioxane cage has been fully polymerised. The sDO3A-(ethyl) (**107**) and pentene-sDO3A-(ethyl) (**133**) are too hygroscopic for the hydrosilylation reactions. Several methods were utilised in the drying of the reactions and of the starting materials. The drying of the catalyst did not make any difference, in that the reactions still produced the gel. This points to the

cyclen as the source of the water, such that the hygroscopic properties of the cyclen were greater than those of the physical drying methods used. It was the presence of this water that, along with the decomposed sDO3A-(ethyl) (**107**), created the conditions for the decomposition. The hydrolysis of the cages competes with the hydrosilylation reaction, and the resulting mixture of hydrolysed and hydrosilylated cages forms the insoluble gel seen in the reaction. It was this insolubility that led to its absences in the ^{29}Si NMR leaving only the signal at −21 ppm, which arose from a trace of the silicon grease used within the laboratory as a general lubricant and sealant of gas-tight joints. It might also have been present in the NMR probe.

This was evident in the T_8H_8 hydrosilylation reactions from the presence of $(RO)_2Si(CH_3)_2$, which gave the signal at ^{29}Si NMR −21 ppm that should not have been formed from the T_8H_8. The $Q_8M_8^H$ (**38**) was different, in that it was possible to form the $HOSi(CH_3)_2OH$ by decomposition of the outer silicon groups (Figure 3.5.6).

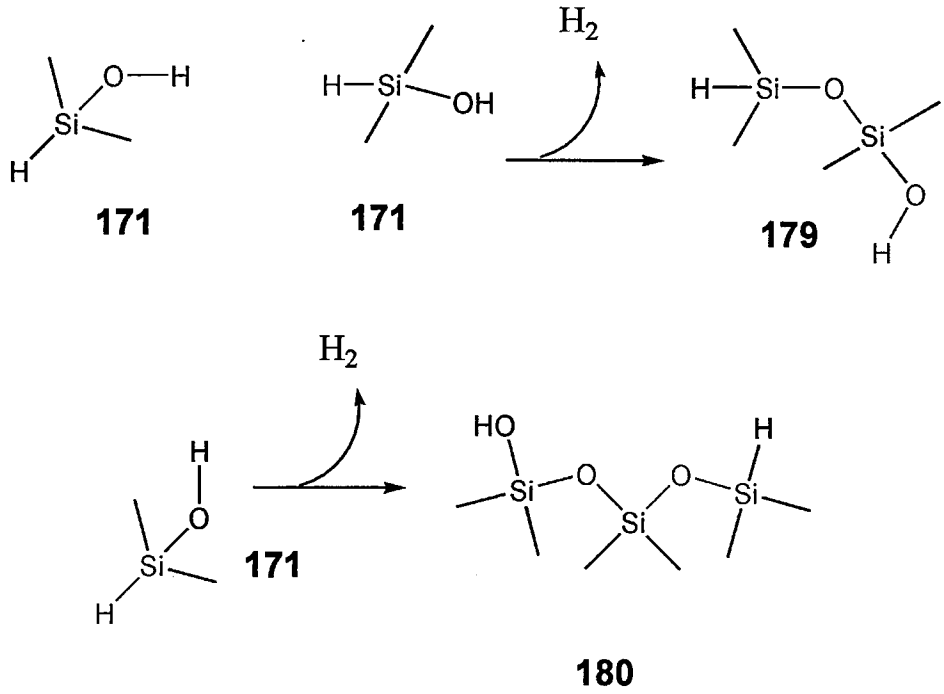

Figure 3.5.6: Formation of –(O-Si(CH$_3$)$_2$-O)n- (180) by the hydrolysis of Q_8M_8H

The water that leads to the hydrolysis of the silicon cages was prevented from being removed by hydrogen bonding to the sDO3A-(ethyl) (**107**) via the carbonyl functional groups, and also the amines. As the sDO3A (**32**) forms a cage-like structure, it effectively traps the water, preventing the drying agents from capturing it. This film of water surrounding the sDO3A-(ethyl) (**107**) leads to the hydrolysis of the Si–N bonds, which are highly labile in the presence of water, and thus regenerates the secondary amine, allowing the cyclen to catalyse the decomposition of the cages. The route with the T_8 and Q_8 cages had to be abandoned because of this hydrolysis, as it was not possible to fully dry the sDO3A-(ethyl) (**107**) or pentene-sDO3A-(ethyl) (**133**) and thus prevent the hydrolysis of the T_8H_8 (**33**) and $Q_8M_8^H$ (**38**) from occurring.

3.6: Reaction of butene-sDO3A-(ethyl) (133) with simple silloxanes and silanes

Since the hydrolysis of the cages occurred in the reactions of both pentene-sDO3A-(ethyl) (**133**) and butene-sDO3A-(ethyl) (**101**), alternative silicon compounds were investigated. Three different substrates were chosen: 1,1,3,3,5,5-hexamethyl-trisiloxane (**182**) was used as a model for the siloxane $Q_8M_8^H$ cages; triethoxysilane (**181**) was chosen as a model for T_8 and to see whether the decomposition affected only the Si–O–Si bonds. The final compound looked at was triethylsilane (**183**), which contains no Si–O bonds and so should not be susceptible to aqueous decomposition (Figure 3.6.1).

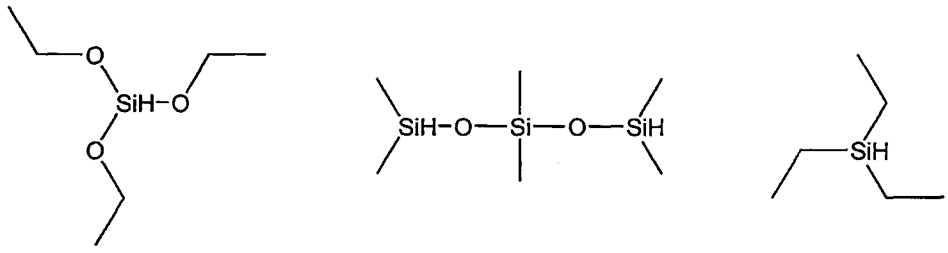

181 **182** **183**

Figure 3.6.1: Structure of triethoxysilane (181), 1,1,3,3,5,5-hexamethyl-trisiloxane (182) and triethylsilane (183)

The first simple siloxane investigated was triethoxysilane (**181**), which was reacted with butene-sDO3A-(ethyl) (**101**) in toluene using Speier's catalyst. The reaction was run in the same manner as for the T_8H_8 (**33**) and $Q_8M_8^H$ (**38**) cages. The reaction produced a large amount of insoluble material, which was removed from the reaction sample. The product was extracted from the solvent by reduced pressure and dissolved in $CDCl_3$. The FTIR of the product showed that the Si–H stretch had disappeared, indicating that the hydrosilylation reaction had occurred. The ^1H and ^{13}C NMR spectra showed a mixture of butane-sDO3A-(ethyl) (**162**) and butene-sDO3A-(ethyl) (**101**). The ^{29}Si NMR gave only a small signal at −21.38 ppm, showing that all the triethoxysilane (**181**) was bound up in the gel formation, as the ^{29}Si NMR signal corresponded to the silicon grease found in the earlier reactions. The majority of the starting material had decomposed during the reaction, forming the insoluble residue in the same manner as in the cage experiments.

The experiment was repeated using 1,1,3,3,5,5-hexamethyl-trisiloxane (**182**) under the same conditions. As with the other reactions, an insoluble residue was formed. The soluble product showed two peaks in the ^{29}Si NMR spectra: a major peak at −21.46 ppm, suggesting decomposition, and a second peak at −7.79 ppm. The ^{29}Si

NMR of 1,1,3,3,5,5-hexamethyl-trisiloxane (**182**) had peaks at −6.20 and −17.30 ppm. The −7.79 ppm peak in the reaction mixture shows that the hydrosilylation reaction had occurred to some extent, although at a lower rate than the decomposition reaction. The decomposition product would be a linear polymer. The 1,1,3,3,5,5-hexamethyl-trisiloxane would first be hydrolysed to the silanol (**184**), which then reacts with another 1,1,3,3,5,5-hexamethyl-trisiloxane (**182**) to give 1,1,3,3,5,5,7,7,9,9,11,11-dodecamethylhexasiloxane (**185**), which in turn could then react further forming longer chain lengths (Figure 3.6.2).

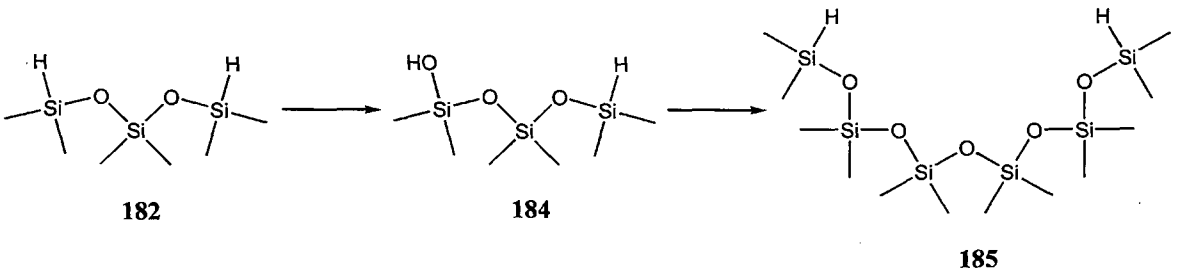

Figure 3.6.2: Decomposition of 1,1,3,3,5,5-hexamethyl-trisiloxane (182) to form 1,1,3,3,5,5,7,7,9,9,11,11-dodecamethylhexasiloxane (185).

The final test compound was triethylsilane (**183**), which was unlike the other test compounds; it was a silane and does not possess an Si–O bond that can be hydrolysed. The reaction was run under the same conditions as before, and yielded a soluble clear gum. The loss of the Si–H stretch at 2101 cm^{-1} in the FTIR confirmed complete hydrosilylation. The ^{1}H and ^{13}C NMR showed the formation of a new Si–C bond giving peaks at 1.09 ppm and 5.18 ppm respectively (Figure 3.6.3). With this success of the hydrosilylation reaction between triethylsilane and pentene-sDO3A (**133**) to give compound (**186**), the target molecule could be redesigned around a silane core instead of a siloxane core.

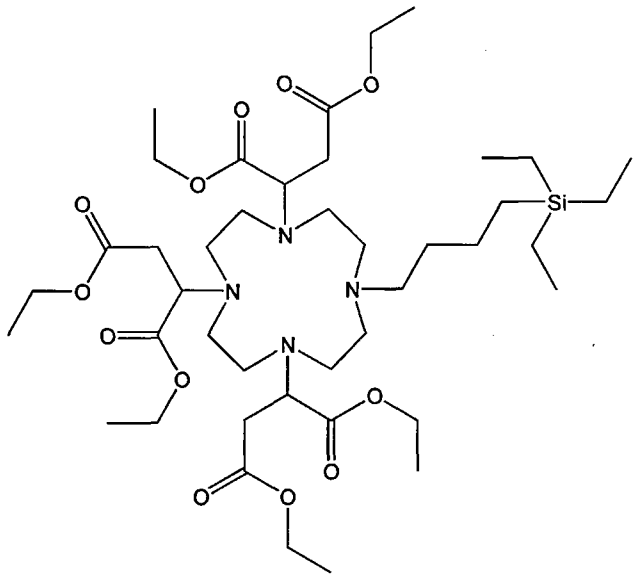

186

Figure 3.6.3: Structure of triethylsilane-butane-sDO3A-(ethyl) (186)

3.7.1: Use of dimethylsilane$_n$-benzenes as the scaffold for the attachment of pentene-sDO3A-(ethyl) via hydrosilylation

The new core was based on a silane-substituted benzene. Three different substituted benzenes were chosen for the experiments. These were the monosubstituted aromatic (pentane-sDO3A-(ethyl))dimethyl(phenyl)silane (**187**), the disubstituted aromatic 1,4-bis((pentane-sDO3A(ethyl))dimethylsilyl)benzene (**218**), and the tri-substituted aromatic 1,3,5-tris((pentane-sDO3A(ethyl))dimethylsilyl) benzene (**289**) (Figure 3.7.1.1).

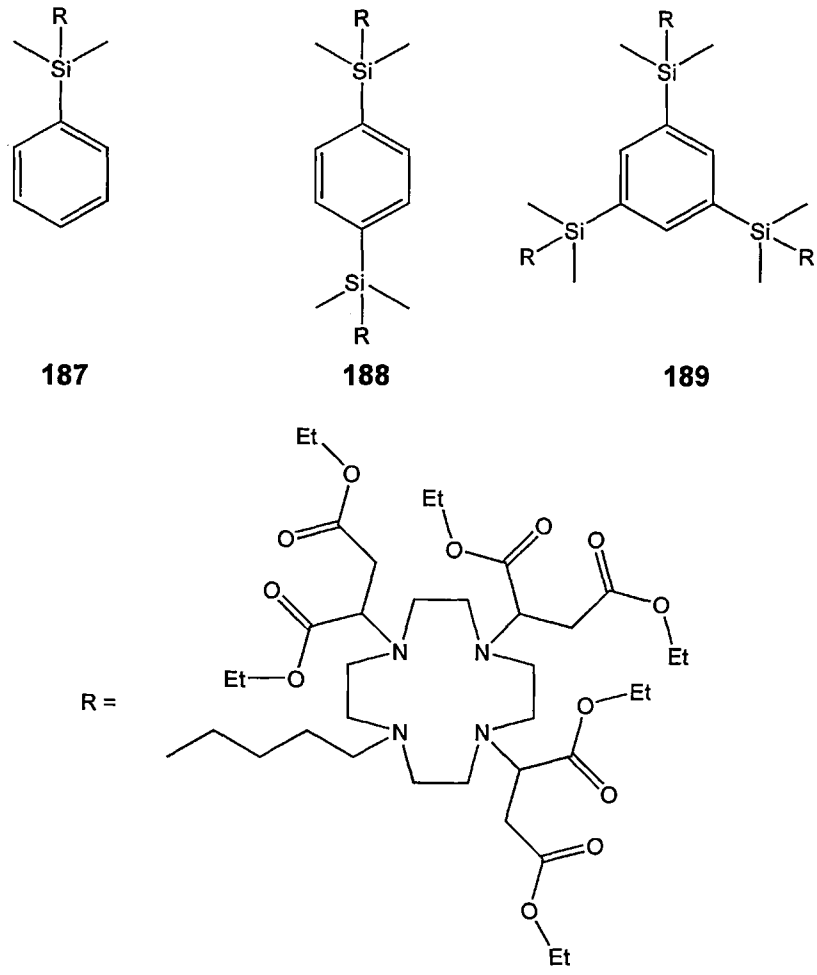

Figure 3.7.1.1: Structure of the new core sDO3A-(ethyl) systems

The new core molecules would allow the formation of a series of three contrast agents. The aim was to show the effect on the relaxivity of the addition of extra groups, by the increase in mass and any interactions between the sDO3A systems, such as the cross-binding as described in Section 1.7.1.

There are two methodologies for the formation of the (pentane-sDO3A-(ethyl)-(dimethylsilyl))benzene (**187**). Route ***H*** was a one-step reaction involving a direct hydrosilylation reaction between dimethylphenylsilane (**190**) and pentene-sDO3A-(ethyl) (**133**), using Speier's catalyst. While this was the same as the routes used earlier, it failed owing to the presence of water that induced the hydrolysis of the

cage. It was repeated with the aryl silanes to see if it was only the hydrolysis that was causing the problems. The second Route, *I*, was a two-step reaction, in which the first step was the hydrosilylation reaction between dimethylphenylsilane (**190**) and 5-bromopent-1-ene (**134**) to give (5-bromopentyl)(dimethylphenyl)silane (**191**). That was then reacted with DO3A-(ethyl) to give the target molecule, (**199**) (Figure 3.7.1.2).

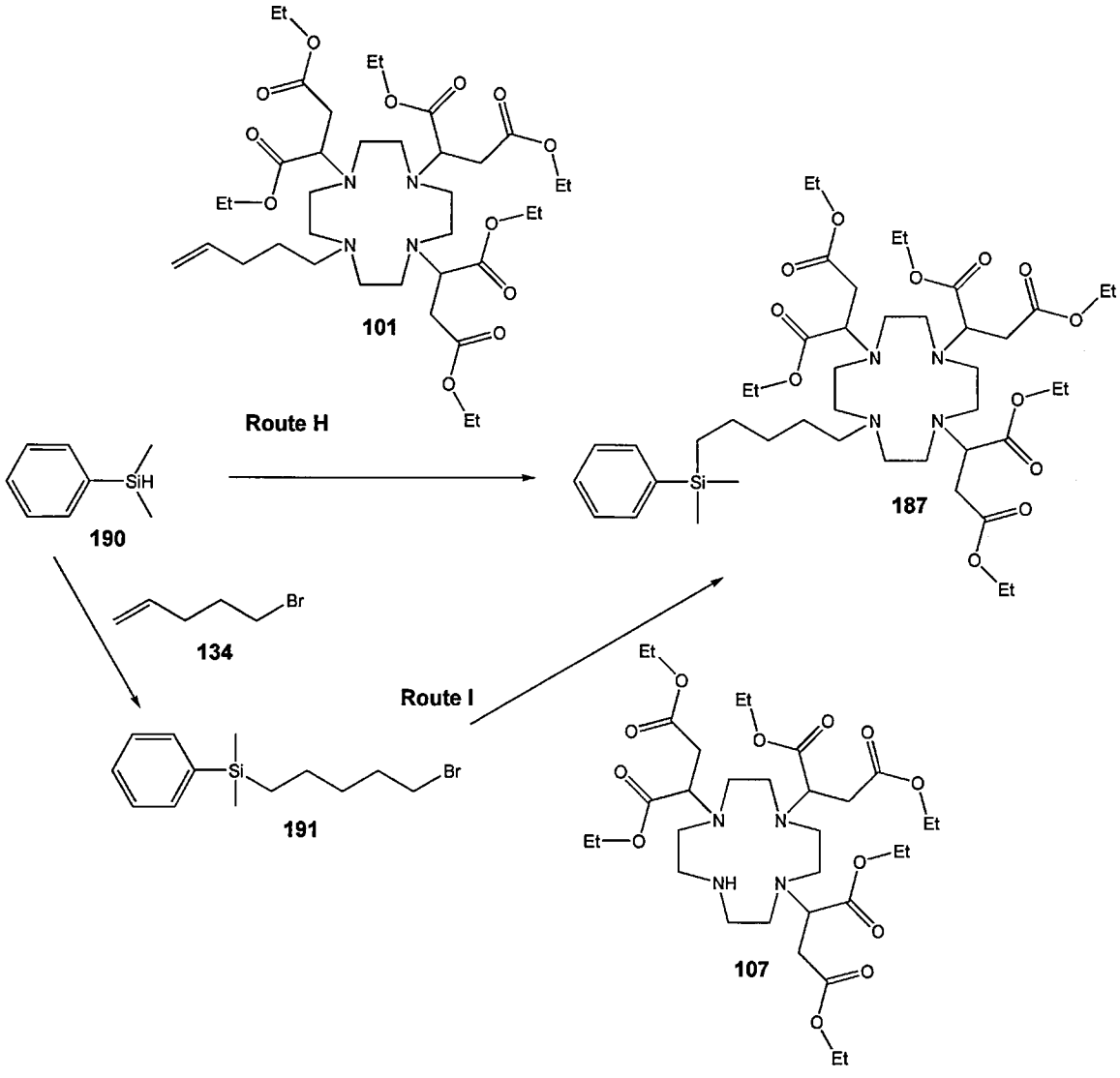

Figure 3.7.1.2: Two routes for the synthesis of (pentane-sDO3A-(ethyl)-(dimethylsilyl)benzene (187)

Both dimethylsilylbenzene (**190**) and 1,4,bis-(dimethylsilyl)benzene (**192**) were purchased from Aldrich, and the 1,3,5,tris-(dimethylsilyl)benzene (**193**) was

synthesised using a Grignard reaction between 1,3,5-tribromobezene (**194**) and dimethylchlorosilane using magnesium, with a yield of around 35%. The compound was characterised by ^{1}H NMR which showed the Me protons at 0.24 ppm, The protons on the silicon atoms at 4.34ppm and the aromatic protons at 7.63 ppm. The structure was also confirmed by the ^{13}C NMR as three proton environments at -3.72, 136.75 and 140.52 ppm. The ^{29}Si NMR spectra showed only one peak at -15.99ppm. (Figure 3.7.1.3).

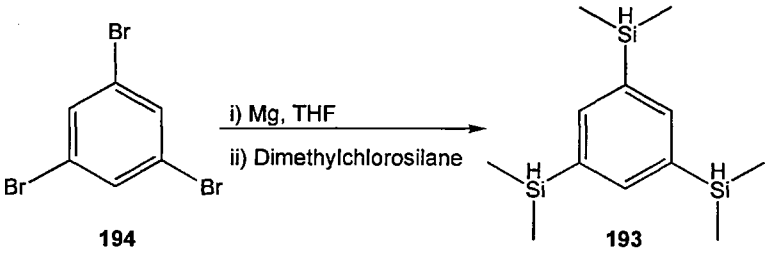

Figure 3.7.1.3: Synthesis of 1,3,5,tri-(dimethylsilyl)benzene (193)

3.7.2: Synthesis of ((pentane-sDO3A(ethyl))dimethylsilyl)$_n$- benzene via Route *H*

The first route investigated was Route ***H***, used in the formation of 1,4-bis((pentane-sDO3A(ethyl))dimethylsilyl)benzene (**188**) and 1,3,5-tris((pentane-sDO3A(ethyl)) dimethylsilyl)benzene (**189**). The first core used was 1,3,5,tri-(dimethylsilyl)benzene (**193**). The pentene-sDO3A-(ethyl) (**133**) was dissolved in toluene, to which Speier's catalyst was added along with 1,3,5-tri-(dimethylsilyl) benzene (**193**), and the mixture was heated to 80 °C for 72 hours. The solvent was removed and the crude product was taken up into DCM and refluxed with activated charcoal for 30 minutes to remove the platinum (Figure 3.7.2.1). The ^{1}H, ^{13}C and ^{29}Si NMR spectra of the crude product showed that a mixture of products had formed, including some polydimethylsiloxane, as shown by a peak at −21.49 ppm in the ^{29}Si NMR. The

crude product was split into two fractions. The first fraction was chromatographed on silica and eluted with DCM and acetone (92%: 8%), which failed to yield a product; the second fraction was vacuum distilled.

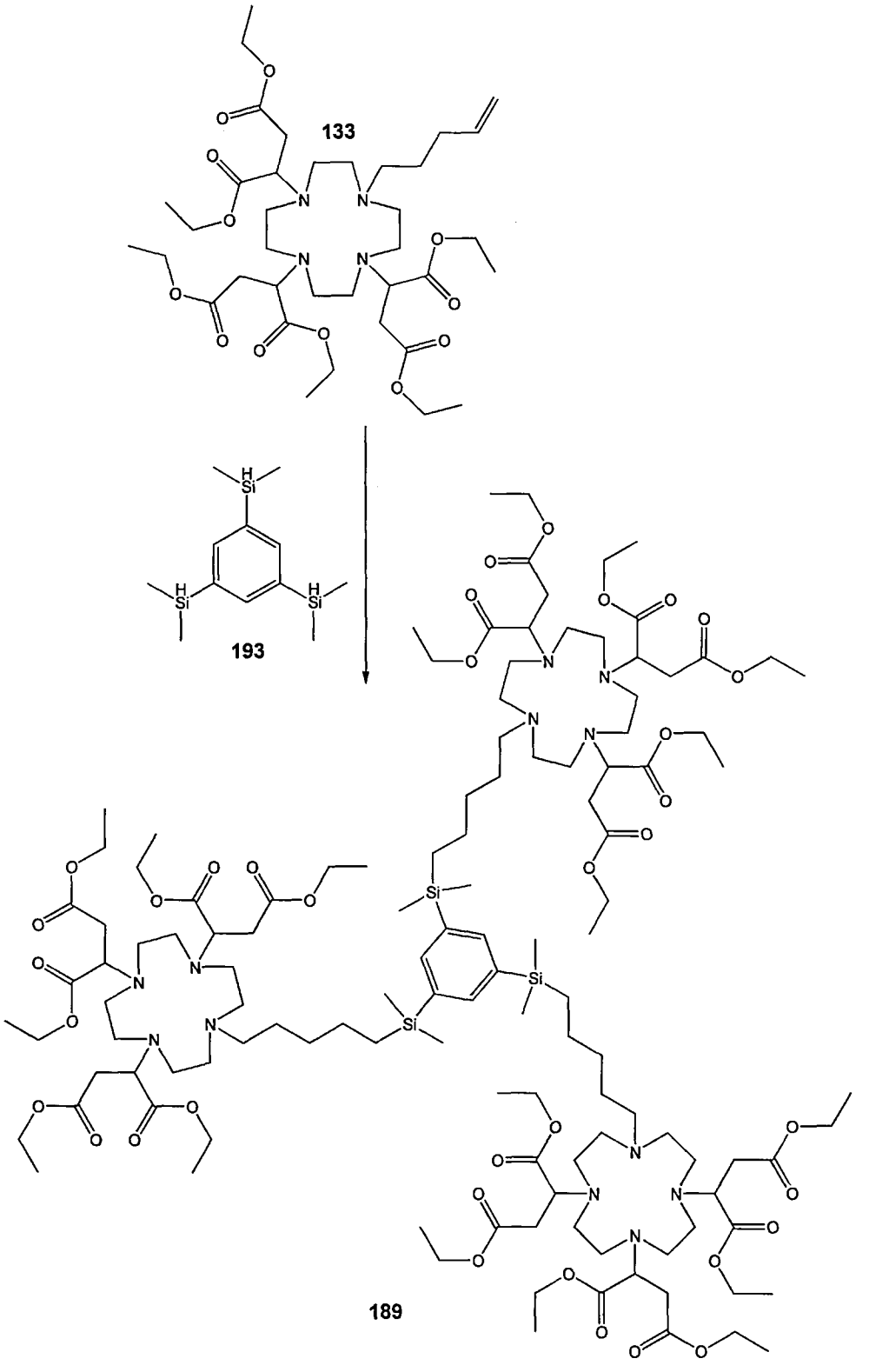

Figure 3.7.2.1: Reaction of pentene-sDO3A-(ethyl) (133) with 1,3,5,tri-(dimethylsilyl)benzene (193)

The distillation of the product was not successful, as the products had such a high boiling temperature that they condensed and stayed in the condenser and on the thermometer. These were extracted and analysed. The thermometer fraction showed a single product with a peak at 5.37 ppm in the ^{29}Si NMR. The ^{1}H and ^{13}C NMR spectra showed the presence of a trace of alkene and, interestingly, there was no characteristic signal of the cyclen. The product from the condenser also showed similar NMR spectra, but with a ^{29}Si NMR signal at 5.71 ppm.

The reaction of pentene-sDO3A-(ethyl) (**133**) with 1,4-bis(dimethylsilyl)benzene (**192**) was run in parallel with the previous reaction under the same conditions. The ^{29}Si NMR showed three signals at 5.22, 5.00, and −0.86 ppm. The ^{13}C NMRs showed that there was evidence of beta-addition, although as a minor product, with the alpha-addition product being in the majority. The presence of beta-addition was seen in the ^{13}C NMR at 21.28ppm as a CH_3 group which was not present in the alpha addition pathway. The TLC of the crude product showed that it was a mixture of three different products. As a result of the unsuccessful separation of the tris-siloxane reaction mixture, further purification of the bis compound was not attempted (Figure 3.7.2.2).

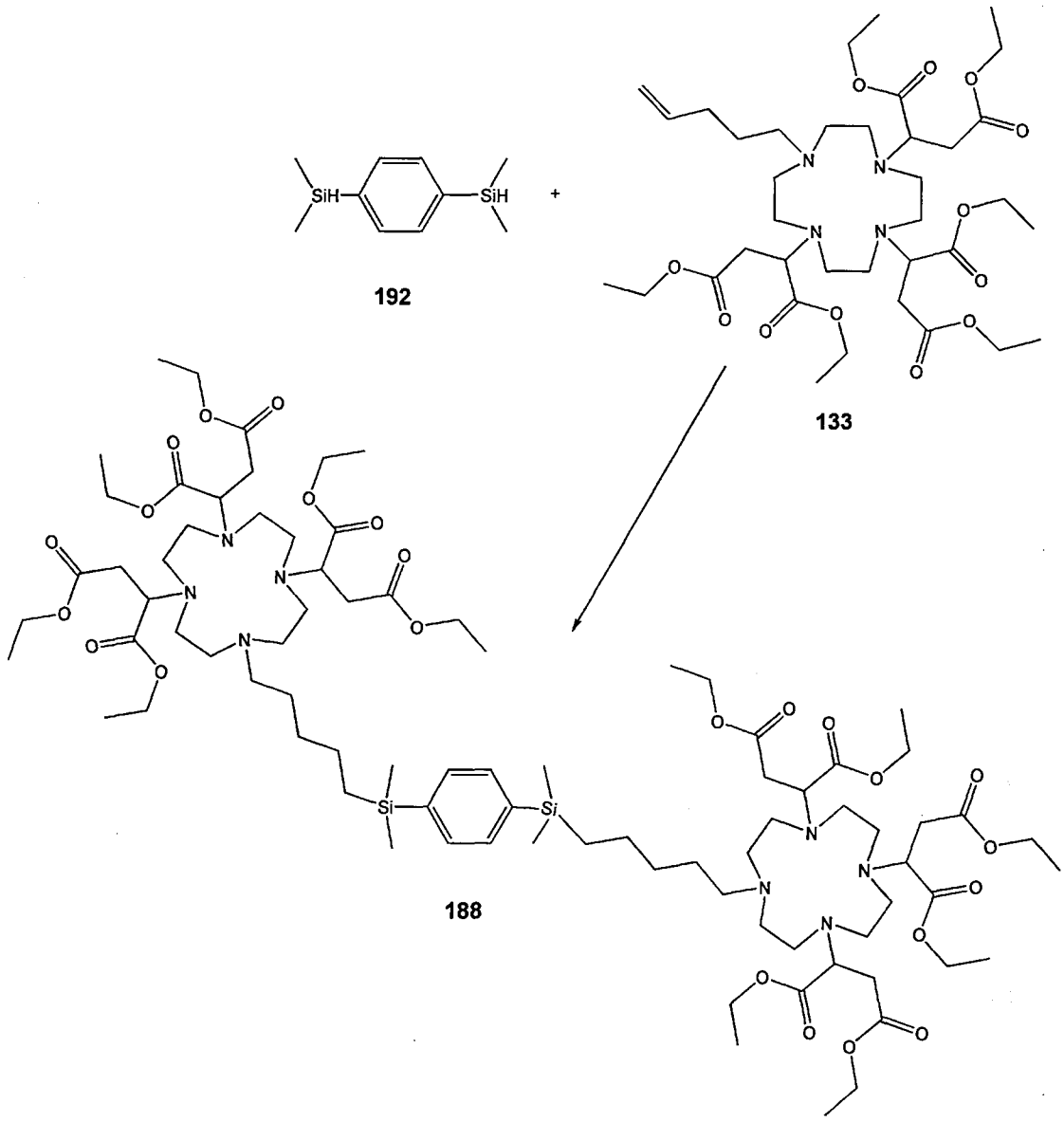

Figure 3.7.2.2: Reaction of pentene-sDO3A-(ethyl) (133) with 1,4-bis(dimethylsilyl)benzene (192)

With several different signals being seen in the ^{29}Si NMR spectra, it was proposed that a secondary side reaction was occurring that was different from the hydrolysis seen with the silsesquioxane cages.

The formation of an alkene by the reaction of the platinum catalyst with pentene-sDO3A-(ethyl) (**133**) was noted earlier. This alkene could react with the silane forming the new compound. Such a compound was noticed in the reaction product

extracted from the distillation of the product of the reaction between pentene-sDO3A-(ethyl) (**133**) and 1,3,5,tri-(dimethylsilyl)benzene (**193**). To see whether or not these reactions were occurring, a model reaction was used.

3.8: Modelling of side reactions between pentene-sDO3A-(ethyi) and dimethylsilylbenzene noticed in Route *H*

1,4-bis(dimethylsilyl)benzene (**192**) was reacted in toluene with diethyl maleate (**127**) using Speier's catalyst, under the same conditions as in the previous reactions. The reaction gave a gum with a yield of 68%. The ^{29}Si NMR of the reaction mixture showed a mixture of 8 different signals, some of which matched the ^{29}Si NMR signals of the reaction mixture from 1,4-bis(dimethylsilyl)benzene (**192**) with pentene-sDO3A-(ethyl) (**133**) (Figure 3.8.1).The accurate mass spectrum (HRMS) of the crude material showed that the target molecule 1,4-bis(diethylsuccinate-dimethylsilyl)benzene (**197**) was present in the reaction as a major constituent.

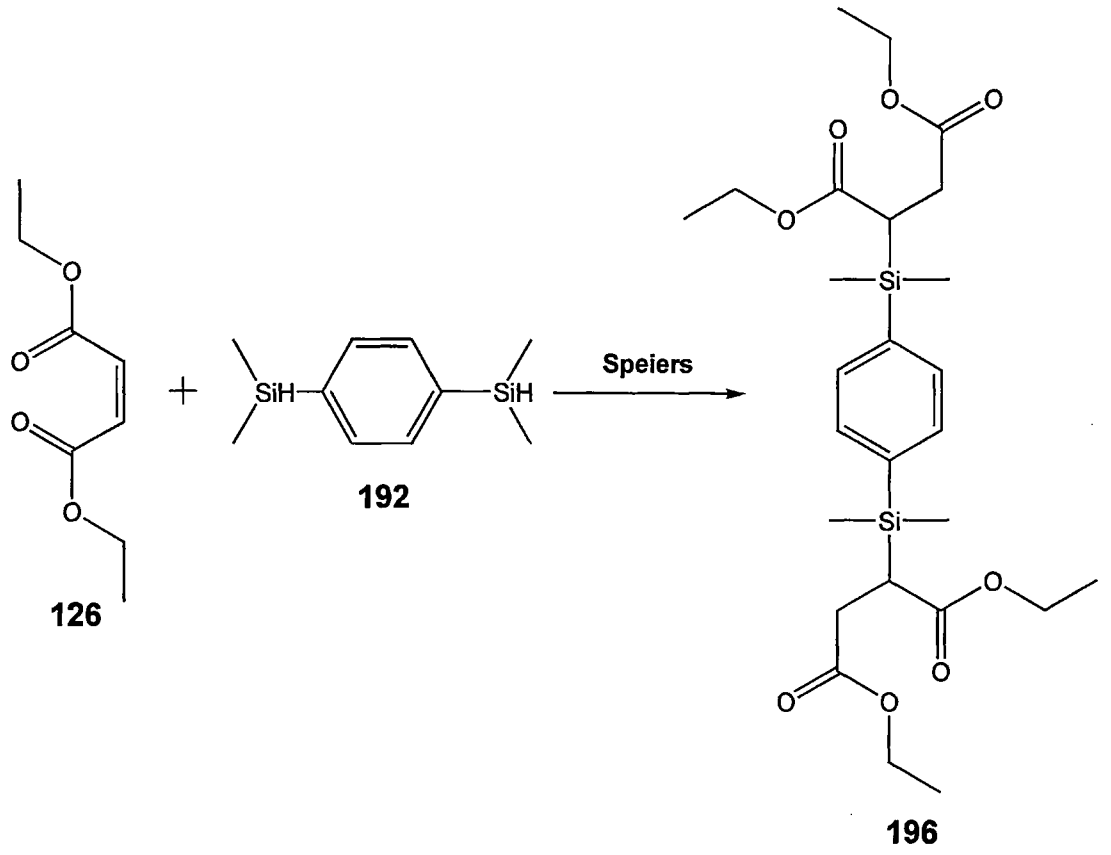

Figure 3.8.1: Reaction of diethyl maleate (126) and 1,4-bis(dimethylsilyl)benzene (192) via Speier's catalyst, producing bis(succinate)dimethyl phenylsilane (196)

To discover whether the succinate was reacting with the silane, a second model compound, diethyl 2-(diethylamino)succinate (**197**), was synthesised from diethylamine (**155**) and diethyl fumarate (**130**) under the same conditions as for the formation of sDO3A-(ethyl) (**107**) (Figure 3.8.2). The compound was purified on silica and eluted with DCM: EtOH (96:4), then identified using ^{1}H NMR spectra which showed the loss of the alkene of the diethyl fumarate (**130**) and the presence of the Et groups of the diethyl amine (**155**). The HRMS, gave the calculated ion mass at 246.1700 [M(**197**)$^{+H}$], and found the ion mass at 246.1697 [M(**197**)$^{+H}$]. The reaction yielded the reaction product at 17.6%.

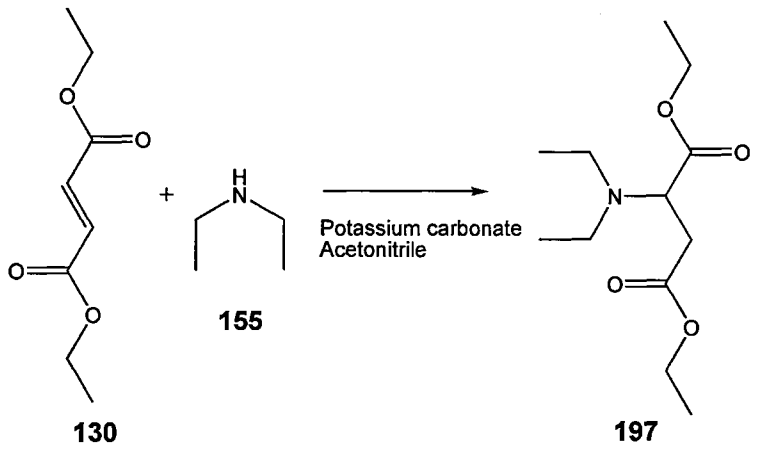

Figure 3.8.2: Synthesis of diethyl 2-(diethylamino)succinate (197) from diethyl fumarate (130) and diethyl amine (155)

Diethyl 2-(diethylamino)succinate (**197**) was reacted with dimethylphenylsilane (**190**) in toluene using Speier's catalyst. After the platinum had been removed the reaction give a viscous oil, which was taken up into $CDCl_3$ leaving a large proportion of product as an insoluble gum. The loss of the Si–H stretch in the FTIR showed that the reaction had taken place. The ^{29}Si NMR showed two signals, with a major peak at 5.91 ppm and a minor one at 5.18 ppm.

The ^{29}Si NMR signals obtained from the reaction of 1,4,bis-(dimethyl)benzene (**192**) / 1,3,5,tris-(dimethylsilyl)benzene (**193**) with pentene-sDO3A-(ethyl) (**133**) are different from the ^{29}Si NMR signals from the reaction of diethyl fumarate (**130**) and bis(dimethylsilyl)benzene (**192**), pointing to the occurrence of several different side reactions. These are the reaction with the diethyl fumarate formed by the reaction of pentene-sDO3A-(ethyl) (**133**), the hydrosilylation reaction with pentene-sDO2A-(ethyl) (**164**), and the hydrosilylation reaction with the carbonyls of the succinate groups on the pentene-sDO3A-(ethyl) (**133**). It was the reaction with the succinate

groups on the cyclen that caused the polymerisation of the silicon cages in the earlier reactions.

3.9.1: The synthesis of ((pentane-sDO3A(ethyl))dimethylsilyl)$_n$- benzene via Route *I*

Owing to the decomposition seen in Route ***H***, an alternative Route ***I*** was investigated. This alternative route had the advantage of avoiding the decomposition of the pentene-sDO3A-(ethyl) (**133**) by the platinum, by having the hydrosilylation reaction between the silane and the alkene occurring before the sDO3A-(ethyl) (**107**) group was attached. The first step was the formation of (5-bromopentyl)dimethyl(phenyl)silane (**191**) by the hydrosilylation reaction between neat dimethylphenyl silane (**190**) and an excess of 5-bromopent-1-ene (**134**), using Speier's catalyst (Figure 3.9.1).

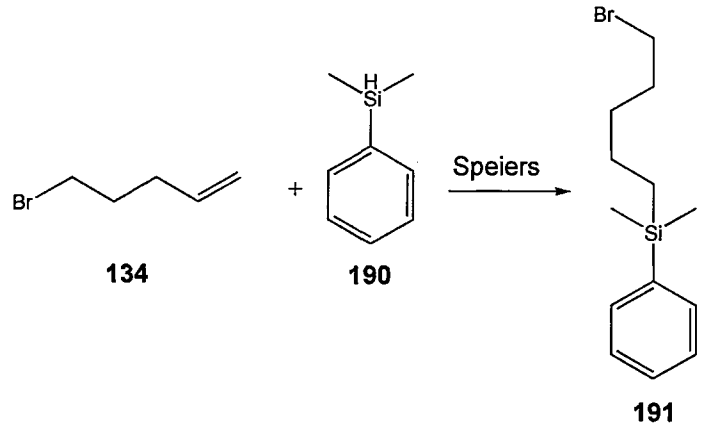

Figure 3.9.1: Synthesis of (5-bromopentyl)dimethyl(phenyl)silane (191)

The reaction was heated to 60 °C for 34 hours, after which the Speier's catalyst was removed using activated charcoal and DCM, as in the previous reaction. The excess

5-bromopent-1-ene (**134**) was removed by reduced pressure (50 mbar) at 40 °C by placing the sample under high vacuum for 48 hours. The product was confirmed by ^{1}H, and ^{13}C NMR, which showed the loss of the alkene and the formation of the new Si–C bond. The loss of the Si–H was seen in the FTIR and in the ^{29}Si NMR, which gave a signal at −2.65 ppm. The formation of both 1,4-bis((5-bromopentyl)dimethylsilyl)benzene (**198**) and 1,3,5-tris((5-bromopentyl) dimethylsilyl)benzene (**199**) was achieved using the same reaction conditions, involving 1,4,bis-(dimethylsilyl)benzene (**192**) and 1,3,5,tri-(dimethylsilyl) benzene (**193**), respectively (Figure 3.9.2). These products were also confirmed by ^{1}H, ^{13}C and ^{29}Si NMR and FTIR – see Table 3.9.1.

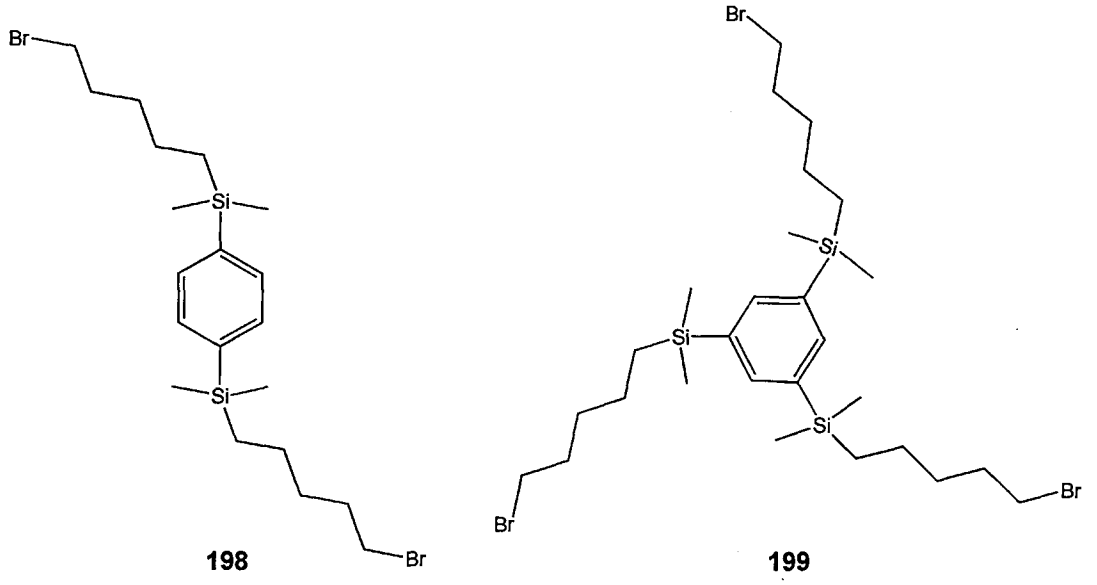

Figure 3.9.2: Structures of 1,4-bis((5-bromopentyl)dimethylsilyl)benzene (198) and 1,3,5-tris((5-bromopentyl)dimethylsilyl)benzene (199).

Compound	*Yield*	*^{29}Si NMR*
(5-bromopentyl)dimethyl(phenyl)silane (**191**)	59.0%	−2.65
1,4-bis((5-bromopentyl)dimethylsilyl)benzene (**198**)	62.3%	−2.66
1,3,5-tris((5-bromopentyl)dimethylsilyl)benzene (**199**)	54.1%	−2.59

Table 3.9.1: Results of the reactions between 5-bromopent-1-ene (134) and dimethylsilyl benzene (190), 1,4,bis-(dimethylsilyl)benzene (192) or 1,3,5-tri-(dimethylsilyl)benzene (193)

The second step was the attachment of the sDO3A-(ethyl) (**107**) to (5-bromopentyl)dimethyl(phenyl)silane (**190**), to form (pentane-sDO3A-(ethyl)) dimethyl(phenyl)silane (**187**) (Figure 3.9.3). The reaction was performed in deuterated acetonitrile with potassium carbonate as the base. The use of the deuterated solvent for the reaction allowed the monitoring of the reaction via ^{1}H NMR, monitoring the protons adjacent to the bromide. This was needed as the size of the molecules made monitoring of the reaction by LCMS less useful, owing to the detection limits and the ionisation abilities of the compounds as mentioned earlier,

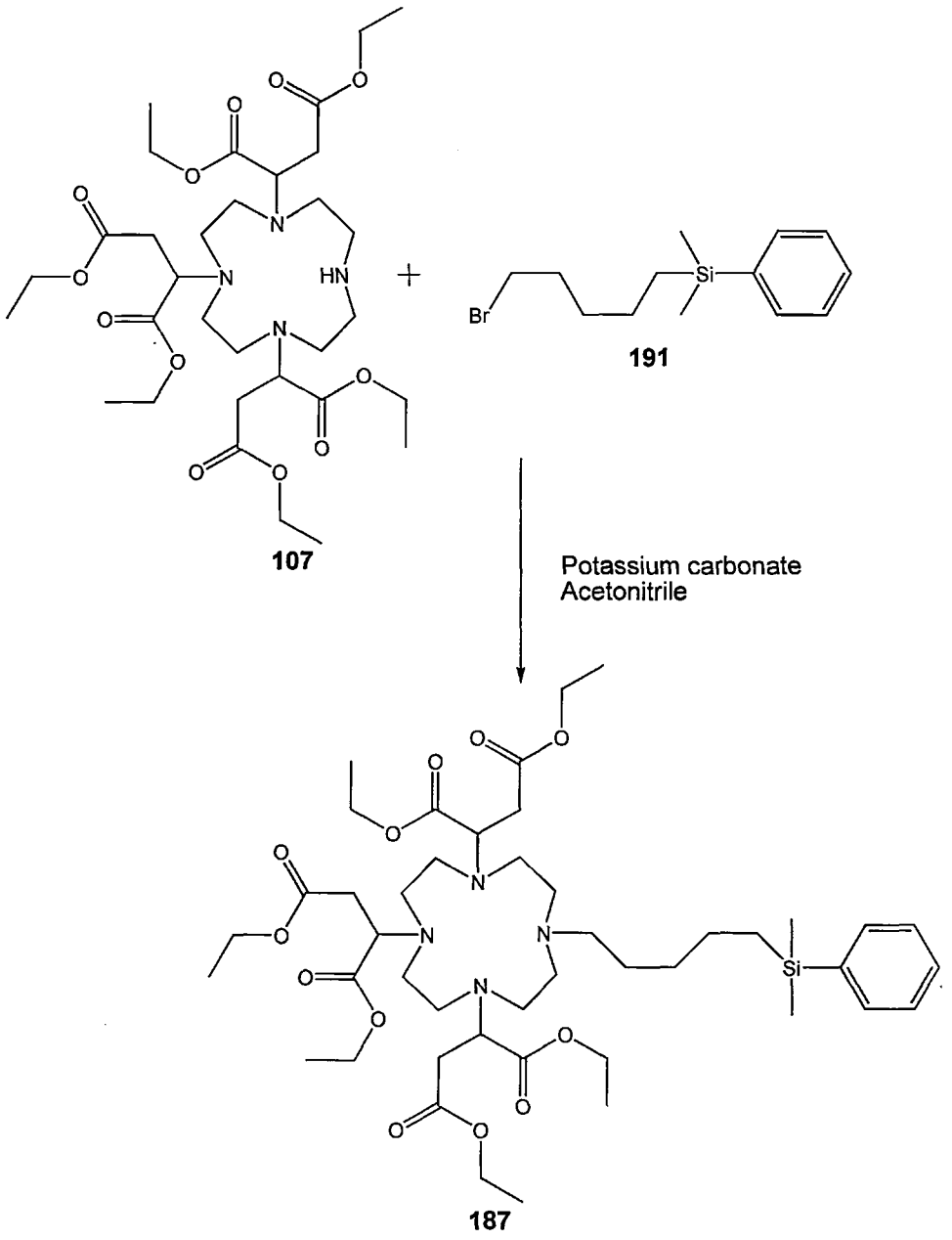

Figure 3.9.3: Synthesis of (pentane-sDO3A-(ethyl))dimethyl(phenyl)silane (187)

The reaction was heated to 60 °C for 48 hours, by which time the ^{1}H NMR signal for CH_2–Br had disappeared. After the solids and solvent had been removed from the reaction, the crude product was chromatographed on silica and eluted with DCM in a gradient from 100% to 95% in relation to EtOH. The pentane-sDO3A-(ethyl))dimethyl(phenyl)silane (**187**) was characterised by ^{1}H, ^{13}C and ^{29}Si NMR spectra and by FTIR and HRMS.

The bis (**228**) and tris (**229**) reactions followed a similar protocol, but needed a slightly different solvent gradient of 100% to 70% during column chromatography, owing to the increased mass of the product increasing the retention times. The reactions gave yields of around 40%, and the compounds were characterised by ^{1}H, ^{13}C and ^{29}Si NMR, as well as FTIR and HRMS. The ^{29}Si NMR showed a slight downfield shift for the products of about 0.1 ppm. This may have been due to a decrease in the shielding of the Si nuclei, as a result of the molecule becoming more linear because of the repulsion of the sDO3A groups (Table 3.9.2; Figure 3.9.4, Figure 3.9.5).

Compound	*Yield*	*^{29}Si NMR*
(pentane-sDO3A-(ethyl))dimethyl(phenyl)silane (**187**)	40.5%	−2.75
1,4-bis((pentane-sDO3A(ethyl))dimethylsilyl)benzene (**188**)	41.5%	−2.85
1,3,5-tris((pentane-sDO3A(ethyl))dimethylsilyl)benzene (**189**)	43.0%	−2.83

Table 3.9.2: Results of the reaction between(5-bromopentyl) dimethyl(phenyl)silane (190), 1,4-bis((5-bromopentyl)dimethylsilyl)benzene (198) and 1,3,5-tris((5-bromopentyl)dimethylsilyl)benzene and sDO3A-(ethyl) (199)

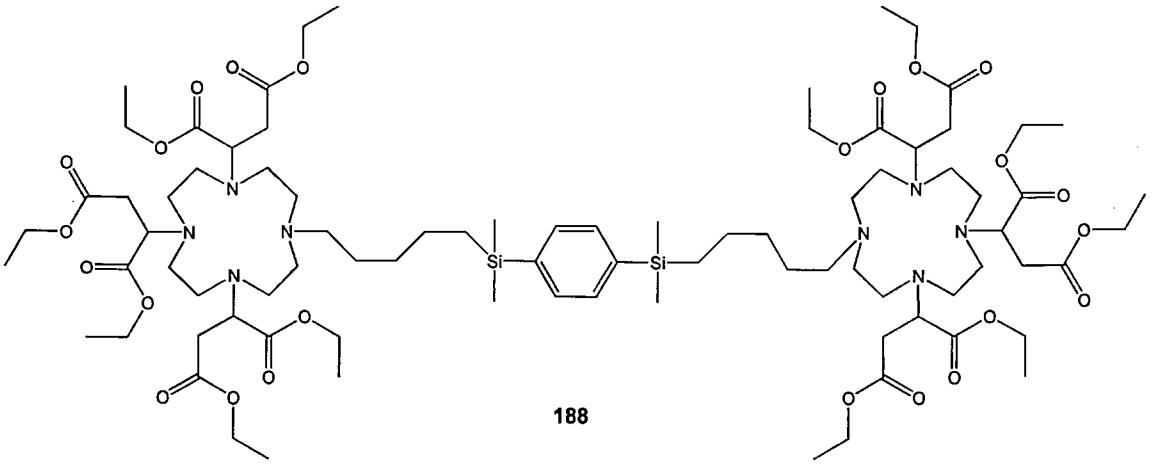

188

Figure 3.9.4: Structure of 1,4-bis((pentane-sDO3A(ethyl))dimethylsilyl)benzene (188)

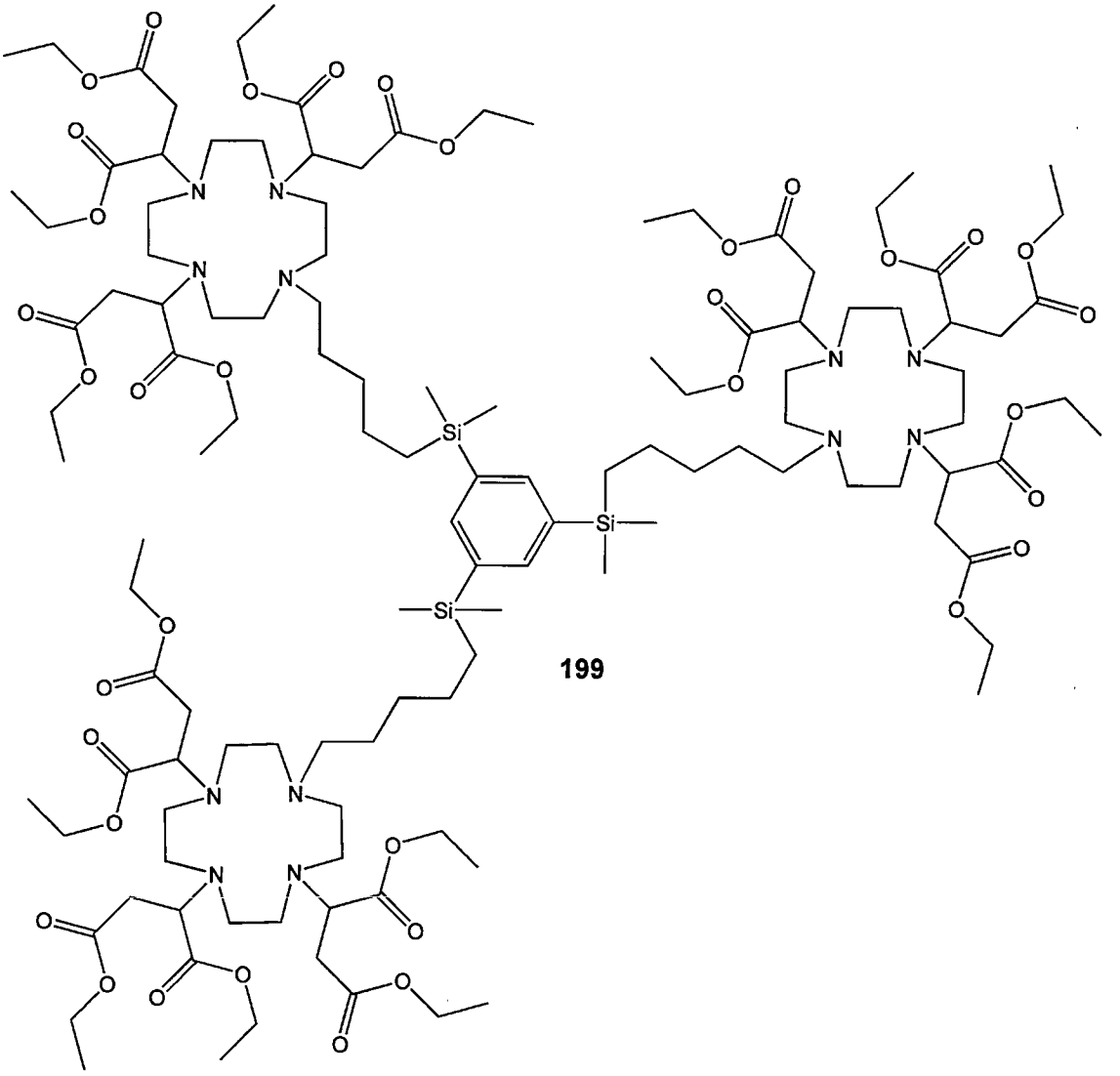

199

Figure 3.9.5: Structure of 1,3,5-tris((pentane-sDO3A(ethyl))dimethylsilyl)benzene (199)

3.10: Hydrolysis of the ethyl ester protecting groups on the ((pentane-sDO3A(ethyl))dimethylsilyl)n-benzene

The final step was the removal of the ester protection groups from the ethyl esters. The hydrolysis was achieved by dissolving the ester in 1M LiOH and heating to 100 °C for 24 hours (Figure 3.10.1). The reaction was worked up by ion-exchange chromatography using a Bio-Rad AG1 A41 resin in the HO^- form, with a bed volume of 500 cm^3.

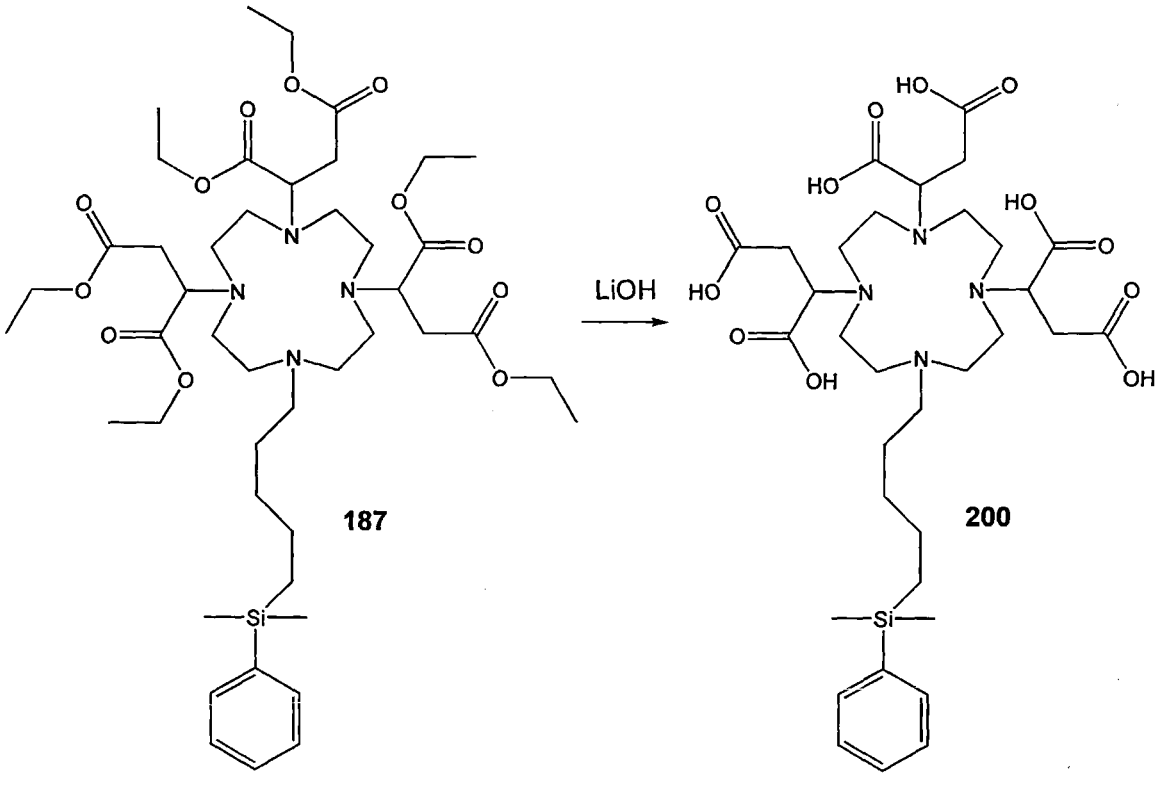

Figure 3.10.1: Hydrolysis of (pentane-sDO3A-(ethyl))dimethyl(phenyl)silane (187) to give (pentane-sDO3A)dimethyl(phenyl)silane (200)

The LiOH reaction solution was injected at the top of the column and was washed though with ultra-pure water, after which the product was eluted using formic acid (1M). The fractions were collected and worked up using lyophilisation. The products were identified using ^{1}H NMR, FTIR and CHN analyses; the results are shown in Table 3.10.1. See Figure 3.10.2 for structures of products.

Compound	*Yield*
(pentane-sDO3A-)dimethyl(phenyl)silane (**200**)	32.0%
1,4-bis((pentane-sDO3A)dimethylsilyl)benzene (**201**)	46.0%
1,3,5-tris((pentane-sDO3A)dimethylsilyl)benzene (**202**)	17.6%

Table 3.10.1: Reaction yields of the hydrolysis of compounds (187), (188)

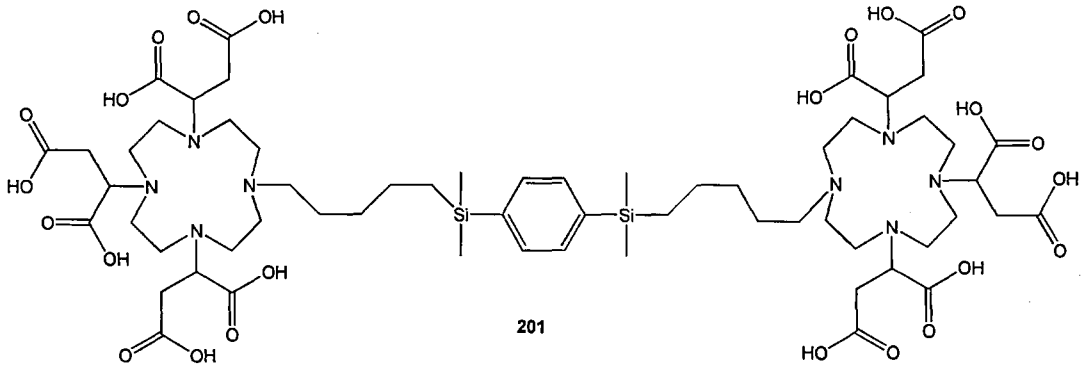

201

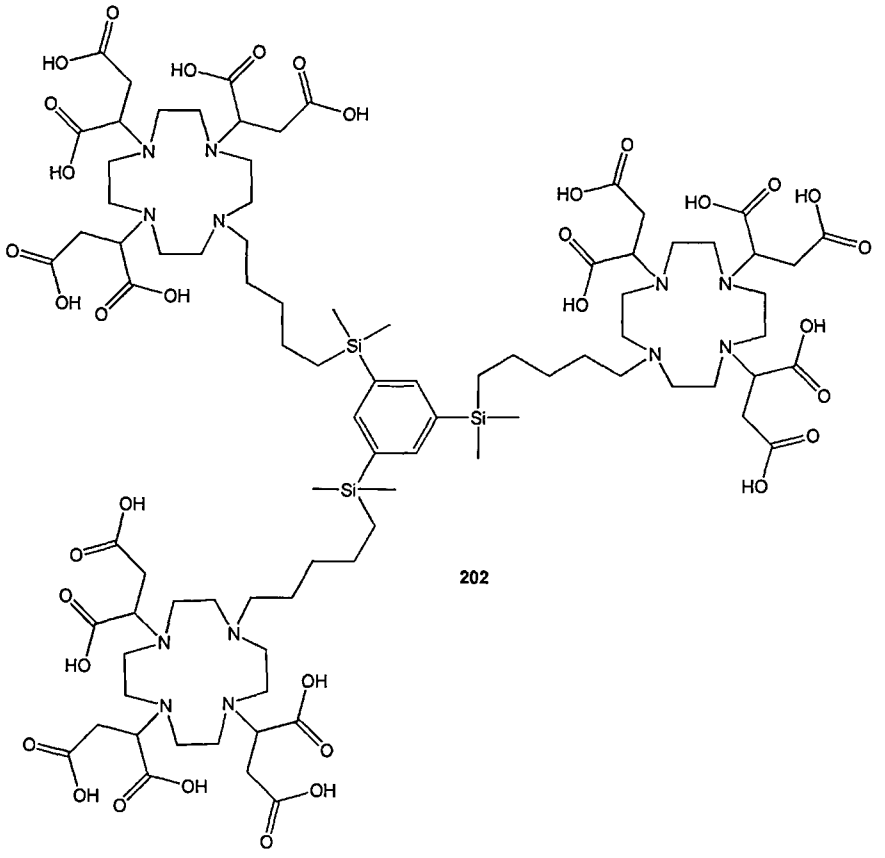

202

Figure 3.10.2: Structures of 1,4-bis((pentane-sDO3A)dimethylsilyl)benzene (201) and 1,3,5-tris((pentane-sDO3A)dimethylsilyl)benzene (202).

The presence of the Si groups was identified by the presence of the Si–CH_3 groups and the protons on the aromatic ring in the ^1H NMR. The yield of 1,3,5-tris((pentane-sDO3A)dimethylsilyl)benzene (**202**) was low owing to the formation of a gum during the hydrolysis step of the reaction. This gum was removed and the sample was purified as normal.

This research has shown that there are several issues that needed to be resolved with the formation of cyclen–silicon compounds. The first issue was the decomposition of the pentene-sDO3A-(ethyl) (**133**) by the platinum catalyst. This produced several difficulties owing to the formation of the secondary amine, which would have decomposed the cages. There was also the side reaction of the diethyl fumarate undergoing a hydrosilylation reaction with the siloxane/silane. The second issue was the reaction of the Si–H with the carbonyls of the succinate groups on the cyclen. In the cage-based reactions, the reaction between the Si–H and succinates on the cyclen would play a major part in the formation of the gel that caused the problems with the silsesquioxane cages. This was due to the sDO3A-(ethyl) (**107**) having multiple succinates, allowing a high amount of cross-linking, and it was that, together with hydrolysis by the cyclen bound water, that was causing the gel formation.

These two issues showed that direct hydrosilylation with the alkene-sDO3A-(ethyl) was not possible, owing to the reaction with the succinate groups. This was circumvented when the 5-bromobutene was reacted with the silane and $Q_8M_8^H$ forming the terminal brominated compounds. These terminal bromide compounds were then reacted with sDO3A-(ethyl) (**107**). While the benzene-based silanes were successful, the $Q_8M_8^H$-based brominated compound failed, and was hydrolysed because the secondary amine in the sDO3A-(ethyl) and the associated water catalysed the decomposition of the $Q_8M_8^H$, forming the gel product. The benzene-based silicon–cyclen compounds were then successfully hydrolysed by a functional-group interconversion of the ethyl ester to the carboxylic acid. The final stage would

be the complexation of the silicon–cyclen compounds with gadolinium to investigate their efficacy as contrast agents.

Chapter 4.0: Complexation and luminescence and relaxivity studies of lanthanide complexes of (13), (101), (107), (138), (141), (200), (201), (202).

4.1: Complexation of the sDO3A-(ethyl)-ligands and the aDO3A-ligands with Gd^{3+} and Eu^{3+}

The complexation of the ligands with the lanthanides may be grouped into two sections. The first group was the ligands, sDO3A-(ethyl) (**107**) and butene-sDO3A-(ethyl) (**101**). The second group was the ligands, sDO3A (**32**), DOTA (**13**), (pentane-sDO3A-)dimethyl(phenyl)silane (**200**), 4-bis((pentane-sDO3A) dimethylsilyl)benzene (**201**) and 1,1,3,5-tris((pentane-sDO3A) dimethyl silyl)benzene (**202**).

The products from both complexation methods were characterised by a combination of FTIR, CHN analysis and the measurements of the *q* number and the relaxivity, which showed a marked difference between complexed and non-complexed lanthanides.

Ester-protected cyclen derivatives, such as sDO3A-(ethyl) (**107**) and pentene-sDO3A-(ethyl) (**133**), were dissolved in ethanol; to the solutions the desired lanthanide – gadolinium or europium – was added as the chloride salt ($GdCl_3$ or $EuCl_{3)}$. The reactions were refluxed under argon for 48 hours. For each lanthanide reaction, the cooled reaction solution was then added to diethyl ether, producing a precipitate that was collected. The product was then purified by dissolving the solid in methanol, and resuspending the precipitate with the addition of the diethyl ether. The solids were extracted, and dried under vacuum.

The ligands that possess carboxylic acid groups, such as sDO3A (**32**), (pentane-sDO3A-)dimethyl(phenyl)silane (**200**) and DOTA (**13**) were complexed with the lanthanides in water, using the oxides Gd_2O_3 and Eu_2O_3. The pH of the solution was

adjusted to pH 8 and the samples heated to 80 °C for 48 hours. The solution was then filtered through a 5 μm PTFE filter, and the filtrate lyophilized to yield a white powder (Table 4.1.1).

Complex	***Lanthanide***	***Yield***
Butene-sDO3A-(ethyl)-Gd (**203**)	$GdCl_3$	25%
Butene-sDO3A-(ethyl)-Eu (**204**)	$EuCl_3$	25%
sDO3A-(ethyl)-Gd (**205**)	$GdCl_3$	46%
sDO3A-(ethyl)-Eu (**206**)	$EuCl_3$	75%
sDO3A-Gd (**207**)	Gd_2O_3	79%
sDO3A-Eu (**208**)	Eu_2O_3	82%
sDO2A-Gd (**209**)	Gd_2O_3	38%
sDO2A-Eu (**210**)	Eu_2O_3	68%
DOTA-Gd (**2**)	Gd_2O_3	96%
DOTA-Eu (**211**)	Eu_2O_3	96%
(pentane-sDO3A-)dimethyl(phenyl)silane-Gd (**212**)	Gd_2O_3	73%
(pentane-sDO3A-)dimethyl(phenyl)silane-Eu (**213**)	Eu_2O_3	83%
1,4-bis((pentane-sDO3A)dimethylsilyl)benzene-Gd_2 (**214**)	Gd_2O_3	83%
1,4-bis((pentane-sDO3A)dimethylsilyl)benzene-Eu_2 (**215**)	Eu_2O_3	80%
1,3,5-tris((pentane-sDO3A)dimethylsilyl)benzene-Gd_3 (**216**)	Gd_2O_3	79%
1,3,5-tris((pentane-sDO3A)dimethylsilyl)benzene-Eu_3 (**217**)	Eu_2O_3	81%

Table 4.1.1: Ligands complexed, with the lanthanide used and the yield of products

4.2.1: Luminescent studies of sDO3A–(ethyl)–Eu-based complexes, sDO3A–Eu-based complexes and the organosilicon Eu^{3+} complexes

From the luminescence of the complexes described in section 4.1, information about the physical properties of the complexes, such as the hydration number and their symmetry in solution, could be obtained.

The Gd^{3+} complexes are not suitable for investigation by luminescence spectroscopy, although the large band gap between the ground state and the lowest excited state of Gd^{3+} will produce fluorescent spectra when excited at 274 nm, with emission in the UV band at 311 nm[116]. The main purpose of the luminescence studies was to calculate the water coordination number (q) from the difference in the excited state lifetime of the complex in H_2O and in D_2O. The problem was that Gd^{3+} does not undergo quenching by OH and OD oscillation, so it would not be possible to calculate the water coordination number using luminescence. The water coordination number may be found by using an alternative lanthanide, Eu^{3+}, in the place of Gd^{3+}. Eu^{3+} was adjacent to Gd^{3+} in the periodic table, and has similar physical characteristics to Gd^{3+} – such as size and charge density. It also forms the same coordinating complex as that of Gd^{3+} and, importantly, the excited state of Eu^{3+} was quenched by OH and OD oscillators. The spectral details obtained from the emission spectrum of Eu^{3+} provide information about the structural symmetry by examination of the peak splitting and intensity ratios in the different ΔJ bands.[117]

The spectra obtained for Eu^{3+} complexes are intense, sharp and well defined; they are due to f–f transitions between the same $4f^n$ configurations that are effectively

shielded from the environment by the $5s^2 5p^6$ orbitals, owing to the small radial extension of the 4f orbital..[116]

When the Eu^{3+} was excited at 394 nm the electrons are excited from the $^7F_0$ energy level to that of the ^5D_J energy level (Figure 4.2.1.1). The emissions from the long-lived ($^5D_0$ / ^7F_J) levels are observed in the Eu^{3+} spectra as $^7F_1$ = 590 nm, $^7F_2$ = 615 nm, and $^7F_4$ = 698 nm, corresponding to the strong emission ΔJ bands 1, 2 and 4 respectively. The actual emission values can shift slightly owing to the nephelauxtic effect the ligands have upon the Eu^{3+} ion as the effective positive charge on the Eu has decreased due to change in the ligands.[118] Bands $^7F_0$ and $^7F_3$ are evident only in some compounds, at 570 nm and 650 nm respectively.[119]

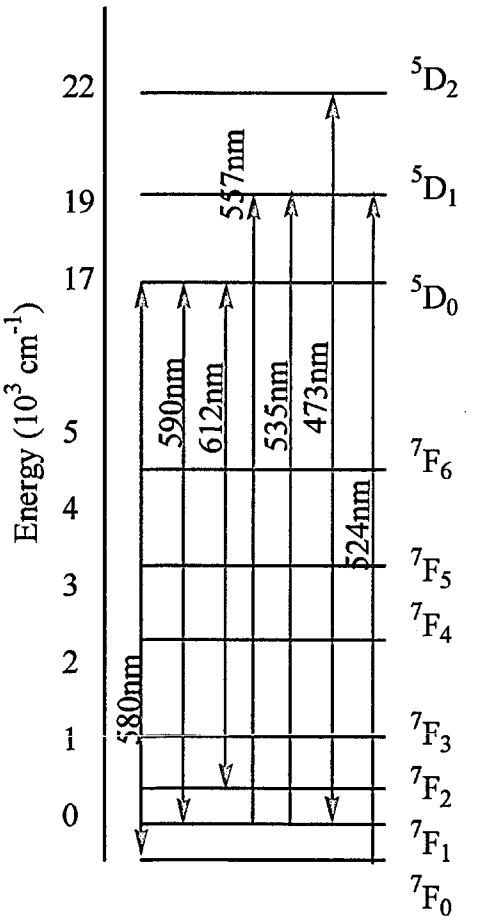

Figure: 4.2.1.1: Energy levels of Eu^{3+} below 30 000 cm^{-1} [116, 120]

4.2.2: Results and analysis of the Eu^{3+} emission spectra for the Eu^{3+} complexes

The emission spectra for the Eu^{3+} complexes were taken between 550nm and 750 nm, with excitation at 395 nm. The spectrum was split into five ΔJ bands: ΔJ = 0, 577–581 nm; ΔJ = 1, 585–600 nm; ΔJ = 2, 611–624 nm; ΔJ = 3, 640–655 nm; and ΔJ = 4, 680–710 nm. These bands have been noted on the spectra in graphs 4.2.2.1 to 4.2.2.7. The bands of the emission spectrum show details of the symmetry, or lack of it, for the complex in which the Eu^{3+} was bound. The ΔJ bands 1, 2 and 3 show sensitivity towards the degree of symmetries.

The ΔJ = 0 band was normally weak, because it was "forbidden" by the selection rules.[121] The emission intensity seen for this magnetic dipole transition was due to band mixing of the electric dipole transitions though interaction with the ligand field or the vibrational states. For example DOTA has C_4 symmetry and shows an intense ΔJ = 0 transition / band. (Figure 4.2.2.1).

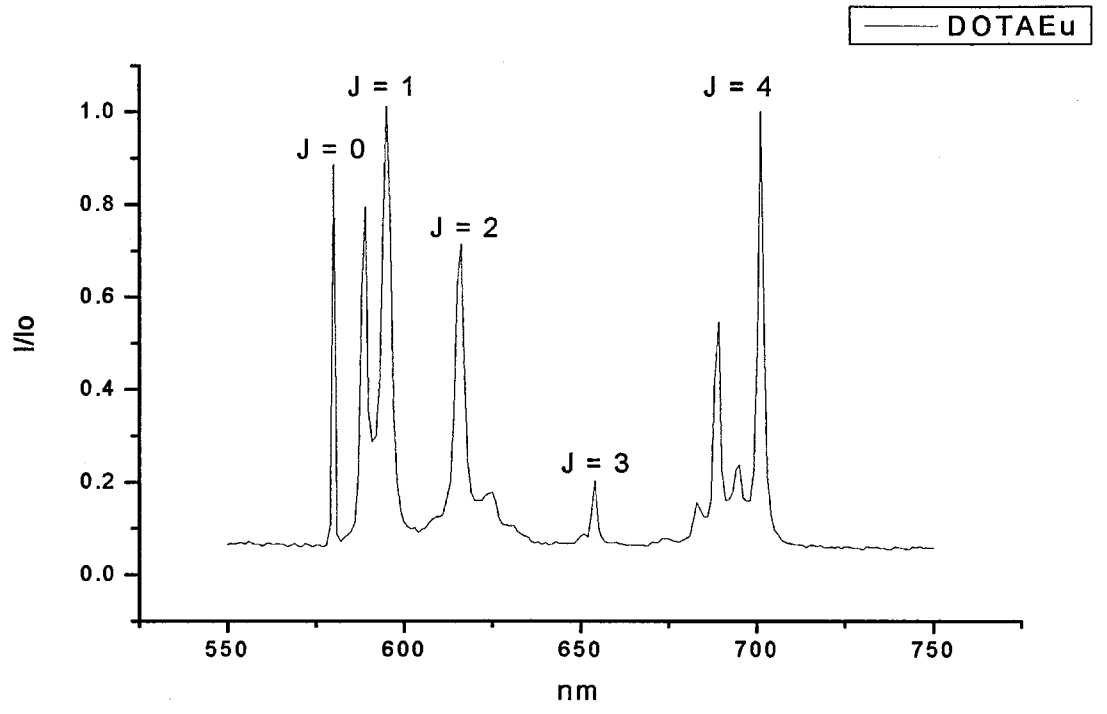

Graph 4.2.2.1: Emission spectrum of DOTA-Eu (3)

The intensity of the ΔJ = 0 band was related to the symmetry of the complex and increases in complexes with C_n or C_{nv} symmetry. As the ΔJ = 0, was non-degenerate therefore If there are two or more peaks present in the spectrum at ΔJ = 0, then it shows that there was more than one complex site for the Eu^{3+} in the solution.[116, 117]

The intensity of the ΔJ = 1 region varies from one coordination environment to another, with the number of peaks within the region relating to the different isomers of the complex present in the solution and to the degree of symmetry. For example, a complex with C_3- or C_4-axis symmetry would lead to two peaks in the band, while a compound with no symmetry in the axis would produce three peaks. Complexes such as DOTA-Eu (3) which C_4 symmetry display 3 peaks with the third peak arising

from the presence of a minor isomer.[116] This isomer mixture was not observed for septadentic complexes as they are a mixture of isomers. These details of the spectrum allow analysis of the binding and symmetry of the molecule to be determined (Table 4.2.2.1).

ΔJ	*λ range (nm)*	*Intensity*	*Notes*
0	577–581	Variable / weak	Intensity increases with symmetry by J-mixing.
1	585–600	Strong	Always present splitting, dependent on symmetry. Three transmissions for low-symmetry complexes; two transmissions for those with C_3 or C_4 symmetry.
2	611–624	Strong / very strong	Hypersensitive; increases when there was a loss of symmetry.
3	640–655	Very weak	Always weak.
4	680–710	Medium / strong	Sensitive to Eu coordination symmetry and donor atom type.

Table 4.2.2.1: Characteristic properties of europium emission spectrum[116]

The ΔJ = 2 band was determined by the complexation site's symmetry, and increases in intensity as the symmetry was reduced. The number of peaks found for this band was also linked to the symmetry, such that a complex with limited symmetry has a greater number of signals than one with a high amount of symmetry.

To confirm the technique and to act as a reference compound the first compound we examined was DOTA-Eu. The spectrum obtained (Graph 4.2.2.2) was sharp and well defined, and matched the published data.[116] The ΔJ = 0 band was intense, because of the high amount of symmetry in the molecule, and because the ratio between different isomers was low. The splitting of the ΔJ = 1 band was characteristic of a compound with C_4 symmetry. This symmetry also influences the ΔJ = 2 band, which was reduced in intensity when compared to the ΔJ = 1 band. The

$\Delta J = 4$ was sensitive to the coordination environment of the Eu^{3+} within the complex, and was identical to that given by the literature data.[116]

The ΔJ bands 0 and 1 for the emission spectrum for sDO3A-Eu (**208**) (Graph 4.2.2.2) are low in intensity, which was indicative of a complex with low symmetry. This was also seen in the $\Delta J = 2$ band, which has a greater intensity due to the limited symmetry of the complex. This was expected, as sDO3A-Eu has symmetry only in the C_1 symmetry in the symmetry axis which was expected for a tri-substituted cyclen.

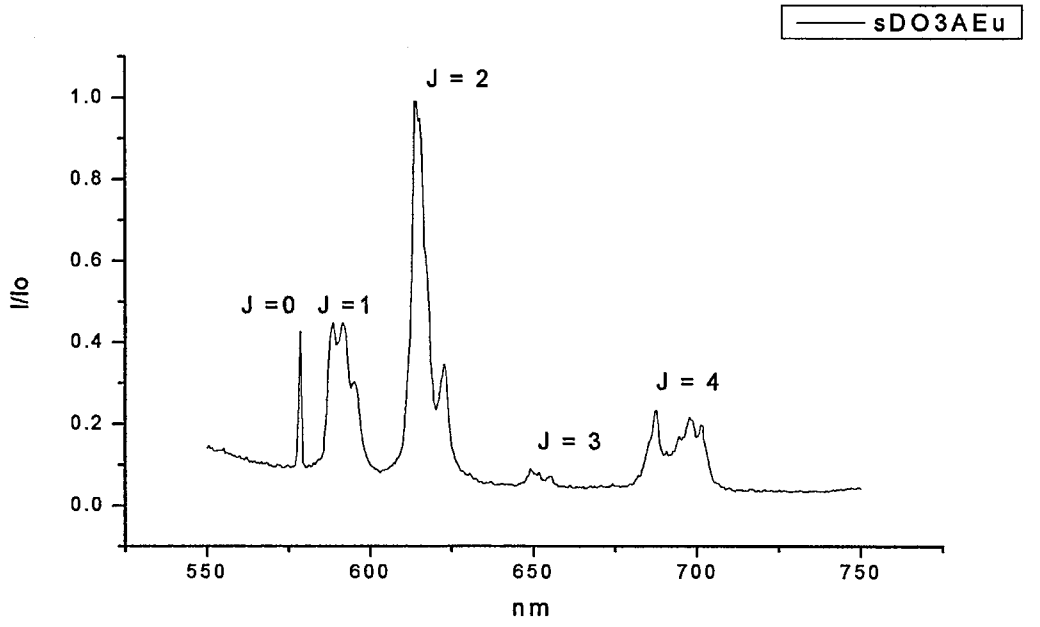

Graph 4.2.2.2: Emission spectrum of sDO3A-Eu (208)

The emission spectrum for sDO3A-(ethyl)-Eu (**206**) (Graph 4.2.2.3) was somewhat similar to that of sDO3A-Eu (**208**) (Graph 4.2.2.2). The main difference was on the $\Delta J = 2$ band, where the sDO3A-(ethyl)-Eu (**206**) has only one peak, whereas the sDO3A-Eu (**208**) has two. This was due to the resolution of the spectrum as the peak was stepped, caused by the hypersensitivity of the band to changes in the groups

binding to the Eu^{3+} emitting closer together than the sDO3A-Eu does. That was due to the change in the coordinating ligands – in the case of sDO3A-(ethyl) (**206**) complexing by the carbonyl group of the ester, and complexing by the carboxylic acid in the case of sDO3A-Eu (**208**).

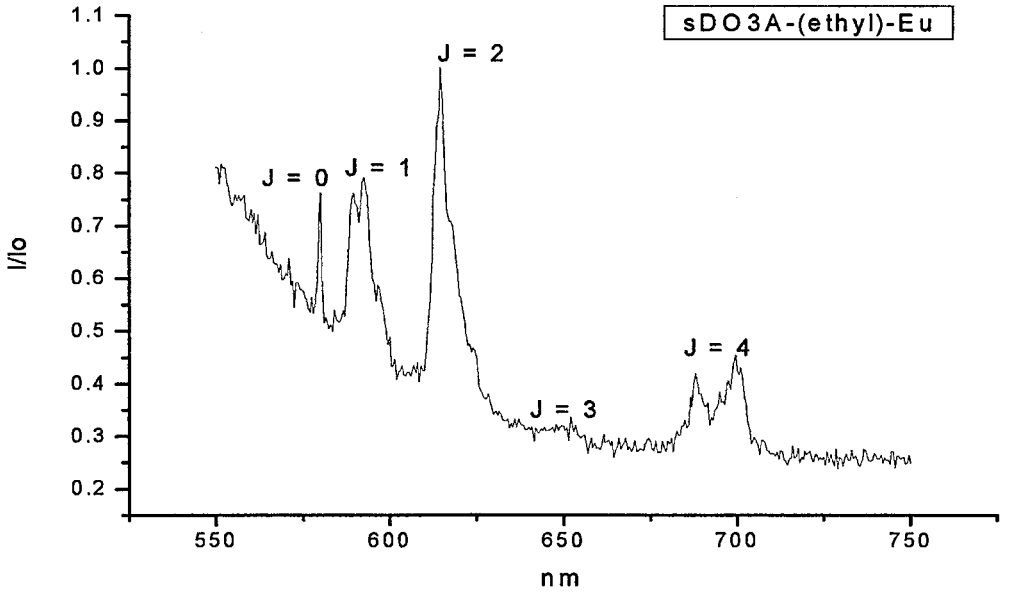

Graph 4.2.2.3: Emission spectrum of sDO3A-(ethyl)-Eu (206)

The spectra for the organosilicon complexes (pentane-sDO3A-)dimethyl (phenyl)silane-Eu (**213**) (Graph 4.2.2.4), 1,4-bis((pentane-sDO3A)dimethylsilyl) benzene-Eu_2 (**215**) (Graph 4.2.2.5) and 1,3,5-tris((pentane-sDO3A)dimethylsilyl) benzene-Eu_3 (**217**) (Graph 4.2.2.6) are all similar in their peak pattern and are a close match to the sDO3A-Eu spectrum. This too was expected as there was unlikely to be coupling between the complexes. It also suggests there is no cross binding occurring. The $\Delta J = 2$ band shows a strong signal, indicating that the molecules have reduced symmetry; that was confirmed by the $\Delta J = 1$ band, which has three transmissions, indicative of low symmetry.

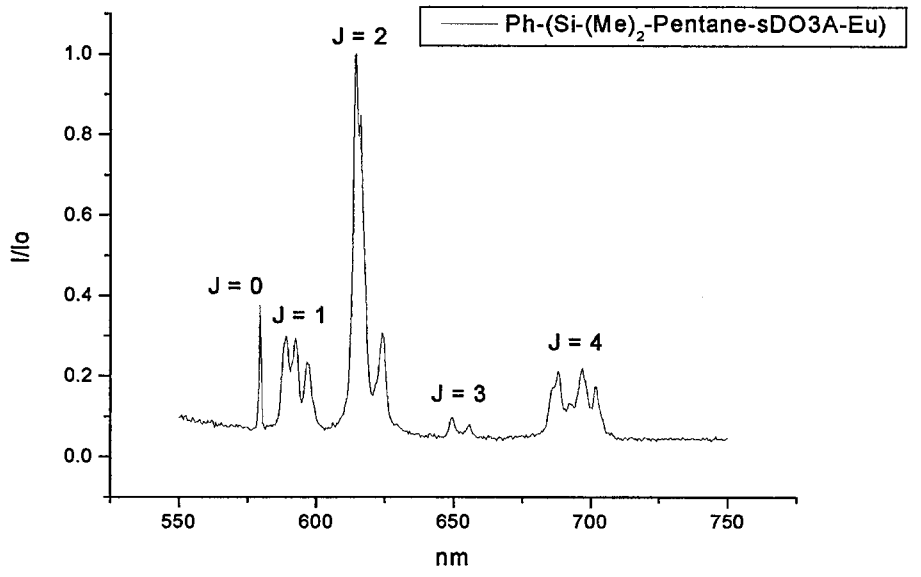

Graph 4.2.2.4: Emission spectrum of Ph-(Si-(Me)$_2$-pentene-sDO3A-Eu) (213)

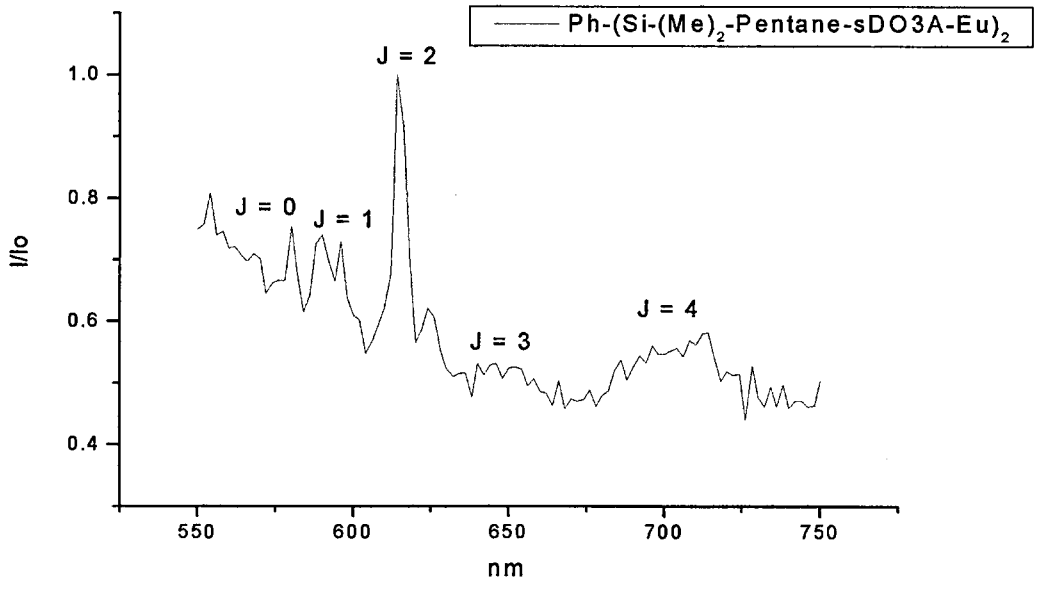

Graph 4.2.2.5: Emission spectrum of Ph-(Si-(Me)3-pentene-sDO3A-Eu)2 (216)

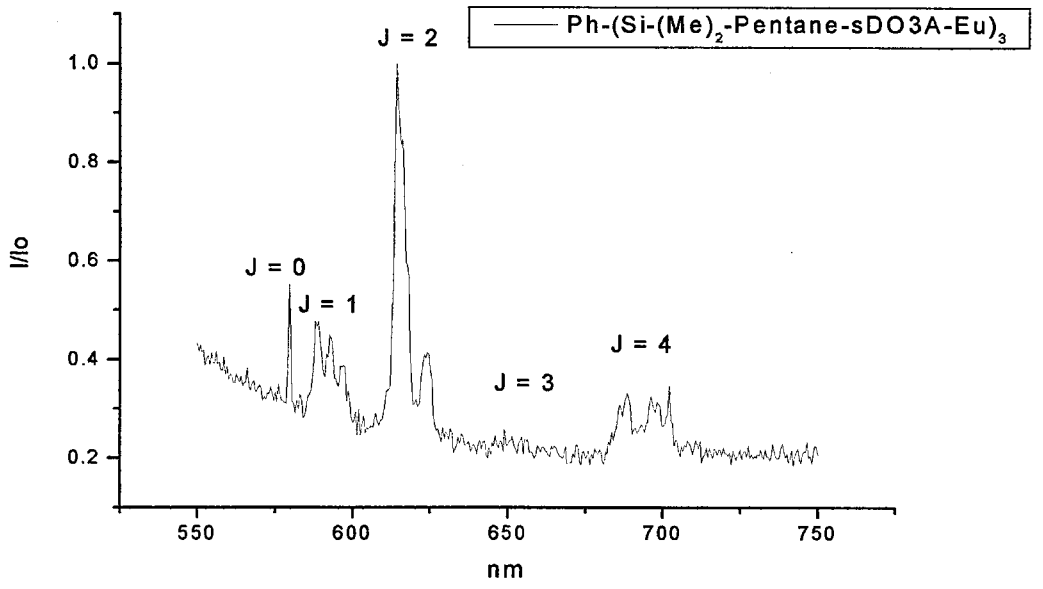

Graph 4.2.2.6: Emission spectrum of Ph-(Si-(Me)3-pentene-sDO3A-Eu)3 (217)

4.3.1: Determination of the water coordination number (*q*) for the Eu^{3+} complexes

The hydration number for the europium complexes was calculated from the decay-rate constant of the excitation state, which was found by measuring the intensity of the phosphorescence emission of the complex solution in both H_2O and D_2O. The difference in the quenching between the two solvents was by a factor of 200, which was seen in the lifetimes of the luminescence.[122]

To measure the luminescence, the solution undergoes excitation by a short pulse of light at 395 nm for 40 ms; after a delay ranging from 0.1 ms to 5 ms (increments of 0.2) the intensity of the phosphorescence was measured through a window of 0.1 ms. The observed wavelength used for all the complexes was the Δ =J2 at 615 nm,

which was an intense peak in the emission spectrum, and was often used for these types of complexes.[18, 56, 117, 118, 121]

4.3.2: Calculation of the Eu^{3+} water hydration number for the Eu^{3+}-complexed ligands

The water coordination number (q) was obtained from *Equation 4.3.2.1* [122, 123], in which A was an empirical constant based on the sensitivity of the lanthanide to quenching (Eu^{3+} = 1.11 water molecules ms, Tb^{3+} = 4.2 water molecules ms). k_{XH} was the combined values of the oscillators in the first coordination sphere, which can shorten the Eu^{3+} excited-state lifetimes by varying degrees.

$$q = A[(k_{H_2O}) - (k_{D_2O}) - k_{XH}] \qquad \textbf{Equation 4.3.2.1}\ ^{122, 123}$$

These oscillators have exchangeable hydrogens, such as alcohols and amines, in which the oxygen or nitrogen was directly coordinated to the metal ion.[123] The constant k_{XH} can be calculated using *Equation 4.3.2.2.*

$$k_{XH} = \alpha + \beta n_{OH} + \gamma n_{NH} + \delta n_{O=CNH} \qquad \textbf{Equation 4.3.2.2}\ ^{123}$$

where n_{OH} was the number of alcoholic O–H oscillators, n_{NH} was the number of amine N–H oscillators and $n_{O=CNH}$ was the number of amide carboxylic oxygen oscillators. The values for these are averages, calculated by Horrocks et al. as β = 0.44 ms^{-1}, γ = 0.99 ms^{-1} and δ = 0.075 ms^{-1}.[122] While β, γ, and δ are related to the first coordination sphere, the α value was the quenching of the excited state Eu^{3+} by the second coordination sphere water molecules. This gives an average value of 0.31 ms^{-1}.[122].

The equation was then rewritten, taking into account the functional groups on the complexes being measured, to give *Equation 4.3.2.3*:

$$q = A[(k_{H_2O}) - (k_{D_2O}) - (\alpha + \gamma n_{NH})] \qquad \textbf{Equation 4.3.2.3}\ ^{122}$$

4.3.3: Results and analysis of the water coordination numbers of the Eu^{3+} complexes

The results from *Equation 4.3.2.3* and the oscillator values are presented in Table 4.3.3.1. The methodology for the calculations was validated by the analyses of DOTA-Eu (**211**). The values obtained for DOTA-Eu are consistent with the published values, where the average was 1.22 (+/− 0.5)[18]. It should be noted that there was some uncertainty with such reported estimates with an experimental error in the rate of between +/−10% and +/−20%.[59, 123] The solutions of the complexes were made at 1 mg per ml of ultra-pure water.

Complex	k_{H_2O}	k_{D_2O}	*q per Gd*	*q N°*
Butene-sDO3A-(ethyl)-Eu (**204**)	3.457	1.81	1.49	1.49
sDO3A-(ethyl)-Eu (**206**)	3.423	0.78	1.5	1.5
sDO3A-Eu (**208**)	4.563	1.75	1.68	1.68
sDO2A-Eu (**210**)	6.549	0.564	4.11	4.11
DOTA-Eu (**211**)	1.93	0.443	1.31	1.31
(pentane-sDO3A-)dimethyl(phenyl)silane-Eu (**213**)	1.758	0.78	0.75	0.75
1,4-bis((pentane-sDO3A)dimethylsilyl)benzene-Eu_2 (**215**)	1.95	0.769	0.97	1.94
1,3,5-tris((pentane-sDO3A)dimethylsilyl)benzene-Eu_3 (**217**)	1.894	0.772	0.9	2.7

Table 4.3.3.1: Lifetime data for Eu^{3+} complexes to calculate q values

The q values of the silicon-sDO3A-Eu compounds are lower than that of sDO3A-Eu alone. This was most likely caused by two effects. In compound (**213**) the benzene ring maybe blocking a potential binding site for the water. By the benzene ring binding to the Eu^{3+} through an electrostatic bond. This would increase the number of coordinating ligands and thus reduce the number of sites to which the water can bind.

The second was that the q values are sensitive to the distance of the coordinating water to the europium. This increasing distance reduces the energy-transfer efficiency, which was manifested as a reduction in the q value.[116] The distancing of the water molecules could happen as a result of the way in which the succinic acid forms a cage around the Eu^{3+}, thus reducing the ability of the water to get close to the Eu^{3+}. This effect could also explain why the results for sDO3A-Eu (**208**), butene-sDO3A-(ethyl) (**204**) and sDO3A-(ethyl) (**206**) are lower than the expected $q = 2$ value predicted.

The predicted q value of sDO2A-Eu was $q = 3$, as the number of ligands binding to the Eu^{3+} was six, with four from the amines and two from the succinic acid donors. The observed value for sDO2A-Eu (**210**) was $q = 4.2$; the difference between the two values for q was greater than the expected error of 20%.

Decomplexation of the unstable hexadentate complex would explain discrepancies in the predicted and experimental results. The decomplexation may be seen in the lifetimes of sDO2A-Eu (**210**) in water, and hence the q values. The solution was measured three times over a total period of 3 hours. The variation in the q value over time indicates that the complex was undergoing some

decomplexation/recomplexation. This instability can be seen in the comparison of *q* values for sDO3A-Eu over time, which shows little variation between the q values (Table 4.3.3.2). This slight decomplexation has been noted in other hexadentate lanthanide ligands.[124, 125]

	sDO2A-Eu			*sDO3A-Eu*		
Run number	k_{H_2O}	k_{D_2O}	q No	k_{H_2O}	k_{D_2O}	q No
1	6.43	0.56	3.79	4.56	1.75	1.67
2	6.48	0.56	4.14	4.58	1.76	1.69
3	6.74	0.56	4.32	4.55	1.75	1.67

Table 4.3.3.2: K_{H2O} and K_{D2O} values for sDO2A-Eu (210) and sDO3A-Eu (208)

4.4.1: Relaxivity measurements of the Gd^{3+} complexes

The relaxation experiments were performed on a Minispec mq60 pulsed time-domain NMR analyzer (Bruker, Massachusetts, USA), with a fixed field of 60 MHz and a magnetic strength of 1.4 Tesla such that for the T_1 measurements could be undertaken near the field of 1.5 T used in clinical MRI systems. The samples were prepared in standard NMR tubes containing 1 ml of the sample. The temperature of the samples was controlled via an external Circulator HAAKE Phoenix II P1-C35P (Thermo electron Corporation) to an accuracy of 0.01 °C.

The samples were measured three times at 25 °C, and were prepared in buffered solution of 10 mmol MOPS (3-(N-Morpholino) propanesulfonic acid) and adjusted to pH 7.4. The buffer was used to keep the experimental conditions identical and allow

the comparison to published data. MOPS was chosen because it has a minimum interaction with gadolinium, compared to phosphate-based buffers that bind to gadolinium.[18] The signal intensity was measured over a period of time by the use of a set of 20 pulse sequences, which varied by the length of time after the pulse before the measurements are taken. The slope of the graph gives the T_1 time for a given sample. The T_1 data used was an average of three stable results. The average T_1 times gained were then plotted as the $1/T_1$ time (in ms) versus concentration (in mmol). The relaxivity ($r_{1p}mM^{-1}$ s^{-1}) was obtained by calculation of the linear regression trend line (Graph 4.4.1). The equation of the line was then used for the calculation of the relaxivity. The R^2 of the linear regression trend line was used to check the validity of the results. We only used data that gave a linear regression line with a (R^2) that was greater than 0.99.

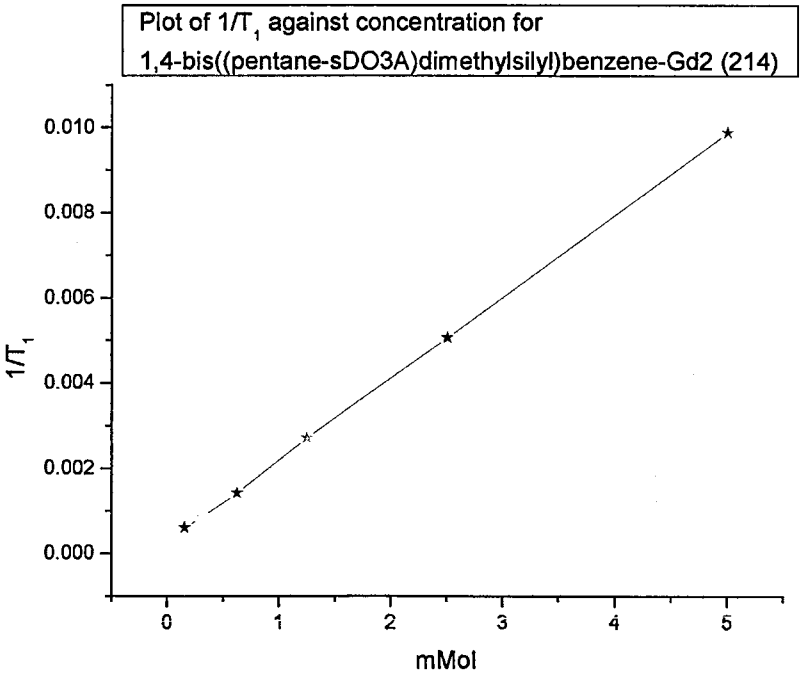

Graph 4.4.1: Example of the plot of $1/T_1$ against concentration for 1,4-bis((pentane-sDO3A)dimethylsilyl)benzene-Gd_2 (214)

Graph 4.4.1: Example of the plot of $1/T_1$ against concentration for 1,4-bis((pentane-sDO3A)dimethylsilyl)benzene-Gd_2 (214)

4.4.2: Relaxation results for the synthesised Gd^{3+} complexes

$GdCl_3$ and DOTA-Gd (**3**) were used as standards to validate the complexation method, analytical technique and calculation methodologies. The results for the DOTA-Gd were performed at both 25 °C and 20 °C, giving relaxation times of 4.3 $r_{1p}/mM^{-1}s^{-1}$ and 3.6 $r_{1p}/mM^{-1}s^{-1}$ respectively, corresponding to known literature values.[19, 54] The relaxivity values of sDO3A-Gd (**207**) and sDO3A-(ethyl)-Gd (**205**) were measured, giving 6.4 $r_{1p}/mM^{-1}s^{-1}$ and 12.6 $r_{1p}/mM^{-1}s^{-1}$ respectively, while the *q* values stayed relatively similar at $q = 1.68$ and $q = 1.50$ (corresponding to acceptable experimental error). The drop in relaxivity suggests the occurrence of cross-binding as was seen in (D. Parker et al)[19] (section 1.6.6). Although the luminescence studies did not suggest this was an issue. This was possibly due to the increased concentrations used in the relaxation studies might influence the degree of cross-binding.

When the relaxivity of sDO3A-Gd (**207**) was compared to the relaxivity of GdaDO3A (**7**) (13.8 $r_{1p}/mM^{-1}s^{-1}$) and GdgDO3A (**8**) (6.2 $r_{1p}/mM^{-1}s^{-1}$), there was an important suggestion that the cross-binding effect of the succinic acid groups was approximately the same as that of glutaric acids. The slight increase in the *q* number and the relaxivity of sDO3A-Gd shows that the effect was less pronounced than that of the GdgDO3A (Table 4.3.2.1).

Complex	$r_{1p}/mM^{-1}s^{-1}$
GdCl3	8.6
Butene-sDO3A-(ethyl)-Gd (**203**)	5.7
sDO3A-(ethyl)-Gd (**205**)	12.6
sDO3A-Gd (**207**)	6.4
sDO2A-Gd (**209**)	5.1
DOTA-Gd (**3**)	4.3
(pentane-sDO3A-)dimethyl(phenyl)silane-Gd (**212**)	4.8
1,4-bis((pentane-sDO3A)dimethylsilyl)benzene-Gd2 (**214**)	4.5
1,3,5-tris((pentane-sDO3A)dimethylsilyl)benzene-Gd3 (**216**)	13.1

Table 4.4.2.1: Results of relaxation measurements

Complex	$r_{1p}/mM^{-1}s^{-1}$	*q*
[GdaDO3A] (**218**)	12.3α (13.8)β	2.2
[GdgDO3A] (**219**)	5.4α (6.2)β	1.2
[GdaDOTA] (**7**)	7.6α (8.9)β	1.0
[GdgDOTA] (**8**)	7.3 α(9.0)β	1.1
[Gd-DO3A] (**220**)	6.0α 4.8γ	1.8
[Gd-DOTA] (**3**)	4.2α 3.5γ	1.0

Table 4.4.2.3: Table of comparative complexes

Note: α 20 MHz, 25 °C; β 65.3 MHz, 25 °C, pH 7.2 [19]; γ 20 °C, 40MHz [54]

The relaxivity of (pentane-sDO3A-)dimethyl(phenyl)silane-Gd (**212**), with a value of 4.8 r_{1p}/ $mM^{-1}s^{-1}$, was substantially lower than the one corresponding to sDO3A-Gd

(**207**). This was due to the low *q* value of (pentane-sDO3A-) dimethyl(phenyl)silane-Gd (**212**) seen while analysing the europium complexes. It can also be noticed in the comparison between Ph-(pentane-sDO3A-)dimethyl(phenyl)silane-Gd (**212**) and DOTA-Gd (**3**) (*q* = 1), which has similar relaxation values, as well as number of coordinated waters. While the relaxivity for (pentane-sDO3A-)dimethyl(phenyl)silane-Gd (**212**) and 1,4-bis((pentane-sDO3A)dimethylsilyl) benzene-Gd_2 (**214**) are similar, at 4.8 r_{1p}/ $mM^{-1}s^{-1}$and 4.5 r_{1p}/ $mM^{-1}s^{-1}$respectively, 1,3,5-tris((pentane-sDO3A)dimethylsilyl)benzene-Gd_3 (**216**) shows a marked difference, with a relaxivity of 13.1 r_{1p}/ $mM^{-1}s^{-1}$. This corresponds to cross-binding between the cyclen systems in the 1,3,5-tris((pentane-sDO3A)dimethylsilyl)benzene-Gd_3 (**216**), which locks the molecule in one position, thus reducing the internal oscillation between the cyclen groups and the aromatic ring and effectively changing the molecule from a branched oligomer to a barycentre. This means that the molecule has only the rotational coefficient to affect the relaxivity, which in turn increases the relaxivity from around 4.5 r_{1p}/ $mM^{-1}s^{-1}$to over 13 r_{1p}/ $mM^{-1}s^{-1}$ (Figure 4.4.2.1). While the increase was a result of the cumulative effect of the gadolinium atoms, it shows the significant effect that the cross-binding has on stabilising the intermolecular movements. The cross-binding effect was not seen in the bis((pentane-sDO3A)dimethylsilyl)benzene-Gd_2 (**214**) complex, pointing to the gadolinium groups being at a comparatively long distance from each other and therefore being unable to cross-bind. This was reflected in the lower relaxivity of 4.5

r_{1p}/ $mM^{-1}s^{-1}$..

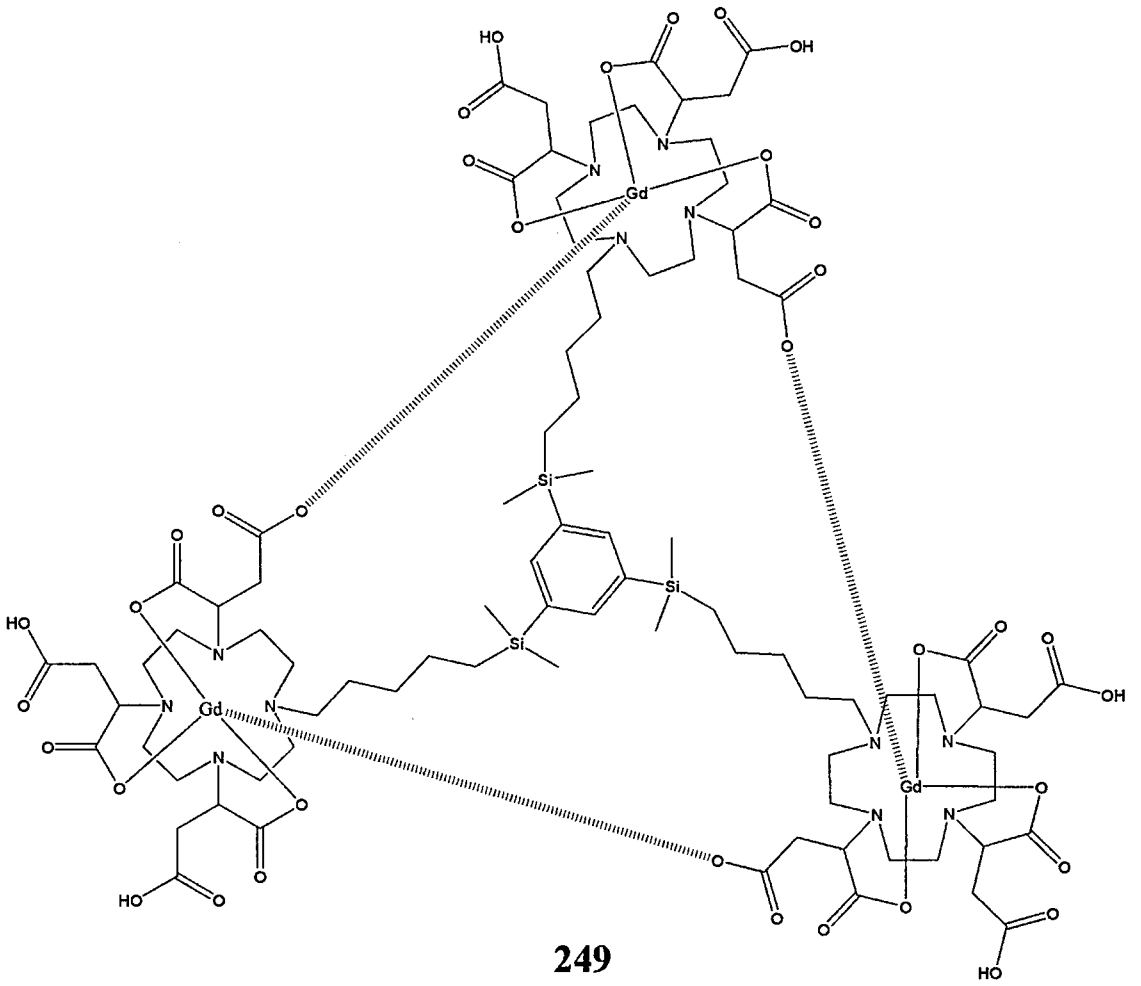

249

Figure 4.4.2.1: Possible configuration of the cross-binding seen within 1,3,5-tris((pentane-sDO3A)dimethylsilyl)benzene-Gd_3 (216)

4.5: Conclusion

Between sDO3A-Eu (**208**) and sDO3A-(ethyl)-Eu (**206**) there was a marked difference in how the cross-binding between the succinic acid groups affects the relaxivity. The series of dimethylsilyl-benzenes shows that it was possible to form lanthanide complexes from a cyclen ligand attached to a silicon core. It was important to note that sDO3A (**32**) pendant groups will cross-bind with each other if they are in close proximity. If the attachment of the sDO3A (**32**) to the silsesquioxane

cages had occurred, then this cross-binding would have been a major part of the relaxivity, as the sDO3A (**32**) pendant groups would have easily cross-linked, because their proximity to each other would have been close to that of the 1,3,5-tris((pentane-sDO3A)dimethylsilyl) benzene-Gd_3 complex (**216**).

The spectral data showed that the complexes were asymmetrical, as indicated by the fluorescence spectra of the individual compounds. This was expected, as the sDO3A-Eu complex has only C_1 symmetry (section 4.2.2). From the analysis of the luminescence emission spectra, it was possible to say that the complexes possess a mixture of different isomers of both [R] and [S]. That was to be expected, since there was no selective pressure during the addition of the maleate/fumarate to the cyclen to produce a predominant isomer. The *q* values of the compounds showed that the butene-sDO3A-(ethyl)-Eu (**204**), sDO3A-(ethyl)-Eu (**206**) and sDO3A-Eu (**208**) have similar values, within experimental error. The organosilicon complexes (pentane-sDO3A-)dimethyl(phenyl)silane-Eu (**213**), 1,4-bis((pentane-sDO3A)dimethylsilyl) benzene-Eu_2 (**215**), and 1,3,5-tris((pentane-sDO3A)dimethylsilyl)benzene-Eu_3 (**217**) had similar *q* values to one another, with a value of $q = 1$; this was a noticeable difference from the non-organosilicon complexes. The critical difference was a result of cross-binding between the pendant groups.

Chapter 5.0: Conclusion

5.1: The formation of sDO3A-(ethyl) (107) and sDO3A (32)

The formation of sDO3A-(ethyl) (**107**) and sDO3A (**32**) gave several different problems, which were mainly due to the reactivity of the cyclen and the need to achieve an asymmetrical substituted pattern. There were two different routes to the formation of the substituted cyclens, the 1+3 and 3+1 routes. The first approach was the formation of pent-4-enoyl-DO3A (**61**) via the 1+3 route, involving the linking arm based on pent-4-enoyl chloride (**63**). The pent-4-enoyl chloride (**63**) was reacted with cyclen, producing an over-alkylated product. The over-reaction was prevented by the use of protection groups. Two methods of protecting three of the cyclen's amines were tried. The first was di-*tert*-butyldicarbonate (**71**), which gave tri-BOC-cyclen (**72**), and the second used 2,2,2-trichloroethane-1,1-diol (**76**) to give triformyl cyclen (**74**).

Both of the protection groups proved effective in preventing over-alkylation, but when the groups were removed the pent-4-enoyl arm was also removed if in the presence of weak base or acid. This ease of elimination of the carboxyl linker arm was a critical problem, as it meant it would be easily removed at later stages of the synthesis of the cage–cyclen complex, especially during the hydrolysis of the ester-protection groups.

This ease of decomposition meant that an alternative linking arm needed to be investigated, and so 4-bromo-butene (**78**) was looked at as a replacement for pent-4-enoyl chloride (**63**). The change in the linking arm presented a possible stability problem, because of the reduction of the number of ligands available for binding to the lanthanide from 8 to 7, due to the loss of the carbonyl on the but-3-enal. The loss

of potential stability was compensated for by the use of di-acid arms, such as malonic acid (**80**) to give mDO3A (**95**) and succinic acid (**100**) to produce sDO3A (**32**). The synthesis of mDO3A (**95**) failed, owing to the decarboxylation of 2-(bromomethyl)-2-methylmalonic acid (**89**) during the esterification of the acids. After that failure the alternative group sDO3A, based on succinic acid (**100**) groups, was investigated. Again the 1+3 route was examined first, and the butene-cyclen 1-but-3-en-1-yl-1,4,7,10-tetraazacyclododecane (**106**) was successfully synthesised by the reaction of 4-bromobutene (**78**) with the tricyclic protected cyclen, octahydro-5H-2a,4a,7,9a-tetraazacycloocta[1,2,3-cd]pentalene (**113**). This was then deprotected using a mild base to yield the butene-cyclen (**106**).

The next step was the reaction of 1-but-3-en-1-yl-1,4,7,10-tetraazacyclododecane (**106**) with diethyl 2-bromosuccinate (**103**), in an attempt to form butene-sDO3A-(ethyl) (**101**). This approach failed to yield butene-sDO3A-(ethyl) (**101**), but instead gave butene-sDO2A-(ethyl) (**123**) and butene-sDO1A-(ethyl) (**124**). This was due to the steric hindrance caused by the attached arms, and the low reactivity of the secondary bromide. The approach to the synthesis was then changed to the (3+1) route, in which sDO3A-(ethyl) (**107**) was synthesised first and then reacted with 4-bromobutene (**78**) to form butene-sDO3A-(ethyl) (**101**). The synthesis of sDO3A-(ethyl) (**107**) from cyclen (**9**) and diethyl 4-bromosuccinate (**103**) was problematic owing to poor separation from the reaction intermediates, mainly sDO2A-(ethyl) (**109**), caused by the diethyl bromo-succinate (**103**) affecting the Rf values of the reaction products. This meant that they eluted together off the column over a wide range of solvent systems and solid-phase media. It was noted during the reaction with potassium carbonate that there was a side reaction occurring to the diethyl 2-bromosuccinate, which underwent elimination of the bromine to give the alkene

diethyl maleate; that then went on to react with the cyclen. These discoveries led to the formation of sDO3A-(ethyl) (**107**) by the Michael addition reaction between cyclen (**9**) and diethyl fumarate (**130**). By not using diethyl 2-bromosuccinate (**103**), it was possible to separate the reaction products with greater yields, as the difference between the Rf values of sDO3A-(ethyl) (**107**) and sDO2A-(ethyl) (**109**) was greater when not in the presence of diethyl 2-bromosuccinate (**103**). Following the successful synthesis of sDO3A-(ethyl) (**107**), the next step was the formation of butene-sDO3A-(ethyl) (**101**) and pentene-sDO3A-(ethyl) (**133**) by reaction with 4-bromobutene (**78**) and 5-bromopentene (**134**), respectively.

The hydrolysis of the alkene-sDO3A-(ethyl)s (**101**) and (**133**) showed that both the succinate and alkene arms were unstable in the presence of strong acids, such as HCl, and organic acids, such as formic acid, when heated. This led to the hydrolysis being performed using LiOH with ion-exchange chromatography to give the sDO3A (**32**).

5.2: Silsesquioxane cage-based contrast agents

The evidence suggested that the pentene-sDO3A-(ethyl) (**133**) was decomposing to give pentene-sDO2A-(ethyl) (**123**), along with several side reactions involving the ester and the amine reacting with the Si–H, as shown by the various model reactions. It became apparent that the original syntheses involving siloxane cages could not succeed using the butene-/pentene-arm-based method for attachment to the cages.

5.3: Silylbenzene based contrast agents

The dimethylsilyl benzenes allowed for the attachment of the cyclen to the silicon core without side reactions involving the hydrolysis of the Si–H group and reaction with the ethyl ester. The measurements using the lanthanide complexes showed that the water coordination number was lower than that of the sDO3A-Eu (**208**). This was most likely due to the water exchange rate being altered by the presence of the benzene group, and by some degree of cross-binding, seen in the difference between the Gd^{3+} complexes of sDO3A (**32**) and the (pentene-sDO3A) dimethyl(phenyl)silane-Eu (**213**) and 1,4-bis((pentene-sDO3A)dimethylsilyl) benzene-Eu_2 (**215**) silylbenzenes that had a reduction of relaxivity of around 26%. The effect of cross-binding was strongly evident in the 1,3,5-tris((pentene-sDO3A)dimethylsilyl)benzene-Gd3 (**217**) complex, with a relaxivity nearly 280% greater than those of the (pentene-sDO3A-)dimethyl(phenyl)silane-Eu (**213**) and 1,4-bis((pentene-sDO3A)dimethylsilyl) benzene-Eu_2 (**215**) complexes.

5.4: Further work on silsesquioxane-cyclen compounds

The decomposition problems associated with the silsesquioxanes could be overcome by the use of a two-part linking arm between the cage and the cyclen. This would allow the attachment of the alkene to the siloxane without the secondary reaction of the Si–H with the ester groups. This step would prevent the decomposition of the cages as seen in section 3.5, where the cage with bromo-alkane arms was decomposed by the secondary amine of the sDO3A-(ethyl) (**107**).

The main concern would be in choosing the type of reaction between the silsesquioxane cage linking arm and the cyclen linking arm. A suitable group would have to be stable around the Si–H groups to avoid unwanted reactions, for example the side reaction with carbonyl groups. This could be achieved by the formation of an ether bond. This particular bond could be formed by the reaction of a short alkane chain with a terminal bromide, from the reaction of T_8H_8 (**33**) with bromoethene (**221**) using Speier's catalyst, which produces a compound with eight terminal bromines (**222**). The product would then be reacted with an alcohol attached to the sDO3A-(ethyl) (**107**) unit. A suitable compound for the formation of the alcohol would be bromoethanol (**223**), giving ethanol-sDO3A-(ethyl) (**224**) (Figure 5.4.1).

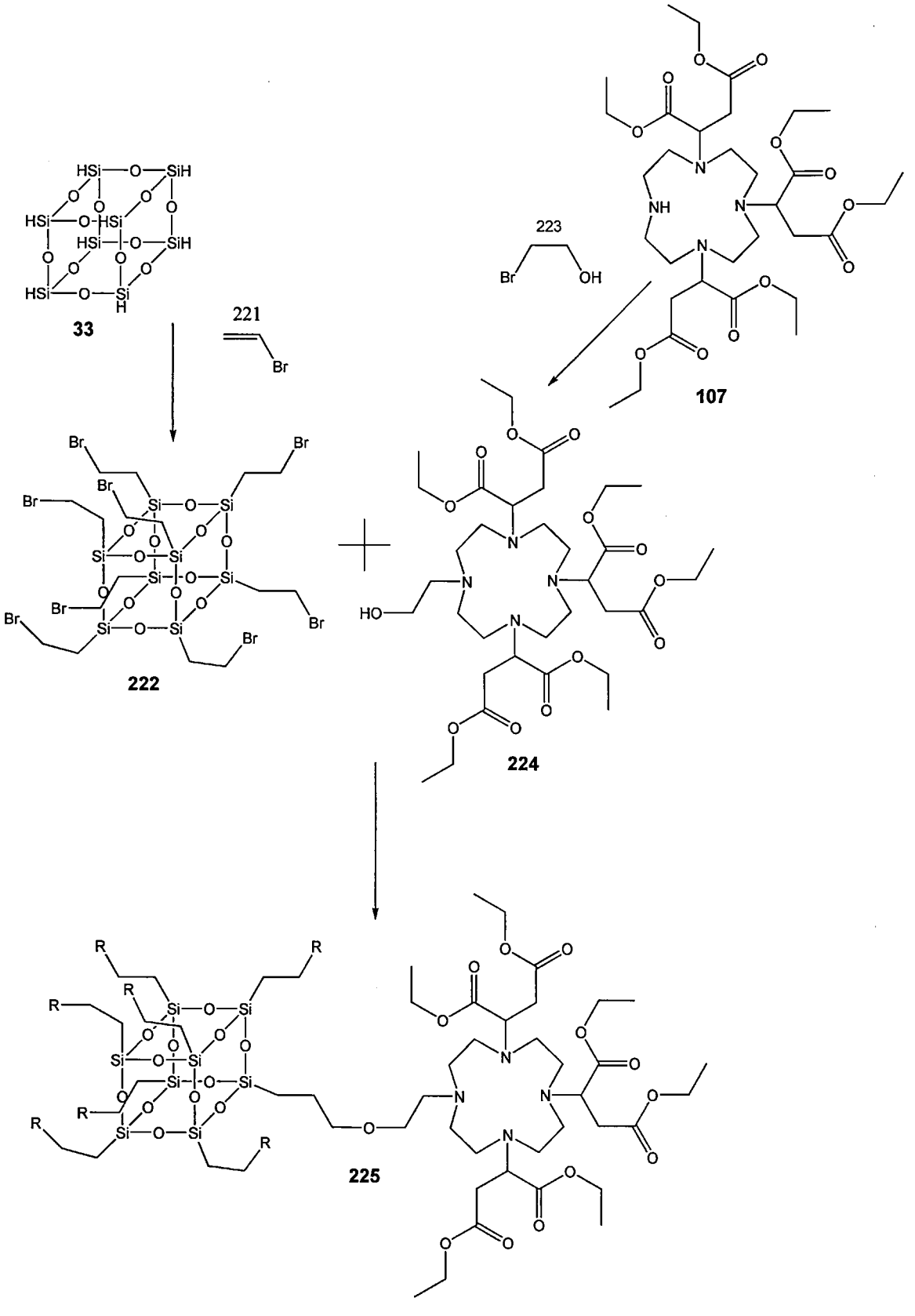

Figure 5.4.1: Possible formation of sDO3A-(ethyl)-T8 (225)

The main obstacle with an ether linked arm was the amount of flexibility that it would acquire. While the length of the chain would be only one unit longer than that found in the T_8-pentane-sDO3A (**225**) molecules, the presence of the ether bond would act effectively as a ball joint. This would increase the anisotropic rotation around the linking arms, having the effect of lowering the relaxivity of the complex.

The hydrolysis of the cyclen-cage compound could present several problems, as the sDO3A group was sensitive to acid, inducing the decomposition of the succinate groups, while the siloxane would be sensitive to an alkali-catalysed decomposition. One possible route around the problem would be to use enzymatic hydrolysis of the ester groups.

5.5: Further work on silylbenzene-based contrast agents

Further work on silylbenzene-based contrast agents could involve expanding the possibilities of silicon-based cores. This would be done by developing a sila substituted benzene suitable for the attachment of oligomers, peptides or proteins to develop targetable contrast agents. The new silicon-based core would have sites for both dimethylsilanes and for targeting groups. A bifunctional silicon core could be synthesised from 2,3,4,5,6-pentabromoanline (**226**) to give the silicon compound 2,3,4,5,6-pentadimethylsilaneanailine (**227**) (Figure 5.5.1). This product could produce a compound in which the amine would allow the attachment of other groups.

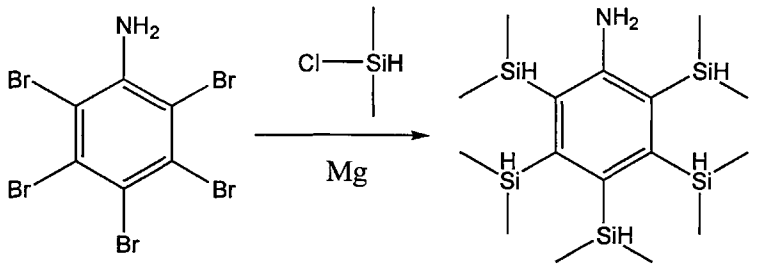

226 227

Figure 5.5.1: Formation of the novel silylbenzene cores 2,3,4,5,6-pentadimethylsilaneanaline (227)

One result of using 2,3,4,5,6-pentabromobenzene as a core for a contrast agent would be that the five sDO3A-Gd groups on the structure would cross-bind, as seen in the 1,3,5-tris((pentane-sDO3A(ethyl))dimethylsilyl)benzene (**207**) complex. This would lead to a higher relaxivity than that of 1,3,5-tris((pentane-sDO3A(ethyl))dimethylsilyl)benzene (**207**). One possible problem with the proposed complexes was the number of sDO3A-Gd (**207**) groups in close proximity to one another. The relaxed water molecule, when relaxed and released from the gadolinium, then was immediately attracted back into the neighbouring complex, which would have the effect of reducing the relaxivity of the complex.

Chapter 6: Experimental Section

6.1: Synthesis of 1-pent-4-enoyl-1,4,7,10-tetraazacyclododecane (66)

Powdered A4 molecular sieve (30 g) was added to a solution of cyclen (**9**) (0.5 g, 0.0029 mol) dissolved in anhydrous chloroform (100 ml). To this was added 4-pentenoylchloride (**63**) (0.3 g, 0.0025 mol, 0.3 ml). The reaction was stirred for 28 hours. Thin Layer Chromatography (TLC) silica (Chloroform 90% methanol 10%) showed that the reaction could not be separated owing to the cyclen binding to the stationary phase seen by the Rf value of 0.01. The reaction produced a mixture of 1-, 2-, 3- and 4-armed cyclens, which were seen by LCMS.

LCMS (positive): 255.21 [M(**66**)$^{+H}$], 337.21 [M(**68**)$^{+H}$], 419.31 [M(**69**)$^{+H}$], 501.33 [M(**70**)$^{+H}$]

6.2: Synthesis of 1,4,7,tetraaza-cyclodecane-1,4,7-tricarboxylic acid tri-*tert*-butyl ester (tri-Boc-cyclen) (72)

A solution of di-*tert*-butyldicarbamate (**71**) (3.6 g, 0.030 mol) dissolved in chloroform (100 ml) was added dropwise to a solution of cyclen (**9**) (1.1 g, 0.00664 mol) and TEA (5.5 ml) dissolved in chloroform (120 ml). The reaction was stirred at room temperature for 18 hours. The solvent was removed using reduced pressure, and the resulting crude product was taken up into DCM (50 ml), and was washed first with 0.5M HCl (1 x 50 ml) and then with water (2 x 50 ml). The organic layer was dried using magnesium sulphate, filtered and the solvent was removed using reduced pressure. The oil produced was then chromatographed on alumina eluting with chloroform (99%) methanol (1%).

Yield, 1.22 g, 40.3%, Rf 0.77 ($CHCl_3$ 99%, MeOH 1%–alumina)

^{1}H NMR ($CDCl_3$): 1.45 (18H, s), 1.47 (9H, s), 2.81–2.89 (4H, m), 3.17–3.44 (8H, m), 3.54–3.72 (4H, m)

FTIR (KBr disk): 2977, 2935, 1690, 1468, 1415, 1366, 1248, 116, 1103

^{13}C NMR ($CDCl_3$): 28.50 (CH_3), 28.70 (CH_3), 45.01 (CH_2), 46.01 (CH_3), 48.88 (CH_2), 49.12 (CH_3), 49.49 (CH_3), 49.90 (CH_3), 50.52 (CH_2), 51.01 (CH_2), 79.20 (C), 155.43 (C=O), 155.62 (C=O), 155.85 (C=O).

FTIR (KBr disk): 3521, 2977, 2121, 1691, 1464, 1418, 1368, 1272, 1172, 1101.

6.3: Synthesis of 1-pent-4-enoyl-4,7,10,tetraaza-cyclodecane-1,4,7-tricarboxylic acid tri-*tert*-butyl ester (73), Scheme C

TriBOC cyclen (**72**) (0.33 g, 0.0007 mol) was dissolved in anhydrous chloroform (100 ml), to which powdered A4 molecular sieve (30 g) was added. To the reaction 4-pentenoylchloride (**63**) (0.43 g, 0.0036 mol, 0.4 ml) was added. The reaction was stirred for 24 hours. The solids were removed using filtration, and the solvent was removed using reduced pressure. The crude product was columned on alumina, eluting with chloroform 95% and methanol 5%.

Yield 0.25 g, 0.00045mol, 64.4%

^{1}H NMR ($CDCl_3$): 1.39 (H 27, s), 2.32 (H 4, d, 2.5 Hz), 3.29–3.42 (H 16, t, 18.5/20.3), 4.92 (H 2, t, 10.27 Hz), 5.76 (H 1, t, 3.48 Hz)

^{13}C NMR ($CDCl_3$): 28.42 (CH_3), 49.54 (CH_2), 50.32 (CH_2), 51.38 (CH_2), 80.08 (CH_2=C), 80.34 (CH=C), 115.38 (O–CH_2), 137.28 (C=O), 155.33 (O–C).

FTIR (NaCl thin film): 3521, 2977, 1761, 2121, 1694, 1464, 1368, 1270, 1175, 1110.

LCMS (positive): 555.72 (M(**70**)$^{+H}$)

6.4: Synthesis of 1-pent-4-enoyl-1,4,7,10-tetraazacyclododecane (66) from 1-pent-4-enoyl-4,7,10-tetraaza-cyclodecane-1,4,7-tricarboxylic acid tri-*tert*-butyl ester (73)

1-pent-4-enoyl-4,7,10-tetraaza-cyclodecane-1,4,7-tricarboxylic acid tri-*tert*-butyl ester (**70**) (0.15 g, 0.00027 mol) was dissolved in acetonitrile (20 ml) to which trifluoroacetic acid (1 ml) was added, and the reaction was stirred at room temperature for 8 hours. After LCMS had shown incomplete hydrolysis, another amount of trifluoroacetic acid (2 ml) was added and the reaction stirred for another 16 hours. The pH of the solution was adjusted to pH 7 by the addition of NaOH (1M).

After 8 hours LCMS (positive): 355.26 [M^{+1}] (semi-hydrolysed product), 455.31 [M^{+1}] (semi-hydrolysed product).

After 24 hours LCMS (positive): 173.19 [M(**9**)$^{+1}$], 255.24 [M(**66**)$^{+1}$] (target product, very small signal).

6.5: Synthesis of 1,4,7,10-tetraazacyclododecane-1,4,7-tricarbaldehyde (triformylcyclen) (74) [87]

Cyclen (**9**) (10 mmol, 1.72 g) was dissolved in ethanol (15 ml) to which chloral hydrate (**76**) (60 mmol, 9.9 g) was added. The reaction was heated to 70 °C for 3 hours. The solvent was then removed using reduced pressure to yield a clear oil. The crude product was then chromatographed on a silica column, eluting with DCM 89.9%, MeOH10% and 0.1%.ammonia solution (35%) to yield a white solid. Yield 2.02 g / 79%

^{1}H NMR ($CDCl_3$): 2.84 (H4, t, 4.5 Hz), 3.09 (H4, t, 4.5 Hz), 3.22 (H8, s), 8.06 (H3, s).

^{13}C NMR ($CDCl_3$): 43.61 (CH_2), 47.89 (CH_2), 45.32 (CH_2), 162.71 (C=O).

FTIR (KBr disk): 3298, 2942, 1669, 1648, 1451, 1408, 1286, 1221, 1155, 1095.

LCMS (positive): 257.39 (M(**74**)$^{+H}$).

6.6: Synthesis of 10-pent-4-enoyl-1,4,7,10-tetraazacyclododecane-1,4,7-tricarbaldeyde (75) version 1

Triformyl cyclen (**74**) (0.5 g, 0.0019 mol) was dissolved in chloroform (100 ml) to which 25 g of activated molecular sieve was added. The reaction was stirred for 10 minutes, after which a solution of pent-4-enoyl chloride (**63**) (0.005 mol, 0.59 g, 0.62 ml) in chloroform (50 ml) was added dropwise over 6 hours. The reaction was then stirred for another 48 hours, after which the solids were removed by filtration and the solvent was removed using reduced pressure.

The crude reaction product was chromatographed on silica, eluting with a mixture of DCM (90%) and MeOH (10%). 0.1 g was collected from the column. LCMS showed that the sample contained the target molecule, but also a large number of unidentifiable peaks.

LCMS (Positive): 270.59 [M?$^{+H}$], 302.59 [M?$^{+H}$], 338.49 [M(**75**)$^{+H}$], 371[M?$^{+H}$].

6.7: Synthesis of 10-pent-4-enoyl-1,4,7,10-tetraazacyclododecane-1,4,7-tricarbaldeyde (75), version 2

Triformyl cyclen (**75**) (1.5 g, 0.0058 mol) was dissolved in DCM (100 ml) to which potassium carbonate (1 g, 0.0072 mol) was added. To this reaction mixture pentyl-4-chloride (**63**) (1.06 g, 0.99 ml, 0.009 mol) was added and the reaction stirred at room temperature for 48 hours, after which TEA (4 ml) was added to the reaction and

stirred for 30 minutes. The solids were removed from the reaction using filtration, and the solvent was removed using reduced pressure. The crude product was then subjected to a high vacuum for 4 hours to remove any residual TEA.

The reaction crude was then taken up into acetone, causing TEA-Chloride to form a powder, which was removed using filtration. The solvent was then removed using reduced pressure, and the resulting crude product was chromatographed on silica, eluting with a mixture of DCM 90%: MeOH 10%: ammonia solution 0.1%.

The target molecule eluted at Rf 0.26.

Yield 0.71 g, 0.0021 mol, 35.7%

^{1}H NMR ($CDCl_3$): 1.18 (H2, s), 1.23 (H2, t, 7.5 Hz), 2.38 (H8, t, 6.7 Hz), 2.52 (H8, t, 6.6 Hz), 3.37 (H3, s,), 4.99 (H, d–d, 10.2 Hz), 5.78 (H2, d–d, H_2C=C, 10.4 Hz),

^{1}C NMR ($CDCl_3$): 28.3 (CH_2), 33.2 (CH_2), 59.3 (CH_2), 68.0 (CH_2), 115.9 (CH_2), 135.8 (CH), 162.7 (C=O), 171.9 (C=O).

LCMS (Positive): 339.41 [M(**75**)$^{+H}$].

FTIR (thin-film NaCl): 3316, 2974, 1715, 1666, 1484, 1380, 1330, 1274, 1089, 1054.

6.8: Synthesis of 1-pent-4-enoyl-1,4,7,10-tetraazacyclododecane (66)

10-pent-4-enoyl-1,4,7,10-tetraazacyclododecane-1,4,7-tricarbaldeyde (**75**) (0.71 g, 0.00207 mol), was dissolved into 0.2M NaOH solution (10 ml) and heated to 70 °C for 72 hours. A 2 ml fraction of the reaction was removed and freeze-dried. The remaining solution was split into two fractions of 4 ml. Purification of the first fraction was attempted by bi-phasic extraction using chloroform (3 x 10 ml); the organic phase was combined and dried over magnesium sulfate. The solvent was removed using reduced pressure to yield zero products. The second 4 ml fraction was passed

though a C18 reverse-phase chromatography column; analysis of the eluent showed that the product had washed through with the sodium hydroxide. The solution was then neutralised using HCl (0.2M), and the reaction was analysed by LCMS.

Crude reaction product LCMS (positive): 254.31 [M(**66**)$^{+H}$]. 282.48 [M(**77**)$^{+H}$].

NMR of freeze-dried crude product

^{1}H NMR ($CDCl_3$): 2.08 (H3, s)(*g*), 2.33 (H4 , m,)(*c,d*), 2.45 (H8, m)(*k ,j*), 2.88 (H4, m,)(*f*), 3.38 (H4, m)(*e*), 4.93 (H1, td, 10.0 Hz,)(*a1*), 5.02 (H1, t, 1.47,)(*a2*), 5.80 (H1, m,)(*b*),

^{13}C NMR ($CDCl_3$): 29.38 (CH_2)(*C*), 30.90 (CH_2)(*D*), 33.12 (CH_2), 115.22 (H_2C=CH–)(*A*), 137.60 (H_2C=CH–)(*B*), 171.21 (C=O)(*E*).

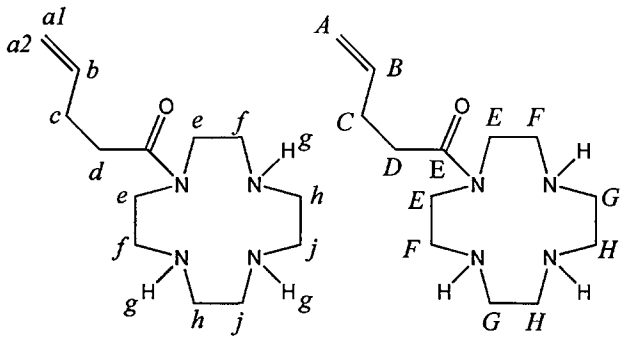

66 **66**

6.8: Characterisation of compound (66), proton (left) carbon (right)

FR (KBr disk): 3435, 2964, 2921, 2851, 2566, 1683, 1645, 1580, 1421

Reverse-phase eluent LCMS (positive): 254.37 [M(**66**)$^{H+}$]. 282.51 [M(**77**)$^{H+}$].

Neutralisation product LCMS (positive): 171.41 [M(**9**)$^{+H}$], 254.32 [M(**77**)$^{+H}$].

6.9: Synthesis of 2-(bromomethyl)-2-methylpropane-1,3-diol (90)

Hydrobromic acid (40%, 28 g) was added dropwise to 3-methyl-3-oxetanemethanol (**91**) (0.1947 mol, 20.00 g) over one hour. The reaction was stirred at 90 °C for 16 hours, and then cooled to 4 °C for 18 hours. The solution was filtered and the crystallised product collected. The resulting crystals were then filtered under vacuum and washed with ice water. The crystalline product was dissolved in DCM (100 ml) and dried over magnesium sulfate. The reaction was filtered and the solvent was removed, using reduced pressure, to yield a white solid.

Yield: 20.99 g, 0.11476 mol, 59%.

^{1}H NMR (CD_3OD): 1.17 (H3, s, $-CH_3$), 3.22 (H2, s, $-CH_2-Br$), 3.47 (H4, s, CH_2-OH).

^{13}C NMR (CD_3OD): 15.6 (CH_3), 35.8 (CH_2-Br) 40.1 (C), 67.7 (CH_2-OH).

LCMS (positive): 91.52 (1/2 M(**90**)$^{+H}$)

6.10: Synthesis of s-(bromomethyl)-2-methylmalonic acid (89)

2-(bromomethyl)-2-methylpropane-1,3,-diol (**90**) (0.0082g, 0.446mmol, 1.50 g) was dissolved in acetone (10 ml) and the reaction was cooled to −15 °C. To the reaction, Jones' reagent* (25 ml) was added dropwise over 1 hour. The reaction was then stirred at room temperature for 16 hours, after which it was quenched with methanol (100 ml) and stirred for 30 minutes. The organic solvents were removed, using reduced pressure, to yield a dark green/black crude solid. The product was extracted using chloroform (2 x 50 ml) and diethyl ether (4 x 200 ml). The organic phases were

combined and dried over magnesium sulfate, filtered and the solvent removed, using reduced pressure, to yield a white, crystalline solid.

Yield 0.81 g, 0.0038 mol, 46.8%

^{1}H NMR (D_2O): 1.78 (H3, s)(*a*), 3.64 (H2, s)(*b*)

^{13}C NMR (D_2O): 18.21 (CH_3)(*A*), 24.28 (CH_2)(*C*), 65.42 (C)(*B*), 182.33 (C=O)(*D*)

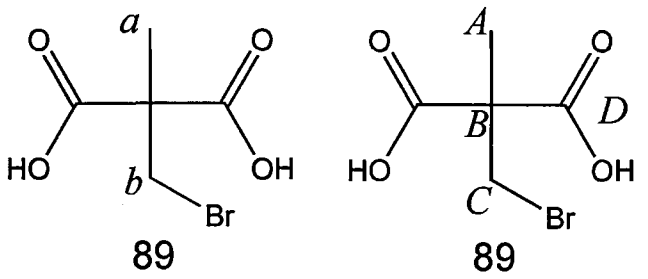

6.10: Characterisation of compound (89), proton (left) carbon (right)

FTIR (KBr disk): 3455, 2975, 1706, 1645, 1571, 1462, 1410, 1263,1172, 1043.

LCMS (positive): 51.75 (1/2M(**89**) $^{-2H}$).

MP 128.1 °C, Lit 126.5 °C [90]

* Jones' reagent: $K_2Cr_2O_7$ (0.0335 mol, 9.86 g) was dissolved in conc. sulfuric acid (6 ml) and diluted with ultra-pure water to make 50 ml of solution.

6.11: Synthesis of dimethyl 2-(bromomethyl)-2-methylmalonate (96)

2-(bromomethyl)-2-methylmalonic acid (**89**) (0.82 g) was dissolved in methanol (30 ml) and sulphuric acid (4 drops). The reaction was then refluxed for 18 hours. The solvent was removed using reduced pressure, and the product taken up into DCM (100 ml) and dried over magnesium sulfate. The reaction was then filtered and the solvent removed, using reduced pressure, to give an oil consisting of (2-(methoxycarbonyl)-3-bromo-2-methylpropanoic acid (**97**).

LCMS (negative): 223.26 [M(**97**)$^{-H}$], 111.20 [1/2M(**97**)$^{-H}$]

6.12: Synthesis of diethyl 2-(bromomethyl)-2-methylmalonate (95)

2-(bromomethyl)-2-methylmalonic acid (**89**) (1.47 g, 0.00696 mol) was dissolved in ethanol (100 ml) and sulfuric acid (4 drops) and heated to reflux for 24 hours. The solvent was removed using reduced pressure and the crude oil was taken up into DCM (50 ml) and dried over magnesium sulfate. The reaction was filtered and the solvent removed to give a red oil.

^{1}H NMR ($CDCl_3$): 1.00 (H ,s), 1.07 (H ,s) 1.27 (H , t, 9.9Hz), 2.09 (H ,s),

^{13}C NMR ($CDCl_3$): 14.04 (CH_3), 19.39 (CH_3), 36.59 (CH_2), 48.74 (CH_2), 61.29 (CH_2), 65.95 (CH_2), 173.12 (C=O).

FTIR (KBr disk): 3479 (C–OH), 2980, 2939, 2880, 1713, 1463, 1368, 1298, 1225, 1175, 1114, 1047.

LCMS (negative): 125.22 [M(2-methylpropanoic acid)+K]

6.13: Synthesis of 1-but-3-en-1-yl-1,4,7,10-tetraazacyclododecane (106)

Cyclen (**9**) (0.5 g, 0.0058 mol) in acetonitrile (20 ml) was added to potassium carbonate (1.5 g, 0.011 mol). The reaction was then cooled to −18 °C (ice/salt/IMS). To the cooled reaction a precooled solution of 4-bromobut-1-ene (**78**) (0.8 g, 0.40 ml, 0.00597 mol) in anhydrous acetonitrile (30 ml) was added dropwise over 4 hours. The reaction was then allowed to warm up to room temperature and stirred for 24 hours. The solid residual waste was removed using filtration. The solvent was then removed using reduced pressure.

The crude was taken up into HCl (2M, 20 ml), the pH adjusted to 10, and then was extracted using chloroform (4 x 100 ml) and the organic component was dried using magnesium sulfate.

TLC – silica (MeOH (5%) $CHCl_3$ (955): Streak from Rf 0.0 to Rf 0.25.

LCMS (positive): 174.26 (M(**9**)$^{+H}$), 227.31 (M(**106**)$^{+H}$), 281.43 (bis-alkene cyclen), 335.49 (M^{+1})(tris-alkene cyclen).

FTIR (thin-film NaCl): 2963, 2876, 1672, 1487, 1464, 1384, 1253, 1153, 11067

6.14: Synthesis of 10-but-3-en-1-yl-1,4,7,10-tetraazacyclodo decane-1,4,7-tricarbaldehyde (111)

Under argon, triformylcyclen (**74**) (0.25 g, 0.00097 mol) was dissolved in acetonitrile (15 ml) to which potassium carbonate (0.67 g, 0.00485 mol, 5 eq) was added. To the reaction was added 4-bromobut-1-ene (**78**) (0.32 g, 0.0024 mol, 2.5 eq) and the reaction was stirred at room temperature for 72 hours. The solid residue was removed via filtration and the solvent by reduced pressure to yield an oil. The crude oil was then placed on high vacuum for 24 hours to yield a yellow oil. The crude product was chromatographed on alumina (neutral) DCM (95%), MeOH (5%).

Yield 0.16 g, 0.000516 mol, 19%

Crude product LCMS (positive): 311.31 [M(**111**)$^{+H}$], 337.51 [M(**112**)$^{+H}$]

Chromatographed product LCMS (positive): 311.21 [M(**111**)$^{+H}$], 337.61 [M(**112**)$^{+H}$].

FTIR (KBr disk): 3112, 2940, 2886, 2484, 1676, 1452, 1313, 1239.

6.15: Synthesis of octahydro-5H-2a,4a,7,9a-tetraazacycloocta[1,2,3-cd]pentalene[92, 93] (113)

Under argon, cyclen (**9**) (2.58 g, 0.0148 mol) was dissolved in toluene (30 ml). To the solution was added N,N-dimethylformamidedimethlyacetal (**114**) (DMF-DMA) (2.32 ml, 2.08 g, 0.0017455 mol), and the reaction was refluxed for 2 hours. It was then cooled and the solvent removed, using reduced pressure, to yield a clear oil.

Yield 86%, 2.38 g

^{1}H NMR ($CDCl_3$): 2.23 (H1, s)(*e*), 2.81 (H16, m)(*a,b*), 4.63 (H1, s)(*c*)

^{13}C NMR ($CDCl_3$): 45.73 (CH_2)(*A*), 53.01 (CH_2)(*B*), 101.44 (CH)(*C*)

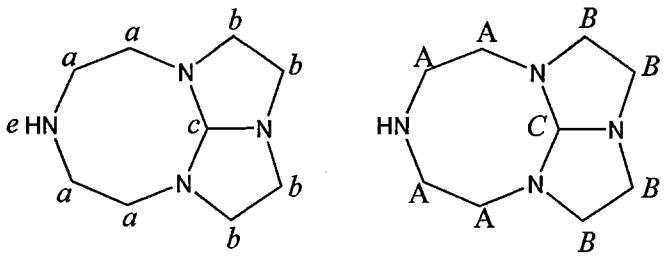

6.15: Characterisation of compound (113), proton (left) carbon (right)

LCMS (positive): 183.15 [M(**113**)$^{+H}$]

FTIR (thin-film NaCl): 3258, 2927, 1678, 1444, 1347, 1291, 1255, 1144, 1065.

6.16: Synthesis of 7-but-3-en-1-yloctahydro-5*H*-2a,4a,7,9a-tetraazacycloocta[1,2,3-*cd*]pentalene (115)

Under argon, octahydro-5*H*-2a,4a,7,9a-tetraazacycloocta[1,2,3-*cd*]pentalene (**113**) (1.00 g, 0.00548 mol) was dissolved in anhydrous acetonitrile (25 ml) to which potassium carbonate (2.25 g, 0.0169 mol) was added. The reaction was cooled using an ice/salt/IMS bath. 4-bromobut-1-ene (**78**) (0.73 g, 0.0054 mol) was added and the reaction was allowed to warm up to room temperature over 18 hours. The solid residue was removed using filtration, and the solvent was removed using reduced pressure to yield a clear oil. The oil was then run though an alumina chromatograph column and eluted with $CHCl_3$ 97%, MeOH 3%.

Yield 0.39 g, 0.001650 mol, 30.1 %

^{1}H NMR ($CDCl_3$): 2.15 (H2, q, 6.95Hz)(*c*), 2.50–2.75 (H18, multiple)(d,*e,f,g*), 4.70 (H, s,)(*h*), 4.92 (H2, t, 8.79Hz)(*a1,a2*), 5.76 (H, d–q, 7.02 Hz–3.42 Hz)(*b*)

^{13}C NMR ($CDCl_3$): 32.79 ($\underline{C}H_2$)(*C*), 51.01 ($\underline{C}H_2$)(*D*), 52.69 ($\underline{C}H_2$)(*D*), 55.44 ($\underline{C}H_2$)(*E*), 58.49 ($\underline{C}H_2$)(*G*), 97.97 ($\underline{C}H$)(*H*), 115.12 (CH_2)(*A*), 130.01 (CH)(*B*)

LCMS: 237.18 [M(**115**)$^{+H}$]

FTIR (thin-film NaCl): 3419, 3258, 2929, 1680, 1444, 1347, 1291, 1257, 1150.

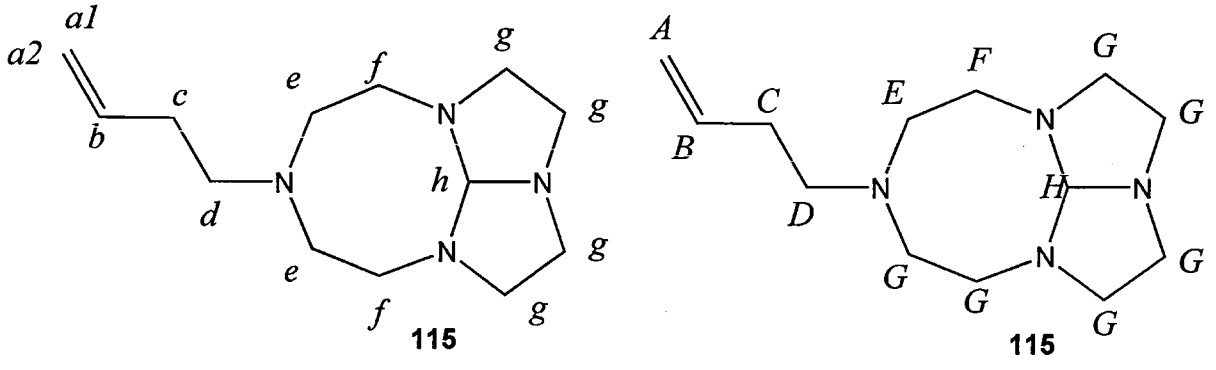

6.16: Characterisation of compound (116), proton (left) carbon (right)

6.17: Synthesis of 7-but-3-en-1-yl-1,4,7,10-tetraazacyclododecane-1-carbaldehyde (121)

7-but-3-en-1-yloctahydro-5*H*-2a,4a,7,9a-tetraazacycloocta[1,2,3-*cd*]pentalene (**115**) (0.51 g, 0.00216 mol) was dissolved in a solution of methanol (90 ml) and water (30 ml) and stirred overnight at room temperature. The solvents were removed using reduced pressure and the crude was taken up into DCM (50 ml) and dried over magnesium sulfate (20 g). The solution was filtered and the solvent removed using reduced pressure.

Yield: 0.42 g, 0.00164 mol, 76%

^{1}H NMR ($CDCl_3$): 2.13 (H2, t, 6.8 Hz)(*c*), 2.21–2.28 (H3, m)(*g*), 2.61 (H2, t, 6.93 Hz)(*d*), 2.66 (H8, s)(e,*f*), 2.88 (H4, t, 6.6 Hz)(*h*), 3.12 (H4, t, 5.31 Hz)(*i*), 4.98 (H, t, 8.35 Hz)(*a1*), 5.03 (H, t, 14.0 Hz)(*a2*), 5.67 (H, m)(*b*).

7-but-3-en-1-yl-1,4,7,10-tetraazacyclododecane-1-carbaldehyde (**121**)

^{13}C NMR ($CDCl_3$): 31.45 ($\underline{C}H_2$)(*C*), 43.64 ($\underline{C}H_2$)(*F*), 45.29 ($\underline{C}H_2$)(*G*), 48.98 ($\underline{C}H_2$)(*H*) 53.50 ($\underline{C}H_2$)(*D*), 55.90 ($\underline{C}H_2$)(*E*), 116.36 ($\underline{C}H_2$)(*A*), 136.20 ($\underline{C}H$)(*B*), 164.31 ($\underline{C}H$=O)(*I*).

4-but-3-en-1-yl-1,4,7,10-tetraazacyclododecane-1-carbaldehyde (**122**)

^{13}C NMR ($CDCl_3$): 31.45 ($\underline{C}H_2$)(*C*), 45.91 ($\underline{C}H_2$)(*I*), 47.51 ($\underline{C}H_2$)(*F*), 50.20 ($\underline{C}H_2$)(*G,H*), 50.44 ($\underline{C}H_2$)(*J*) 51.25 ($\underline{C}H_2$)(*D*), 55.90 ($\underline{C}H_2$)(*E*), 116.36 (H_2C=)(*A*), 136.20 ($\underline{C}H$)(*B*), 164.31 ($\underline{C}H$)(*M*).

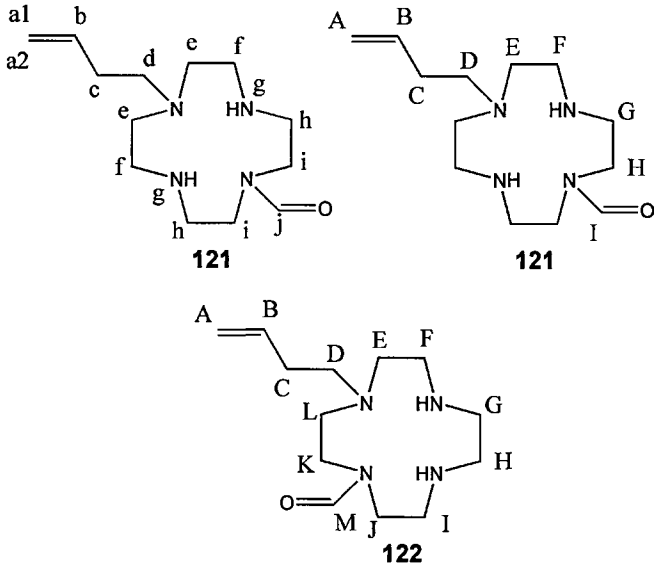

6.17: Characterisation of compound (121), proton (left) carbon (right)and (122) carbon (bottom)

LCMS (positive): 255.21 [M(121/122)$^{+h}$].

FTIR (thin-film NaCl plate): 3419, 3000, 2753, 2420, 1686, 1576, 1496, 1442, 1379, 1291, 1254, 1171, 1116.

6.18: 1-but-3-en-1-yl-1,4,7,10-tetraazacyclododecane (106)via potassium hydroxide

7-but-3-en-1-yl-1,4,7,10-tetraazacyclododecane-1-carbaldehyde (**121**) / 4-but-3-en-1-yl-1,4,7,10-tetraazacyclododecane-1-carbaldehyde (**122**) (0.40 g, 0.00156 mol) was dissolved in a solution of methanol (5 ml) and potassium hydroxide solution (0.2 M, 10 ml). The reaction was refluxed for 24 hours. The reaction was cooled and the

pH was adjusted to pH 7 using HCl (2 M). The solvents were removed using reduced pressure, after which the crude was taken up in DCM (50 ml) and centrifuged to remove the solid residue. Then it was dried over magnesium sulfate, filtered and the solvent removed using reduced pressure to yield a clear oil.

Yield: 0.21 g, 9.28 mmol, 59 %.

^{1}H NMR ($CDCl_3$): 2.13 (H2, d–d, 6.7 Hz), 2.57 (H2, t, 7.0 Hz), 2.76 (H4, multiple), 2.86 (H12, multiple), 4.94 (H2, t, 5.2), 5.73 (H1, multiple).

^{13}C NMR ($CDCl_3$): 31.62 ($\underline{C}H_2$–CH=CH_2), 44.75 (N–$\underline{C}H_2$–CH_2–N), 46.61 (N–CH_2–$\underline{C}H_2$–N), 48.83 (OC–N–$\underline{C}H_2$–CH_2) 50.92 (N–$\underline{C}H_2$–CH_2–CH=CH_2), 54.12 (–CH_2–N–(CH_2–R)–$\underline{C}H_2$–CH_2–N), 116.44 (CH_2–CH=$\underline{C}H_2$), 135.99 (CH_2–$\underline{C}H$=CH_2), 169.07 (N–$\underline{C}H$=O).

LCMS (positive): 227.35 [M(106)$^{+H}$]

6.19: 1-but-3-en-1-yl-1,4,7,10-tetraazacyclododecane (106) via ammonium hydroxide

7-but-3-en-1-yl-1,4,7,10-tetraazacyclododecane-1-carbaldehyde (**121**) (0.42 g, 0.00164 mol) was dissolved in ammonia solution (6 ml of 35% in 44 ml of water) and heated to 100 °C for 48h. The solvent was removed using reduced pressure. The crude product was taken up into water (10 ml) and was extracted with chloroform (2 x 50 ml). The organic component was combined and dried using magnesium sulfate, filtered, and the solvent removed using reduced pressure.

Yield: 0.24 g, 0.00106 mol, 64.7 %

^{1}H NMR ($CDCl_3$): 2.12 (H2, d–d, 6.6 Hz), 2.58 (H2, t, 7.02 Hz), 2.76 (H4, d–m, 9.54 Hz), 2.85 (H12, m), 4.93 (H2, t, 5.2), 5.73 (H1, m).

^{13}C NMR ($CDCl_3$): 31.60 ($\underline{C}H_2$–CH=CH_2), 44.85 (N–$\underline{C}H_2$–CH_2–N), 46.60 (N–CH_2–$\underline{C}H_2$–N), 50.90 (N–$\underline{C}H_2$–CH_2–CH=CH_2), 53.78 (–CH_2–N–(CH_2–R)–$\underline{C}H_2$–CH_2–N), 116.42 (CH_2–CH=$\underline{C}H_2$), 136.58 (CH_2–$\underline{C}H$=CH_2)

FTIR (thin-film NaCl plate): 3075, 2879, 2780, 1657, 1513, 1446, 1351, 1296, 1218.

LCMS (positive): 227.24 [M(**106**)$^{+1}$]

6.20: Synthesis of diethyl 2-bromosuccinate (103)

2-Bromosuccinic acid (**104**) (3.5 g, 0.0177 mol) was dissolved in 100% ethanol (25 ml), to which sulfuric acid (conc., 0.5 ml) was added. The reaction was refluxed for 24 hours under argon; it was then cooled, the solvent was removed using reduced pressure, and the crude oil was taken up into DCM (100 ml) and dried over magnesium sulfate (20 g). The solids were removed and then the solvent was

removed using reduced pressure. The resulting oil was passed though an alumina plug (neutral, 10 g) and was stored over molecular sieve (3 A, 10% of weight).

Yield 4.01 g, 0.0159 mol, 89%.

^{1}H NMR ($CDCl_3$): 1.12 (H3, t, 7.14 Hz,)(*a*), 1.14 (H3, t, 7.16 Hz,)(*f*), 2.83 (H1, d–d, 6.21 Hz)(*c*), 3.11 (H1, d–d, 8.97 Hz)(*c*), 4.05 (H2, q, 7.14 Hz)(*b*), 4.12 (H2, q, 7.15 Hz) (*e*), 4.44 (H, d–d, 2.73 Hz, 6.06 Hz)(*d*).

^{13}C NMR ($CDCl_3$): 13.48 ($\underline{C}H_3$)(*A*), 13.71($\underline{C}H_3$)(*H*), 38.22 ($\underline{C}H_2$)(*D*), 39.14 (*E*), 60.81 ($\underline{C}H_2$)(*G*), 61.85 ($\underline{C}H_2$)(*B*), 168.63 ($\underline{C}$)(*F*), 169.25 ($\underline{C}$)(*C*).

FTIR (thin-film NaCl): 2985, 1739, 1364, 1301, 1257, 1170, 1027.

LCMS (positive): 174 [M(**103**)- **Br** $^{+H}$], 253 [M(**103**)$^{+H}$]

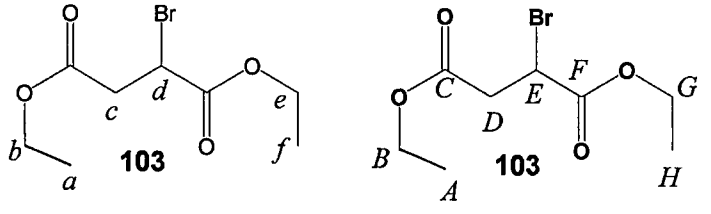

6.20: Characterisation of compound (108), proton (left) carbon (right)

6.21: Synthesis of butene-sDO3A-(ethyl) (101) from 1-but-3-en-1-yl-1,4,7,10-tetraazacyclododecane (106)

1-but-3-en-1-yl-1,4,7,10-tetraazacyclododecane (**106**) (0.67 g, 0.0029 mol) was dissolved in dry acetonitrile (20 ml) to which potassium carbonate (4 g, 0.0298 mol) was added. To this diethyl 2-bromosuccinate (**103**) (3.68 g, 0.0145 mol) was added dropwise. The reaction was heated to reflux for 78 hours, then cooled. The solid residues were removed using a centrifuge. The solvent was removed to yield an oil.

LCMS (positive): 571.32 [M(**123**)$^{+H}$], 398.12 [M(**124**)$^{+H}$].

6.22: Synthesis of sDO3A-(ether) (107) from cyclen (9)

1,4,7,10-tetraazacyclododecane (**9**) (0.5 g, 0.0029 mol) was dissolved in anhydrous acetonitrile (25 ml) to which potassium carbonate (1.35 g, 0.0098 mol) was added. The reaction was cooled to −15 °C in an ice/NaCl/IMS bath. Diethyl 2-bromosuccinate (**103**) (3.2 eq, 0.00896 mol, 2.26 g) was added in 0.5 ml aliquots every 5 minutes. The reaction was stirred at room temperature for 24 hours, after which another amount of diethyl 2-bromosuccinate (1.00 g, 0.0039 mol) was added and stirred for a further 24 hours. The reaction was then filtered, and the solvent was removed using reduced pressure to yield a clear oil.

Yield = (0.045 g) (0.000065 mol) (2.25%); this was chromatographed on silica eluted with chloroform (95%)/methanol (5%).

TLC – mixture from column (silica, eluted with (MeOH 5%, $CHCl_3$ 95%) sDO2A-ethyl (**109**) (Rf 0.15), sDO3A-ethyl (**107**)(Rf 0.20)).

LCMS (positive): 689.37 [M(**107**)$^{+H}$], 728.37 [M(**107**)+ K^{+H}]

^{1}H NMR ($CDCl_3$): 1.21 (H18, t, 4.7 Hz), 2.52–2.91 (H22, m), 3.63 (H3, q, 4.2 Hz), 4.10 (H12, t, 7.5)

^{13}C NMR ($CDCl_3$): 13.99 (CH_3), 14.97 (CH_3), 35.52 (CH_2), 47.53 (CH_2), 49.41 (CH_2), 60.70 (CH), 63.40 (CH_3), 170.94 (C=O), 171.29 (C=O)

FTIR (NaCl plate): 2985, 1737, 1464, 1368, 1301, 1170, 1027

6.23: Synthesis of sDO3A-(ethyl) (107) from cyclen (9) – universal method

1,4,7,10-tetraazacyclododecane (**9**) (0.50 g, 0.00285 mol) was dissolved in anhydrous acetonitrile (50 ml),. To this potassium carbonate (1.9 g, 0.0137 mol) was added. To the reaction a solution of diethyl 2-bromosuccinate (**103**) (4.50 g, 0.01775 mol) in anhydrous acetonitrile (50 ml) was added dropwise over one hour. The reaction was stirred at room temperature for 18 hours, after which the mixture was refluxed for 72 hours. The reaction was cooled and the solids removed by centrifuge and the liquid decanted. The solvent was then removed using reduced pressure to yield a crude oil.

6.24: Purification method (1) – biphasic separation: silica chromatography eluted with DCM (70%), THF (30%)

The crude from reaction 6.23 was taken up into DCM (10 ml) and washed with water (3 x 10 ml); the organic was dried over magnesium sulfate and filtered. The solvent was removed using reduced pressure. The resulting oil was then chromatographed

on a silica column eluted with DCM 70%, THF 30%. The eluting solvent system was then slowly changed via a gradient to a system eluting with DCM 66.5%, THF 30%, MeOH 3%, 0.5% ammonia (33% in water). Two major products were extracted.

Product A: TLC (silica, DCM 66.5%, THF 30%, MeOH 3%, ammonia 0.5%) showed a streak between Rf 0.00 and Rf 0.40

Yield 0.46 g, (mixture)

LCMS (positive): 689.23 [M(**107**)$^{+1}$], 517.55 [M(**109**)$^{+1}$]

Product B: TLC (silica, DCM 66.5%, THF 30%, MeOH 3%, ammonia 0.5%) showed at Rf 0.35.

Yield 0.023 g, 1.1%,

LCMS = 689.24 [M(**107**)$^{+H}$]

^{1}H NMR ($CDCl_3$): 1.20 (H18, q, 4.77 Hz), 2.45–2.85 (H22, m), 3.75 (H3, q, 7.14 Hz), 4.10 (H12, d–t, 7.32 Hz).

^{13}C NMR ($CDCl_3$): 14.03 (CH_3), 14.18 (CH_3), 35.43 (CH_2), 47.42 (CH_2), 49.19 (CH_2), 60.67 (CH), 61.24 (CH_2), 61.97 (CH_2), 170.96 (C=O), 171.24 (C=O).

FTIR (NaCl plate): 2986, 1732, 1461, 1370, 1303, 1182, 1025

6.25: Purification method (2) – biphasic separation: silica chromatography eluted with DCM 95%, MeOH 5%

The crude from reaction 6.23 was taken up into DCM (10 ml) and washed with water (3 x 10 ml); the organic was dried over magnesium sulfate and filtered. The solvent was removed using reduced pressure. The resulting product was chromatographed

on a silica column eluted with a mixture of dichloromethane (95%) and methanol (5%). The column yielded three products: at Rf 0.12 (sDO2A-(ethyl) (**109**)), at 0.34 (sDO3A-(ethyl) (**107**)) and at 0.73 diethyl 2-bromosuccinate (**103**) (obtained on silica TLC plates eluted with DCM (95%) MeOH (5%)).

LCMS crude: 172.75 [M(**9**)$^{+H}$] , 210.78 [M(**9**)+K^{+H}], 346.14 [M(**108**)$^{+1}$], 385.10 [M(**108**)+K^{+H}, 518.70 [M(**109**)$^{+H}$], 556.10 [M(**109**)+K^{+H}], 689.84 [M(**107**)$^{+H}$], 728.74 [M(**107**)+K^{+H}).

Fraction with Rf 0.34

Yield = 0.07 g, 0.0001013 mol, 3.7%

LCMS (positive): 689.32 [M(**107**)$^{+H}$]

^{1}H NMR ($CDCl_3$): 1.20 (H18, q, 3.1 Hz), 2.5-2.8 (H22, m), 3.77 (H3, q, 7.2 Hz), 4.09 (H12, d–t, 7.3 Hz).

^{13}C NMR ($CDCl_3$): 14.04 (CH_3), 14.18 (CH_3), 35.44 (CH_2), 47.42 (CH_2), 49.20 (CH_2), 60.67 (CH), 61.25 (CH_2), 61.99 (CH_2), 170.98 (C=O), 171.24 (C=O).

FTIR (NaCl plate): 2984, 1730, 1464, 1387

6.26: Purification method (3) – biphasic separation: alumina chromatography eluted with DCM 95%, MeOH 5%

The crude from reaction 6.23 was taken up into DCM (10 ml) and washed with water (3 x 10 ml); the organic was dried over magnesium sulfate and filtered. The solvent was removed using reduced pressure. The resulting product was then chromatographed on alumina eluting with DCM (100%), giving one product from the

column as a streak on TLC (alumina DCM 95%, MeOH 5%) between Rf 0.35 and Rf 0.00. There was found to be no separation between sDO2A-(ethyl) and sDO3A-(ethyl).

Yield of mixture 0.42 g

LCMS (positive): 517.31 [M(**109**)$^{+H}$], 556.10 [M(**109**)+K^{+H}], 689.84 [M(**107**)$^{+H}$], 728.74 [M(**107**)+K^{+H}].

6.27: Purification method (4) – biphasic separation: alumina chromatography eluted with DCM 70%, THF 30%

The crude from reaction 6.23 was taken up into DCM (10 ml) and washed with water (3 x 10 ml); the organic was dried over magnesium sulfate and filtered. The solvent was removed using reduced pressure. The resulting product was then chromatographed on alumina eluting with DCM (100%), giving one product from the column as a streak on TLC (alumina DCM 70%, THF 30%) at Rf 0.86 (diethyl 2-bromosuccinate (**103**)) and a streak between Rf 0.1 and Rf 0.00. There was found to be no separation between sDO2A-(ethyl) and sDO3A-(ethyl).

LCMS (positive): 517.32 [M(**109**)$^{+H}$], 689.74 [M(**107**)$^{+H}$]

6.28: Purification method (5) – biphasic separation: alumina chromatography eluted with DCM 99%, MeOH 1%

The crude from reaction 6.23 was taken up into DCM (10 ml) and washed with water (3 x 10 ml); the organic was dried over magnesium sulfate and filtered. The solvent was removed using reduced pressure. The resulting product was chromatographed

on alumina using DCM and MeOH (99:1). The TLC showed three products 0.78 (diethyl 2-bromosuccinate), 0.30 (sDO3A-(ethyl)(**107**), and 0.21 (sDO2A-(ethyl)(**109**).

Yield = 0.11 g, 0.000159 mol, 5.6%

^{1}H NMR ($CDCl_3$): 1.19 (H18, q, 3.0 Hz)(*a*), 2.5–2.8 (H22, m)(*e*), 3.75 (H3, q, 7.1 Hz)(*c*), 4.10 (H12, d–t, 7.3 Hz)(d).

^{13}C NMR ($CDCl_3$): 14.03 (CH_3)(*A*), 14.18 (CH_3)(*G*), 35.43 (CH_2)(*D*), 47.42 (CH_2)(*I*), 49.19 (CH_2)(*H*), 60.67 (CH)(*E*), 61.24 (CH_2)(*B*), 61.97 (CH_2), 170.96 (C=O)(*F*), 171.24 (C=O)(*C*).

HRMS 689.3892 [M(**107**)$^{+H}$] (found), 689.3895 [M(**107**)$^{+1}$] (predicted)

FTIR (NaCl plate): 2985, 1731, 1465, 1389

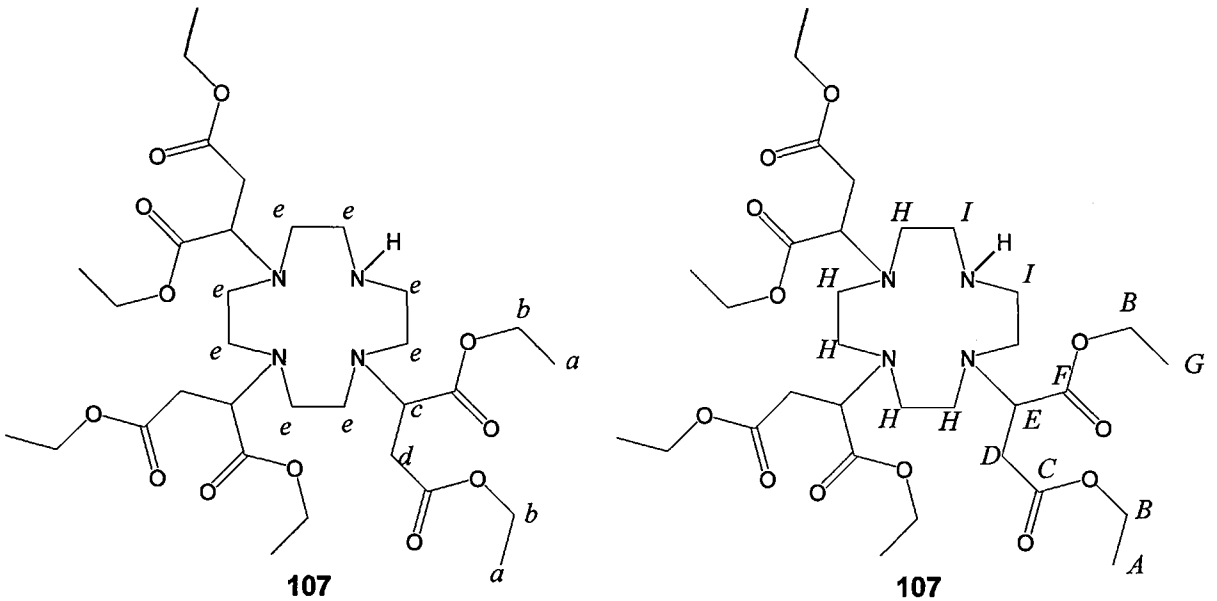

6.28: Characterisation of compound (107), proton (left) carbon (right)

6.29: Synthesis of sDO3A-(ethyl) (103) via cyclen (9) using Sep-Pak columns.

1,4,7,10-tetraazacyclododecane (**9**) (0.50 g, 0.00285 mol) was dissolved in anhydrous acetonitrile (50 ml),. To this potassium carbonate (1.9 g, 0.01 mol) was added. To the reaction a solution of diethyl 2-bromosuccinate (**103**) (4.50 g, 0.01775 mol) in anhydrous acetonitrile (50 ml) was added dropwise over 1 hour. The reaction was stirred at room temperature for 18 hours, after which the reaction was refluxed for 72 hours. The reaction was cooled, the solids removed by centrifuge and the liquid decanted. The solvent was then removed using reduced pressure to yield a crude oil. Chromatography of the crude product was performed on a Sep-Pak (Si–60) 25 g column. 500 mg of the crude oil was infused onto the Sep-Pak chromatographic column, which was then eluted with DCM 95% / EtOH **5%.**

The product from the column:

Rf = 0.91 = diethyl 2-bromosuccinate (**103**)

Rf = 0.55 = diethyl maleate (**126**), 0.20 mg, 0.001416 mol, 40% of crude oil

Rf = 0.19 = sDO3A-(ethyl) (**107**), 0.12 g, 0.000174 mol, 24% of crude oil product (for 500 mg sample of crude oil).

Reaction product = sDO3A-(ethyl) (**107**)

^{1}H NMR ($CDCl_3$): 1.22 (18H, q, 7.5 Hz), 2.48–2.76 (22H, m), 3.79 (3H, t, 6.2 Hz), 4.12 (12H, t, 7.1 Hz),

^{13}C NMR ($CDCl_3$): 14.25 (CH_3), 14.39 (CH_3), 35.32 (CH_2), 49.87 (CH_2), 51.21 (CH_2), 60.47 (CH_2), 171.46 (C=O), 171.90 (C=O).

LCMS (positive): 688.32 [M(**107**)^{H}]

Reaction product = diethyl maleate (**126**)

^{1}H NMR ($CDCl_3$): 1.25 (H6, t, 6.8 Hz), 4.20 (H4, q, 7.0 Hz), 6.80 (H2, s).

^{13}C NMR ($CDCl_3$): 14.2 (CH_3), 61.4 (CH_2), 133.7 (CH), 165.1 (C=O).

FTIR (thin-film $CDCl_3$ NaCl): 3431, 2985, 2255, 1719, 1644, 1368, 1303, 1262, 1160

LCMS (positive): 212.81 [M(**126**)+K^{+H}]

6.30: Reaction of diethyl 2-succinate (103) with potassium carbonate to form diethyl maleate (126)

Potassium carbonate (1.00 g, 0.0072 mol) was combined with diethyl 2-bromosuccinate (**103**) (3.00 g, 0.0118 mol). The sealed flask was then heated to 60 °C for 72 hours. The reaction was cooled and the product was extracted by washing with DCM (2 x 50 ml), and any solids removed by filtration. The solvent was then removed using reduced pressure.

Yield 1.78 g, 87%, 0.001034 mol

^{1}H NMR ($CDCl_3$): 1.25 (H6, t, 6.9 Hz), 4.20 (H4, q, 7.1 Hz), 6.81 (H2, s).

^{13}C NMR ($CDCl_3$): 14.2 (CH_3), 61.46 (CH_2), 133.7 (CH), 165.1 (C=O).

FTIR (thin-film $CDCl_3$ NaCl): 3428, 2985, 2255, 1718, 1646, 1370, 1303, 1262, 1159, 1036.

LCMS (positive) 212.99 [M(**126**)+K^{+H}]

6.31: Synthesis of sDO3A-(ethyl) (107) from cyclen (9) via caesium carbonate – version 1

Cyclen (**9**) (0.5 g, 0.0028 mol) and caesium carbonate (4.56 g, 0.0014 mol) were dissolved in anhydrous acetonitrile (50 ml) under argon. To this solution diethyl 2-bromosuccinate (**103**) (1.90 g, 0.0075 mol) in acetonitrile (50 ml) was added dropwise over a period of 1.5 hours. The reaction was stirred at room temperature for 18 hours, after which the mixture was refluxed for 24 hours. Then another amount of diethyl 2-bromosuccinate (**103**) (1.00 g, 0.00395 mol) was added and the reflux continued for a further 24 hours. The reaction was cooled to room temperature and the solids removed using a centrifuge. The solvent was removed using reduced pressure, yielding a viscous oil. The crude oil was chromatographed on silica eluted with DCM (98%), MeOH (2%).

18 hours LCMS (positive): 307.87 [M(**9**)+Cs^{+H}], 477.26 [M(**108**)+Cs^{+H}], 649.12 [M(**109**)+Cs^{+H}].

32 hours LCMS (positive): 515.39 [M(**109**)$^{+H}$], 649.12 [M(**109**)+Cs^{+H}], 821.61 [M(**107**)+Cs^{+H}].

92 hour LCMS (positive): 516.40 [M(**109**)$^{+H}$], 690 [M(107)$^{+H}$].

The crude was then chromatographed on alumina eluting with DCM (99%), MeOH (1%). Yield = 0.11 g, 0.000159 mol, 5.6%

^{1}H NMR ($CDCl_3$): 1.19 (H18, q, 3.1 Hz), 2.5–2.9 (H22, m), 3.76 (H3, q, 7.0 Hz), 4.08 (H12, d–t, 7.1 Hz).

^{13}C NMR ($CDCl_3$): 14.03 (CH_3), 14.20 (CH_3), 35.44 (CH_2), 47.42 (CH_2), 49.20 (CH_2), 60.65 (CH), 61.23 (CH_2), 61.98 (CH_2), 170.97 (C=O), 171.26 (C=O).

LCMS positive: 689.38 [M(**107**)$^{+H}$]

FTIR (NaCl plate): 2986, 1729, 1464, 1388

6.32: Synthesis of sDO3A-(ethyl) (107) from cyclen (9) via caesium carbonate – version 2

1,4,7,10-tetraazacyclododecane (**9**) (0.50 g, 0.00286 mol) and caesium carbonate (4.5 g, 0.01385 mol) were cooled to −15 °C using ice/NaCl/IMS. To this mixture diethyl 2-bromosuccinate (**103**) (7 g, 0.02755 mol) was added and the reaction was stirred for 48 hours at room temperature, after which the reaction was heated to 60 °C for 48 hours. The reaction was cooled and the crude was taken up into DCM (2 x 50 ml). The solids were removed by centrifugation, and the solvent was extracted using reduced pressure to yield a viscous oil.

The oil was split into two aliquots.

After 10 minutes-at room temperature LCMS (positive): 173.60 [M(**9**)$^{+H}$] or [M(**130**)$^{+H}$], 516.29 [M(109)$^{+H}$].

After 48 hours at room temperature LCMS (positive): 341.70 [M(**108**)$^{+H}$], 516.32 [M(**109**)$^{+H}$], 689.98 [M(**107**)$^{+H}$].

After 96 hours (48 hours at room temperature, 48 hours at 60 °C)

516.34 [M(**109**)$^{+H}$], 689.71 [M(**107**)$^{+H}$].

6.32.1: Work-up method 1: Chromatography

The crude product was chromatographed on silica eluting with DCM (95%) MeOH (5%). sDO3A-(ethyl) (**107**) was collected at Rf 0.2.

LCMS (positive): 690.53 [M(**107**)$^{+H}$]

Yield 22 mg, 0.0000319 mol, 1.1%

^{1}H NMR ($CDCl_3$): 1.20 (H18, t, 5.0 Hz), 1.81–2.42 (H22, m), 3.54 (H1, q, 5.38 Hz), 3.78 (H3, q, 7.003 Hz), 4.10 (H12, q, 7.00).

^{13}C NMR ($CDCl_3$): 14.20 (CH_3), 35.58 (CH_2), 46.49 (CH_2), 47.46 (CH_2), 50.18 (CH_2), 50.41 (CH_2), 59.58 (C=O), 60.53 (CH_2), 170.94 (C=O), 171.47 (C=O).

FTIR (thin-film, KBr disk): 2983, 1736, 1464, 1368, 1302, 1256, 1170.

6.32.2: Work-up method 2: Vacuum distillation

The oil underwent vacuum distillation. The sample was slowly heated using an oil bath to 80 °C, yielding a white solid which was collected at 60 °C.

Product found (*E*)-3-(ethoxycarbonyl) acrylic acid (**125**)

^{1}H NMR ($CDCl_3$): 2.12 (H3, t, 7.14 Hz)(*a*), 5.05 (H2, q, 7.14 Hz)(*b*), 7.66 (H2, q, 15.72 Hz)(*c*+*d*).

^{13}C NMR ($CDCl_3$): 14.04 (CH_3)(*A*), 61.60 (CH_2)(*B*), 132.54 (CH)(*E*), 135.84 (CH)(*D*), 164.65 (C=O)(*C*), 170.21 (C=O)(*F*)

LCMS (negative): 143.20 [M(**125**)$^{-H}$], 287.12 [2M(**125**)$^{-H}$].

MP: 68 °C

HRMS: 145.0495 [M(125)$^{+H}$] (Found), 145.0423 [M(125)$^{+H}$) (predicted)
FTIR (KBr disk): 3155, 2904, 2254, 1708, 1306, 1269, 1174

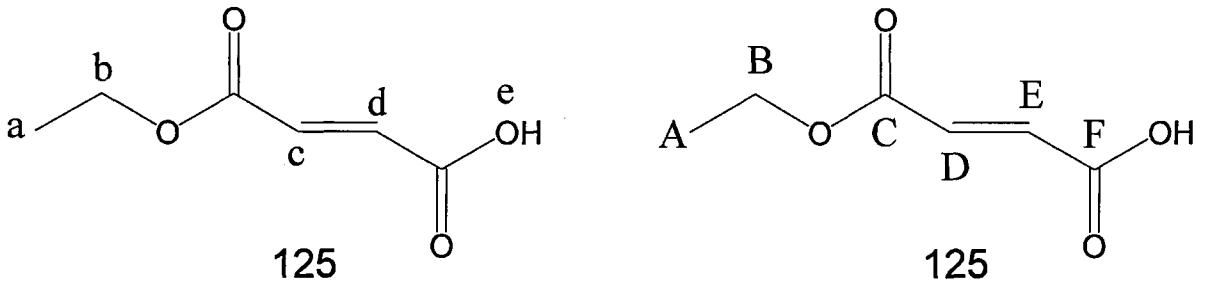

6.32: Characterisation of compound (125), proton (left) carbon (right)

6.33: Reaction of diethyl 2-bromosuccinate (103) with caesium carbonate to form (*E*)-3-(ethoxycarbonyl) acrylic acid (125)

Diethyl 2-bromosuccinate (**103**) (1.00 g, 0.0039 mol) was added to caesium carbonate (1.3 g, 0.0039 mol). The reaction was heated to 60 °C for 1 hour. The reaction was then cooled and the product was extracted from the solid residue by washing with DCM (2 x 25 ml). The solvent was removed using reduced pressure to yield a crude, light-yellow oil. The oil was then distilled under vacuum to yield a white solid.

Before heating LCMS (negative): 143.20 [M(**125**)$^{-H}$], 287.13 [2M(125)$^{-H}$].

LCMS (positive): 174.19 [M(**103**)-Br^{+H}].

White solid produced:

Yield = 0.11 g, 0.000076 mol, 19% MP: 69.5 °C.

LCMS (negative ion): 143.21 [M(**125**)$^{-H}$], LCMS (positive ion): no ions detected

^{1}H NMR ($CDCl_3$): 2.11 (H3, t, 7.14 Hz), 5.05 (H2, q, 7.16 Hz), 7.66 (H2, q, 15.70 Hz).

^{13}C NMR ($CDCl_3$): 14.05 (CH_3), 61.60 (CH_2), 132.54 (CH), 135.84 (CH_2), 164.65 (C=O), 170.21 (C=O).

FTIR (KBr disk): 3155, 2904, 2254, 1710, 1306, 1269, 1174

6.34: Synthesis of sDO3A-(ethyl) (107) from diethyl maleate

Cyclen (**9**) (0.5 g, 0.0029 mol) was dissolved in anhydrous acetonitrile (30 ml) containing potassium carbonate (1.40 g, 0.0101 mol). To this a solution of diethyl maleate (**153**) (2.7 g, 0.0157 mol, 2.54 ml) dissolved in anhydrous acetonitrile (30 ml) was added dropwise over a period of 2 hours. The reaction was stirred for 24 hours at room temperature, after which it was heated to 60 °C for 6 hours. Then diethyl maleate (**126**) (2.00 g, 0.0116 mol) was added and the reaction continued for another 48 hours. The reaction was cooled, the solid residue was removed, the liquid layer was decanted, and the solvent removed using reduced pressure. The crude was then chromatographed on silica eluted with 95% DCM and 5% EtOH.

Yield 200 mg, 0.00029 mol, 10.02%

(1 hour) LCMS (positive): 211.07 [M(**9**)+K^{+H}], 345.30 [M(**108**)$^{+H}$], 384.28 [M(108)+K^{+H}], 517.33 [M(**109**)$^{+H}$].

(24 hours) LCMS (positive): 210.89 [M(**9**)+K^{+H}], 383.15 [M(**108**)+K^{+H}], 516.82 [M(**109**)$^{+H}$], 554.08 [M(**109**)+K^{+H}], 727.24 [M(**107**)+K^{+H}]

(30 hours) LCMS (positive): 210.91 [M(9)+K^{+H}], 382.77 [M(108)+K^{+H}], 516.82 [M(**109**)$^{+H}$], 554.08 [M(109)+K^{+H}], 727.24 [M(107)+K^{+H}].

(54 hours) LCMS (positive): 210.83 [M(**9**)+K^{+H}], 382.92 [M(**108**)+K^{+H}], 516.82 [M(**109**)$^{+H}$], 554.08 [M(**109**)+K^{+H}], 728.62 [M(**107**)+K^{+H}].

^{1}H NMR ($CDCl_3$) 1.19 (H18, q, 3.4 Hz), 2.40–2.81 (H25, m), 3.73 (H3, q, 5.31 Hz), 4.08 (H12, q, 4.95 Hz).

^{13}C NMR ($CDCl_3$): 13.99 (CH_3), 14.97 (CH_3), 35.52 (CH_2), 47.53 (CH_2), 49.41 (CH_2), 60.70 (CH), 63.40 (CH_3), 170.94 (C=O), 171.29 (C=O)

FTIR (thin-film, KBr disk): 2984, 1736, 1462, 1370, 1300, 1255, 1170.

6.35: Synthesis of sDO3A-(ethyl) (107) via diethyl fumarate (130)

Cyclen (**9**) (0.5 g, 0.0029 mol) was dissolved in anhydrous acetonitrile (30 ml) containing potassium carbonate (1.40 g, 0.0101 mol). To this a solution of diethyl fumarate (**130**) (2.7 g, 0.0157 mol, 2.57 ml) dissolved in anhydrous acetonitrile (30 ml) was added dropwise over a period of 2 hours. The reaction was stirred for 24 hours at room temperature, after which it was heated to 60 °C for 6 hours. Then diethyl fumarate (2.00 g, 0.0116 mol) was added and the reaction continued for another 48 hours. The reaction was cooled, the solid residue was removed, the liquid layer was decanted and the solvent removed using reduced pressure. The crude was then chromatographed on silica eluted with 95% DCM and 5% EtOH.

Yield 200 mg, 0.00029 mol, 10%.

^{1}H NMR: 1.21 (18H, q, 7.5 Hz), 2.49–2.78 (22H, m), 3.72 (3H, t, 6.0 Hz), 4.07–4.14 (12 m),

^{13}C NMR: 14.39 ($\underline{C}H_3$–CH_2–O), 35.37 (CH–$\underline{C}H_2$–C=O), 49.87 ($H_2\underline{C}$–N–$\underline{C}H_2$), 51.19 (–N–$\underline{C}H_2$), 60.49 (–CH_2–CH_3), 171.44 (O–$\underline{C}$=O–CH), 171.90 (O–$\underline{C}$=O–CH_2).

FTIR (thin-film, KBr disk): 2987, 1737, 1464, 1367, 1302, 1255, 1172.

LCMS: 689.32 [M(**107**)$^{+H}$]

HRMS: predicted 711.3787 [M(**107**)+Na^{+H}], found 711.3796 [M(**107**)+Na^{+H}]

6.36: Synthesis of sDO3A-(ethyl) (107) via diethyl maleate (126) – scaled-up version (final version)

1,4,7,10-tetraazacyclododecane (**9**) (3 g, 0.01734 mol) and potassium carbonate (7.8 g, 0.05652 mol) were dissolved in anhydrous acetonitrile (100 ml). To this a solution of diethyl maleate (**126**) (42 g, 0.2439 mol) in anhydrous acetonitrile (100 ml) was added dropwise over 2 hours. The reaction was heated to 80 °C and stirred for 72 hours. The reaction was cooled to room temperature and the solids were removed. The solvent was removed using reduced pressure to yield a crude oil.

The crude extract was chromatographed on silica (Si–60) (350 g), made up of slurry packed into a sintered glass filter column with an internal diameter of 95 mm. The most relevant factor for successful purification was the way the bed was compacted before and after the addition of the crude reaction mixture. When the silica–solvent mixture was added first, the solvent was drained until the solvent layer was just below the top of the silica. The column was then compacted using a heavy steel rod fitted with a suba seal to stop contamination. This step enabled a greater replication of the chromatographic performance, as well as removing small imperfections in the column bed. The chromatography column was eluted with DCM/EtOH (95:5).

Product at Rf 0.2. The solvent was removed using reduced pressure yielding a clear, viscous oil.

Yield = (4.25 g, 0.00617 mol, 35.58%).

^{1}H NMR ($CDCl_3$): 1.21 (H18, t, 5.01 Hz), 1.80–2.41 (H22, m), 3.54 (H1, q, 5.35 Hz), 3.77 (H3, q, 7.03 Hz), 4.08 (H12, q, 7.01).

^{13}C NMR ($CDCl_3$): 14.18 (CH_3), 35.58 (CH_2), 46.46 (CH_2), 47.44 (CH_2), 50.18 (CH_2), 50.40 (CH_2), 59.58 (C=O), 60.52 (CH_2), 170.93 (C=O), 171.46 (C=O).

FTIR (thin-film, KBr disk): 2983, 1736, 1464, 1368, 1302, 1256, 1170.

LCMS: 689.39 [M(**107**)$^{+H}$]

HRMS: predicted 711.3787 [M(**107**)+Na^{+H}], found 711.3792 [M(**107**)+Na^{+H}]

6.37: Synthesis of butene-sDO3A-(ethyl) (101) via sDO3A-(ethyl) (107)

sDO3A-(ethyl) (**107**) (0.64 g, 0.00093 mol) was dissolved in anhydrous acetonitrile (20 ml) to which potassium carbonate (1.00 g, 0.0072 mol) had been added. The reaction was cooled in an Ice/NaCl/IMS bath. To this 4-bromobutene (**78**) (2.66 g, 0.0197 mol, 2.00 ml) was added and the reaction was allowed to warm up to room temperature overnight. The reaction was then stirred for 78 hours at room temperature. The solids within the reaction mixture were removed using a centrifuge, and the solvent was decanted. The solvent was then removed using reduced pressure, followed by 24 hours on high vacuum to yield a clear, light-yellow oil. The crude product was then chromatographed on silica eluted with DCM and EtOH (95:5%)

Yield 0.54 g, 0.00072, 77.92%

Crude sample LCMS (positive): 742.40 [M(**101**)$^{+H}$], 799.31 [M(**132**)$^{+H}$]

Product LCMS (positive): 742.40 [M(**101**)$^{+H}$]

^{1}H NMR ($CDCl_3$): 1.18 (H18, q, 5.7 Hz)(*a*), 2.09 (H2, d, 6.98 Hz)(*j*), 2.3–2.8 (H24, m)(*c,e,f,g,h,i*), 3.75 (H3, t, 6.0 Hz)(*d*), 4.11 (H12, m)(*b*), 4.93 (H2, q, 17.4 Hz)(*m*), 5.71 (H1, t–t, 6.75 Hz)(*k*).

^{13}C NMR ($CDCl_3$): 14.12 (CH_3)(*A*), 14.38 (CH_3)(*A1*), 29.64 (CH_2)(*M*), 35.52 (CH_2)(*D*), 49.87 (CH_2)(*E*), 50.60 (CH_2)(*F*), 51.18 (CH_2)(*G*), 53.55 (CH_2)(*H*), 53.92 (CH_2)(*J*), 54.66 (CH_2)(*L*), 59.57 (CH)(*E*), 59.84 (CH)(*E*), 59.92 (CH)(*E*), 60.44 (CH_2)(*B*), 60.84 (CH_2)(*B2*), 115.31 (CH_2)(*O*), 137.09 (CH)(*N*), 171.39 (C=O)(*F*), 171.89 (C=O)(*C*).

HRMS: calculated 743.4437 [M(**101**)$^{+H}$], found 743.4445 [M(**101**)$^{+H}$].

FTIR (thin-film $CDCl_3$ NaCl): 2982, 2253, 1723, 1461, 1371, 1300, 1260.

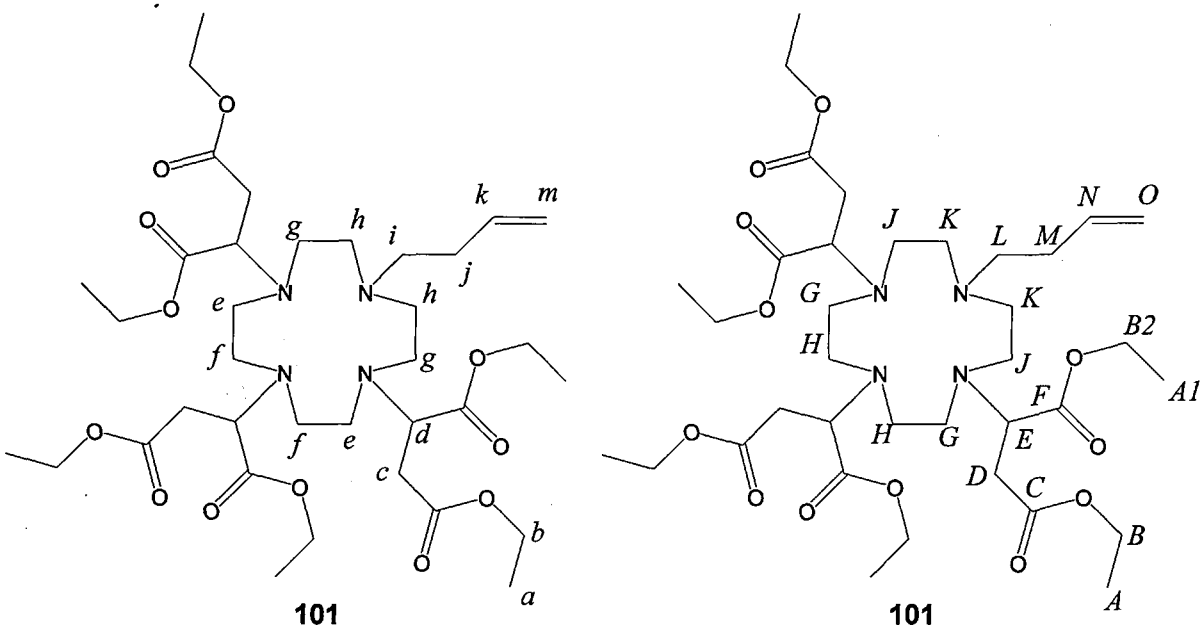

6.37: Characterisation of compound (101), proton (left) carbon (right)

6.38: Synthesis of pentene-sDO3A-(ethyl) (133) from sDO3A-(ethyl) (107)

sDO3A-(ethyl) (**107**) (4.06 g, 0.0059 mol) was dissolved in anhydrous acetonitrile (40 ml) to which potassium carbonate (4.1 g, 0.03 mol) was added. The reaction was cooled to −18 °C, then 5-bromopent-1-ene (**134**) (2.65 g, 0.0177 mol) was added, followed by stirring for a period of 48 hours while being kept at room temperature. The solid was removed using a centrifuge, and the solvent layer was decanted. The solvent was then removed using reduced pressure to yield a dark-yellow oil. The crude product was then chromatographed on silica eluted with DCM and EtOH (95:5%)

Yield, 2.77 g, 0.00366 mol, 62%

^{1}H NMR ($CDCl_3$): 1.18 (H18, q, 5.6 Hz)(*a*), 2.10 (H2, d, 6.70 Hz)(*i*), 2.3-2.8 (H26, m)(*e,f,m,c*) 3.76 (H3, t, 6.0 Hz)(*d*), 4.11 (H12, m)(*b*), 4.94 (H2, q, 17.5Hz)(*k*), 5.72 (H1, t–t, 6.75 Hz)(*j*).

^{13}C NMR ($CDCl_3$): 14.12 (CH_3)(*A1*), 14.40 (CH_3)(*A2*), 29.71 (CH_2)(*J*), 30.21 (CH_2)(*K*), 35.50 (CH_2)(*D*), 49.90 (CH_2)(*G*), 50.58 (CH_2)(*G*), 51.19 (CH_2)(*G*), 53.55 (CH_2)(*H*), 53.92 (CH_2)(*H*), 54.67 (CH_2)(*I*), 59.60 (CH)(*E1*), 59.82 (CH)(*E2*), 59.90 (CH)(*E3*), 60.46 (CH_2)(*B1*), 60.82 (CH_2)(*B2*), 115.30 (CH_2)(*N*), 137.11 (CH)(*M*), 171.41 (C=O)(*F*), 171.91 (C=O)(*C*).

FTIR (thin-film NaCl): 2981, 2940, 2832, 1728. 1448, 1372, 1297, 1258, 1175, 1117

LCMS: (positive): 757.98 [M(**133**)$^{+H}$]

HRMS: predicted 757.4593 [M(**133**)$^{+H}$], found 757.4590 [M(**133**)$^{+H}$]

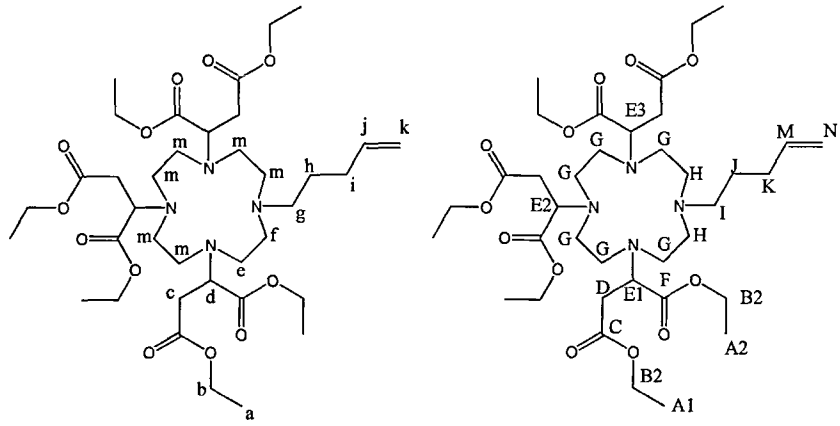

133 133

6.38: Characterisation of compound (133), proton (left) carbon (right)

6.39: Hydrolysis of sDO3A-(ethyl) (107) to form sDO3A (32) – DCl method

sDO3A-(ethyl) (**107**) (1.00 g, 0.00145 mol) was dissolved in D_2O (5 ml) to which DCl (0.8 ml, 35%) was added. The reaction was heated to 90 °C in a sealed tube for 24 hours. The DCl was removed using reduced pressure and the D_2O was removed using freeze-drying. The sample was retaken up into water (20 ml) and freeze-dried again. Yield 588 mg, 0.001339 mol, 92.3%

^1H (CD_3OD): 0.56 (H4, t, 3.3 Hz), 2.16 (H7, m), 2.35 (H8, s) 2.52 (H6, s), 2.54 (H3, s), 3.42 (H4, m) 4.15 (H3, s)

^{13}C NMR (CD_3OD): 13.960 (CH_3), 43.235 (CH_2), 58.122 (CH_2), 134.816 (CH), 169.232 (C=O), 175.253 (C=O), 175.944 (C=O), 176.478 (C=O)

FTIR (KBr disk): 3414, 2969, 1722, 1408, 1273, 1229, 1174.

LCMS (positive): 231.35 [1/2M(**138**)-$NaCl^{+H}$], 403.69 [M(**138**) $^{+H}$], 439.97 [M(**109**)Cl^{+H}].

6.40: Hydrolysis of sDO3A-(ethyl) (107) to form sDO3A via formic acid

sDO3A-(ethyl) (**107**) (0.25 g, 0.00036 mol) was dissolved in ethanol (1 ml), and was added to a solution of formic acid (2.5 ml, 3.05 g, 0.06587 mol) and water (2 ml). The reaction was heated to 90 °C for 24 hours, then cooled to room temperature. The solvents and formic acid were removed using lyophilisation. The lyophilisation was repeated three times by dissolving the crude material in water (10 ml).

^{1}H (D_2O): 1.31 (H4, t, 3.3 Hz), 2.16 (H7, m), 2.35 (H8, s) 2.52 (H6, s), 2.54 (H3, s), 3.42 (H4, m) **4**.15 (H3, s)

^{13}C NMR (CD_3OD): 13.960 (CH_3), 43.235 (CH_2), 58.122 (CH_2), 134.816 (CH), 169.232 (C=O), 175.253 (C=O), 175.944 (C=O), 176.478 (C=O)

6.41: Hydrolysis of butene-sDO3A-(ethyl) (101) to form butene-sDO3A (105) via 1.4M formic acid

Butene-sDO3A-(ethyl) (**101**) (0.25 g, 0.0003355 mol) was dissolved in formic acid (1.4M, 15 ml), and heated to 60 °C for 48 hours. The temperature was increased to 70 °C for 24 hours. The solvent was removed using lyophilisation, the solid residue was taken up into water (20 ml) and the reaction underwent a second round of lyophilisation.

Yield 0.21 g, 0.000305 mol, 91%

^{1}H NMR ($CDCl_3$): 1.26 (H12, t, 6.01 Hz), 2.05 (H2, q, 8.61 Hz), 2.54–2.99 (H24, m), 3.77 (H3, q, 3.87 Hz), 4.12 (H8, 4.98 Hz), 5.02 (H2, q, 8.43 Hz), 5.66 (H, q, 10.53 Hz).

^{13}C NMR ($CDCl_3$): 14.09 (CH_3), 35.33 (CH_2), 44.82 (CH_2), 48.11 (CH_2), 49.89 (CH_2), 61.10 (CH_2), 63.16 (CH_2), 116.87 (CH_2), 134.85 (CH), 166.59 (C=O–formic acid), 170.79 (C=O), 170.81 (C=0), 170.92 (C=O).

LCMS (positive): 687.81 [M(**107**)$^{+H}$] [$C_{32}H_{54}N_4O_{12}$]–

FTIR ($CDCl_3$–NaCl): 2983, 2858, 2254, 1729, 1609, 1465, 1372, 1299, 1262, 1180.

6.42: Hydrolysis of butene-sDO3A-(ethyl) (101) to form butene-sDO3A (105) via 2.2M formic acid

Butene-sDO3A-(ethyl) (**101**) (0.25 g, 0.0003365 mol) was dissolved in formic acid (2.2M, 10 ml) and heated to 80 °C in a sealed tube for 48 hours. The reaction was cooled, the solvent removed using lyophilisation, then the solid residue was taken up into water (20 ml) and the reaction underwent a second lyophilisation step.

24 hour LCMS (positive): 744.47 [M(**101**)$^{+H}$]

48 hours LCMS (positive): 257.93 [½M(**109**)$^{+H}$], 286.45 [½M(butene-sDO2A-(ethyl)$^{+H}$], 516.26 [M(**109**)$^{+H}$], 542.74 [M(**32**)+Na^{+H}], 572.45 [M(butene-sDO2A)$^{+H}$]

FTIR (thin-film $CDCl_3$): 3400, 2254, 1793, 1726, 1630, 1599, 1469, 1383, 1095, 908, 733.

HRMS (positive): 571.3708 – [M($C_{28}H_{51}O_8N_4$)$^{+H}$] minor peak 625.4173 – [M($C_{32}H_{57}O_8N_4^{+H}$]

6.43: Hydrolysis of sDO3A-(ethyl) (107) via sodium hydroxide in D_2O

The reaction was performed in a sealed-tube vessel sDO3A-(ethyl) (**107**) (0.1 g, 0.000145 mol) was dissolved in deuterium dioxide (5 ml) in which sodium hydroxide

(0.2 g, 0.005 mol) was dissolved. The reaction was stirred for 1.5 hours at room temperature, after which a sample was taken for NMR. The reaction was then heated to 80 °C for 24 hours.

After 1.5 hours

^{1}H NMR (D_2O): 1.22 (t, 15H, 5.5 Hz), 2.2–3.05 (m, 22H,), 3.69 (q, 7H, 6.9 Hz). 3.84 (m, 3H).

After 25.5 hours

^{1}H NMR (D_2O): 2.2–3.05 (m, 22H,), 3.84 (m, 3H)

6.44: Preparation of ion-exchange resins

The ion-exchange resins have to be prepared with the correct counter ion before use. This was done using a batch method, in which the resin was added to a solution of the desired counter ion. For example in the cation-exchange system, the H^+ counter ion was needed for the absorption of Na^+ ion. This was achieved by adding the resin to a large volume (500 ml to 100 g of resin) of 1M hydrochloric acid; this was stirred for around 30 minutes and then the acid was decanted and the resin washed with water until the pH of the eluent stabilised. The same principle was used for the generation of the anion-exchange resins, using NaOH, to give the hydroxide counter ion form. The resin was then placed in a glass-walled preparative HPLC column designed for protein purification. The solvents were pumped into the column using a gradient pump (Dionex, UK), which allowed for elution and gradient control. A Foxy Fraction Collector (ISCO, USA) was used for the collection of the fractions. The size of the column used depended on the volume of resin needed. For large-scale chromatography a 3 cm (internal diameter) by 100 cm (length) column was used, and for the small-scale chromatography a 3 cm (internal diameter) by 30 cm (length) column was used.

6.44.2: Cation-exchange resin preparation

Dowex 50W x 8 (H^+ form) was converted from the (NH_4^+) form by suspension of the resin in hydrochloric acid solution (1M) (6 times the volume of resin) for 20 minutes. The used acid was decanted and the resin was washed with ultra-pure water (5 x 200 ml) so that the pH was stabilised.

6.44.3: Anion-exchange resin preparation

Bio-Rad AG1 A4I was supplied in the Cl^- ion form; the experiment required the conversion of the resin to the HO^- form. This was performed by stirring the resin in sodium hydroxide (5 times the volume of the resin), for 10 minutes. The solvent was decanted and the resin was washed with ultra-pure water (5 x 200 ml) until the pH reached a stable, constant pH value of 6–7.

6.45: Cation-exchange chromatography of reaction solution from the hydrolysis of sDO3A-(ethyl) (107) via NaOD

The reaction solution from the hydrolysis of sDO3A-(ethyl) (**107**) via NaOD (500µl) was injected into the head of the ion-exchange column containing Dowex 2x-8 (OH^- form), bed volume 8 cm^3, eluting with ultra-pure water at a rate of 4 ml/min. The pH was monitored until it reached equilibrium at a pH of 6–7. The ion-exchange column was then eluted with a gradient of ammonia solution (2%). The fractions were collected and analysed using negative-ion LCMS. The solvent was removed from the product containing fractions by lyophilisation, to yield a brown solid.

NMR H^1 d = 2.49 (s, H?) , 2.84 (s, H?), 3.07 (s, H?), 3.59 (s, H?), 4.28 (s, H?) (base line meant no integration possible).

LCMS (negative): 278.55 [1/2M(sDO3A-$(NH_4)_2)^{-H}$], 403.07 [M(**138**)$^{-H}$], 521.05 [M(**32**)$^{-H}$], 559.03 [M(**32**)+$(NH_4)_2{}^{-H}$]

6.46: Hydrolysis of sDO3A-(ethyl) (107) via lithium hydroxide

The reaction was performed in a sealed-tube vessel. sDO3A-(ethyl) (**107**) (0.1 g, 0.000145 mol) was dissolved in deuterium dioxide (5 ml) in which 1M LiOH (5 ml) was dissolved. The reaction was then heated to 90 °C for 38 hours.

6.47: Anion-exchange chromatography of sDO3A (32)

The crude reaction mixture from the LiOH hydroxide hydrolysis method was injected into the head of an ion-exchange column containing Bio-Rad AG1 A4I (OH^- form), bed volume 500 cm^3, eluting with ultra-pure water at a rate of 4 ml/min. The pH was monitored until it reached equilibrium. The column was then eluted with a gradient of formic acid (1M). The fractions were collected and analysed using negative-ion LCMS. The solvent was removed from the product containing fractions by lyophilisation, yielding a white solid.

Yield: = 350 mg, 0.000672 mol, 46.3%
^{1}H NMR (D_2O): 2.4-2.7 (H 22, m), 3.83 (H3, m)

^{13}C NMR (D_2O): 37.5 (CH_2), 43.9 (CH_2), 50.2 (CH_2), 52.4 (CH_2) 60.6 (CH), 174.9 (C=O), 177.3 (C=O).

CHN analysis: found C = 43.3%, H = 6.52%, N = 9.84%; calculated C = 43.17%, H = 6.52%, N = 10.06% as $C_{20}H_{32}N_4O_{12}.(H_2O)_2$

HRMS: (electro spray (positive)): found 521.2088 [M(**32**)$^{+H}$], predicted 521.2089 [M(**32**)$^{+H}$].

6:48: Anion-exchange chromatography of sDO2A (162)

Crude reaction mixture from formic acid hydrolysis of sDO3A-(ethyl) (**107**) (588 mg) was dissolved into water (5 ml) and injected into the head of an ion-exchange column containing Bio-Rad AG1 A4I (OH^- form), bed volume 500 cm^3, eluting with ultra-pure water at a rate of 4 ml/min. The pH was monitored until it reaching equilibrium. The column was then eluted with a gradient of ammonia solution (2%). The fractions were collected and analysed using negative-ion LCMS. The solvent was removed from the product containing fractions by lyophilisation to yield a white solid.

Yield: = 212 mg

^{1}H NMR (D_2O): 2.06–2.53 (H20, m), 3.42 (H2, dd, 6.78 Hz)

LCMS (negative): 405.18 [M(**138**)$^{-H}$]

FTIR: (KBr disk): 3414, 2969, 1722, 1408, 1273, 1229, 1174.

6.49: Formation of T_8H_8 $[HSiO_{3/2}]_8$ (33)

Ferric chloride (anhydrous) (100 g, 0.625 mol), hydrochloric acid (conc., 40 cm^3) methanol (80 cm^3), hexane (700 cm^3) and toluene (100 cm^3) were placed in a 2 l reaction vessel. To this a solution of $HSiCl_3$ (**154**) (54 g, 0.4 mmol, 40 cm^3) in hexane (250 cm^3) was added dropwise over 8 hours and stirred for another 30 minutes. The upper hexane layer was removed and was added to a mixture of sodium carbonate (28 g) and calcium chloride (20 g). The mixture was stirred overnight. The solid was removed by filtration and the solvent was removed using reduced pressure to yield a white, crystalline solid.

This was then recrystallised from hexane to yield a white powder.

Yield: 2.5 g, 0.0059 mol, 11.8%.

^1H NMR ($CDCl_3$): 4.27 (H8, s)

^{29}Si NMR ($CDCl_3$): −84.44

FTIR (KBr disk): 2305, 2214, 1668.

6.50: Formation of *N,N*-diethylbut-3-en-1-amine (156)

4-bromobut-1-ene (**78**) (5 ml, 6.65 g, 0.04925 mol) was dissolved in acetonitrile (5 ml) to which diethylamine (**155**) (3.3 ml, 2.33 g, 0.03189 mol) was added. The reaction was heated in a sealed tube for 48 hours at 60 °C. The solvent was removed using reduced pressure and the crude product was then dissolved into water (25 ml) and the pH adjusted to pH 9 using potassium carbonate. The product was extracted using DCM (2 x 50 ml); the organic layer was then dried using

magnesium sulfate and filtered to remove solid residue. The solvent was removed using reduced pressure.

^{1}H NMR ($CDCl_3$): 1.06 (H6, t, 7.1 Hz)(*a*), 2.26 (H2, q, 6.9 Hz)(*d*), 2.61 (H6, q, 7.1 Hz)(*b,c*), 4.98 (H2, t, 11.0 Hz)(*f*), 5.73 (H, d–t, 6.7 Hz)(*e*).

^{13}C NMR ($CDCl_3$): 10.53 (CH_3)(*A*), 30.11 (CH_2)(*D*), 46.42 (CH_2)(*B*), 51.43 (CH_2)(*C*), 115.95 (CH_2)(*F*), 135.42 (CH)(*E*).

LCMS (positive): 128.15 [M(**156**)$^{+H}$]

FTIR (thin-film NaCl): 3436, 2922, 2738, 2690, 2653, 2360, 1701, 1653, 1639, 1543, 1472, 1438, 1397, 1261, 1166, 1099, 1035.

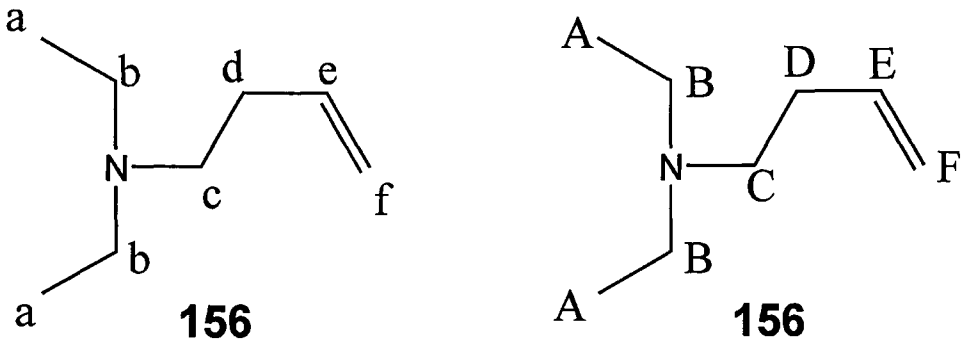

650: Characterisation of compound (156), proton (left) carbon (right)

6.51: Reaction of *N,N*-diethylbut-3-en-1-amine (156) with T_8H_8 to form compound (167)

N,N-diethylbut-3-en-1-amine (**156**) (6.7 mg, 0.00005112 mol) was dissolved in anhydrous toluene (1 ml) to which T_8H_8 (**33**) (2.7 mg, 0.0000064 mol) was added. To this Speier's catalyst (10 µl) was added and the flask was flushed with argon. The reaction was heated to 60 °C for 48 hours, forming a white precipitate that was removed by centrifugation. The solvent was removed using reduced pressure to yield a clear gum. This was then taken up into $CDCl_3$. The white solid formed was not soluble in any solvent studied.

Yield: 8mg.

^1H NMR ($CDCl_3$): 0.01(H, s), 0.68 (H1.6, d, 4.2 Hz), 1.14 (H0.7, s), 1.37 (H6, t, 7.3 Hz), 1.88 (H1.4, s), 2.19 (H0.4, s), 2.24 (H0.9, d, 2.4 Hz), 3.08 (H6, s)

^{13}C NMR ($CDCl_3$): 8.95 (CH_3), 20.89 (CH_3), 46.26 (CH_2), 66.42 (CH_2)

^{29}Si NMR ($CDCl_3$): −66.0

6.51: Reaction of *N,N*-diethylbut-3-en-1-amine with Q_8H_8 to form compound (168)

N,N-diethylbut-3-en-1-amine (**156**) (58 mg, 0.00045 mol) was dissolved in anhydrous toluene (1 ml) to which Q_8H_8 (**38**) (11 mg, 0.0000108 mol) was added. To this Speier's catalyst (10 µl) was added and the flask was flushed with argon and sealed. The reaction was heated to 80 °C for 48 hours. The solvent was removed using reduced pressure. The resulting gel was taken up into $CDCl_3$. Yield extracted 50mg, 72%

^{1}H NMR ($CDCl_3$): 0.14 (H158, s), 1.14 (H150, d, 6.03 Hz), 1.41 (H27, t, 7.32 Hz), 1.58 (H8, s), 2.33 (H72, s,), 3.11 (H18.90, s,), 4.13 (H15, t, 5.85), 5.21 (H4, t, 11.7 Hz), 5.71 (H1, m), 7.16 (H65, d, 7.53 Hz), 7.26 (H65, d, 6.95 Hz).

^{29}Si NMR ($CDCl_3$): −11.31, −109.5 8

6.52: Reaction of butene-sDO3A-(ethyl) (101) with T_8H_8 (33) via Speier's catalyst – version 1

$[HSiO_{3/2}]_8$ (**33**) (0.1 g, 0.000236 mol) and butene-sDO3A-(ethyl) (101) (0.57 g, 0.000767 mol) were dissolved in a solution of 0.02 mol H_2PtCl_6 in propan-2-ol (10 µl) and placed in a 1.5 ml sealed-tube reaction vessel. The reaction was heated to 80 °C for 24 hours. The reaction was then cooled to room temperature and the reaction mixture was dissolved into chloroform (10 ml). The solution was then passed though an activated charcoal plug. The fractions collected were centrifuged to collect the gel formed in the chloroform, the solution layer was decanted and the solvent was removed using reduced pressure to yield a mixture of oil and solid. The oil was extracted by washing the reaction mixture with $CDCl_3$ (1.5 ml) and extraction of the resulting solid with $CDCN_3$ (1.5 ml) was then attempted. The remaining solid was placed under high vacuum for 24 hours.

Yield 40 mg ($CDCl_3$-soluble)

^{1}H NMR ($CDCl_3$): 1.20 (H18, q, 5.8 Hz,), 2.12 (H2, s,), 2.3–28 (H24, m), 3.75 (H3, t, 6.1 Hz), 4.11 (H12, m), 4.93 (H2, q, 17.5 Hz), 5.71 (H1, t-t, 6.69 Hz).

^{13}C NMR ($CDCl_3$): 14.13 (CH_3), 14.16 (CH_3), 29.38 (CH_2), 35.13 (CH_2), 49.61 (CH_2), 50.40 (CH_2), 50.96 (CH_2), 53.34 (CH_2), 54.44 (CH_2), 54.66 (CH_2), 59.32 (CH), 59.69 (CH), 59.84 (CH), 60.44 (CH_2), 61.00 (CH_2), 115.307 (CH_2), 133.34 (CH), 171.15 (C=O), 171.63 (C=O).

^{28}Si NMR ($CDCl_3$): −109.15, −111.12, −111.44, −112.31, −113.00

FTIR ($CDCl_3$, thin-film NaCl): 2982, 2824, 2256, 1724, 1458, 1447, 1261, 1176.

6.53: Reaction of butene-sDO3A-(ethyl) (101) with T_8H_8 (33) via Speier's catalyst – version 2

Butene-sDO3A-(ethyl) (**101**) (10 eq, 0.15 g, 2.07^{-4} mol), T_8H_8 (**33**) (2.07^{-5} mol, 8.7mg) and Pt solution (20 µl) were combined in a sealed-tube reaction vessel and heated to 80 °C for 24 hours. The cooled reaction was extracted with chloroform (5 ml), producing a precipitate. The ppt was removed using a centrifuge, forming a gel. The chloroform layer was removed using reduced pressure and the resulting product was taken up into $CDCl_3$. The gel from the centrifuge was then washed using hexane (2 x 20 ml), yielding a white solid. The hexane layer did not yield any product after the solvent was removed using reduced pressure. The solid was then placed under high vacuum, yielding an insoluble, glass-type product.

Yield of $CDCl_3$-soluble product 20 mg

^1H NMR ($CDCl_3$): 1.31 (H18, t, 2.7 Hz), 1.87 (H2, s), 2.34–3.2 (H28, m), 4.12–4.32(H15, m), 5.31 (H2, q, 17.2 Hz), 6.05 (H, m).

^{29}Si ($CDCl_3$): −21.49

FTIR ($CDCl_3$, thin-film NaCl): 2926, 2855, 2254 ($CDCl_3$), 1713, 1465, 1378, 1303, 1262, 1216.

6.54: Reaction of butene-sDO3A-(ethyl) (101) with T_8H_8 (33) via Speier's catalyst dried over molecular sieve

Butene-sDO3A-(ethyl) (**101**) (250 mg, 3.35–4 mol, 10 eq) was toluene (1 ml) and dried over activated molecular sieve (4 Å) for 24 hours. The solution was filtered through a 5-micron filter to which T_8H_8 (**33**) (0.0000355 mol, 14 mg) was added. To the reaction Speier's catalyst (20ul) was added. The reaction vessel was flushed with argon and sealed, then heated to 80 °C for 48 hours. The reaction was cooled and the solvent was removed using reduced pressure. The crude product was taken up in $CDCl_3$ (1.5 ml), and the remaining crude was then extracted using $C_6D_5CD_3$ (1.0 ml), leaving a trace of insoluble material.

Silica TLC plate (glass backed as opposed to plastic backed 95% DCM with 5% EtOH) two spots: one at zero, and the other at Rf 0.56, co-spotted to butene-sDO3A-(ethyl).

6.54.1: Chloroform extraction

^1H NMR ($CDCl_3$): 0.04 (H1, s), 1.21 (H18, t, 2.5 Hz), 2.12 (H1.05, d, 7.1 Hz), 2.28–2.82 (H18.99, m,), 3.75 (H2.17, t, 5.67 Hz), 4.01 (H10.59, m), 4.98 (H1.12, t, 16 Hz), 5.77 (H0.56, td, 6.75 Hz, 10.26 Hz)

^{13}C NMR ($CDCl_3$): 0.94 (CH_3), 14.10 (CH_3), 14.36 (CH_3), 31.95 (CH_2), 35.25 (CH_2), 35.53 (CH_2), 49.89 (CH_2), 50.30 (CH_2), 50.63 (CH_2), 51.21 (CH_2), 53.58 (CH_2), 53.93 (CH_2), 54.67 (CH_2), 59.58 (CH), 59.85 (CH), 59.93 (CH), 60.07 (CH_2), 60.35 (CH_2),

60.45 (CH_2), 61.23 (CH_2), 115.26 (CH_2), 133.46 (CH), 137.09 (CH), 171.36 (C=O), 171.89 (C=O).

^{29}Si NMR ($CDCl_3$): −21.41, −116.27, 171.47

FTIR (NaCl plate, thin-film): 2980, 2937, 2819, 2360 (minor), 2257 (minor), 1733, 1640 (minor), 1464, 1448, 1372, 1256, 1162, 1113, 1032.

6.54.2: Toluene extraction

^{1}H NMR ($C_6D_5CD_3$): 1.18 (H18, s), 2.09–2.80 (H26, m), 4.00 (H15, m), 4.93 (H2, t,), 5.71 (H1, m).

^{29}Si NMR ($C_6D_5CD_3$): −21.40, −111.06, −116.14.

FTIR ($C_6D_5CD_3$ thin-film NaCl): 2275, 2240, 2211, 2120, 2084, 2051, 1582, 1571, 1387, 1331, 1283, 1256, 1200, 1174, 1051.

6.55: Reaction of butene-sDO3A-(ethyl) (101) with $Q_8M_8^H$ (38) via Speier's catalyst dried over molecular sieve

Butene-sDO3A-(ethyl) (**101**) (628 mg, 0.000778 mol) was dissolved in toluene (3 ml) (dried over 4 Å molecular sieve) along with Speier's catalyst (20 µl), to which $Q_8M_8^H$ (38) (0.00009 mmol, 96.7 mg) was added. The reaction was then flushed with argon and sealed. The mixture was then heated for a total of 65 hours at 80 °C. The reaction was cooled and the product filtered through an activated charcoal filter and the solvent removed using reduced pressure, yielding a clear, gum-like product. The gum was then extracted using $C_6D_5CD_3$ (1 ml), leaving a gel that formed a glass-type product after being placed in high vacuum.

After 24 hours FTIR (thin-film NaCl): 3027, 2961, 2920, 2866, 2365, 2141, 1940, 1861, 1801, 1734, 1604, 1495, 1461, 1379, 1257, 1174, 1100, 1031.

After 47 hours FTIR (thin-film NaCl): 3027, 2971, 2921, 2866, 2141, 1940, 1857, 1735, 1604, 1496, 1462, 1376, 1259, 1170, 1099, 1031.

After 57 hours FTIR (thin-film NaCl): 2980, 2929, 2365, 2143, 1735, 1602, 1495, 1460, 1372, 1201, 1257, 1161, 1098.

After 65 hours FTIR (thin-film NaCl): 2980, 2930, 2357, 1944, 1861, 1733, 1604, 1496, 1463, 1370, 1266, 1160, 1098.

Soluble product

^{1}H NMR ($C_6D_5CD_3$): 0.14 (H26, s), 0.22 (H22, s), 0.95 (H18, s), 1.17 (H12, s), 2.20–2.66 (H28, m), 3.91 (H15, s), 4.91 (H1.6, s)

^{13}C NMR ($C_6D_5CD_3$): 0.00 (CH_3), 1.16 (CH_3), 14.08 (CH_3), 14.28 (CH_3), 25.86 (CH_2), 28.90 (CH_3), 35.64 (CH_3), 51.47 (CH_2), 60.05 (CH), 65.05 (CH_2), 137.26 (CH), 171.01 (C=O), 171.47 (C=O)^{29}Si NMR ($C_6D_5CD_3$): −1.10 (trace), −11.23 (trace), −21.47, −108.06, −109.22, −109.49

6.56: Reaction of butene-sDO3A with Q_8H_8 via Speier's catalyst (Dean–Stark reaction method)

Butene-sDO3A-(ethyl) (101) (400 mg, 0.000538 mol) was dissolved in toluene (26ml), and the reaction was then refluxed in a Dean–Stark apparatus with a 12 ml trap for 4 hours, with 12 ml of solvent removed.

From the dried solution 5 ml was removed, containing butene-sDO3A-(ethyl) (101) (205 mg, 0.000276 mol). It was added to Speier's catalyst (dried solvent) (10 µl), to which $Q_8M_8^H$ (38) (0.0000338 mol, 34.5 mg) was added and the reaction sealed under argon and heated to 60 °C for 48 hours. The solvent was removed using reduced pressure, yielding a yellow gel. The product was then taken up into $CDCl_3$ (2 ml) leaving an insoluble product, which formed a glassy solid under high vacuum.

^{1}H NMR ($CDCl_3$): 0.017 (H48, s), 1.18 (H198.8, q, 7.71 Hz), 2.11 (H10.5, 3.48 Hz), 2.19–2.82 (H194, m), 3.64 (H14.25, q, 6.96 Hz), 3.73 (H14.25, t, 8.58 Hz), 4.08 (H94.33, m), 4.92 (H8.17, 4.32 Hz), 5.71 (H4.08, 6.75 Hz).

^{29}Si NMR ($CDCl_3$) (593-ii) −21.50 ppm

FTIR (thin-film NaCl): 2980, 2931, 2358, 1732, 1604, 1495, 1463, 1371, 1264, 1160.

6.57: Reaction of pentene-sDO3A (133) with Q_8H_8 via Karstedt's catalyst

Pentene-sDO3A-(ethyl) (**133**) (2.27 g, 0.003 mol) was dissolved in toluene (20 ml) and then dried over 4Å molecular sieve (2 x 10 g). The reaction was then placed in a sealed tube, to which $Q_8M_8^H$ (**38**) (368 mg, 0.000362 mol) and Karstedt's catalyst (100 µl) were added. The reaction was sealed under argon, and heated to 80 °C for 18 hours. The reaction was cooled and the solvent was removed using reduced pressure. The crude was then taken up into DCM (50 ml) to which activated charcoal was added, and the reaction was heated to reflux for 30 minutes. The solids were removed using filtration, and the solvent removed using reduced pressure. The product was then washed with $CDCl_3$ leaving a residual product, which formed a glass-type solid after drying in a high vacuum.

^{1}H NMR ($CDCl_3$): 0.00 (H7, s), 0.06 (H35, s), 0.53 (H8, s), 0.81 (H105, t, 6.9 Hz), 1.18 (H409, t, 3.6 Hz), 2.19–2.82 (H87, m), 3.73 (H13, 4.4 Hz), 4.0 (H70, q, 7.1 Hz)

^{13}C NMR ($CDCl_3$): 0.00 (v small), 1.43 (minor), 14.78 (major), 14.78 (minor), 23.02 (major), 29.30 (minor), 30.07 (minor), 31.96 (major) 35.82 (small), 60.81 (minor), 61.00 (minor), 61.64 (minor), 133.99 (minor), 165.33 (small), 171.89 (small), 172.31 (small), 172.68 (small)

^{29}Si NMR ($CDCl_3$): −21.49

FTIR (thin-film NaCl plate): 3027, 2920, 2868, 2361, 1942, 1861, 1801, 1734, 1604, 1495, 1461, 1379, 1255, 1177, 1082, 1031.

6.58: Test reaction of T_8H_8 (33) with Speier's catalyst

T_8H_8 (**33**) (0.0000335 mol, 14 mg) was dissolved in toluene (2 ml) to which Speier's catalyst (10 µl) was added. The reaction was sealed under argon and heated to 80 °C for 48 hours. The solvent was then removed using reduced pressure, yielding a white solid. The solid was taken up into $C_6D_5CD_3$.

Yield 13.5 mg 96.4%

^{1}H NMR ($CDCl_3$): 4.28 (H8, s)

^{29}Si NMR ($CDCl_3$): −84.46

FTIR (KBr disk): 2305, 2215, 1667.

6.59: Formation of Q_8-(1-bromobutane)$_8$ (166)

$Q_8M_8^H$ (**38**) (50 mg, 0.0000491 mol) was dissolved in toluene (1 ml) to which 5-bromopent-1-ene (**134**) (0.10 ml, 133 mg, 0.000985 mol) and Speier's catalyst (10 µl) were added. The reaction was sealed under argon and heated to 80 °C for 24 hours. The solvent was then removed using reduced pressure to yield a clear gum. The crude product was taken up into DCM (50 ml) to which activated charcoal was added and the solution was refluxed for 30 minutes. The solids were removed using filtration, and the solvent removed using reduced pressure. This was then taken up into $CDCl_3$.

Yield 90.7 mg, 0.0000412 mol, 83.9%

^{1}H NMR ($CDCl_3$): 0.00 (H48, s)(*f*), 0.47 (H16, t, 8.9 Hz)(*e*), 1.23 (H32, t, 7.1 Hz)(*c,d*), 1.74 (H16, t, 7.1 Hz)(*b*), 3.27 (H16, t, 6.8 Hz)(*a*).

^{13}C NMR ($CDCl_3$): 0.60 (CH_3)(*F*), 17.81 (CH_2)(*E*), 22.53 (CH_2)(*D*), 32.07 (CH_2)(*C*), 32.88 (CH_2)(*B*), 34.14 (CH_2)(*A*).

^{29}Si NMR ($CDCl_3$): −11.32, −109.5

FTIR (thin-film NaCl): 2980, 2930, 2357, 1496, 1370, 1265

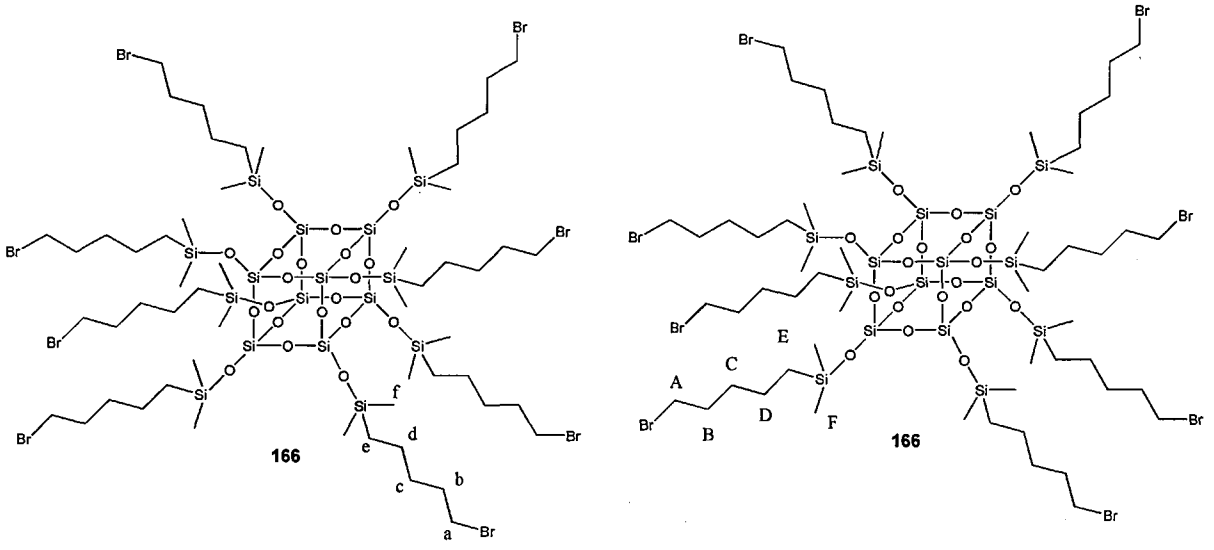

6.59: Characterisation of compound (166), proton (left) carbon (right)

6.60: Reaction of Q_8(1-bromopentene)$_8$ (166) with sDO3A-(ethyl) (107) to form compound (167)

Q_8(5-bromopentane)$_8$ (**166**) (0.000034 mol, 53.6 mg) was dissolved in acetonitrile (15 ml) to which potassium carbonate (15 eq, 0.00051 mol, 71 mg) and sDO3A-(ethyl) (**107**) (10 eq, 0.000343 mol, 236 mg) were added. The reaction was then heated to 60 °C for 48 hours.

The solids were removed from the reaction by centrifuge, and the liquid was decanted. The solvent was then removed using reduced pressure to yield a yellow solid. The solid was washed with DCM (2 x 10 ml). The organic phases were combined and the solvent removed using reduced pressure, yielding an oil.

^{1}H NMR ($CDCl_3$): 0.00 (H48, s), 1.19 (H163, t, 7.86 Hz), 1.942.91 (H230, m), 3.81 (H22, m), 4.08 (H103, m)

^{13}C NMR ($CDCl_3$): 0.96 (CH_3), 14.24 (CH_3), 14.37 (CH_3), 34.05 (CH_2), 35.58 (CH_2), 42.63 (CH_2), 45.01 (CH_3), 48.50 (CH_2), 49.44 (CH_2), 58.51 (CH_2), 59.93 (CH), 60.60 (CH_2), 171.52 (C=O), 171.66 (C=O).

^{29}Si NMR ($CDCl_3$): −21.40, −97.21 (trace)

FTIR (thin-film NaCl): 2981, 2930, 2357, 1732, 1605, 1497, 1463, 1371, 1266, 1160, 1098.

6.61: Reaction of triethoxysilane (13) and butene-sDO3A-(ethyl) (101)

Butene-sDO3A-(ethyl) (**101**) (114 mg, 0.00015 mol) was dissolved into toluene (1 ml) to which triethoxysilane (**183**) (0.0002 mol, 0.0328 g, 0.037 ml) was added, along with Speier's catalyst (20µl), sealed under argon and heated to 80 °C for 48 hours. The reaction produced large amounts of insoluble material, which were removed using a centrifuge; the liquid layer was decanted and the solvent removed using reduced pressure, giving rise to a clear, gum-like product, which was taken up into $CDCl_3$.

^{1}H NMR ($CDCl_3$): 1.19 (H18, t, 6.8 Hz), 1.79 (H2, m), 2.20–2.82 (H28, m), 3.81 (H3, q, 7.1 Hz), 4.09 (H12, m). 5.02 (H1, t, 19.0 Hz), 5.73 (H0.45 , m).

^{13}C NMR ($CDCl_3$): 1.3 (CH_3), 14.10 (CH_3), 14.36 (CH_3), 18.07 (CH_2), 18.36 (CH_2), 25.50 (CH_2), 35.25 (CH_2), 50.62 (CH_2), 58.31 (CH_2), 59.25 (CH_2), 60.00 (CH), 60.53 (CH_2), 67.87 (CH_2), 172.65 (C=O), 173.32 (C=O)

^{29}Si ($CDCl_3$): −21.38

FTIR (thin-film NaCl plate): 3030, 2921, 2868, 2362, 1943, 1734, 1604, 1495, 1461, 1379.

6.62: Reaction of 1,1,3,3,5,5 hexamethyl-trisiloxane (182) with butene-sDO3A-(ethyl) (101)

Butene-sDO3A-(ethyl) (**101**) (114 mg, 0.000153 mol) was dissolved in toluene (1 ml) to which 1,1,3,3,5,5-hexamethyl-trisiloxane (**182**) (160 mg, 0.019 ml, 0.0000765 mol) was added along with Speier's catalyst (20µl). The reaction was heated to 80 °C for 48 hours. The solvent was removed using reduced pressure to yield a clear gel. The gel was taken up into $CDCl_3$, leaving an insoluble residue.

^{1}H NMR ($CDCl_3$): 0.00 (H9, d, 8.6 Hz), 0.07 (H9, t, 7.5 Hz), 1.18 (H33, m), 1.78 (H4.2, pent, 3.1 Hz), 2.4–2.7 (H14.03, m,), 3.7 (H4.72, t, 9.7 Hz), 4.11 (H17.9, m), 4.99 (H1.2, m), 5.81 (H0.4, m)

^{13}C NMR ($CDCl_3$): −0.69 (CH_3), −0.13 (CH_3), 13.82 (CH_3), 14.08 (CH_3), 21.68 (CH_2), 25.27 (CH_2), 27.52 (CH_2), 60.22 (CH), 67.62 (CH_2), 133.27 (CH_2), 171.09 (C=O), 171.22 (C=O), 171.73 (C=O).

^{28}Si NMR ($CDCl_3$): minor −7.79, major −21.46

Hexamethyl-trisiloxane (**182**)

^{1}H NMR ($CDCl_3$): −0.15 (H6, s), 0.01 (H12, s), 4.57 (H2, t, 2.7Hz)

^{28}Si ($CDCl_3$): −6.20, −17.30

6.63: Reaction of triethylsilane (181) with butene-sDO3A-(ethyl) (101) to give compound (186)

Butene-sDO3A-(ethyl) (250 mg, 0.000336 mol) was dissolved in toluene (1 ml), to which triethylsilane (58 mg, 0.0005 mol, 0.08 ml) was added. To the stirred reaction mixture Speier's catalyst (20 µl) was added and the reaction was heated to 80 °C for 24 hours. The reaction was cooled and passed though an activated charcoal plug. The solvent was then removed using reduced pressure, yielding a clear gum.

^{1}H NMR (CDCl3): 0.53 (H6, q, 7.86 Hz)(*k*), 0.98 (H9, t, 5.54 Hz)(*l*), 1.09 (H2, d, 6.03 Hz)(*j*), 1.21 (H20, t, 7.14 Hz)(*a*), 1.67 (H1, s,)(, 2.28–2.83 (H22, m)(*e,f,c,m*), 3.73 (H3, m)(*e*), 4.09 (H12, q, 4.57 Hz)(*b*).

^{13}C NMR ($CDCl_3$):0.93 (CH_3)(*O*), 5.75 (CH_2)(*N*), 6.51 (CH_2)(*M*), 14.02 (CH_3)(*A1*), 14.35 (CH_3)(*A2*), 21.35 (CH_2)(*K*), 22.57 (CH_2)(*I*), 26.59 (CH_2), 29.13(CH_2), 29.78 (CH_2), 35.22 (CH_2)(*D*), 35.40 (CH_2)(*D*), 49.98 (CH_2), 50.65 (CH_2), 51.05 (CH_2), 51.19 (CH_2), 53.68 (CH_2), 53.98 (CH_2), 55.40 (CH_2), 59.59 (CH)(*E*), 60.43 (CH_3), 171.39 (C=O)(*F*), 171.44 (C=O)(*F*), 171.86 (C=O)(*C*).

^{29}Si NMR ($CDCl_3$): 19.57, −21.49

FTIR (thin-film NaCl): 3027, 2920, 2874, 1734, 1604, 1495, 1461, 1379, 1177

LCMS (positive): 859.53 [M(**186**)$^{+H}$]

Triethylsilane FTIR (thin-film NaCl plate): 2955, 2912, 2876, 2101, 1460, 1415, 1379, 1235, 1016, 975, 811.

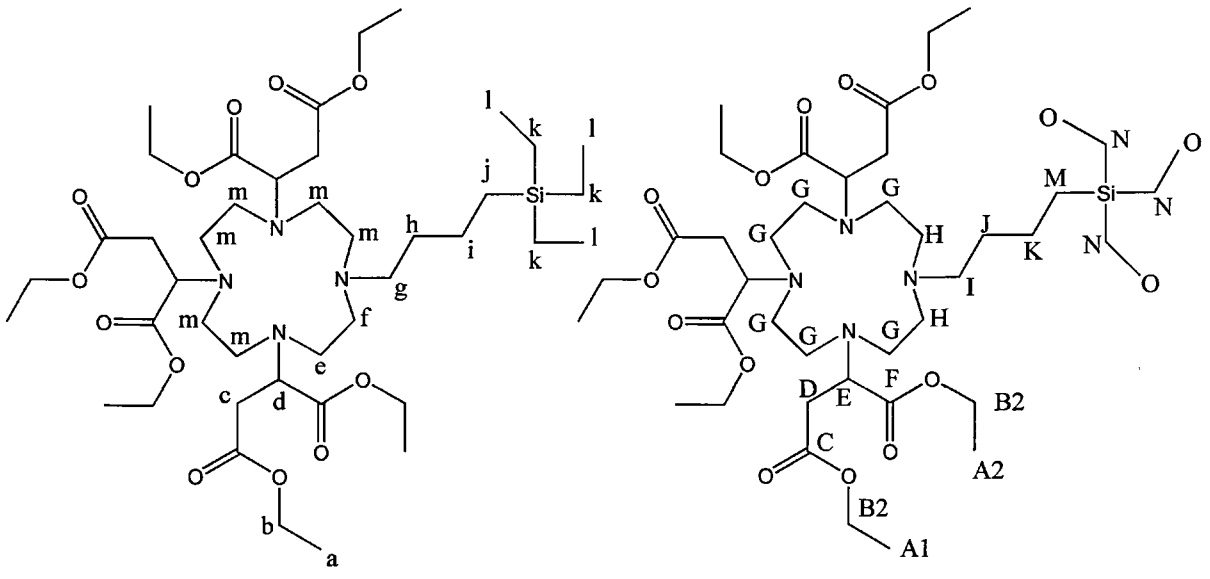

186 186

6.63: Characterisation of compound (188), proton (left) carbon (right)

6.64: Formation of tri-(dimethylsilyl) benzene (193)

Dimethyl chlorosilane (37.60 g, 0.3968 mol) was dissolved in THF (120 ml) to which magnesium turnings (9.68 g, 0.3968 mol) were added and stirred until dissolved. The solution was then added dropwise to a slowly refluxing solution of 1,3,5-tribromobenzene (**194**) (25 g, 0.078 mol) dissolved in THF (80 ml). The reaction was then refluxed for 3 hours, after which the solvent was removed using reduced pressure to yield an orange solid. The product was extracted using hexane (4 x 50 ml); the organic phases were combined and filtered and the solvent removed using reduced pressure, yielding a crude oil. The oil was then distilled under high vacuum and a product collected at 60–65°C.

Yield 6.98 g, 0.02768 mol, 35.5%

FTIR (thin-film NaCl plates): 3004, 2960, 2902, 2122, 1558, 1426, 1380, 1365, 1249

HRMS calculated 251.1102 [M(**193**)$^{+H}$], found 251.1104 [M(**193**)$^{+H}$]

^{1}H NMR ($CDCl_3$): 0.24 (H18, t, 2.7 Hz)(*a*), 4.34 (H3, q, 3.7H)(*b*), 7.63 (H3, s)(*c*)

^{13}C NMR ($CDCl_3$): −3.72 (CH_3)(*A*), 136.75 (CH)(*C*), 140.54 (C)(*B*).

^{29}Si NMR ($CDCl_3$): −15.99

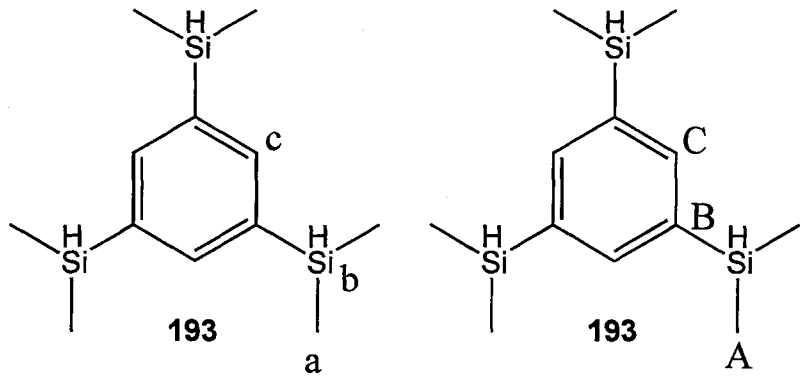

6.64: Characterisation of compound (193), proton (left) carbon (right)

6.65: Reaction of tri-(dimethylsilyl) benzene (193) with pentene-sDO3A-(ethyl) (133) to form 1,3,5-tris((pentane-sDO3A(ethyl))dimethylsilyl) benzene (189)

Pentene-sDO3A-(ethyl) (**133**) (417 mg, 0.0005508 mol) was dissolved in toluene (20 ml), to which Speier's catalyst (100 µl) was added. To the reaction 1,3,5-dimethylsilane benzene (**193**) (46.3 mg, 0.0001836 mol) was added and the reaction sealed under argon was heated to 80 °C for 72 hours, after which the solvent was removed using reduced pressure. The crude was taken up into DCM (50 ml) to which activated charcoal was added, and then refluxed for 30 minutes. The solids were filtered out, and the solvent removed using reduced pressure to yield a crude product. The sample was then split into two fractions; the first one was

chromatographed on silica eluted with DCM (92%) and acetone (8%), while the second one was vacuum distilled.

Crude = 440 mg, 0.00017437 mol, 94.9%

^{1}H NMR ($CDCl_3$): −0.29 (H2, s), −0.02 (H18, s), 0.50 (H3, d, 4.6 Hz), 0.74 (H12, d, 6.2 Hz), 0.94 (H18, t, 4.7 Hz), 1.78 (H8, d), 3.60 (H2, m), 3.86 (H7, q, 7.1 Hz), 4.93 (H11, s), 6.46 (H2, s), 6.88 (H, s).

^{13}C NMR ($CDCl_3$): −1.11 (CH_3), 0.00 (CH_3), 0.97 (CH_3), 14.06 (CH_3), 25.60 (CH_3), 29.14 (CH_2), 39.66 (CH_2), 30.88 (CH), 53.40 (CH_2), 60.64 (CH_2), 61.29 (CH_2), 65.26 (CH), 164.97 (C=O).

^{29}Si NMR ($CDCl_3$): 5.19, 4.38, −0.80, −21.49

FTIR (thin-film NaCl plate): 2981, 2935, 2872, 2256, 1725, 1468, 1464, 1372, 1301, 1257.

6.65.1: Distillation results:

Thermometer:

^{1}H NMR ($CDCl_3$): −0.01 (H16, s), 0.045 (H2, s), 0.78 (H18, t, 7.8 Hz), 3.61 (H2.6, pent, 6.1 Hz), 3.87 (H10, q, 7.1 Hz), 6.47 (H0.74, s), 7.24 (H3, s).

^{13}C NMR ($CDCl_3$): −1.11 (CH_3), 14.15 (CH_3), 61.37 (CH_2), 65.36 (CH), 133.67 (CH), 139 (C), 165.06 (C=O).

^{29}Si NMR ($CDCl_3$): 5.37

FTIR 2972, 2930, 1716, 1467, 1370, 1303, 1261, 1160, 1032, 905

Condenser:

^{1}H NMR ($CDCl_3$): −0.19 (H4, s), −0.02 (H18, s), 0.73 (H18, d, 7.1 Hz), 0.91 (H54, t, 5.3 Hz), 1.19 (H15, s), 3.89 (H24, q, 7.1 Hz), 6.46 (H12, s), 6.88 (H8, s), 7.24 (H3, s).

^{13}C NMR ($CDCl_3$): −1.18 (CH_3), 14.08 (CH_3), 61.29 (CH_2), 132.71 (CH), 133.61 (C), 164.99 (C=O).

^{29}Si NMR ($CDCl_3$): 5.71

Flask:

^{1}H NMR ($CDCl_3$): 0.01 (H2, s), 0.25 (H2, s), 0.29 (H3, s), 0.84 (H3, 3.2 Hz), 1.07 (H2, d, 6.0 Hz) 1.18 (H18, q, 6.0 Hz), 2.18–2.85 (H22, m), 3.74 (H3, t, 4.2 Hz), 4.10 (H12, q, 6.5 Hz), 7.46–7.52 (H2, s).

^{13}C NMR ($CDCl_3$): −1.35 (CH_3), 0.00 (CH_3), 13.96 (CH_3), 14.23 (CH_3), 17.79 (CH_2), 25.48 (CH_2), 26.46 (CH_2), 29.57 (CH_2), 31.51 (CH_2), 34.78 (CH_2), 35.26 (CH_2), 45.08 (CH_2), 45.36 (CH_2), 45.70 (CH_2), 46.89 (CH_2), 48.89 (CH_2), 49.79 (CH_2), 50.15 (CH_2), 50.45 (CH_2), 50.87 (CH_2), 51.03 (CH_2), 51.16 (CH_2), 53.54 (CH_2), 53.81 (CH_2), 53.92 (CH_2), 54.96 (CH_2), 55.23 (CH_2), 59.35 (CH_2), 60.00 (CH_2), 60.18 (CH_2), 60.20 (CH_2), 60.24 (CH_2), 60.44 (CH_2), 60.60 (CH_2), 61.08 (CH_2), 65.08 (CH_2), 132.19 (CH), 133.46 (CH), 138.48 (C), 139.53 (C),171.32 (C=O), 171.72 (C=O).

^{29}Si NMR ($CDCl_3$): 6.25, 5.19, 5.09, 0.73, 0.63

6.66: Reaction of pentene-sDO3A-(ethyl) (133) with bis(dimethyl silyl)benzene (192) to form 1,4-bis((5-bromopentyl) dimethylsilyl) benzene (198)

A solution of pentene-sDO3A-(ethyl) (**133**) (1.00 g, 0.001321 mol), was dissolved in toluene (10 ml) to which Speier's catalyst (10µl) was added. To this reaction bis(dimethylsilyl)benzene (**192**) (0.000629 mol, 0.12 g) was added. The reaction was

flushed with argon and the reaction sealed within a tube. The reaction was then heated to 80 °C for 48 hours. The solvent was removed using reduced pressure and the crude material was then taken up into DCM (100 ml) and refluxed with activated charcoal for 30 minutes. The solids were removed using filtration and the solvent was removed using reduced pressure, yielding a clear, gum-like residue.

TLC (100% DCM alumina) shows three spots: Rf 0.02, Rf 0.30 (pentene-sDO3A-(ethyl), Rf 0.97.

^{1}H NMR ($CDCl_3$): 0.23 (H2, s), 0.27 (H10, s), 1.04 (H4, d, 5.9 Hz), 1.17 (H36, q, 6.7 Hz), 1.42 (H2, s), 1.95 (H4, d, 6.6 Hz), 2.24 (H4, s), 2.4–2.77 (H48, m), 3.71 (H6, s), 4.05 (H24, m), 4.87 (H3, q, 5.85 Hz), 5.69 (H1.5, m), 7.10 (H4, m), 7.46 (H3, m).

^{13}C NMR ($CDCl_3$): –3.22 (CH_3), –1.28(CH_3), 0.00(CH_3), 0.72(CH_3), 14.04(CH_3), 14.30(CH_3), 21.28(CH_3), 22.52 (CH_2), 25.56(CH_3), 26.13 (CH_2), 29.00 (CH_2), 31.58 (CH_2), 35.13 (CH_2), 35.27 (CH_2), 49.85 (CH_2), 50.56 (CH_2), 50.90 (CH_2), 51.07 (CH_2), 53.44 (CH_2), 53.61 (CH_2), 53.86(CH_2), 54.72 (CH_2), 59.46(CH_2), 59.73 (CH_2), 59.83 (CH_2), 60.28 (CH_2), 60.38 (CH_2), 61.13(CH_3), 65.14(CH_3), 114.36(CH_2), 125.166 (CH), 128.07 (CH), 128.86 (CH), 132.10 (CH), 132.25 (CH), 133.47(CH), 137.59(C), 138.51 (C), 164.73 (COOH), 171.24 (C=O), 171.28(C=O), 171.34(C=O), 171.72(C=O).

^{29}Si NMR ($CDCl_3$): 5.22, 5.00, −0.86

FTIR (thin-film NaCl): 3535 (small), 2981, 2938, 2844, 2257, 1726, 1641, 1464, 1448, 1372, 1347, 1299, 1256, 1175, 1137, 1096, 1030.

6.67: Synthesis of bis(succinate)dimethyl phenylsilane (196)

Bis(dimethylsilyl)benzene (**192**) (350 mg, 0.0018229 mol), was mixed with diethyl maleate (**126**) (2.1 eq, 659 mg, 0.003828 mol) to which Speier's catalyst (100 µl) was added, along with toluene (5 ml). The reaction was sealed under argon and heated to 80 °C for 72 hours. The reaction was then dissolved in DCM (150 ml) to which activated charcoal was added, and then the reaction was refluxed for 30 minutes. The solids were filtered out and the solvent was removed using reduced pressure, yielding a clear oil.

Yield 670 mg, 0.0012 mol, 68%

^{1}H NMR ($CDCl_3$): 0.00 (H12, s), 0.89 (H12, t, 7.1 Hz), 1.84 (H2, d, 2.2 Hz), 2.33 (H2, m), 3.66 (H8, t, 5.5 Hz), 3.90 (H2, q, 4.6 Hz), 7.18 (H2, s), 7.22 (H2, s).

^{13}C NMR ($CDCl_3$): −4.9 (CH_3), −3.71 (CH_3), −1.77 (CH_3), 0.00 (CH_3), 14.10 (CH_3), 25.67 (CH), 29.19 (CH_2), 60.61 (CH_2), 128.20 (CH), 128.99 (CH), 129.81 (CH), 132.74 (C), 133.90 (C), 172.31 (C=O), 172.73 (C=O).

^{29}Si 5.72, 5.63 (minor), 5.37, 5.22, 4.87, 4.79, 0.70, 0.60 (major)

FTIR (neat thin-film NaCl): 3536, 2979, 1736, 1466, 1447, 1409, 1372, 1301, 1254, 1136, 1036

HRMS: calculated 556.2756 [M(**196**)$^{+NH4}$], found 556.2761 [M(**196**)$^{+NH4}$]

6.68: Formation of diethyl 2-(diethylamino)succinate (197)

Diethylamine (**155**) (5.00 g, 0.0683 mol) was dissolved in acetonitrile (100 ml) to which potassium carbonate (28.3 g, 0.205 mol) was added. To the stirred reaction diethyl fumarate (**130**) (28.3 g, 0.13672 mol) was added. The reaction was then refluxed for 48 hours. The solids were removed by filtration and the solvent was removed using reduced pressure to yield a crude oil. The oil was then chromatographed on silica eluted with DCM (96%) EtOH (4%), eluting the product at Rf 0.28. The remaining diethyl fumarate was eluted at Rf 0.86.

^{1}H NMR ($CDCl_3$): 1.28 (H6, t, 5.3 Hz)(*h*), 1.49 (H6, t, 5.5 Hz)(*a,f*), 2.77 (H4, q, 4.1 Hz)(*g*), 2.91 (H1, d, 4.2 Hz)(*d*), 3.02 (H1, t, 4.5 Hz)(*c*), 4.38 (H4, q, 8.8 Hz)(*b*).

^{13}C NMR ($CDCl_3$): 13.51 (CH_3)(*J*), 14.31 (CH_3)(*A,H*), 34.34 (CH_2)(*D*), 46.56 (CH_2)(*I*), 59.89 (CH)(*E*), 61.23 (CH_2)(*B,G*), 171.39 (C=O)(*C*), 173.23 (C=O)(*F*).

Yield 2.96 g, 0.012 mol, 17.66%

HRMS: calculated 246.1700 [M(**197**)$^{+H}$], found 246.1697 [M(**197**)$^{+H}$]

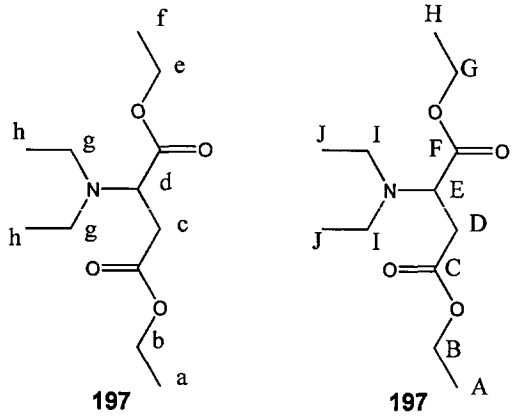

6.68: Characterisation of compound (197), proton (left) carbon (right)

6.69: Reaction of diethyl 2-(diethylamino)succinate (197) with dimethylphenyl silane (190)

Diethyl 2-(diethylamino)succinate (**197**) (300 mg, 0.0012195 mol) was dissolved in toluene (5 ml) to which dimethylphenyl silane (**190**) (150 mg, 0.0011086 mol) and Speier's catalyst (100 µl) were added. The reaction was then heated to 60 °C for 48 hours. The solvent was removed using reduced pressure, and the resulting gum was taken up into DCM (50 ml) along with activated charcoal and refluxed for 30 minutes. The solids were removed using filtration and the solvent was removed using reduced pressure. The product was then taken up into $CDCl_3$, leaving an insoluble, gum-like residue.

^1H NMR (CDCl3): 0.12 (H, s), 0.48 (H ,s), 1.10 (H6, s),1.13 (H , s), 1.28 (H6, s,), 2.15 (H , d, 3.7 Hz), 2.36 (H1,s), 2.56 (H4, q, 3.1 Hz), 2.62 (H2 m), 2.81 (H1, m), 3.97 (H1, t, 3.28 Hz), 4.17 (H4, m), 5.29 (H , d, 3.7 Hz), 7.17 (H2, t, 7.1 Hz), 7.25 (H3, t, 7.3 Hz).

^{29}Si NMR ($CDCl_3$): 5.91 (major), 5.18.

FTIR (thin-film NaCl plate): 2978, 2936, 1729, 1475, 1447, 1372, 1299, 1259, 1178.

6.70: Stability of pentene-sDO3A-(ethyl) (133) with Speier's catalyst

Pentene-sDO3A-(ethyl) (**133**) (25 mg, 0.000033 mol) was dissolved in $CDCl_3$ (1.25 ml) to which Speier's catalyst (10 µl) was added, and the reaction was placed in an NMR tube. The tube was then warmed for 48 hours, after which the ^1H and ^{13}C NMR spectra were taken.

^1H NMR ($CDCl_3$): 1.12 (H60, dd, 6.0 Hz), 1.21 (H18, q, 6.5 Hz), 2.10 (H1, s), 2.42 (H2, d, 5.5 Hz), 2.49 (H4, d, 5.7 Hz), 2.69 (H22, s), 3.72 (H3, q, 3.1 Hz), 3.92 (H15, pent, 6.0 Hz), 4.07 (H20, m), 4.90 (H2, m), 5.71 (H1, dq, 6.8 Hz), 6.77 (H0.26, s).

^{13}C NMR ($CDCl_3$): 13.83 (CH_3), 13.89 (CH_3), 14.16 (CH_3), 24.72 (CH_2), 24.99 (CH_2), 25.24 (CH_3), 25.98 (CH_2), 27.39 (CH_2), 29.71 (CH_2), 30.64 (CH_2), 31.50 (CH_2), 35.16 (CH_2), 49.71 (CH_2), 50.41 (CH_2), 50.78 (CH_2), 53.62 (CH_2), 54.62 (CH_2), 59.38 (CH_2), 57.73 (CH_2), 60.37 (CH_2), 61.51 (CH), 63.79 (CH_2), 64.53 (CH), 114.24 (CH_2), 115.27 (CH_2), 116.3 (CH_2), 133.31, (CH), 133.41 (CH), 133.48 (CH), 138.44 (CH), 164.82 (C=O), 171.31 (C=O), 171.73 (C=O)

6.71: Stability of pentene-sDO3A-(ethyl) (133) with Karstedt's catalyst

Pentene-sDO3A-(ethyl) (**133**) (25 mg, 0.000033 mol) was dissolved in $CDCl_3$ (1.25 ml) to which Karstedt's catalyst (10 µl) was added, and the reaction was placed in an NMR tube. The tube was then warmed for 48 hours, after which ^1H and ^{13}C NMR spectra were taken.

^{1}H NMR ($CDCl_3$): 0.00 (H0.5, s), 0.05 (H0.5, s), 1.16 (H18, q, 6.1 Hz), 1.45 (H2, m), 1.95 (H2, d, 7.1 Hz), 2.01 (H2, s), 2.24 (H14, s, toluene), 2.40–2.72 (H24, m), 3.72 (H3, t, 5.7 Hz), 4.07 (H12, m), 4.98 (H2, m), 5.89 (H, m), 7.12 (H25, m, toluene).

^{13}C NMR ($CDCl_3$): 0.00 (CH_3), 0.79 (CH_3), 13.81 (CH_3), 13.89 (CH_3), 14.14 (CH_3), 21.15 (CH_3), 25.29 (CH_2), 26.03 (CH_2), 27.38 (CH_2), 29.70 (CH_2), 30.51 (CH_2), 31.46 (CH_2), 31.74 (CH_2), 35.00 (CH_2), 49.76 (CH_2), 50.46 (CH_2), 50.80 (CH_2), 50.96 (CH_2), 53.48 (CH_2), 53.76 (CH_2), 54.61 (CH_2), 59.33 (CH), 59.60 (CH), 59.81 (CH), 59.98 (CH_2), 60.15 (CH_2), 60.19 (CH_2), 60.24 (CH_2), 60.99 (CH_2), 114.22 (CH_2), 115.22 (CH_2), 125.03 (CH), 128.16 (CH), 128.75 (CH), 131.19 (CH), 133.33 (CH), 137.52 (C) (toluene), 138.42 (CH), 164.65 (C=O), 171.81 (C=O), 171.62 (C=O).

6.72: Synthesis of (5-bromopentyl)dimethyl(phenyl)silane (191)

Dimethylphenyl silane (**190**) (1.0 ml, 876 mg, 0.007338 mol) was added to 5-bromopent-1-ene (**134**) (1.4 eq, 1.04 ml, 1.31 g, 0.008806 mol) along with Speier's catalyst (100 µl). The reaction mixture was sealed under argon and heated to 60 °C for 34 hours. The cooled reaction was added to DCM (150 ml) and activated charcoal was added; the reaction was then refluxed for 30 minutes. The solids were removed using filtration and the solvent was removed by reduced pressure. The excess 5-bromopent-1-ene was removed using reduced pressure (50 mbar) at 40 °C; the product was then placed under high vacuum for 34 hours. The resulting oil was centrifuged to remove trace amounts of activated charcoal, yielding a pure product as shown by TLC.

Yield 1.23 g, 0.00433 mol, 59.0%.

^{1}H NMR ($CDCl_3$): 0.03 (H6, s)(*f*), 0.52 (H2, t, 6.2 Hz)(*e*), 1.13 (H4, m)(*c,d*), 1.54 (H2, t, 6.8 Hz)(*b*), 3.03 (H2, t, 6.9 Hz)(*a*), 7.07 (H3, t, 3.8 Hz)(*h,i*), 7.26 (H2, q, 3.5 Hz)(*g*).

^{13}C NMR ($CDCl_3$): −1.15 (CH_3)(*F*), 15.49 (CH_2)(*E*), 23.01 (CH_2)(*D*), 31.80 (CH_2)(*C*), 32.27 (CH_2)(*B*), 33.52 (CH_2)(*A*), 127.60 (CH)(*J*), 129.27 (CH)(*I*), 133.35 (CH)(*H*), 139.02 (C)(*G*).

^{29}Si NMR ($CDCl_3$): −2.65

FTIR (thin-film NaCl plate): 3068, 2961, 2935, 1642, 1579, 1475, 1252, 1119.

LCMS (positive): 206.15 [M(**191**)-Br^{+H}]

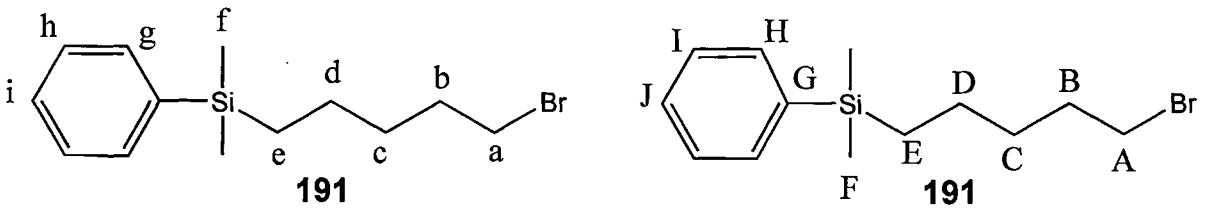

672: Characterisation of compound (191) proton (left) carbon (right)

6.73: Formation of 1,4-bis((5-bromopentyl)dimethylsilyl)benzene (198)

1,4-Bis(dimethylsilyl)benzene (**192**) (1 ml, 875 mg. 0.0045 mol) and 5-bromo-pent-1-ene (**134**) (2.8 eq, 0.0126 mol, 1.877 g, 1.50 ml) were combined in a sealed tube, to which Speier's catalyst (100 µl) was added. The reaction was sealed under argon and heated to 60 °C for 48 hours. After this step the reaction was added to DCM (100 ml) and activated charcoal was added; a further stage of reflux for 30 minutes followed. The solids were filtered out and the solvent removed using reduced

pressure, yielding a clear oil. The oil was then placed under high vacuum for 48 hours.

Yield 0.0028035 mol, 1.37 g, 62.3%

^{1}H NMR ($CDCl_3$): 0.00 (H12, s)(*f*), 0.49 (H4, t, 6.8 Hz)(*e*), 1.18 (H8, m)(*c,d*), 1.53 (H4, pent, 7.3 Hz)(*b*), 3.03 (H4, t, 6.9 Hz)(*a*), 7.22 (H4, s)(*h*).

^{13}C NMR ($CDCl_3$): −3.09 (CH_3)(*F*), 23.03 (CH_2)(*E*), 30.67 (CH_2)(*D*), 31.87 (CH_2)(*C*), 33.58 (CH_2)(*A*), 132.22 (CH)(*H*), 139.66 (C)(*G*).

^{29}Si NMR ($CDCl_3$): −2.66.

FTIR (thin-film NaCl plate): 2955, 2926, 1459, 1438, 1379, 1250, 1135, 1056

HRMS: calculated 508.1061 [M(**198**)$^{+NH4}$], found 508.1054 [M(**198**)$^{+NH4}$]

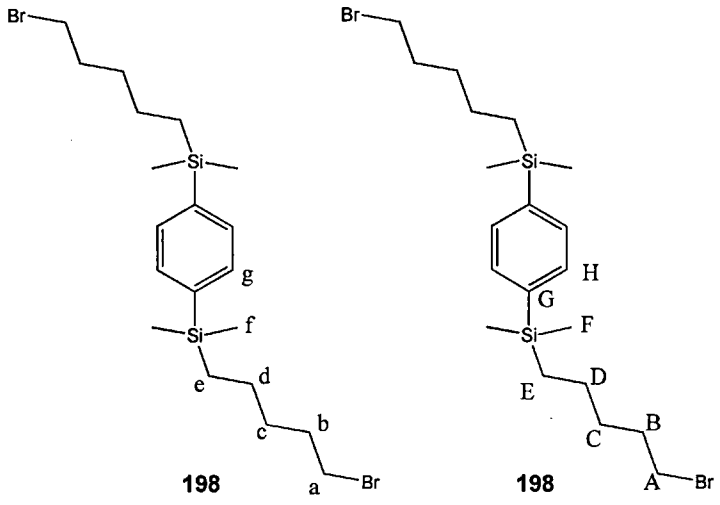

6.73: Characterisation of compound (198), proton (left) carbon (right)

6.74: Synthesis of 1,3,5-tris((5-bromopentyl)dimethylsilyl)benzene (199)

1,3,5-tri(dimethylsilyl)benzene (**193**) (1.00 g, 0.004 mol), was added to 5-bromopent-1-ene (**134**) (4 eq, 2.39 g, 0.016 mol, 1.90 ml) along with Speier's catalyst (100 µl). The reaction was sealed under argon and heated to 60 °C for 48 hours. The cooled reaction was added to DCM (100 ml) alongside activated charcoal, and refluxed for

30 minutes. The solids were removed using filtration and the solvent removed, yielding a clear oil. The oil was then placed under high vacuum for 48 hours.

Yield 1.51 g, 0.002169 mol, 54.1%

^{1}H NMR ($CDCl_3$): 0.00 (H18, s)(*f*), 0.49 (H6, t, 6.9 Hz)(*e*), 1.14 (H12, m)(*d,c*), 1.54 (H6, t, 6.8 Hz)(*b*), 3.08 (H6, t, 6.8 Hz)(*a*), 7.35 (H3, s)(*g*).

^{13}C NMR ($CDCl_3$): −3.08 (CH_3)(*F*), 15.46 (CH_2)(*E*), 23.05 (CH_2)(*D*), 31.79 (CH_2)(*C*), 32.39 (CH_2)(*B*), 33.66 (CH_2)(*A*), 137.02 (CH)(*H*), 139.11 (C)(*G*).

^{29}Si NMR ($CDCl_3$): −2.59

FTIR (thin-film NaCl plate): 2957, 2927, 1711, 1460, 1439, 1411, 1367, 1252, 1222, 1138, 1070.

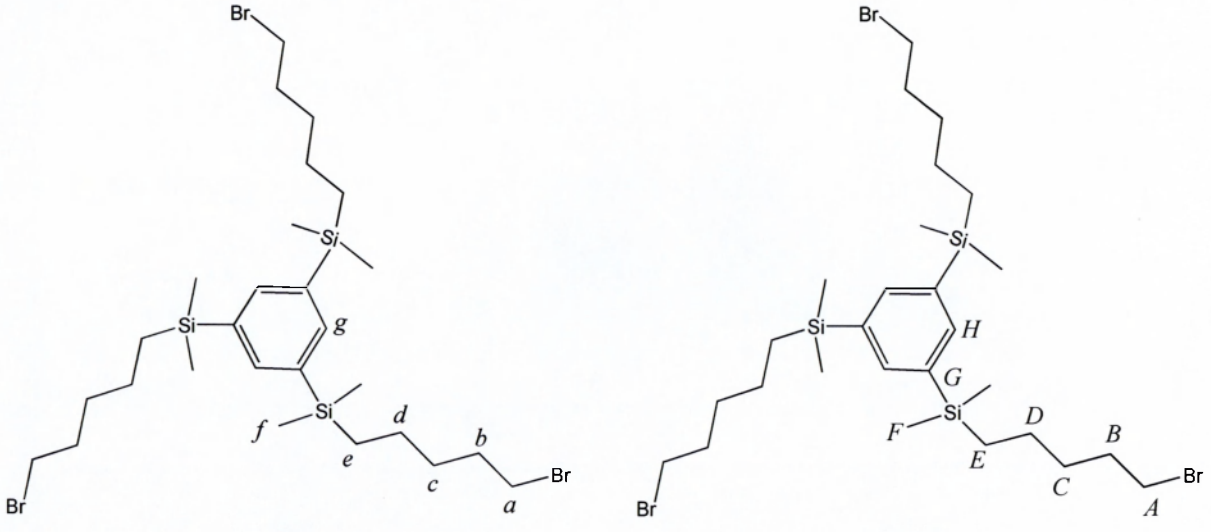

6.74: Characterisation of compound (199), proton (left) carbon (right)

6.75: Synthesis of (pentane-sDO3A-(ethyl))dimethyl(phenyl)silane (187)

sDO3A-(ethyl) (**107**) (1.15 g, 0.00152 mol) was dissolved in anhydrous acetonitrile (10 ml) to which potassium carbonate (0.90 g, 0.00666 mol) was added along with

(5-bromopentyl)dimethyl(phenyl)silane (**191**) (450 mg, 0.00158 mol). The reaction was sealed under argon and heated to 60 °C for 48 hours. The reaction was cooled and the solids removed using a centrifuge. The solvent was then removed using reduced pressure to yield a yellow oil.

The crude product was then chromatographed on silica, eluted with a gradient of 100% DCM to 95% DCM + 5% EtOH, with the fractions monitored using LCMS. Yield 550 mg, 0.0006144 mol, 40.5%

^{1}H NMR ($CDCl_3$): 0.20 (H6, s)(*n*), 0.69 (H2, t, 6.4 Hz)(*m*), 1.16 (H2, d, 3.5 Hz)(*l*), 1.19 (H4, t, 2.7 Hz)(*k,j*), 1.24 (H18, t, 6.9 Hz)(*a*), 2.20 (H2, s)(*i*), 2.43–2.65 (H22, m)(*e,f,g,h*), 3.74 (H3, m)(*d*), 4.10 (H12, q, 7.0 Hz)(*c*), 7.29 (H3, t, 3.3 Hz)(*p,q*), 7.64 (H2, dd, 2.5 Hz)(*o*).

^{13}C NMR ($CDCl_3$): −3.17 (CH_3)(*P*), 14.09 (CH_3)(*A*), 14.30 (CH_3)(*A2*), 15.65 (CH_2)(*O*), 18.28 (CH_2)(*N*), 23.77 (CH_2)(*M*), 26.43 (CH_2)(*L*), 31.48 (CH_2)(*D*), 35.31 (CH_2), 49.81 (CH_2)(*K*), 50.51 (CH_2)(*H*), 51.06 (CH_2)(*G*), 53.94 (CH_2)(*J*), 55.26 (CH_2)(*I*), 58.09 (CH)(*E*), 59.89 (CH_2), 60.38 (CH_2), 127.56 (CH)(*T*), 128.61 (CH)(*S*), 133.39 (CH)(*R*), 139.43 (C)(*Q*), 171.28 (C=O)(*C*), 171.76 (C=O)(*F*).

^{29}Si NMR ($CDCl_3$): −2.73.

FTIR: 2922, 2361, 1724, 1634, 1645, 1284, 1252, 1180, 1110, 1088.

HRMS: calculated 893.5302 [M(**187**)$^{+H}$], found 893.5286 [M(**187**)$^{+H}$]

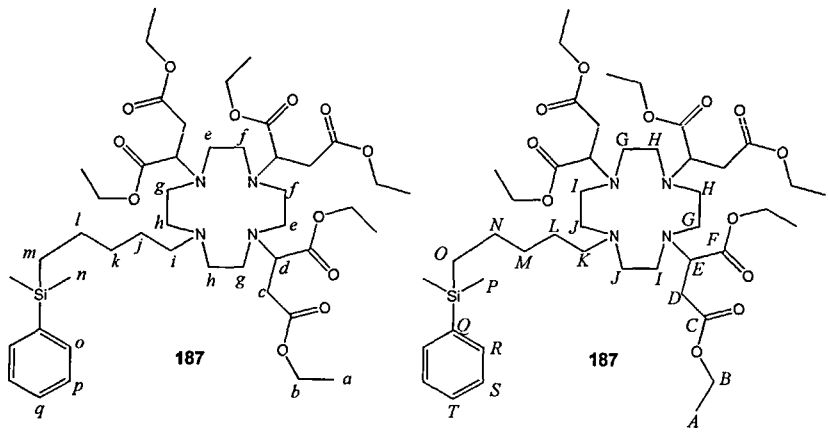

6.75: Characterisation of compound (187), proton (left) carbon (right)

6.76: Synthesis of 1,4-bis((pentane-sDO3A(ethyl))dimethylsilyl) benzene (188)

sDO3A-(ethyl) (**107**) (590 mg, 0.0008576 mol) was dissolved in acetonitrile (10 ml) to which potassium carbonate (1.00 g, 0.007407 mol) was added. To the reaction mixture 1,4-bis((5-bromopentyl)dimethylsilyl)benzene (**198**) (211 mg, 0.0004288 mol) was added and the reaction was sealed under argon and heated to 60 °C for 48 hours. The solids were removed using centrifugation and the solvent was extracted by reduced pressure. The crude product was then taken up into DCM (100 ml) to which activated charcoal was added, and then refluxed for 30 minutes. The solids were removed by filtration and the solvent by reduced pressure to yield a clear oil. The product was then chromatographed on silica eluted with a gradient of DCM (100%) to DCM (95%) / EtOH (5%), then elution with DCM (70%) / EtOH (30%), yielding the product.

Yield 0.000 1778mol, 303.7 mg, 41.5%

^{1}H NMR ($CDCl_3$): 0.22 (H12, s), 0.72 (H4, s), 1.21 (H8, m), 1.26 (H36, m), 1.9 (H4, s), 2.23–2.75 (H48, m), 3.71 (H6, m), 4.07 (H24, m), 7.49 (H4, s).

^{13}C NMR ($CDCl_3$): −3.21 (CH_3), 14.09 (CH_3), 14.30 (CH_3), 15.65 (CH_2), 18.28 (CH / CH_3), 23.77 (CH_2), 26.43 (CH_2), 31.48 (CH_2), 35.31 (CH_2), 49.81 (CH_2), 50.51 (CH_2),

51.06 (CH_2), 53.94 (CH_2), 55.26 (CH_2), 58.09 (CH), 59.89 (CH_2), 60.38 (CH_2), 127.56 (CH), 128.61 (CH), 133.39 (CH), 139.43 (C), 171.28 (C=O), 171.76 (C=O).

^{29}Si NMR ($CDCl_3$): −2.85

FTIR (thin-film NaCl plates): 2983, 2930, 1724, 1465, 1447, 1371, 1302, 1260, 1170, 1031, 909

The isotope pattern from the FAB mass spectrum matches the predicted pattern for compound (**188**)

Theoretical isotope profile: 1708.0 (92%), 1709.0 (100%), 1710.0 (62%), 1711.0 (32%), 1712 (10%). Found 1707.9 (90%), 1709.0 (100%), 1709.9 (50%), 1710.9 (36%), 1712.0(10%). Also present was a compound at 1917 m/z. 208 difference.

6.77: Synthesis of 1,3,5-tris((pentane-sDO3A(ethyl))dimethylsilyl) benzene (189)

1,3,5-bis((5-bromopentyl)dimethylsilyl)benzene (**199**) (674.5 mg, 0.00109 mol), was dissolved in acetonitrile (10 ml) to which sDO3A-(ethyl) (**107**) (2.25 g, 0.00327 mol) was added, along with potassium carbonate (2.20 g, 0.016 mol). The reaction was heated to 60 °C for 48 hours under argon, after which the solids were removed using centrifugation and the solvent was removed using reduced pressure. The crude oil was then taken up into DCM (100 ml) to which activated charcoal was added. The reaction was refluxed for 30 minutes, and the solids were removed using filtration. The solvent was then removed using reduced pressure to yield the crude product. The oil was chromatographed on silica eluted with a gradient of DCM (100%) to

DCM (95%) EtOH (5%), then to DCM (70%) EtOH (30%). The main product was found in the fractions of the DCM 70% / EtOH 30% elution range.

Yield: 0.000469 mol, 1.18 g, 43.0%

^{1}H NMR ($CDCl_3$): 0.33 (H18, s), 0.72 (H6, m), 1.37 (H72, m), 2.36–2.71 (H72, m), 3.88 (H9, m), 4.12 (H36, m), 7.69 (H3, s).

^{13}C NMR ($CDCl_3$): −3.13 (CH_3), 13.98 (CH_3), 14.25 (CH_3), 15.68 (CH_2), 18.19 (CH_3), 23.90 (CH_2), 25.96 (CH_2), 28.12 (CH_2), 31.66 (CH_2), 35.52 (CH_2), 35.17 (CH_2), 35.31 (CH_2), 46.58 (CH_2), 47.83 (CH_2), 49.81 (CH_2), 51.06 (CH_2), 53.70 (CH_2), 57.92 (CH_2), 58.54 (CH), 59.88 (CH), 60.33 (CH_2), 60.37 (CH_2), 60.53 (CH_2), 137.23 (CH), 139.05 (C), 171.33 (C=O), 171.82 (C=O).

FTIR (flush sample $CDCl_3$, NaCl plate): 2981, 2932, 2854, 2360, 2258, 1729, 1448, 1372, 1299, 1254, 1175, 1030

^{29}Si NMR ($CDCl_3$): −2.83

6.78: Hydrolysis of (sDO3A- (ethyl)-pentyl)dimethyl(phenyl) (187) to form (pentane-sDO3A-)dimethyl(phenyl)silane (200)

(sDO3A- (ethyl)-pentyl)dimethyl(phenyl) (187) (0.55 g, 0.0006162 mol) was dissolved in 1M LiOH (5 ml) and heated to 100 °C for 24 hours. The solution was cooled to room temperature, then was injected into the head of the ion-exchange column containing Bio-Rad AG1 A4I (OH^- form), bed volume 500 cm^3, eluting with ultra-pure water at a rate of 5 ml/min. After collection of 500 ml of eluent, the eluent was changed to formic acid (1M), while the fraction was collected in 5 ml units and

analysed using negative-ion LCMS. The solvent was removed from the product-containing fractions by lyophilisation to yield a white solid, which was then dissolved in water (10 ml) and the lyophilisation repeated.

Yield 143 mg, 0.0001974 mol, 32%.

^{1}H NMR (D_2O): 0.00 (H6, s), 0.53 (H2, s), 1.09 (H4, s), 1.43 (H2, s), 2.11–2.79 (H24, m), 3.83 (H3, m), 7.17 (H3, m), 7.39 (H2, m).

^{13}C NMR (D_2O): −3.21 (CH_3), 129.03 (CH), 131.52 (CH), 135.11 (CH), 137.21 (C).

^{29}Si NMR (D_2O): −2.80

CHN analyses: found C 46.64%, H 6.69%, N 6.9%; calculated to be dimethyl(phenyl)silane-pentyl-sDO3A $(HCOOH)_3$, $(H_2O)_3$, $(NH_4)_{0.5}$ (C 46.72%, H 7.13%, N 6.81%).

FTIR (KBr disk): 3012, 2880, 2583, 1726, 1512, 1485, 1376, 1327, 1296.

6.79: Hydrolysis of 1,4,bis-(sDO3A-(ethyl)-pentyl)dimethyl(phenyl) (188) to form 1,4-bis((pentane-sDO3A)dimethylsilyl)benzene (201)

Bis-dimethyl(phenyl)silane-pentyl-sDO3A-(ethyl) (**188**) (1.72 g, 0.001 mol) was dissolved in LiOH (5 ml) and heated to 100 °C for 24 hours. The solution was cooled to room temperature, then was injected into the head of the ion-exchange column containing Bio-Rad AG1 A4I (OH^- form), bed volume 500 cm^3, eluting with ultra-pure water at a rate of 5 ml/min. After collection of 500 ml of eluent, the eluent was changed to formic acid (1M), while the fraction was collected in 5 ml units and analysed using negative-ion LCMS. The solvent was removed from the product-containing fractions by lyophilisation to yield a white solid, which was then dissolved in water (10 ml) and the lyophilisation repeated.

Yield, 629 mg, 0.00046 mol, 46%

^{1}H NMR (D_2O): 0.00 (H12, s)(*j*), 0.89 (H4, s)(*i*), 1.06 (H4, s,)(*h*), 1.09 (H4, s)(*g*), 2.47 (H44, m)(*b,d,e,f*), 3.89 (H6, m)(*c*), 7.62 (H4, m)(*k*).

FTIR: 3218, 3052, 2953, 2576, 1927, 1725, 1631, 1580, 1467, 1392, 1248, 1187, 1135, 1086.

CHN analysis: found C 40.45%, H 6.27%, N 6.61%; calculated bis-dimethyl(phenyl)silane-pentyl-sDO3A $-(HCOO^-)_{10}$, $(NH_4)_1$, $(H_2O)_{12}$ (C 40.91%, H 6.62%, N 6.13%).

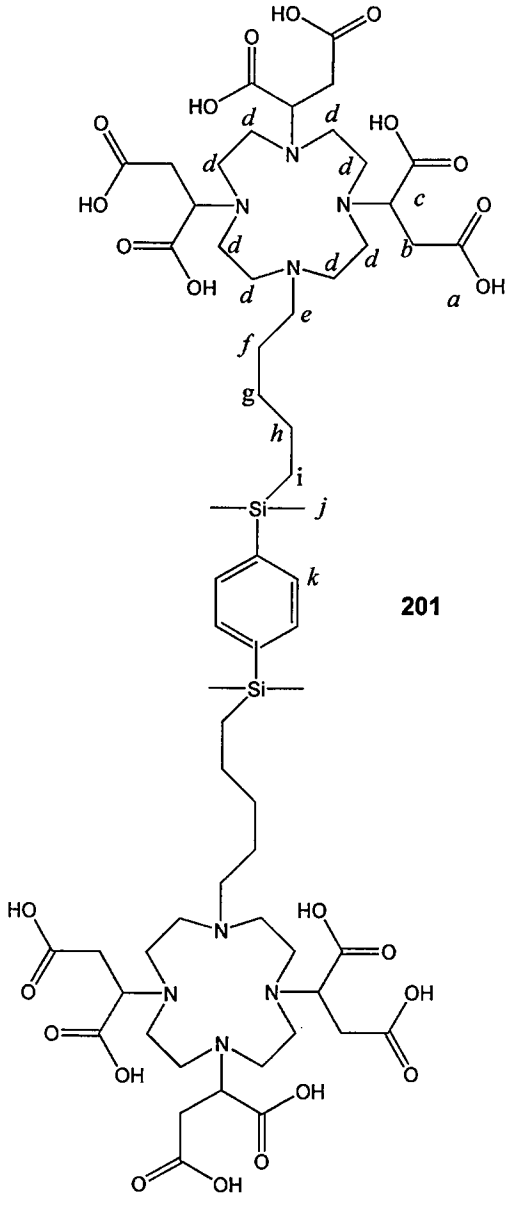

201

6.79: Characterisation of compound (201), proton (left) carbon (right)

6.80: Hydrolysis of 1,3,5,-tris-(sDO3A-(ethyl)-pentyl)dimethyl(phenyl) (232) to form 1,3,5-tris((pentane-sDO3A)dimethylsilyl)benzene (202)

1,3,5-Tris-dimethyl(phenyl)silane-pentyl-sDO3A-(ethyl) (**189**) (2.00 g, 0.000788 mol) was dissolved in LiOH (25 ml) and heated to 100 °C for 48 hours, forming a colloidal solution. The solution was filtered through a 5 µm glass-fibre filter pad, then the solution was neutralised using formic acid (1M). The solution was lyophilised to form

a white solid, which was then taken up into LiOH (1M) (50 ml) forming a clear solution. The solution was injected into the head of the ion-exchange column containing Bio-Rad AG1 A4I (OH^- form), bed volume 500 cm^3, eluting with ultra-pure water at a rate of 5 ml/min. After collection of 500 ml of eluent, the eluent was changed to formic acid (1M), while the fraction was collected in 5 ml units and analysed using negative-ion LCMS [$1/32M(202)^{-H}$] ≈ 64. The solvent was removed from the product-containing fractions by lyophilisation to yield a white solid, which was then dissolved in water (10 ml) and lyophilisation was repeated.

Yield 283 mg, 0.00014 mol, 18%

^1H NMR (D_2O): −0.05 (H18, s), 0.48 (H6, s), 0.87 (H6, s), 1.15 (H6, s), 1.60 (H6, s), 2.35–3.03 (H72, m), 3.93 (H9, m), 7.46 (H3, s).

^{13}C NMR (D_2O): −3.41, 20.25, 30.79, 31.27, 31.32, 67.40, 179.48.

^{29}SI NMR (D_2O): −2.83

FTIR (KBr disk): 3402, 3132, 2975, 2858, 1734, 1639, 1597, 1384, 1251, 1179.

Elemental analyses C 0.32%, H 7.25%, N 7.82%; theory C 51.77%, H 7.16%, N 8.32%; calculated C 50.92%, H 7.30%, N 7.82% for $C_{87}H_{144}N_{12}O_{36}Si_3$ $(H_2O)_{3.3}$

6.81: Luminescence emission defaults

The luminescence emissions were recorded on a Fluoromax-P (Jobin–Yvon, England). Samples were placed in a 3 ml, 1 cm path-length quartz fluorescence cuvette and measured using right-angle geometry. The excitation wavelength was set at 395 nm with a slit size of 2 nm, and the emissions obtained were in the range 550–750 nm with 0.5 nm increments, with slits set at 0.2 nm. These settings were derived by experimentation until the optimum resolution of the graph was obtained.

The samples were dissolved in ultra-pure water, at a concentration of 1 mg/ml. As the lanthanides are not quenched by O_2, there was no need for degassing of the solvent prior to luminescence analysis.[119] The measurements were taken at room temperature and at the compounds' natural pH.

6.82: Formation of butene-sDO3A-(ethyl)-Gd (203)

Butene-sDO3A-(ethyl) (**101**) (600 mg, 0.00081 mol) was dissolved in EtOH (3 ml), to which $GdCl_3$ (180 mg, 0.00068 mol) was added. The reaction was refluxed for 48 hours. The cooled reaction was added to ice-cold diethyl ether (25 ml). The solid formed was collected by centrifuge and washed with cold diethyl ether (2 x 50 ml) and dried under vacuum. The solid was taken up into methanol (1 ml) and room-temperature diethyl ether added until precipitation occurred. The sample was then cooled to −18°C for 18 hours. The solid formed was collected by centrifugation.

Yield 180 mg, 24.6%. Decomposes at 275 °C. FTIR (KBr disk): 3376, 2360, 1732, 1615, 1440, 1242.

Elemental Analyses: Found C% 27.66, H 5.28%, N, 4.64%, Calculates to butene-sDO3A-(ethyl) –Gd .$35H_2O$. $K_{11}Cl_{16}N_6H_{18}$. predicted as (C 22.68%, H 4.04.45%, N 3.31%)

6.83: Formation of butene-sDO3A-(ethyl)-Eu (204)

Butene-sDO3A-(ethyl) (**101**) (370 mg, 0.00049 mol) was dissolved in EtOH (3 ml), to which $EuCl_3$ (118 mg, 0.000456 mol) was added. The reaction was refluxed for 48 hours. The cooled reaction was added to ice-cold diethyl ether (25 ml). The solid formed was collected by centrifuge and washed with cold diethyl ether (2 x 50 ml) and dried under vacuum. The solid was taken up into methanol (1 ml) and room-temperature diethyl ether added until precipitation occurred. The sample was then cooled to −18 °C for 18 hours. The solid formed was collected by centrifugation.

Yield 109 mg, 0.000127 mol, 24.8%

FTIR (KBr disk): m 2268, 2984, 2360, 1728, 1641, 1467, 1278, 1179.

MADLI-MS: Predicted 757.92 [butene-sDO3A-(ethyl)-Eu+H]-Eu. Found 757.4 [butene-sDO3A-(ethyl)-Eu+H]-Eu.

6.84: Formation of sDO3A-(ethyl)-Gd (205)

sDO3A-(ethyl) (**107**) (400 mg, 0.00058 mol) was dissolved in EtOH (2 ml) to which $GdCl_3$ (139 mg, 0.00051 mol) was added. The reaction was refluxed for 24 hours. The cooled reaction was added to ice-cold diethyl ether (25 ml). The solid formed was collect3ed by centrifuge and washed with cold diethyl ether (2 x 50 ml) and dried under vacuum. The solid was taken up into methanol (1 ml) and room-temperature diethyl ether added until precipitation occurred. The sample was then cooled to −18 °C for 18 hours. The solid formed was collected by centrifugation.

Yield: 227 mg, 0.000268 mol, 46.3%.

FTIR (KBr disk): 3397, 1729, 1594, 1439, 1371, 1302, 1179, 1089.

Elemental Analyses: Found C% 22.69, H 4.11%, N, 3.32%, Calculates to sDO3A-(ethyl) –Eu .10.25H_2O. 9KCl predicted as (C 22.58%, H 4.53%, N 3.29%)

6.85: Formation of sDO3A-(ethyl)-Eu (206)

sDO3A-(ethyl) (**107**) (457 mg, 0.00069 mol) was dissolved in EtOH (2 ml) to which $EuCl_3$ (162 mg, 0.000627 mol) was added. The reaction was refluxed for 24 hours. The cooled reaction was added to ice-cold diethyl ether (25 ml). The solid formed was collected by centrifuge and washed with cold diethyl ether (2 x 50 ml) and dried under vacuum. The solid was taken up into methanol (1 ml) and room-temperature diethyl ether added until precipitation occurred. The sample was then cooled to −18 °C for 18 hours. The solid formed was collected by centrifugation.

Yield: 356 mg, 0.00052 mol, 75.4%.

FTIR (KBr disk): 3429, 2920, 2857, 2360, 1601, 1441, 1314, 1268, 1185, 1153, 1094.

Elemental Analyses: Found C% 22.37, H 4.01%, N, 3.98%, Calculates to sDO3A-(ethyl) –Eu .$6H_2O$. 10KCl predicted as (C 22.68%, H 4.45%, N 3.31%)

6.86: Formation of sDO3A-Gd (207)

sDO3A (**32**) (108 mg, 0.0002105 mol) was dissolved in HCl solution (2 ml, pH 3) to which Gd_2O_3 (37.8 mg 0.000105 mol) was added. The reaction was then heated to 80 °C for 24h, after which it was allowed to cool, and then passed through a 5 µm filter. The resulting filtrate was freeze-dried, producing a white solid.

Yield 112 mg, 0.0001659 mol, 78.8%

FTIR (KBr disk): 3229, 2981, 2830, 2254, 1631, 1415, 1368, 1311, 1274, 1222, 1204, 1174.

CHN analyses: found C 23.17%, H 3.69%, N 5.1%; calculated sDO3A-Gd-K_6 $(HCOOH)_{3.4}$ (C 23.50%, H 3.24%, N 5.48%).

6.87: Formation of sDO3A-Eu (208)

sDO3A (**32**) (20 mg, 0.0000384 mol) was dissolved in water (5 ml) to which to which Eu_2O_3 (6.8 mg 0.0000194 mol) was added. The reaction was then refluxed for 24 hours, after which it was allowed to cool, and then passed through a 5 μm filter. The resulting filtrate was freeze-dried, producing a white solid.

Yield 21 mg, 0.00003133 mol, 81.5%

FTIR (KBr disk): 3420, 2975, 2921, 2884, 1720, 1592, 1413, 1186, 1091

MALDIMS: Predicted 743.91 [sDO3A-(ethyl)-Eu^{+H}]-Eu, Found 743.40 [sDO3A-Ethyl)-Eu^{+H}]-Eu.

6.88: Formation of sDO2A-Gd (209)

sDO2A (**138**) (200 mg, 0.00049 mol) was dissolved in MeOH (2 ml) to which $GdCl_3$ (118 mg, 0.00045 mol) was added and the reaction refluxed for 48 hours, after which it was allowed to cool, and then passed though a 5 μm filter. The resulting filtrate was freeze-dried, producing a white solid.

Yield: 104 mg, 0.000186 mol, 38%

FTIR (KBr disk): 3366 (OH), 2357, 1724 (C=O), 1630 (N–C), 1440, 1368, 1289, 1229, 1090.

Sample used for relaxation measurements resulting in not enough sample for elemental analysis.

6.89: Formation of sDO2A-Eu (210)

sDO2A (**138**) (200 mg, 0.00049 mol) was dissolved in MeOH (2 ml) to which $EuCl_3$ (116 mg, 0.00045 mol) was added and the reaction refluxed for 48 hours, after which it was allowed to cool, and then passed though a 5 μm filter. The resulting filtrate was freeze-dried, producing a white solid.

Yield: 235 mg, 0.0004233mol, 68.3%

FTIR (KBr disk): 3501, 3261, 2951, 2759, 2415, 2141, 1730, 1627, 1440, 1361, 1280, 1220, 1094, 1003.

Elemental Analyses: Found C% 28.54, H 4.95%, N, 9.03%, Calculates to sDO2A-Gd.$6H_2O$ predicted as (C 28.86%, H 5.45%, N 8.41%)

6.90: Formation of DOTA-Gd (2)

DOTA (**13**) (43 mg, 0.000106 mol) and Gd_2O_3 (19.25 mg, 0.0000531 mol) were dissolved in HCl solution (2 ml, pH 3) and refluxed for 25 hours, after which the mixture was allowed to cool and was then passed through a 5 μm filter. The resulting filtrate was freeze-dried, producing a white solid.

Yield: 57 mg, 0.000102mol, 96%

FTIR (KBr disk): 3400, 2984, 2916, 2361, 1728, 1579, 1448, 1407, 1321, 1243, 1156, 1084, 1003.

Elemental Analyses: Found C% 28.54, H 4.95%, N, 9.03%, Calculates to DOTA-Gd. $(H_2O)_{5.75}$ predicted as (C 29.06%, H 5.411%, N 8.47%)

6.91: Formation of DOTA-Eu (211)

DOTA (**13**) (75mg, 0.000185 mol) and Eu_2O_3 (45.5mg, 0.0000531 mol) were dissolved in HCl solution (2ml, pH 3) and refluxed for 25 hours, after which the mixture was allowed to cool and was then passed through a 5 μm filter. The resulting filtrate was freeze-dried to produce a white solid.

Yield: 57 mg, 0.000102 mol, 96%

FTIR (KBr disk): 3400. 3099, 2359, 1731, 1576, 1443, 1411, 1322, 1250, 1217, 1158, 1084.

Florescence spectra match that of published data.

6.92: Formation of (pentane-sDO3A-)dimethyl(phenyl)silane-Gd (212)

Dimethyl(phenyl)silane-pentyl-sDO3A (**188**) (11.3 mg, 0.0000157 mol) was dissolved in water (10 ml) to which Gd_2O_3 (2.8 mg, 0.00000785 mol) was added. The pH of the solution was adjusted from pH 5 to pH 8–8.5 by addition of LiOH (1M) solution. The reaction was then heated to 80 °C for 48 hours. The solution was cooled and the

solids removed using a centrifuge, then the solution was decanted and passed though a 0.5 μm filter. The solution was lyophilised, producing a white powder.

Yield 10mg, 0.000011487 mol, 73%

CHN analyses: found C 41.15%, H 5.34%, N 6.05%; calculated [dimethyl(phenyl)silane-pentyl-sDO3A-Gd]-$(HCOOH)_{1.5}$, $(H_2O)_{2.8}$ (C 41.49%, H 5.81%, N 5.61%).

FTIR (KBr disk): 3415, 2954, 2932, 2867, 2359, 1587, 1392, 1317, 1252, 1182, 1153, 1115, 1084.

6.93: Formation of (pentane-sDO3A-)dimethyl(phenyl)silane-Eu (213)

(pentane-sDO3A-)dimethyl(phenyl)silane (**188**) (26.7 mg, 0.000031 mol) was dissolved in water (20 ml) to which Eu_2O_3 (5.5 mg, 0.0000155 mol) was added. The pH was adjusted from pH 5 to pH 8.5 using LiOH and the reaction was heated to 80 °C for 48 hours. The solution was centrifuged and then passed though a 0.5 µm filter, after which it was lyophilised, producing a white powder.

Yield 22.5 mg, 0.0000257 mol, 83%

FTIR (KBr disk): 3417, 2954, 2932, 2867, 2359, 1588, 1393, 1317, 1253, 1184, 1152, 1115, 1083.

6.94: Formation of 1,4-bis((pentane-sDO3A)dimethylsilyl)benzene-Gd_2 (214)

1,4-bis((pentane-sDO3A)dimethylsilyl)benzene (**188**) (60 mg, 0.00004377 mol) was dissolved in water (10 ml) to which Gd_2O_3 (7.9 mg, 0.00002188 mol) was added. The pH of the solution was raised from pH 5 to pH 8.5 by addition of LiOH (1M). The reaction was then heated to 80 °C for 24 hours. The cooled reaction was passed though a 0.5 µm filter and lyophilised, producing a white powder.

Yield 61 mg, 0.000036 mol, 83%

CHN analysis: found C = 38.78%, H = 6.04%, 5.94%; calculated C = 38.74%, H = 6.07%, N = 6.02%. $C_{60}H_{92}N_8O_{24}Si_2Gd_2.(H_2O)_{10}$

FTIR (KBr disk): 3427, 2957, 2849, 1592, 1418, 1248, 1102.

6.95: Formation of 1,4-bis((pentane-sDO3A)dimethylsilyl)benzene-Eu_2 (215)

1,4-bis((pentane-sDO3A)dimethylsilyl)benzene (**188**) (60 mg, 0.00004377 mol) was dissolved in water (10 ml) to which Eu_2O_3 (7.7 mg, 0.00002188 mol) was added. The pH of the solution was raised from pH 5 to pH 8.5 by addition of LiOH (1M). The reaction was then heated to 80 °C for 24 hours. The cooled reaction was passed though a 0.5 µm filter and lyophilised, producing a white powder.

Yield 59mg, 0.0000352 mol, 80%

FTIR (KBr disk): 3427, 2959, 2851, 1623, 1599, 1589, 1417, 1368, 1248, 1168, 1135.

CHN analysis: found C = 31.06%, H = 5.51%, N = 4.78%; calculated C = 31.12%, H = 6.18 %, N = 4.83 %. $C_{60}H_{92}N_8O_{24}Si_2Eu_2.(H_2O)_{25}K_4$

6.96: Formation of 1,3,5-tris((pentane-sDO3A)dimethylsilyl) benzene-Gd_3 (216)

1,3,5-tris((pentane-sDO3A)dimethylsilyl) benzene (**189**) (60 mg, 0.0000297 mol) was dissolved in water (10 ml) to which Gd_2O_3 (5.4 mg, 0.0000148 mol) was added. The pH of the solution was raised from pH 5 to pH 8.5 by addition of LiOH (1M). The reaction was then heated to 80 °C for 24 hours. The cooled reaction was passed though a 0.5 µm filter and lyophilised, producing a white powder.

FTIR (KBr disk): 3399, 2360, 1596, 1419. 1315, 1249, 1085

Yield: 58.3 mg, 0.0000235 mol, 79.2%

CHN analysis: found C = 28.51%, H = 5.21%, N = 4.41%; calculated C = 28.84%, H = 5.81%, N = 4.41%. 1,3,5-tris((pentane-sDO3A)dimethylsilyl) benzene-$Gd_3.(H_2O)_{22}(HCOOH)_{15}$, K_6.

6.97: Formation of 1,3,5-tris((pentane-sDO3A)dimethylsilyl) benzene-Eu_3 (217)

1,3,5-tris((pentane-sDO3A)dimethylsilyl) benzene (**189**) (60 mg, 0.0000297 mol) was dissolved in water (10 ml) to which Eu_2O_3 (5.2 mg, 0.0000148 mol) was added. The pH of the solution was raised from pH 5 to pH 8.5 by addition of LiOH (1M). The reaction was then heated to 80 °C for 24 hours. The cooled reaction was passed though a 0.5 µm filter and lyophilised, producing a white powder.

FTIR (KBr disk): 3414, 2964, 2927, 2857, 1589. 1414.30

Elemental analysis: found C 40.72%, H 5.67%, N 6.18%; calculated C 40.60%, H 5.75%, N 6.52% for 1,3,5-tris((pentane-sDO3A)dimethylsilyl)benzene-Eu + $6H_2O$.

Yield: 59 mg, 0.000024 mol, 81%

6.98: MOPS buffer – (10mmol)

4-Morpholinepropanesulfonic acid (2.09 g, 10 mmol) was dissolved in ultra-pure water (1000 ml). The pH of the solution was then adjusted using ammonia solution to pH 7.72.

6.99: Anionic background, simulated extracellular environment

The anionic background used for the pH measurements was taken from Messeri et al.[19] The original make-up of the background required potassium lactate and potassium citrate. These were not available, so were substituted by the sodium forms. This was accounted for and the amount of NaCl added was adjusted, along with the addition of KCl to keep the ion concentration and composition the same.

	concentration	*water – 500 ml*	*D_2O – 25 ml*
$NaHCO_3$	30 mM	126 mg	63 mg
NaCl	96.57 mM	2819 mg	140 mg
KCl	3.43 mM	128 mg	6.4 mg
KH_2PO_4	0.9 mM	103 mg	5.1 mg
Na lactate	3.3 mM	185 mg	9.2 mg
Na citrate	0.13 mM	19 mg	1 mg

Chapter 7: References

1. Lauterbur, P. C., Image Formation by Induced Local Interactions: Examples Employing Nuclear Magnetic Resonance. . Nature 1973, (242), 190-191.

2. Clow, H.; Young, I. R., Britain's brains produce first NMR scans New Scientist 1979, 1978, p 8.

3. McRobbie, D. W.; Moore, E. A.; Graves, M. J.; Prince, M. R., MRI from picture to proton. University Press: Cambridge, 2003; p 359.

4. Bottrill, M.; Kwok, L.; Long, N. J., Lanthanides in magnetic resonance imaging. Chem. Soc. Rev. 2006, 35, 557-571.

5. Cajoling Wilhelm, Image: MRI head saggital.jpg. In Wikipedia: 2007.

6. Hollas, J. M., Modern Spectroscopy. Third ed.; Wiley: Chichester, 1996; p 391.

7. Mansson, S.; Bjornerud, A., Physical principles of medical imaging by nuclear magnetic resonance. . In The chemistry of contrast agents in medical magnetic resonance imaging, Merbach, A. E., Ed. John Wiley & sons, LTD: 2001; pp 1-44.

8. Silverstein, R. M.; Webster, F. X., Spectrometric Identification of Organic Compounds. 6 ed.; John Wiley & Sons, Inc: New York, 1998; p 482.

9. Willard, H. H.; Merritt, L. L.; Dean, J. A.; Settle, F. A., Instrumental methods of analysis. 7th ed.; Wadsworth: 1988; p 895.

10. Mohr, P. J.; Taylor, B. N., CODATA recommended values of the fundamental physical constants: 1998. Reviews of Modern Physics 2000, 72, (2), 145.

11. Hendee, W. R.; Ritenour, E. R., Medical Imaging Physics. 4th ed.; Wiley-Liss: New York, 2002; p 511.

12. Farr, R. F.; Allisy-Roberts, P. J., Physics for Medical Imaging. Harcourt Publishers Limited: London, 1998; p 276.

13. Portal, M. R.-T. I. Sagittal Knee MRI Images STIR http://www.mr-tip.com/serv1.php?type=img&img=Sagittal%20Knee%20MRI%20Images%20STIR

14. MR-TIP Sagittal Knee MRI Images T1 weighted. http://www.mr-tip.com/serv1.php?type=img&img=Sagittal%20Knee%20MRI%20Images%20T1%20Weighted (9th June 2007),

15. Caravan, P., Strategies for increasing the sensitivity of gadolinium based MRI contrast agents. Chem. Soc. Rev. 2006, 35, 512-523.

16. Jacques, V.; Desreux, J. F., New Classes of MRI Contrast Agents. Topics in Current Chemistry 2002, 221, 125-164.

17. Song, B.; Storr, T.; Lui, S.; Orvig, C., Synthesis and solution studies of the complexes of trivalent lanthanides with the tetraazamacrocycle TETA-(PO)2. Inorg. Chem. 2002, 41, 685-692.

18. Caravan, P.; Ellison, J. J. E.; McMurry, T. J.; Lauffer, R. B., Gadolinium (III) chelates as MRI contrast agents: structure, Dynamics and applications. Chem. Rev. 1999, 99, 2293-2352.

19. Messeri, D.; Lowe, M. P.; Parker, D.; Botta, M., A stable, high relaxivity, diaqua gadolinium complex that suppresses anion and protein binding. Chem. Commun. 2001, 2742-2743.

20. Elst, L. V.; Raynal, I.; Port, M.; Tisnes, P.; Muller, R. N., In vitro relaxometric and luminescence characterization of P792 (Gadomelitol, Vistarem), an efficient and rapid clearance blood pool MRI contrast agent. Eur. J. Inorg. Chem. 2005, (6), 1142-1148.

21. Crespigny, A. J.; Howard, D.; DÁrceuil, H.; Muller, H.; Agoston, A. T.; Seri, S.; Hashiguchi, Y.; Fujimoto, C.; Nakatani, A.; Moseley, M. E., Dynamic contrast-enhanced MRI of implanted VX2 tumours in rabbit muscle: comparison of Gd-DTPA and NMS60. Magnetic Resonance Imaging 1999, 17, (9), 1297-1305.

22. Xu, H.; Regino, C. A. S.; Bernardo, M.; Koyama, Y.; Kobayashi, H.; Choyke, P. L.; Breachiel, M. W., Towards improved syntheses of dendrimer-based magnetic resonance imaging contrast agents: New bifunctional diethylenetriaminepentaacetic acid ligands and non aqueous conjugation chemistry. . J. Med. Chem. 2007, 50, 3185-3193.

23. Dewey, M.; Kaufels, N.; Laule, M.; Schnorr, J.; Wagner, S.; Kivelitz, D.; Raynaud, J.; Robert, P.; Hamm, B.; Taupitz, Assessment of myocardial infarction in pigs using a rapid clearance blood pool contrast medium. Magnetic Resonance in Medicine 2005, 51, 703-709.

24. Jebasingh, B.; Alexander, V., Synthesis and relaxivity studies of a tetranuclear gadolinium(III) complex of DO3A as a contrast-enhancing agent for MRI. Inorg. Chem. 2005, 44, (25), 9434-9443.

25. Messeri, D.; Lowe, M. P.; Parker, D.; Botta, M., A stable, high relaxivity, diaqua gadolinium complex that suppresses anion and protein binding. Chem. Commun 2001, 2742-2743.

26. Doble, D. M. J.; Botta, M.; Wang, J.; Aime, S.; Barge, A.; Raymond, K. N., Optimization of the relaxivity of MRI contrast agents: Effect of poly(ethylene glycol) chains on the water-exchange rates of Gd(III) complexes. J. Am. Chem. Soc 2001, 123, 10758-10759.

27. Xu, J.; Churchill, D. G.; Botta, M.; Raymond, K. N., Gadolinium(III) 1,2-hydroxypyridonate-based complexes: Towards MRI contrast agents of high relaxivity. Inorg. Chem. Commun. 2004, 43, 5492-5494.

28. Aime, S.; Botta, M.; Bruce, J. I.; Mainero, V.; Parker, D.; Terreno, E., Modulation of the water exchange rates in [Gd-DO3A] complex by formation of ternary complexes with carboxylate ligands. Chem. Commun 2001, 115-116.

29. Messeri, D.; Lowe, M. P.; Parker, D.; Botta, M., A stable, high relaxivity, diaqua gadolinium complex that suppresses anion and protein binding. Chem. Commun 2001, 2742-2743.

30. Woods, M.; Aime, S.; Botta, M.; Howard, J. A. K.; Moloney, J. M.; Navet, M.; Parker, D.; Port, M.; Rousseau, O., Correlation of water exchange rate with isomeric composition in diasteroisomeric gadolinium complexes of tetra(carboxyethyl)dota and related macrocyclic ligands. J. Am. Chem. Soc 2000, 122, 9781-9792.

31. Lewin, A.; Hill, J. P.; Boetzel, R.; Georgiou, T.; James, R.; Kleanthous, C.; Moore, G. R., Site-specific labelling of proteins with cyclen-bound transition metal ions. Inorganica. Chemica. Acta 2002, 331, 123-130.

32. Hancock, R. D.; Dobson, S. M.; Evers, A.; Wade, P. W.; Ngwenya, M. P.; Boeyens, J. C. A.; Wainwright, K. P., More rigid macrocyclic ligands that show metal ion size-based selectivity. A crystallographic, molecular mechanics, and formation constant study of the complexes of bridged cyclen. J. Am. Chem. Soc 1988, 110, 2788-2794.

33. Antunes, P.; Campello, P. M.; Delgado, R.; Drew, M. G. B.; Felix, V.; Santos, I., Metal complexes of a tetraazacyclophane: solution and molecular modelling studies. Dalton Trans 2003, 1852-1860.

34. Li, C.; Wong, W. T., A convenient method for the preparation of mono N-alkylated cyclams and cyclens in high yields. Tetrahedron letters 2002, 43, 3217-3220.

35. Zucchi, G.; Scopelliti, R.; Bunzli, J. C. G., Importance of the chromophore orientation to the ligand-to-metal energy transfer in lanthanide complexes with pendant-arm fitted cyclen derivatives. J. Chem. Soc. Dalton Trans 2001, 13, 1975-1985.

36. Hovland, R.; Aasen, A. J.; Klaveness, J., Preparation and in vitro evaluation of GdDOTA-(BOM)4; a novel angiographic MRI contrast agent. Org. Biomol. Chem. 2003, 1, 1707-1710.

37. Raghunand, R.; Zhang, S.; Sherry, A. D.; Gilles, R. J., In vivo magnetic resonance imaging of tissue pH using novel pH-sensitive contrast agent, GdDOTA-4AmP1. Acad Radiol 2002, 9, (2), S481-S483.

38. Woods, M.; Zhang, S.; Ebron, V. H.; Sherry, A. D., pH-Sensitive modulation of the second hydration sphere in lanthanide (III) tetraamide-DOTA complexes: A novel approach to smart MR contrast media. Chemistry, A European Journal. 2003, 9, (19), 4634-4640.

39. Gerweck, L. E.; Seetharaman, K., Cellular pH gradient in tumour versus normal tissue: Potential exploitation for the treatment of cancer. Cancer Research 1996, 56, 1194-1198.

40. Elst, L. V.; Port, M.; Raynal, I.; Simonot, C.; Muller, R. N., Physicochemical characterization of P760, a new macromolecular contrast agent with high relaxivity. Eur. J. Inorg. Chem. 2003, 2495-2501.

41. Simon, G. H.; Daldrup-Link, H. E.; Rummeny, E. J., MR Imaging of hepatic metastases. MR. Imaging. Decisions. 2003, 1, 19-28.

42. Schuhmann-Giampieri, G., Invest. Radiol 1993, 8, 753-761.

43. Peters, J. A.; Huskens, J.; Raber, D. J., J. Prog. Nucl. Magn. Reson. Spectroscopy. 1996, (28), 283-350.

44. Jin, T.; Zhao, S.; Xu, G.; Han, Y.; Shi, N.; Ma, Z., Huaxue Xuebao 1991, (1991), 569-575.

45. Inoue, M. B.; Inoue, M.; Fernando, Q., Inorg. Chem. Acta 1995, 232, 203-206.

46. Caravan, P.; Ellison, E. T.; McMurry, T. J.; Lauffer, R. B., Gadolinium(III) chelates as MRI contrast agents: Structure, dynamics, and applications. Chem. Rev. 1999, 99, 2293-2352.

47. Strijkers, G. J.; Mulder, W. J.; van Heeswijk, R. B.; Frederik, P. M.; Bomans, P.; Magusin, P. C.; Nicolay, K., Relaxivity of liposomal paramagnetic MRI contrast agents. MAGMA 2005, 18, (4), 186-192.

48. Jacques, V.; Desreux, J. F., New Classes of MRI Contrast Agents. Topics in Current Chemistry 2002, 221, 125-164.

49. Andre, J. P.; Toth, E.; Fischer, H.; Seelig, A.; Macke, H. R.; Merbach, A. E., High relaxivity for monomeric Gd(DOTA)-based MRI contrast agents, Thanks to micellar self-organization. J. Eur. Chem. 1999, 5, (10), 2977-2983.

50. Group, B. http://www.neuro.gatech.edu/groups/bellamkonda/newprojects/contrast.html.

51. Botnar, R. M.; Buecker, A.; Wiethoff, A. J.; Parsons, E. C.; Katoh, M.; Katsimaglis, G.; Weisskoff, R. M.; Lauffer, R. B.; Gramham, P. B.; Gunther, R. W.; Manning, W. J.; Spuentrup, E., In vivo magnetic resonance imaging of coronary thrombosis using a fibrin-binding molecular magnetic resonance contrast agent. Circulation 2004, 110, 1463-1466.

52. Pharmaceuticals, E. EXIP Pharmaceuticals: MS-325.

53. Caravan, P.; Greenfield, M. T.; Li, X.; Sherry, A. D., The Gd3+ complex of a fatty acid analogue of DOTP binds to multiple albumin sites with variable water relaxivity. Inorganic Chemistry 2001, 40, 6580-6587.

54. Kang, S. I.; Ranganthan, R. S.; Emswiler, J. E.; Kumar, K.; Gougoutas, J. Z.; Malley, M. F.; Tweedle, M. F., Synthesis, characterization and crystal structure of the gadolinium (III) chelates of (1R, 4R, 7R)-a,a',a''=trimethyl-1,4,7,10-tetraazacyclododecane-1,4,7-triacteic acid (DO3MA). Inorg. Chem. 1993, 32, 2912-2918.

55. Masui, T.; Saeed, M.; Wendland, M. F.; Higgins, C. B., Occlusive and reperfused myocardial infarcts: MR imaging differentiation with non-ionic Gd-DTPA-BMA. Radiology 1991, 181, (1), 77-83.

56. Aime, S.; Botta, M.; Crick, S. G.; Giovenzana, G.; Pagliarin, R.; Sisti, M.; Terreno, E., NMR relaxometric studies of Gd(III) complexes with heptadentate macrocyclic ligands. Magnetic Resonance in Chemistry 1999, 36, (S1), S200 - S208.

57. Pulukkody, K. P.; Norman, T. J.; Parker, D.; Royle, L.; Broan, C. J., Synthesis of charged and uncharged complexes of gadolinium and yttrium with cyclic polyazaphosphinic acid ligands for in vivo applications. J. Chem. Soc. Perkin. Trans. 2 1993, 99, 605-620.

58. Howard, J. A. K.; Kenwright, A. M.; Moloney, J. M.; Parker, D.; Port, M.; Navet, M.; Rousseau, O.; Woods, M., Structure and dynamics of all of the stereoisomers of europium complexes of tetra(carboxyethyl) derivatives of dota: ring inversion is decoupled from cooperative arm rotation in the RRRR and RRRS isomers. Chem. Commun. 1998, 13, 1381-1382.

59. Parker, D.; Dickins, R. S.; Pushchmann, H.; Crossland, C.; Howard, J. A. K., Being excited by lanthanide coordination complexes: Aqua species, chirality, excited-state chemistry, and exchange dynamics. Chem. Rev. 2002, 102, 1977-2010.

60. Eisenwiener, K. P.; Powell, P.; Macke, H. R., A convenient synthesis of novel bifunctional prochelators for coupling to bioactive peptides for radiometal labelling. Bioorganic and Medicinal Chemistry Letters 2000, 10, 2133-2135.

61. Harrison, P. G., Silicate Cages: Precursors to new materials. J. Organometallic Chemistry 1997, 542, 141-183.

62. Muller, R.; Kohne, R.; Sliwinski, S., J. Prakt. Chem. 1959, 9, 71.

63. Frye, C. L.; Collins, W. T., J. Am. Chem. Soc 1970, 92, 5596.

64. Feher, F. J.; Soulivong, D.; Eklund, A. G., Controlled cleavage of R8Si8O12 frame works: a revolutionary new method for manufacturing precursors to hybrid inorganic-organic materials. Chem. Commun. 1998, 399-400.

65. Gillett, S. L. In Towards a silicate-Based Molecular Nanotechnology 1. Background and Review, Fifth Foresight Conference on Molecular Nanotechnology., Palo Alto, California, 1998, 1998; Palo Alto, California, 1998.

66. Kuhnle, A.; Jost, C.; Abbenjuis, H. C. L. Nanofiller, production and use. 2005.

67. Gillett, S. L. In Towards a Silicate-Based Molecular Nanotechnology II. Modelling, Synthesis Review, and Assembly Approaches., Fifth Foresight Conference on Molecular Nanotechnology., Palo Alto, California, 1998, 1998; Palo Alto, California, 1998.

68. Feher, F. J.; Soulivong, D.; Lewis, G. T., Facile framework cleavage reaction of a completely condensed silsesquioxane framework. J. Am. Chem. Soc 1997, 119, 11323-11324.

69. Feher, F. J.; Soulivong, D.; Nguyen, F., Practical methods for synthesizing four incompletely condensed silsesquioxanes from a single R8Si8O12 framework. Chem. Commun. 1998, 1279-1278.

70. Annand, J.; Aspinall, H. C., Lanthanide silsesquioxanes: monomeric and functionalised complexes. J. Chem. Soc. Dalton Trans 2000, 1867-1871.

71. Annand, J.; Aspinall, H. C.; Steiner, A., Novel Heterometallic Lanthanide Silsesquioxane.

Inorganic Chemistry 1999, 38, 3941-3943.

72. Feher, F. J.; Terroba, R.; Ziller, J. W., A new route to incompletely-condensed silsesquioxanes: Base-mediated cleavage of polyhedral oligosilsesquioxanes. Chem. Commun. 1999, 2309-2310.

73. Feher, F. J.; Terroba, R.; Ziller, J. W., Base-catalyzed cleavage and homologation of polyhedral oligosesquixanes. Chem. Commun. 1999, 2153-2154.

74. Feher, F. J.; Wyndham, K. D.; Soulivong, D.; Nguyen, F., Syntheses of highly functional cube-octameric polyhedral oligosilsesquioxanes (R8Si8O12). J. Chem. Soc. Dalton Trans 1999, 1491-1497.

75. Brook, M. A., Silicon in organic , organometallic and polymer chemistry. John Wiley &Sons, INC.: Ontario, 2000; p 680.

76. Burgy, H.; Calzaferri, G., J. Chromatograph 1990, 507, 481.

77. Calzaferri, G.; Imhof, R., J. Chem. Soc. Dalton Trans 1992, 3391.

78. Bassindale, A. R.; Gentle, T. E., J. Mater. Chem. 1993, 3, 1319.

79. Boukherroub, R. C., C.: Manuel, G., Organometallics 1996, 15, 1508.

80. Lukevics, E. D., M., J. Orgabomet. Chem. 1985, 295, 265.

81. Brook, M. A., Silicon in organic, organometallic and polymer chemistry. John Wiley &Sons, INC.: Ontario, 2000; p 171-188.

82. Kaden, T. A., Ten-membered rings or larger with one or more nitrogen atoms. In Comprehensive heterocyclic chemistry II: A review of the literature 1982-1995. , Katritzky, A. R.; Rees, C. W.; Scriven, E. F., Eds. Pergamon: 1995; Vol. 9, pp 790-807.

83. Rosenthatal, M. T.; Czarnit, A. W., Rapid transacylations of activated ester substrates bound to the primary side B-cyclodextrin-cyclen conjugate and its M+2 J. of Inclusion Phenomena and Macrocyclic Chemistry 1991, 10, (1), 119-126.

84. Padwa, A., Tandem methodology for heterocyclic synthesis. Pure Appl. Chem. 2004, 76, (11), 1933-1952.

85. Yoo, J.; Reichert, D. E.; Welch, M. J., Regioselective N-substitution of cyclen with two different alkyl groups: synthesis of all possible isomers. Chem. Commun. 2003, 766-767.

86. Boldrini, V.; Giovenzana, G.; Pagliarin, R.; Palmisano, G.; Sisti, M., Expeditious N-monoalkylation of 1,5,7,10-tetraazacyclododecane (cyclen) via formamido protection. Tetrahedron Let 2000, 41, 6527-6530.

87. Boldrini, V.; Giovenzana, G. B.; Pagliarin, R.; Palmisano, G.; Sisti, M., Expeditious N-monoalkylation of 1,4,7,10-tetraazacyclododecane (cyclen) via formamido protection. Tetrahedron letters 2000, 41, 6527-6530.

88. March, J.; Smith, M. B., March's Advanced Organic Chemistry. 5th ed.; Wiley-Interscience Publication: 2001.

89. Reiff, H.; Dieterich, D.; Braden, R.; Ziewmann, H., Neue 1,3-Propandiole durch nuclephile ringoffnung von 3-alkyl-3-hydroxymethyl-oxetanen. Liebig Ann. Chem. 1973, 365-374.

90. Flohr, H.; Pannhorst, W.; Retey, J., Ein sythetisches modell fur die aktivstelle der conenzym-B12-abhangigen methylmalonyl-CoA-mutase. Helvetica. Chemica. Acta 2004, 61, (5), 1565-1587.

91. McMurry, T. J.; Parmelee, D. J.; Sajiki, H.; Scott, D. M.; Ouwllet, H. S.; Walovitch, R. C.; Tyeklar, Z.; Dumas, S.; Bernard, P.; Nadler, S.; Midelfort, K.; Greenfield, M.; Troughton, J.; Lauffer, R. B., The effect of a phosphodiester linking group on albumin binding, blood half-life, and relaxivity of intravascular diethylenetriaminepentaacetato aqua gadolinium(III) MRI contrast agents. J. Med. Chem. 2002, 45, 3465-3474.

92. Glogard, C.; Hovland, R.; Fossheim, S. L.; Aasen, A. J.; Klaveness, J., Synthesis and physicochemical characterisation of new amphiphilic gadolinium DO3A complexes as contrast agents for MRI. J. Chem. Soc. Perkin Trans. 2 2000, 1047-1052.

93. Hovland, R.; Glogard, C.; Aasen, A. J.; Klaveness, J., Gadolinium DO3A derivatives mimicking phospholipids; preparation and in vitro evaluation as pH responsive MRI contrast agents. J. Chem. Soc. Perkins Trans. 2 2001, (929-933).

94. Anelli, P. L.; Murru, M.; Uggeri, F.; Virtuani, M., Highly regioselective synthesis of 1,7-diprotected 1,4,7,10-tetraazacyclododecane derivatives. Chem. Commun. 1991, 1317-1318.

95. Anelli, P. L.; Calabi, L.; Dapporto, P.; Murru, M.; Paleari, L.; Paoli, P.; Uggeri, F.; Verona, S.; Virtuani, M., Highly regioselective access to 7-substituted 1,4,7,10-tetraazacyclododecane-1-carbaldehyde derivatives: synthetic aspects and NMR elucidation of the structures. X-ray crystal structures of 7-triphenylmethyl-1,4,7,10-tetraazacyclododecane-1-carbaldehyde and 7-triphenylmethyloctahydro-5H,9bH-2a,5a,7,9a-tetraazacycloocta[cd]pentalene. J. Chem. Soc. Perkins Trans. 1 1995, 2995-3004.

96. Bruce, J. I.; Dickins, R. S.; Govenlock, L. J.; Gunnlaugsson, T.; Lopinski, S.; Lowe, M. P.; Parker, D.; Peacock, R. D.; Perry, J. J. B.; Aime, S.; Botta, M., The selectivity of reversible oxy-anion binding in aqueous solution at a chiral europium and terbium centre: Signalling of carbonate chelation by changes in the forma and circular polarization of luminescence emission. J. Am. Chem. Soc 2000, 122, 9674-9684.

97. Bornstein, D.; Mandelbaum, A.; Vidavsky, I.; Domon, B.; Mueller, D. R.; Richter, W. J., Mechanism of electron impact ionization-induced halogen elimination from 2-methyl-2-bromosuccinate. Org. Mass. Spec 1992, 28, (3), 230-234.

98. Bornstein, D.; Mandelbaum, A.; Vidavsky, I.; Domon, B.; Mueller, D. R.; Richter, W. J., Behaviour of isomeric methyl ethyl and ethyl methyl halosuccinates under electron impact. Elimination of a halogen atom by a multi-step mechanism. Org. Mass. Spec 1991, 26, (9), 793-798.

99. Lee, J. D., Concise Inorganic Chemistry. 5th ed.; Chapman & Hall: 1996; p 1032.

100. Liu, S.; Edwards, D. S., Bifunctional chelators for the therapeutic lanthanide radiopharmaceuticals. Bioconjugate chem. 2001, 12, (1), 7-34.

101. Gunnlaugsson, T.; Davies, R. J.; Nieuwenhuyzen, M.; Stevenson, C. S.; Viguier, R.; Mulready, S., Rapid hydrolytic cleavage of the mRNA model compound HPNP by glycine based macrocyclic lanthanide ribonuclease mimics. Chem. Commun. 2002, (18), 2136-7.

102. Eisner, U.; Elvide, J. A.; Linstead, R. P., Unsaturated lactones and related substance. Part V. Dihydro-B-ketomuconic acid and carboxyl-lactones of the protoanemonin type. J. Chem. Soc. 1951, 1501-1512.

103. Quiros, M.; Astorga, C.; Rebolledo, F.; Gotor, V., Enzymatic selective transformations of diethyl fumarate. Tetrahedron 1995, 51, (28), 7715-7720.

104. Pratt, L.; Smith, B. B., Proton resonance spectra of some unsaturated carboxylic acids. Trans. Faraday. Soc 1967, 2858-2867.

105. Ganguly, S.; Roundhill, D. M., Hydration of diethyl maleate in the presence of bimetallic hydroxy palladium(II) complexes of 1,2-Bis(diphenylphosphino)ethane(dppe) as catalysts. Chem. Commun. 1991, 639-640.

106. Levene, O. A.; Mikeska, L. A., On a possible asymmetry of aliphatic diazo compounds. IV. The Journal of Biological chemistry 1922, 55, (4), 794-800.

107. McMurry, J., Organic Chemistry. 4th ed.; Brooks/Cole Publishing Company: 1996.

108. Fensterbank, H.; Berthault, P.; Larpent, C., A tuneable one-step N,N'- disubstitution of 1,4,8,11- tetraazacyclotetradecane with acrylamide. Eur. J. Org. Chem. 2003, 3985-3990.

109. Fensterbank, H.; Zhu, J.; Riou, D.; Larpent, C., A convenient one-step synthesis of mono-N-functionalized tetraazamacrocycle. J. Chem. Soc. Perkins Trans. 1 1999, 881-815.

110. Channa, A.; Steed, J. W., Anion and cation binding by a pendant arm cyclam and its macrobicyclic derivatives. Dalton Trans 2005, 2455-2461.

111. Bartoil, G.; Bosco, M.; Marcantoni, E.; Petrini, M.; Sambri, L.; Torreglant, E., Conjugate addition of amines to a-b-Enones promoted by CeCl3.7H2O-NaI system supported in silica gel. J. Org. chem. 2001, 66, (26), 9052-9055.

112. Areces, P.; Gil, M. V.; Higes, F. J.; Roman, E.; Serrano, J. A., Stereoselective Michael addition reactions of 5-glyco-4-nitrocyclehex-1-enes. Tetrahedron Let 1998, 39, 8557-8560.

113. LTD, T. B. D. H., Ion Exchange Resins. 5 ed.; BDH: Poole, UK, 1965; p 80.

114. Faglioni, F.; Blanco, M.; Goddard, W. A.; Saunders, D., Heterogeneous inhibition of homogeneous reactions: Karstedt's catalyzed hydrosilylation. J. Phys. chem. B 2002, 106, 1714-1721.

115. Lewis, L. N.; Stein, J. S.; Gao, Y.; Colborn, R. E.; Hutchins, G., Platinum catalysts used in the silicones industry. Platinum Metals Rev 1997, 41, (2), 66-75.

116. Bruce, J. I.; Lowe, M. P.; Parker, D., Photophysical Aspects of Lanthanide(III) complexes. In The Chemistry of Contrast Agents in Medical Magnetic Resonance Imaging, Merbach, A. E., Ed. John Wiley & Sons: Chichester, 2001; pp 437-463.

117. Cotton, S., Lanthanides & Actinides. 1st ed.; MacMillan Education: London, 1991; p 192.

118. Frey, S. T.; Horrocks, W. J., On correlating the frequency of the 7F0 --> 5D0 transition in Eu3+ complexes with the sum of "nephelauxtic parameter' for all of the coordinating atoms. Inorganica Chimica Acta 1995, 383-390.

119. Barja, B. C.; Remorino, A.; Roberti, M. J.; Aramendia, P. F., Luminescence quenching of europium (III) and terbium (III) carboxylates by transition metals in solution. J. Argent. Chem. Soc 2005, 93, (4), 81-91.

120. Ofelt, G. S., Structure of the f5 configuration with application to rare-earth ions. J. Chem. Phys. 1962, 38, (9), 2171-2180.

121. Buenzli, J. C. G.; Choppin, G. R., Lanthanide Probes in Life, Chemical and Earth Sciences: Theory and Practice. . Elsevier: 1989.

122. Supkowski, R. M.; Horrocks, W. J., On the determination of the number of water molecules, q,

coordinated to europium(III) ions in solution

from luminescence decay lifetimes. Inorganica Chimica Acta 2002, 340, (1), 44-48.

123. Beeby, A.; Clarkson, I. M.; Dickins, R. S.; Faulkner, S.; Parker, D.; Royle, L.; Sousa, A. S.; Williams, J. A. G.; Woods, M., Non-radiative deactivation of the excited states of europium, terbium and ytterbium complexes by proximate energy-matched OH, NH and CH oscillators: an improved luminescence method for establishing solution hydration states. J. Chem. Soc. Dalton Trans 2 1999, 493-503.

124. Batsanov, A. S.; Bruce, J. I.; Ganesh, T.; Low, P. J.; Kataky, R.; Pushchmann, H.; Steel, P. G., Synthesis, characterisation and application of lanthanide cyclen complexes in organic synthesis. J. Chem. Soc. Perkins Trans. 1 2002, 932-937.

125. Bianchini, C.; Giambastiani, G.; Laschi, F.; Mariani, P.; Vacca, A.; Vizza, F.; Zanello, P., Synthesis, characterization and coordination chemistry of the new tetraazamacrocycle 4,10-dimethyl-1,4,7,10-tetraazacyclododecane-1,7-bis(methanephosphonic acid monoethyl) dipotassium salt. Org. Biomol. Chem. 2003, (1), 879-886.